VŠB - Technical University of Ostrava
Faculty of Electrical Engineering
and Computer Science

Energy Harvesting Enabled Relaying Network: Design System and Performance Analysis

Ph.D. THESIS

2018 **Hoang-Sy Nguyen**

VŠB - Technical University of Ostrava
Faculty of Electrical Engineering and Computer Science
Department of Telecommunications

Energy Harvesting Enabled Relaying Network: Design System and Performance Analysis

Ph.D. Thesis

Doctoral Study Branch: 2601V018 Communication Technology
Doctoral Study Programme: P1807 Computer Science, Communication Technology and Applied Mathematics

2018 **Hoang-Sy Nguyen**

VYSOKÁ ŠKOLA BÁŇSKÁ–TECHNICKÁ UNIVERZITA OSTRAVA
VŠB–TECHNICAL UNIVERSITY OF OSTRAVA

FAKULTA ELEKTROTECHNIKY A INFORMATIKY
FACULTY OF ELECTRICAL ENGINEERING AND COMPUTER SCIENCE

KATEDRA TELEKOMUNIKAČNÍ TECHNIKY
DEPARTMENT OF TELECOMMUNICATIONS

Energy Harvesting Enabled Relaying Network: Design System and Performance Analysis

Ph.D. Thesis; Delivered in November, 2018
Doctoral Study Programme:
P1807 Computer Science, Communication Technology and Applied Mathematics
Doctoral Study Branch:
2601V018 Communication Technology

PhD. Student: Ing. Hoang-Sy Nguyen
VŠB - Technical University of Ostrava
Faculty of Electrical Engineering and Computer Science
Department of Telecommunications
17. listopadu 15/2172, 708 33 Ostrava, Czech Republic
sy.nguyen.hoang.st@vsb.cz

Supervisor: Prof. Ing. Miroslav Vozňák, PhD.
VŠB - Technical University of Ostrava
Faculty of Electrical Engineering and Computer Science
Department of Telecommunications
17. listopadu 15/2172, 708 33 Ostrava, Czech Republic
miroslav.voznak@vsb.cz

OSTRAVA, 2018

DECLARATION

I myself declare that this thesis is conducted as the result of my original research done by myself with the guidance of my supervisor in the faculty of electrical engineering and computer science at VŠB - Technical University of Ostrava as a candidate for the Doctor of Communication Technology.

My works included below were carried out under the supervision of Prof. Miroslav Vozňák. It is noted that this thesis has never been submitted for any other degrees or awards in any other universities or educational institutions.

This is a true copy of the thesis, including any required final revisions, as accepted by my examiners.
I understand that my thesis may be made electronically available to the public.

. . . .
(author's signature)

ACKNOWLEDGEMENT

Firstly, I would like to express my gratitude to my supervisor prof. Ing. Miroslav Vozňák, Ph.D. for his kind support of my Ph.D. study and research activities. His instructions helped me well through all my research works and the completion of this thesis. His not only advises me on how to be a great researcher, but also shows me how to be a good person.

Secondly, I would like to thank my little family for their motivations. Over the course of my student life, my wife and my son play a very important role in my study. I am grateful to my parents and siblings who have provided me with moral, emotional, and sometimes financial support. I also would like to express my gratitude to other family members and friends who have motivated me along the way.

Last by not least, my study would be really challenging if I did not receive much support from my dear colleagues in WiCOM research group, especially Mr. Thanh-Sang Nguyen who has supported me a lot. His valuable suggestions and insightful comments have significantly improved the quality of my papers.

. . . .

(author's signature)

ABSTRAKT

Tato dizertační práce se věnuje návrhu nových protokolů pro bezdrátově napájené komunikační sítě, jejichž efektivita je následně podrobena analýze. V této práci jsou probrány přístupy k bezdrátovému napájení komunikačních zařízení, a sice SP (Separated Power) a HP (Harvested Power), kdy energie je získána z okolí. Tyto techniky jsou zkoumány z pohledu tzv. relay uzlu R (Relay node) v plně duplexních sítích RN (Relaying Networks) pracujících v režimu DF (Decode-and-Forward).

Mimoto, jsou v práci rozebrány i faktory snižující výkonnost a efektivitu bezdrátově napájených komunikačních systémů využívajících navržený hybridní protokol HTPSR (Hybrid Time Switching-based and Power Splitting-based Relaying). Pro tyto účely je využita zejména informace o stavu kanálu CSI (Channel State Information), přičemž detekovány a vyhodnoceny jsou i vlivy jednotlivých zařízení HWIs (Hardware Impairments). Pro zmíněný protokol HTPSR je v práci taktéž řešen problém optimalizace poměru mezi intervaly časového přepínání TS (Time Switching) a děleného napájení PS (Power Splitting), kde byl využit genetický algoritmus.

Další oblastí, která je v této práci zkoumána, je síť umožňující současný přenos informací i energie pro napájení, pro niž byly v rámci této práce navrženy, nasazeny a vyhodnoceny dva protokoly, a to PTSTW (Power Time Splitting-based Two-slot) a PTSTH (Power Time Splitting-based Three-slot).

Následně jsou v dizertaci zkoumány tři navržená schémata, ve kterých může být provozován uzel R a je provedena jejich výkonnostní analýza, konkrétně jde o režim:

- poloduplexní využívající techniku kombinování maximálních poměrů HDMRC (Half-duplex Deploying Maximal Ratio Combine),
- plně duplexní využívající sdružené dekódování FDJD (Full-duplex Deploying Joint Decoding),
- a hybridní kombinující oba výše zmíněné způsoby v režimu HTS (Hybrid Transmission Scheme).

Všechna tato tři schémata jsou provozována v optimalizovaných režimech provozu, přičemž v práci jsou rozebrány dva – optimální napájení s individuálními limity OPIPC (Optimal Power Under the Individual Power Constraints) a optimální napájení s možností využití získávání energie OPEHA (Optimal Power with Energy Harvesting Ability). Z následných simulací pak bylo zjištěno, že HTS svou efektivitou předčí jak HDMRC, tak FDJD a že režim OPEHA je výhodnější než režim OPIPC.

Posledním přínosem této práce jsou dva navržené způsoby určení časových poměrů OTPS (Optimal Time for transmitting Power at Source) a OTPR (Optimal Time for transmitting Power at Relay) s cílem optimalizovat přenos energie v CR (Cognitive Relaying) sítích. Rovněž byly pečlivě zkoumány výkonnostní parametry jako pravděpodobnost

výpadku, poměr mezi přenosovou rychlostí systému a dodanou energií a průměrná efektivita systému při přenosu energie, a to za účelem zlepšení vlastností datových přenosů.

KLÍČOVÁ SLOVA

Získávání energie, pravděpodobnost výpadku, ergodická kapacita, průchodnost, energetická účinnost.

ABSTRACT

The thesis deals with the design of new protocols and the analysis of wireless-powered communications networks' performance. In order to bring the contribution to the science in field of my topic, this thesis starts with the study of wireless power supply policies, namely the separated power (SP) and harvested power (HP) techniques at the relay node in the full-duplex (FD) decode-and-forward (DF) relaying networks (RNs).

In the second emphasis, the thesis deals with the factors degrading the system performance, i.e., channel state information (CSI) and hardware impairments (HWIs) using Hybrid time switching-based and power splitting-based relaying (HTPSR) protocol. Besides that, an optimization problem regarding time switching (TS) and power splitting (PS) ratios are solved in this thesis, where a genetic algorithm was used.

In the third emphasis of this thesis, a two-way simultaneous wireless information and power transfer (SWIPT) network is considered to be an important technique, in which two new proposed protocols, namely power time splitting-based two-slot (PTSTW) and power time splitting-based three-slot (PTSTH) are deployed and compared with each other. The throughput performance is analyzed for both developed protocols.

The following emphasis is the study of relay selection (RS) schemes. The three optimal RS schemes are proposed to examine the system performance, namely:

- Half-duplex (HD) deploying maximal ratio combine (HDMRC),
- FD deploying joint decoding (FDJD),
- and hybrid FD/HD relaying transmission scheme (HTS).

All of them operate in two optimal power supply policies - optimal power under the individual power constraints (OPIPC) and optimal power with energy harvesting ability (OPEHA). The simulation results show that the HTS outperforms HDMRC and FDJD, and OPEHA is better than OPIPC.

Finally, Optimal time for transmitting power at source (OTPS) and Optimal time for transmitting power at relay (OTPR) are proposed to optimize the transmit power in a cognitive relaying network (CRN). For performance analysis, the outage probability (OP), the rate-energy trade-off and the average energy efficiency are studied to enhance the successful data transmission.

KEYWORDS

Energy harvesting, outage probability, ergodic capacity, throughput, energy efficiency.

CONTENTS

LIST OF FIGURES

LIST OF TABLES

LIST OF ABBREVIATIONS AND SYMBOLS

Abbreviations

AF	Amplify-and-Forward
AWGN	Additive White Gaussian Noise
BER	Bit error rate
BSs	Base stations
CDF	Cumulative distribution function
CEEs	Channel Estimation Errors
CEs	Channel Errors
CRN	Cognitive Relaying Network
CSCG	Circularly Symmetric Complex Gaussian
CSI	Channel State Information
CU	Central Unit
D	Destination node
D2D	Device-to-Device
DF	Decode-and-Forward
EE	Energy efficiency
EH	Energy Harvesting
FD	Full-duplex
FDJD	FD deploying joint decoding
GA	Genetic Algorithm
HDMRC	HD deploying maximal ratio combine
HP	Harvested power
HTS	Hybrid FD/HD relaying transmission scheme
HWIs	Hardware impairments
IoT	Internet of things

IT	Information Transmission
LI	Loop Interference
MPR	Macro Cell Primary Receiver
MPT	Macro cell primary transmitter
NOMA	non-orthogonal multiple access
OMA	orthogonal multiple access
OP	Outage Probability
OPEHA	Optimal power with EH ability
OPIPC	Optimal power under the individual power constraints
OTPR	Optimal time for transmitting power at relay
OTPS	Optimal time for transmitting power at source
P2P	Peer-to-Peer
PDF	Probability distribution function
PS	Power Splitting
PSR	Power splitting-based relay
PTSTH	Power time splitting-based three-slot
PTSTW	Power time splitting-based two-slot
PUs	Primary users
QoS	Quality of Service
R	Relay node
RF	Radio frequency
RNs	Relaying networks
RSI	Residual Self-Interference
RVs	Random variables
S	Source node
SE	Spectral efficiency
SER	Symbol Error Rate

SI	Self-interference
SIR	Signal-to-interference Ratio
SNDR	Signal-to-noise-plus-distortion ratio
SNR	Signal-to-noise ration
SP	Separated power
STP	Successful transmission probability
SUs	Secondary users
SWIPT	Simultaneous wireless information and power transfer
TS	Time Switching
TSM	Time-Sharing selection method
TWRNs	Two-way relaying networks
UEs	User equipments
WBNs	Wireless body networks
WET	Wireless Energy Transfer
WPNs	Wireless-Powered networks
WPT	Wireless power transmission
WSNs	Wireless sensor networks

Symbols

$(1-\alpha)T$	TS for IT from R to D
$(1-\beta)P_S$	PS for IT from S to R
αT	TS for IT from S to R
βP_S	PS for EH at R
η	The energy efficiency
γ_0	The SNR threshold
$\mathrm{E}\{.\}$	The expectation operation
$\Pr(.)$	The probability function
B	The signal bandwidth

d_{LI}	The distances between two antennas
d_{RD}	The distances between R and D
d_{SR}	The distances between S and R
$E_i(x)$	Exponential integral
E_{Ci}	The circuit power for UEs
E_{Di}	The transmit power for UEs
F_X	The CDF of the RVs, X.
f_X	The PDF of the RVs, X.
$K_n(.)$	The modified Bessel function of the second kind with order n
m	The path-loss exponent
P_R	The transmit powers at relay
P_S	The transmit powers at source
R_0	The transmission target rate
T	The transmission block time

1 INTRODUCTION

In this chapter, I present the general background for the dissertation. Specific background material relevant to only one chapter is provided in the introduction of the appropriate chapter. I provide an overview of the specific technical problems in Section 1.1, and the organization of this thesis is presented in Section 1.2.

1.1 Background and Motivation

Thanks to the increasing demand for services requiring wireless connection in recent years, wireless networks have caught more attention. In principle, wireless systems, i.e. wireless sensor or wireless body sensor networks often face with limited lifetime. Thus, in order to overcome that limitation, energy harvesting (EH) has emerged as a promising technology. In particular, energy can be extracted from the surrounding environment (e.g. solar, geothermal, wind, etc.) to help prevent the short lifetime and the recharge or replacement of batteries. Now, I am going to go through some fundamental knowledge on elements in wireless systems.

1.1.1 RF Energy Transfer

Recently, RF-EH techniques, which enable the process of generating electricity from the received RF signals, have received considerable research interests [1]. Thus, a number of solutions have been proposed in terms of RF-EH to enhance power energy-constrained wireless networks for information transmission (IT) and signal processing due to a lack of radio resources. Since RF-EH technology has been deployed in wireless sensor networks (WSNs) [2], wireless body networks [3], and wireless charging systems [4], it is increasingly challenging to come up with new models to make RF-EH more efficient. Furthermore, wireless energy transfer has been presented in wireless systems for RF-EH, where a robust model was introduced so-called simultaneous wireless information and power transfer (SWIPT) [5]. In such a technique, both energy and information can be carried by RF signals. Hence, it is worth noting that wireless-powered networks can become a vital and irreplaceable building block of large-scale wireless systems, including WSNs [6] and the Internet of Things (IoT) .

Here, as illustrated in Fig. 1.1, a RF-EH network model consisting of three main components is considered, including information gateways, the sources and the nodes. Base stations (BSs) , the information gateways represent wireless routers or relays. In principle, RF sources can be deployed as RF transmitters or ambient RF sources, where nodes representing the user equipments (UEs) communicate with the information gateways. Note that the gateways and sources are equipped with a fixed power supply while energy from RF sources can be used to power the network nodes.

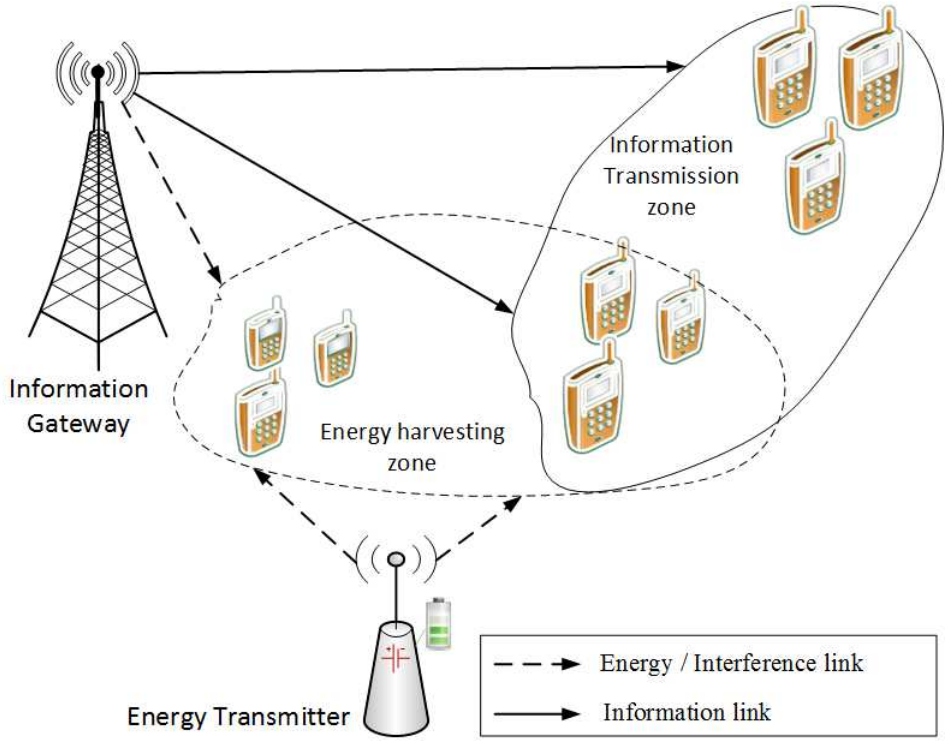

Fig. 1.1: Infrastructure-based Architecture RF-EH

Regarding Fig. 1.1, devices located in the EH zone (the dashed line zone) scavenge energy from BS, while components in the IT zone (the line zone) can decode information. It is noted that each node in the EH and IT zone is equipped with separate RF energy harvester and RF transceiver, respectively. Thus, both EH and IT can be done simultaneously.

1.1.2 Relaying Networks

Relaying networks (RNs), which have been comprehensively studied, improve the energy efficiency (EE) with the help of relay nodes, and this kind of network also enables short multi-hop communication with low system energy consumption compared to the direct communication. RNs can help achieve larger coverage area and longer network lifetime. Besides that, both relaying protocols, namely amplify-and-forward (AF) and decode-and-forward (DF) protocol were deployed in [7], where DF relaying scheme enables the relay node to receive the transmitted signals from the source node (S) , after that the received signal is decoded and then forwarded to the destination node (D) . Meanwhile, the relay node (R) in AF relaying scheme receives the source signal, amplifies and forwards to D. In [8] and [9], a receiver model was considered, in which wireless power transmission (WPT) and information decoding from the same RF was evaluated. Nonetheless, SWIPT was mentioned in [8] and [9], since the work in [10] showed that circuits used for EH from RF signals cannot decode the information.

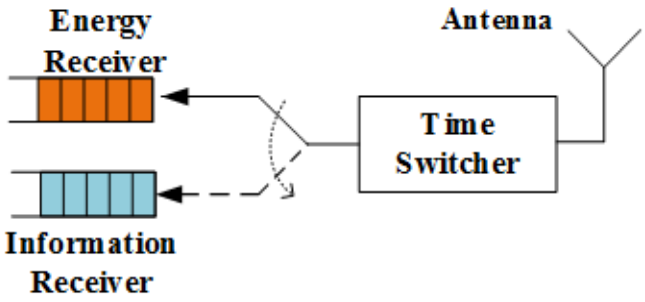

Fig. 1.2: Time Switcher Architecture

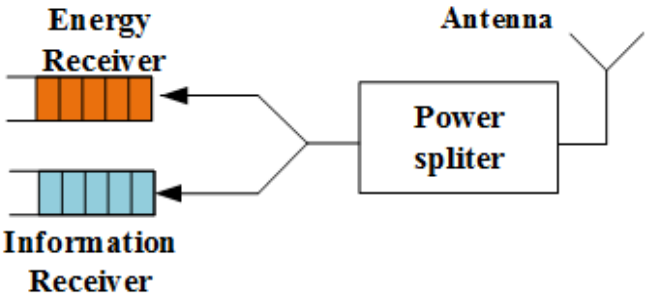

Fig. 1.3: Power Splitter Architecture

Motivated from these limitations, two practical receiver policies illustrated in Fig. 1.2 and Fig. 1.3 were put forward based on TS or PS architecture. The main goal of the TS architecture is coordinating the time for information reception and RF EH. However, for the PS architecture, its aim is to achieve an optimal ratio to split the received RF signals, if the circuit power consumption is negligible.

A. Time switching-based relay protocol (TSR):

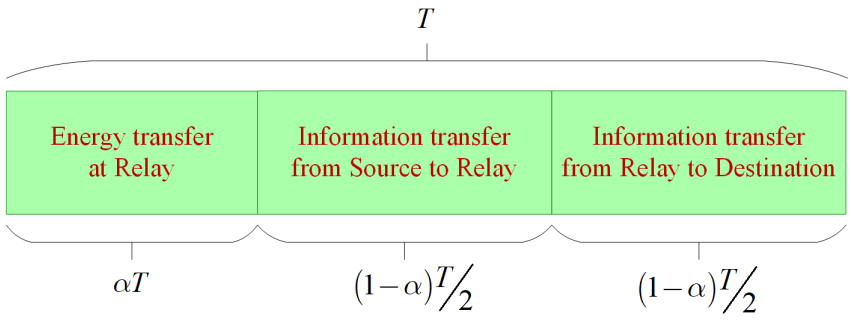

Fig. 1.4: Time switching-based relay protocol

In Fig. 1.4, TS receiver model switches between EH and information decoding mode. The received signal denoted by y_R is transmitted to the EH receiver for an amount of

time, αT, and then to the information receiver in $(1-\alpha)T$, where T stands for time duration for information being transmitted between S and D.

B. Power splitting-based relay protocol (PSR):

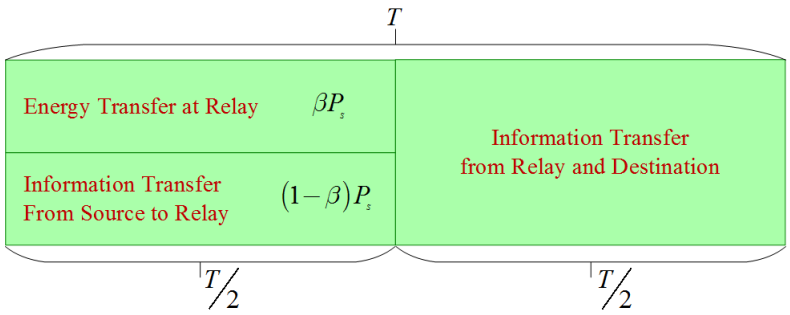

Fig. 1.5: Power splitting-based relay protocol

In addition, in Fig. 1.5, the power of the received signal is split into two parts in PS receiver architecture so-called the PS ratio denoted by β. A portion, $\sqrt{\beta}y_R$, of the received signal is transmitted to the EH receiver, while the remaining portion, $\sqrt{(1-\beta)}y_R$ is used for the information receiver. The considered architecture have been deployed in a number of systems, i.e. [11], [12] and [13].

C. Hybrid power time switching-based relay protocol (HPTSR)

In addition, a hybrid TSR-PSR protocol (HPTSR) is also proposed in this thesis which is illustrated in Fig. 1.6.

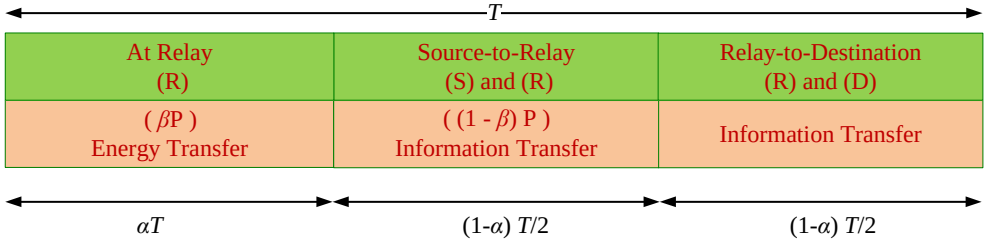

Fig. 1.6: The HPTSR protocol

In Fig. 1.6, T stands for the time block, where S transmits data to D, and the ratio of T is αT where R harvests power from the transmitted signal from S ($0 < \alpha < 1$). The remaining time, $(1-\alpha)T$ used for IT is split into two equal portions, in which $(1-\alpha)T/2$ is for S-R link while R-D link accounts for $(1-\alpha)T/2$, respectively. Furthermore, R consumes all the harvested energy during energy transfer process to forward signals from S to D. Most importantly, βP_S is used for EH with P_S being the transmit power at S, while $(1-\beta)P_S$ denoted as PS ratio is utilized for IT.

D. Energy Harvesting (EH)

Therefore, the harvested energy in TSR, PSR and HPTSR protocol at R can be respectively expressed as

$$E_h^{TSR} = \eta P_S |h_S|^2 \alpha T, \tag{1.1}$$

$$E_h^{PSR} = \frac{1}{2} \eta P_S |h_S|^2 \beta T, \tag{1.2}$$

and

$$E_h^{HPTSR} = \eta P_S |h_S|^2 \alpha \beta T, \tag{1.3}$$

where $0 \leq \eta \leq 1$ denotes the EH efficiency at the energy receiver relying on the EH circuitry and the rectifier.

1.2 Thesis Organization

The structure of the thesis is as follows:

- Chapter 1 is the introduction to this thesis which provides a background. Besides that, the description of each task and the thesis organization are also given.
- Chapter 2 presents the state-of-the-art of all the related research works in this thesis.
- Chapter 3 consists of the primary goals in the thesis.
- Chapter 4 examines the performance of RNs with WPT constraint policies.
- In Chapter 5, the impact of CSI when HTPSR protocol is examined.
- Chapter 6 focuses on the presence of HWIs in cognitive device-to-device (D2D) communications.
- In Chapter 7, the system performance of two-way relaying networks (TWRNs) is examined, where different time slots are going to be investigated.
- In Chapter 8 and 9, RS policies in different situations are studied, where a hybrid FD and HD RS scheme with optimal power under individual power constraints and EH is taken into consideration.
- Chapter 10 studies the TS policies, i.e., OTPS and OTPR in a HD DF small-cell CRN to enhance the maximum transmit power at S and R.
- Chapter 11 draws conclusions from our works and also suggests some possible directions for future research.

2 STATE OF THE ART

This chapter begins with a discussion of the motivation and context for the problems considered in this dissertation.

These days, thanks to the advancement of RF-EH circuit, powering wireless devices in wireless communication systems is the primary focus in both academia and industry [14], [15]. In particular, the work in [14] considered a network model of a set of RF charging stations overlaying with an uplink cellular network, while a harvest-then-transmit protocol was put forward for wireless power transfer [15]. Additionally, different kinds of up-to-date beamforming methods were implemented to enhance power transfer efficiency [8, 15, 16].

Recently, to assist wireless energy and information transfer, the dual use of RF signals was thoroughly discussed [11], [17]. Besides that, the authors in [9] proposed SWIPT to transmit RF energy in low-power systems (i.e. body sensor networks). There are a number of benefits associated with SWIPT in terms of bringing information and energy simultaneously efficiently, and it is a cost-effective choice for sustainable wireless systems without requiring further hardware update on transmitting devices. Nonetheless, it is worth noting that SWIPT can be optimized to bring more efficient network performance [17], [18].

Moreover, different kinds of low-power electronics, (i.e. smart watch, wireless keyboard and mouse, etc.) can be powered by energy scavenged from RF signals, since the majority of them only consume a little amount of power ranging from approximately micro-watts to milli-watts. An RF circuit was designed in [19] to assist non-stop charging of mobile electronics in areas filling with lots of people, in which more ambient RF signals are scavenged. Due to the fluctuations in entropy rate, RF signals determine the amount of data sent, while the average squared value of RF signals represents its power. As a result, the transmitted information and energy cannot be optimized concurrently. Therefore, new designs for next wireless systems are needed.

2.1 Power supply policies

In principle, the energy harvester powers communications or other processing, otherwise the unused energy will be put in an energy storage, i.e., a capacitor. Nevertheless, different from traditional wireless communication devices which suffer from a power constraint or a sum energy constraint, EH transmitters are subject to other EH constraints. In particular, each transmitter in each time slot can only consume at most the amount of stored energy available despite the availability of more energy in upcoming slots. Therefore, the use of the harvested energy is the biggest constraint the needs discussing.

There are a number of works considering the use of energy harvester as an energy source [20, 21, 22, 23, 24, 25]. In particular, the technique of dynamic programming was discussed [20], while the optimization problem of a reward which is linear with the used

energy was discussed in [21]. In [22], the throughput performance was optimized over an infinite horizon, in which [23] data queuing was also studied. Besides, an adaptive duty cycling was employed for throughput optimization. In [24], an information-theoretic technique was considered where the energy is harvested at the level of channel uses. The work in [25] presented optimal methods for throughput maximization over additive white Gaussian noise (AWGN) or fading channels.

2.2 Different factors affecting wireless relaying networks

According to studies related to EH in RNs, authors most assumed the ideal transceiver hardware is at all nodes. In fact, the transceiver hardware is imperfect because of some issues, i.e., phase noise, I/Q imbalance and amplifier nonlinearities [26]. In particular, HWIs of dual-hop RNs in terms of the capacity, throughput and symbol error rate (SER) were discussed in [27]. Meanwhile, the authors in [28] evaluated the issue of designing linear precoding and decoding for a TWRN between two MIMO FD nodes, in which the presence of HWIs and CSI are comprehensively studied.

Regarding the imperfect CSI, the work in [29] obtained the closed-form expression for the OP of two-way FD RNs with the residual loop interference (LI) and the imperfect CSI, but they did not study EH. Meanwhile, although the imperfect CSI in a FD RN was discussed in [29], the system performed badly in HD mode. In [30], the imperfect CSI at S was studied, and an opportunistic regenerative relaying deployed to guarantee the quality of service (QoS) in a CRN. Nonetheless, in most previous works, ergodic capacity was not comprehensively discussed in terms of PS and TS protocols for both AF and DF RNs under the impact of imperfect CSI.

2.3 Two-way Relaying Networks

Considering on TWRNs, a number of works have been carried out on this subject. In particular, the authors in [31] studied the ergodic capacity, the OP and the finite-SNR of SWIPT for TWRNs, while the work in [32] studied three TS EH policies, namely dual source power transfer, single-fixed source power transfer, and single-best-source power transfer. In addition, the impact of HWIs in TWRNs was also studied, where the authors derived the closed-formed expressions for throughput to study the trade-off between throughput and TS/PS ratios. The work in [33] considered TS-based network coding relaying protocol in a TWRN. However, to evaluate the performance of two-way transmission, the time-slot processing was studied to balance EH and IT. Besides, the system performance of TWRN also faces with several a number of technical limitations, e.g., the direct transmission of information cannot be processed. Thus, the use of multiple S-D pairs is considered as a potential solution in [34], where information is exchanged via EH R, and the allocation of energy among users is also a concern.

2.4 Relay selection techniques in CRNs

In terms of opportunistic multiple relay selection (RS) which is a goal of this thesis, we have found several interesting works. In particular, the work in [35] studied an issue associated with RS between AF and FD relaying protocols, where the best RS helps optimize instantaneous capacity of FD channel, and more importantly, several less-than-standard policies of RS with the assistance of partial CSI knowledge, including i) the communication between S and R; ii) the communication between R and D; iii) the loop interference. The authors in [36] put forward a scheme of power assignment in DF RNs with multi-relay over Rayleigh fading channels.

2.5 Cognitive radio in wireless communication networks

There is no doubt that combining EH with CRNs leads to better SE in the demand of green communications [37, 38, 39, 40]. In principle, both primary users (PUs) and secondary users (SUs) in a CRN can gain access to the spectrum concurrently. To guarantee QoS of PUs, the interference caused by SUs should be remained under an acceptable threshold [37]. In particular, the work in [38] studied the EH cooperative CRN, where SU, which shares the spectrum owned by PU, is equipped with EH capability and has finite capacity battery for energy storing. In return, SU transfers portion of its energy to PU.

There have been significant improvements in the deployment of CRNs [39], [40]. In [39], the work focused on a CRN, where SU uses portion of the primary time for IT, and it is deployed as a R for PU, SU can help in primary transmission. In the aforementioned model, the work implemented two RF EH techniques at R. Meanwhile, the authors in [40] considered SUs in case they are used as cooperative R nodes. An optimal stopping rule was proposed which selects a R node from a group of them to support the IT process.

3 GOALS OF DISSERTATION THESIS

The structure of the dissertation is based on the state-of-the-art research and requirements. All goals of the dissertation describe the dissertation schedule based on the new trends in current wireless communication networks. The contributions of each goal are going to be discussed in this chapter.

3.1 Goal 1: Performance analysis with wireless power transfer constraint policies

Regarding the first goal, wireless power supply policies are put forward to not only extend the coverage but also lengthen the network lifetime. The main contributions regarding this research problem include:

- Closed-form expressions for outage probability (OP) and the delay-tolerant and delay-limited throughput over independent and identically distributed Rayleigh fading channels are obtained.
- Simulation results are given in terms of some parameters like SI, power allocation schemes, transmit power at S and TS schemes for EH and FD mode. Additionally, SP and HP mode are compared.
- The proposed EH architecture helps boost the throughput performance. Furthermore, with the obtained optimal TS, the optimal transmission rate is achieved for HP mode.

3.2 Goal 2: Different factors affecting wireless relaying networks and measures to deal with them

Regarding this goal, new methods to address HWIs and CSI are presented. Therefore, I am going to summarize the contributions of each work.

In particular, the first research area is how to cope with the impact of CSI. The contributions can be summarized as follows:

- Under the impact of CSI, closed-form expressions for the end-to-end signal-to-noise ratio (SNR) and ergodic capacity are obtained. Besides, policies to choose optimal TS and PS ratios in HPTSR protocol are also evaluated.
- The closed-form analytical expressions of throughput in delay-limited and delay-tolerant modes are provided.
- We derive expressions of the instantaneous transmission mode and delay-limited transmission mode in both AF and DF protocols. The performance of bit error rate (BER) is evaluated by OP and signal modulation techniques.
- The appropriate choice of ideal PS and TS ratios in the proposed HTPSR is done carefully in close form for DF and AF.

In the second research problem, we propose ways to cope with the impact of HWIs in a D2D communication underlaying a cellular network. This study's contributions can be listed as follows:

- The energy consumption is quantified by deriving closed-form expressions for the STP, average EE and average spectral efficiency (SE) in case all nodes are affected.
- Comparisons between AF and DF transmission schemes in the multi-hop D2D communication and the direct P2P communication are given, and the optimization problem related to TS and PS ratios is also solved with the proposed HTPS protocol.
- Most importantly, our main goal is to optimize the successful transmission probability (STP).

3.3 Goal 3: Different time slots in two-way relaying networks

The study of different time slots contribute to the development of TWRNs in these listed following ways:

- Two newly proposed EH relaying protocols, namely PTSTW and PTSTH are deployed, where the role of TS and PS ratios is balanced.
- The throughput performance for these protocols under the impact of TS and PS ratios is studied.
- Following that, closed-form and approximate expressions for OP are provided, and we also achieve delay-limited and delay-tolerant throughput. It is noted that position allocation for R is determined to analyze OP.
- Most importantly, PTSTW is better than PTSTH regarding OP and throughput, since three times slot are occupied by PTSTH which result in more delay time compared to PTSTW.

3.4 Goal 4: Multiple relay selection schemes in both full-duplex and half-duplex transmission

In this work, optimal RS in a multi-relay RN is going to be investigated. In particular, the contributions of this research area include:

- The optimization problem of both TS and PS ratios is studied.
- The expressions for OP and throughput in delay-limited and delay-tolerant mode are derived.
- The trade-off between ergodic capacity and average EH is evaluated using HTPSR protocol.
- Thanks to the numerical results, the system throughput is proved to be greatly improved when RS is applied at high SNR, where delay-tolerant throughput is better than delay-limited throughput. In addition, the transmission data rate is boosted by the joint optimal TS and PS ratios.

In addition to the above work, more contributions can be shown as:

- OP at high SNR regime considering three proposed RS schemes, i.e. HDMRC and FDJD and HTS is comprehensively studied to minimize the impact of SI.
- In addition, two optimal power supply policies, i.e., OPIPC and OPEHA are used to study each RS scheme.
- The asymptotic results are also given besides the closed-form expressions.
- With the quantified power consumption model, EE can be improved.
- The numerical results prove that the proposed HTS scheme is superior to HDMRC and FDJD schemes in terms of OP.

3.5 Goal 5: The optimization of time-switching ratios in small cell cognitive relaying networks

Regarding this research goal, a HD DF small cell CRN is studied to examine the optimal TS ratio with the following summarized contributions:

- We put forward two optimal time switching policies so-called OTPS and OTPR to maximize the instantaneous transmit power at S and R.
- Closed-form expressions for OP, where the choice of an appropriate power allocation allows the proposed policies to enjoy better outage performance.
- The EE in the considered system is evaluated, where the average EE based on different impacts of power circuits and transmit powers is considered. In addition, the throughput performance in delay-limited transmission mode and the rate-energy trade-off are also obtained.

4 PERFORMANCE ANALYSIS WITH WIRELESS POWER TRANSFER CONSTRAINT POLICIES

In this chapter, we develop wireless power supply policies, SP and HP to propose a flexible architecture at R in FD DF RNs considering TSR to achieve optimal time used for a communication process. This transmission mode requires more processing procedure at R, i.e. antenna installations and SI cancellation. We evaluate the optimal power constraints in case of SP and HP to achieve better power consumption efficiency R. More importantly, closed-form expressions for outage probability and throughput are derived. To prove the correctness of the system, comparisons between SP and HP are given using numerical and simulation results, in which HP outperforms SP due to the amount of energy harvested.[NHS01]

4.1 Motivation

In practice, FD transmission mode[1] not only helps extend the coverage but also lengthen network lifetime, has attracted much research interest in recent years [41, 42]. In principle, thanks to the use of FD transmission mode, the SE in advanced communication systems can be significantly increased compared to HD mode. Besides that, FD mode is considered as an attractive mechanism to enhance data rate to satisfy the requirements of high transmission rate.

Furthermore, FD mode acquires more benefits than HD mode regarding SI. Particularly, SI resulted from FD was evaluated in [43]. However, a few disadvantages were discussed in that work [43]. For example, it is intractable and approximations are required. There was a rise in noise floor because of the interfering signal according to the model of self-inference in [44]. In such a model, better SI cancellation and SI channel estimation are achieved thanks to higher transmit power. Though perfect SI cancellation was able to achieve an upper bound on FD mode performance, it was considered to be unfeasible [45].

In addition, there are some special cases of the use of EH transmitters in multi-hop scenario which were considered [46, 47, 48]. In [47], unlike traditional battery powered wireless nodes, EH transmitters must deploy transmission to harvest available energy at any time. In [48], a HD relaying channel using DF protocol was considered, in which two delay constraints were proposed, namely delay-constrained and no-delay-constrained traffic were analysed. The work in [49] focused on promising FD methods such as SI cancellation solutions which were divided in to passive suppression, analog cancellation and digital cancellation. Recently, SE loss has been overcome with the help of FD transmission mode by allowing users to exchange information at the same frequency band [50, 51].

[1] In wireless communications, FD transmission mode, which allows the transmitter and receiver to be operated simultaneously in the same frequency band.

However, power allocation was not addressed comprehensively in the aforementioned studies in terms of opportunistic EH-assisted relay scheme. Therefore, we are going to focus on the power supply policies in DF FD RNs.

The rest of this chapter is organized as follows: We present the system model in Section 2. In Section 3, the optimal power constraints for R are studied for system performance. The simulation results are provided in Section 4. Section 5 gives a brief conclusion for the chapter.

4.2 System Model

As illustrated in Fig 4.1, we study a two-hop system consisting of R, S, and D. In particular, R is used to assist the communication between S and D. Assuming that S and D are respectively provided with a single antenna while R has one receiving and one transmitting antenna. We denote the channel coefficients of S-R link, R-D link and the residual LI respectively as h, g and f. The channel power gains, $|h|^2$, $|g|^2$, $|f|^2$ are exponentially distributed random variables (RVs) with means $\Omega_h = d_{SR}^{-m}$, $\Omega_g = d_{RD}^{-m}$, and $\Omega_f = d_{LI}^{-m}$. The distances between S and R, R and D are d_{SR} , d_{RD}, respectively. Besides that, the distance between two antennas is denoted as d_{LI}, and m is the path-loss exponent . We assume that the AWGN denoted as N_0 is with variance σ^2.

In addition, perfect CSI is assumed at S and R. Since information is transmitted and received at the same frequency band at R, this leads to residual SI, $|f|^2$ although SI cancellation techniques are deployed at R.

In this chapter, we use TSR protocol to study EH with T being the time block for an information transfer period. In particular, transmitting energy in the first phase makes up αT while the remaining amount of time, $(1-\alpha)\,T$ is used for IT in the second phase.

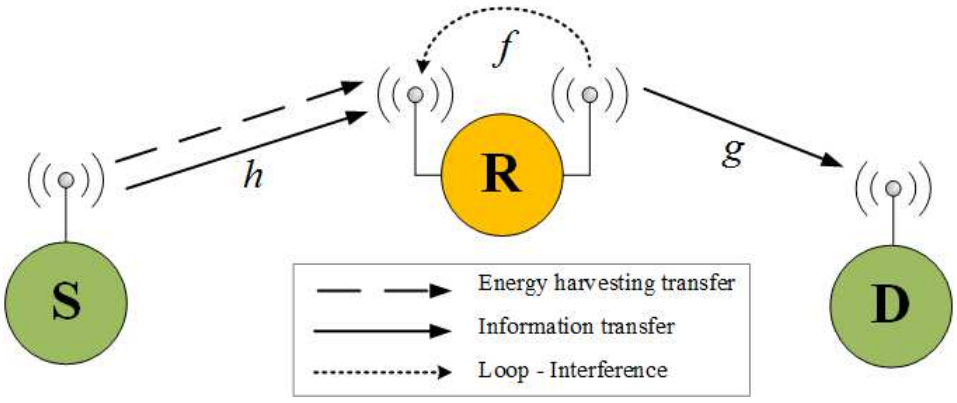

Fig. 4.1: The system model for EH FD RNs.

Note that P_S and P_R represent the transmit powers at S and R which are considered as individual constraints, i.e., $P_S \leq 1$ and $P_R \leq 1$. The received signal at R can be given

as

$$y_R = hx_S + fx_R + N_0, \tag{4.1}$$

where the energy symbols of S and R are defined as $\mathrm{E}\left\{|x_S|^2\right\} = P_S$ and $\mathrm{E}\left\{|x_R|^2\right\} = P_R$, respectively.

The high SNR at R when small noise term is available can be given as

$$\gamma_R = \frac{P_S|h|^2}{P_R|f|^2 + \sigma^2} = \frac{P_S|h|^2}{P_R|f|^2}. \tag{4.2}$$

The received SNR at D can be similarly computed as

$$\gamma_D = P_R|g|^2/\sigma^2. \tag{4.3}$$

The overall end-to-end SNR deploying DF relaying protocol is written by

$$\gamma_{eq} = \min\left\{\gamma_R, \gamma_D\right\}. \tag{4.4}$$

4.3 Performance Analysis

In order to evaluate the system performance, we separate the optimal power constraints at S and R. It is worth noting that the transmit powers at S and R are defined as $\{P_S = 1, P_R = 1\}$. Hence, the instantaneous rate of FD relaying in DF protocol can be computed as

$$R_1 = B\beta\log_2\left(1 + \gamma_{eq}\right), \tag{4.5}$$

where the values for SP and HP are defined as $\beta = 1/2$ and $\beta = (1 - \alpha)$, respectively, and the signal bandwidth is B.

In order to analyse OP denoted as P_{out}, we should consider following points. In particular, an outage event happens if the given target rate is higher than the system data rate. As a result, OP corresponds with the given target rate R_0 (bps/Hz) which can be computed by

$$OP^k_{out}\left(R_1 < R_0\right) \underset{k\in\{SP,HP\}}{=} \Pr\left(\gamma^k_{eq} < \gamma_0\right), \tag{4.6}$$

where two scenarios including SP and HP are taken into consideration. Therefore, the SNR threshold is defined as $\gamma_0 = 2^{R_0} - 1$.

4.3.1 Separated power mode

Thanks to optimal power constraints, the instantaneous rate can be maximized. Besides that, we can also optimize the optimal transmit powers of S, P^*_S and R, P^*_R by solving the following optimization problem which is given as

$$(P^*_S, P^*_R) = \arg\max\left(R_1\right), \tag{4.7}$$

where $0 \leq (P_S, P_R) \leq 1$. Note that R is under the impact of CSI, and each SNR value corresponds with the received power at R. Hence, the given optimization issue can be given as

$$\begin{cases} \frac{P_S^*|h|^2}{P_R^*|f|^2} = P_R^* \frac{|g|^2}{\sigma^2} \\ P_S^* = 1 \end{cases} , 0 \leq (P_S^*, P_R^*) \leq 1 \tag{4.8}$$

We solve the proposed optimization problem as

$$P_R^* = \min \left\{ P_S^*, \sqrt{\frac{\sigma^2|h|^2}{|g|^2|f|^2}} \right\}. \tag{4.9}$$

Similarly, we compute the average optimal transmit power at R as

$$\bar{P}_R^* = \min \left\{ \bar{P}_S^*, \sqrt{\frac{\sigma^2\Omega_h}{\Omega_g\Omega_f}} \right\}. \tag{4.10}$$

Proposition 4.1: In this mode, the analysis of OP can be done by giving a expression as

$$OP_{out}^{SP}(\gamma_0) = 1 - \frac{P_S\Omega_h}{P_S\Omega_h + P_R\Omega_f\gamma_0} \exp\left(-\frac{\sigma^2\gamma_0}{P_R\Omega_g}\right). \tag{4.11}$$

Proof: See in Appendix A.1

4.3.2 Harvested power assisted relay

In the second phase, R can harvest energy from the received RF signal because it is not equipped with any fixed power supplies (i.e., batteries). Therefore, the transmitted power at R can be computed as [52]

$$P_R = \frac{E_h}{(1-\alpha)\,T} = \rho P_S|h|^2, \tag{4.12}$$

where the energy conversion efficiency is defined by $0 < \eta < 1$. Besides, this coefficient illustrates the impact of EH circuitry, and the harvested energy is written as $E_h = \eta\alpha P_S|h|^2T$, and $\rho = \eta\alpha(1-\alpha)^{-1}$.

Following from (4.2), the high SNR at R can be rewritten as

$$\gamma_R = \frac{P_S|h|^2}{\rho P_S|h|^2|f|^2}. \tag{4.13}$$

As in [53], the end-to-end SNR in HP mode is given by

$$\gamma_{eq}^{HP} = \min\{\gamma_R, \gamma_D\} = \min\left\{\frac{1}{\rho|f|^2}, \rho\frac{P_S}{\sigma^2}|h|^2|g|^2\right\} \tag{4.14}$$

We achieve the optimal transmission rate by giving the following expression

$$\frac{1}{\eta\alpha\,(1-\alpha)\,|f|^2} = \eta\alpha\,(1-\alpha)\,\frac{P_S}{\sigma^2}|h|^2|g|^2. \tag{4.15}$$

The optimal TS coefficient is achieved after some manipulations as follows

$$\alpha_{opt} = \left[\frac{2\eta \frac{P_S}{\sigma^2} \Omega_h \Omega_f}{\left(\sqrt{1 + 4\frac{P_S}{\sigma^2} \frac{\Omega_h \Omega_f}{\Omega_g}} - 1 \right)} + 1 \right]^{-1}. \tag{4.16}$$

Remark 4.1: Thanks to the careful choice of α_{opt} and understanding of its impact on the instantaneous rate, more energy can be harvested at S and R. However, worse throughput performance is seen at D.

Proposition 4.2: The expression for OP in HP mode can be given as

$$OP_{out}^{HP}(\gamma_0) = 1 - L \times \Psi K_1(\Psi), \tag{4.17}$$

where $\Psi = 2\sigma^2 \sqrt{\gamma_0 (\rho P_S \Omega_h \Omega_g)^{-1}}$, $L = 1 - \exp\left(-\frac{1}{\rho \gamma_0 \Omega_f}\right)$.

Proof: See in Appendix A.2.

4.3.3 Asymptotic Outage Probability Analysis:

In this part, upper bound expressions for OP in case of both SP and HP modes are derived. However, SP mode is first studied.

1) SP Case:

Since designing low interference systems are in demand for future wireless networks, several insights into the fundamental impact of SI should be provided. Thus, we upper bound the expression for OP using ideal FD relaying protocol with ($\Omega_f \to 0$) as

$$P_{out}^{SP\_Upper}(\gamma_0) \approx 1 - \exp\left(-\frac{\sigma^2 \gamma_0}{P_R \Omega_g}\right). \tag{4.18}$$

2) HP Case:

On the other hand, when the approximation of $\Psi K_1(\Psi) \approx \Psi \frac{1}{\Psi} = 1$ with respect to ($\Psi \to 0$) in the high-power regime ($P_S \to \infty$) is used, the OP for HP mode can be given as

$$P_{out}^{HP\_Upper}(\gamma_0) \approx \exp\left(-\frac{1}{\rho \gamma_0 \Omega_f}\right). \tag{4.19}$$

4.3.4 Throughput Performance

1) Delay-Limited Transmission:

In this part, the throughput performance in delay-limited transmission mode is first given with the knowledge of the derived OP. As a consequence, the expression for throughput at the fixed rate R_0 is given by

$$\tau_{LM}^{k} \underset{k \in \{SP,HP\}}{=} \beta \left(1 - P_{out}^{k}\right) R_0. \tag{4.20}$$

2) Delay-Tolerant Transmission:

In terms of the delay-tolerant throughput, the ergodic capacity, $C^k, k \in \{SP, HP\}$ at D has to be studied first. It is noted that less transmission rate is needed by S than or equal to the values of ergodic capacity. Therefore, neither S nor R has knowledge of CSI to obtain ergodic capacity. It is noted that the fixed transmission rate at S corresponds with the ergodic capacity. Hence, the throughput in delay-tolerant transmission mode at D, τ_{TO}^k is given by

$$\tau_{TO}^k \underset{k\in\{SP,HP\}}{=} \beta \mathrm{C}^k, \tag{4.21}$$

where $C^k = E_{|h|^2,|g|^2,|f|^2} \log_2\left(1+\gamma_{eq}^k\right)$ for both case in (4.4). It is noted that ergodic capacity at (D) can be computed as

$$C^k \underset{k\in\{SP,HP\}}{=} \frac{1}{\ln 2} \int_{x=0}^{\infty} \frac{1-P_{out}^k(x)}{1+x} dx. \tag{4.22}$$

4.4 Numerical Results

In this section, to prove the robustness of the analytical expressions derived, we provide numerical results. The simulation results follow some parameters specified in Table 4.1. In these simulations, we present $\bar{\gamma}_{SR} = \Omega_h$, $\bar{\gamma}_{RD} = \Omega_g$ and $\bar{\gamma}_{LI} = \Omega_f$.

Parameters	**Values**
Transmission fixed rate, R_0	2 (bps/Hz)
Transmit power at S, P_S	1 (Joules/s)
EH efficiency, η	0.5
Bandwidth, B	1
Noise variances for all nodes, σ^2	1/2

Tab. 4.1: Main Simulation Parameters (WPT Constraint Policies)

As illustrated in Fig. 4.2 and Fig. 4.3, the throughput is presented as a function of SNRs in the communication between S and R with $\bar{\gamma}_{SR} = \bar{\gamma}_{RD}$. It is evident that, we set $\alpha = 0.5$ for SP mode while the optimal TS ratio, α_{opt} is is used for HP mode.

In Fig. 4.4 and Fig. 4.5, we present the optimal throughput performance in both delay-limited and delay-tolerant transmission modes obtained with the optimal TS ratio in HP mode.

Regarding the considered protocol, throughput increase as α climbs from 0 to the optimal value, $\alpha = 0.1$, resulting in the best performance than SP mode when $\alpha = 0.5$. When values of α are smaller than the optimal values of α_{opt}, EH consumes more time. It is evident that SI degrades the throughout performance at any time. However, in both transmission modes, the appropriate choice of α for HP can lead to better throughput performance regardless of SI factors.

In addition, the delay-limited throughput of HP mode in Fig. 4.6 increases to the peak which later drops slightly. It is clear that the highest throughput can be achieved

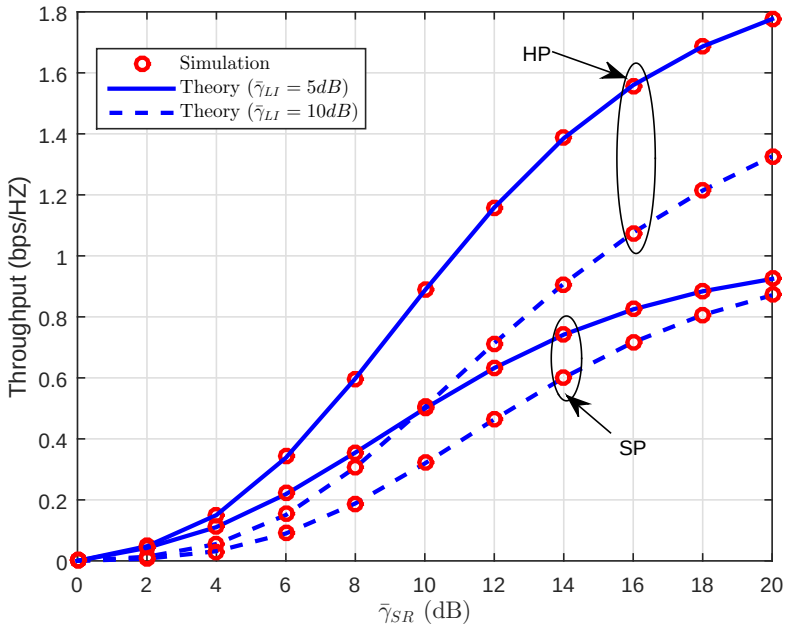

Fig. 4.2: Theory and simulation results of throughput vs. $\bar{\gamma}_{SR}$ under different impacts of SI $\bar{\gamma}_{LI} = 5dB$ or $\bar{\gamma}_{LI} = 10dB$ and α_{opt} , (Delay-limited mode).

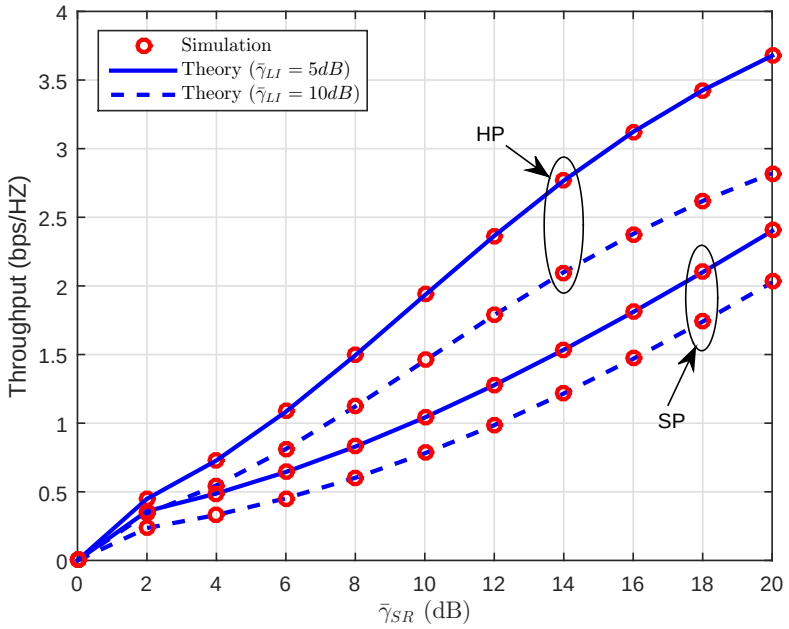

Fig. 4.3: Theory and simulation results of throughput vs. $\bar{\gamma}_{SR}$ under different impacts of SI $\bar{\gamma}_{LI} = 5dB$ or $\bar{\gamma}_{LI} = 10dB$ and α_{opt} , (Delay-tolerant mode).

regardless of the increase in the transmit power at S, and the tight upper bound is close to the simulation results. The throughput performance varies significantly with respect to

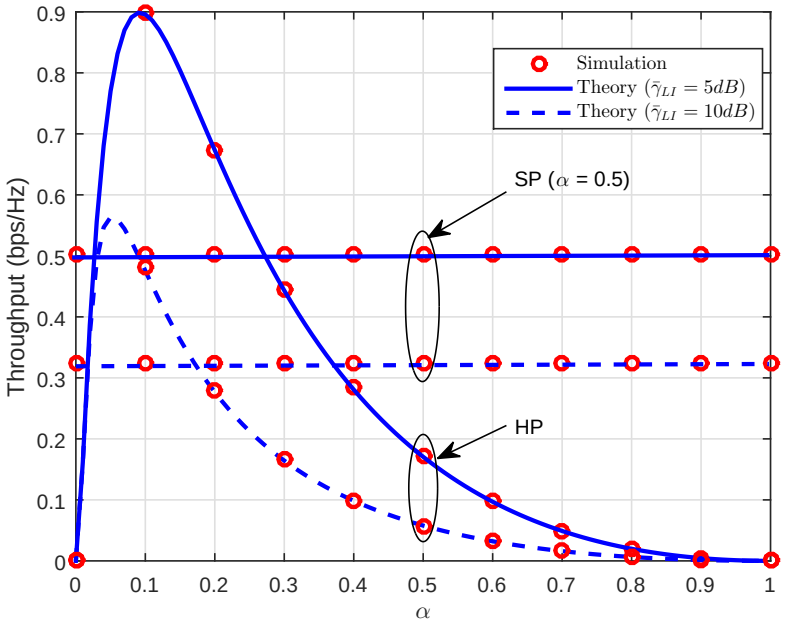

Fig. 4.4: Throughput performance versus time switching coefficients with $\bar{\gamma}_{SR} = \bar{\gamma}_{RD} = 10dB$ in the delay-limited mode.

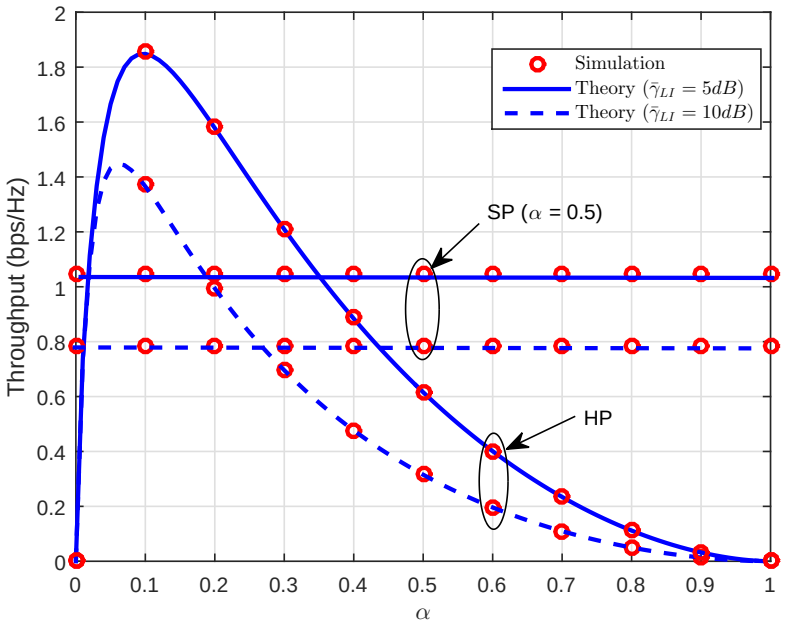

Fig. 4.5: Throughput performance versus TS coefficients with $\bar{\gamma}_{SR} = \bar{\gamma}_{RD} = 10dB$ in the delay-tolerant mode.

different values of the SNR threshold. As a consequence, R with EH circuitry can satisfy proper applications for wireless communications with an acceptable SNR level.

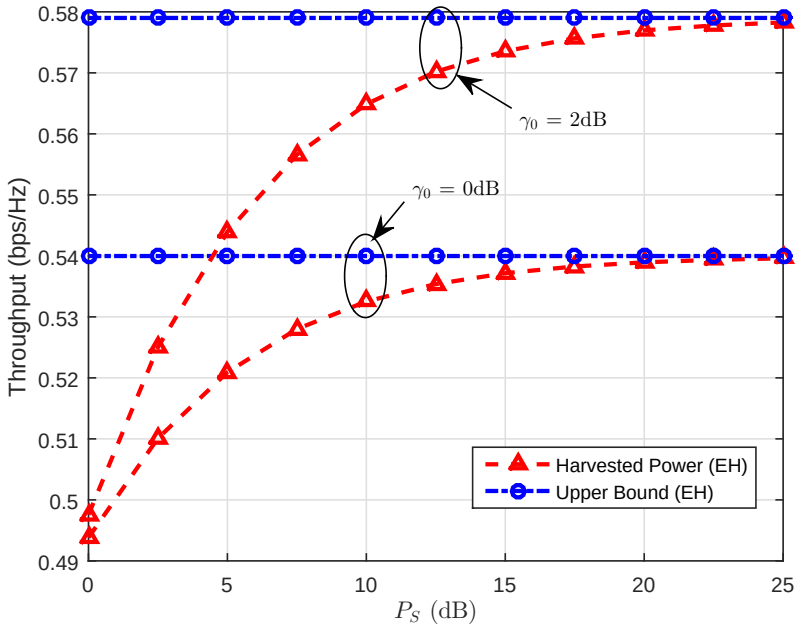

Fig. 4.6: The asymptotic throughput performance with different transmit power in the delay-limited mode $\bar{\gamma}_{SR} = \bar{\gamma}_{RD} = 10dB$ and $\bar{\gamma}_{LI} = 5dB$.

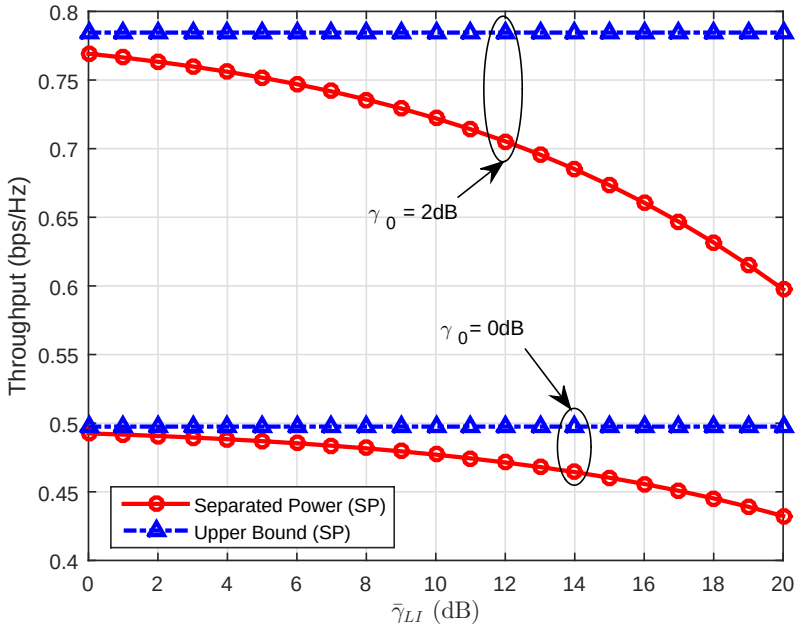

Fig. 4.7: The asymptotic throughput performance under impact of self-interference with $\bar{\gamma}_{SR} = \bar{\gamma}_{RD} = 20dB$.

In Fig. 4.7, the throughput performance under the impact of SI is illustrated. We observe that the throughput declines as SI rises while the upper bound of SP is appro-

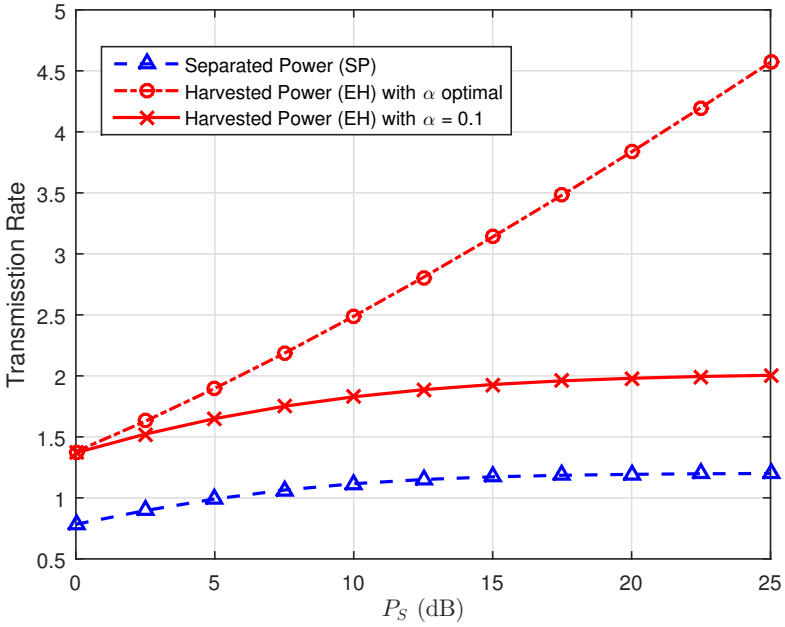

Fig. 4.8: The transmission rate vs P_S other parameters: $\bar{\gamma}_{LI} = 5dB$, $\bar{\gamma}_{SR} = \bar{\gamma}_{RD} = 20dB$, $\alpha = 0.1$ and α_{opt}.

ximately 0. Due to both pre-defined SNR thresholds, i.e., $0dB$ and $2dB$, the throughput performance is degraded.

As shown in Fig. 4.8, the transmission rate in terms of the optimal TS ratios is presented. More energy cannot be harvested to assist the communication process in SP mode, so the transmission rate is observed to remain stable. However, HP enjoys higher transmission rate due to its EH capacity and the the installation of energy storage at R.

4.5 Summary

In this chapter, wireless power supply policies, including SP and HP in FD RNs were proposed. In particular, thanks to the deploying of TSR protocol and the achievement of optimal TS ratio, R can function without using completely the energy like SP. For system performance analysis, we provided the exact expressions for OP and throughput in delay-limited and delay-tolerant transmission modes. Besides that, an acceptable outage performance between HP and SP mode was achieved, in which our simulation results matched well with the exact expressions for OP. In addition, we also provided insights into the impact of several parameters, i.e., SI, TS ratio, and the transmit power on the system throughput.

5 EVALUATING THE IMPACT OF CSI USING HTPSR PROTOCOL

In this chapter, the proposed HTPSR protocol is exploited, and the comparisons between the performance of AF and DF under the impact of imperfect CSI are provided. Besides that, the instantaneous rate and the achievable BER are determined, and closed-form expressions for throughput in delay-tolerant and delay-limited transmission mode are derived. In addition, the optimization of TS and PS ratios is achieved to enhance the overall system performance. With the simulation results, we are able to provide better insights into the differences between AF and DF and the impact of TS and PS ratios on the performance of BER, OP, and throughput. It is noted that DF outperforms AF, and the optimization of TS and PS ratios helps obtain the optimal instantaneous rate [NHS02].

5.1 Motivation

There are a number of studies on perfect and imperfect CSI conducted in [54, 55, 56, 57, 58, 59]. In particular, a MISO system was studied in [54] while the authors in [55] considered a transmit power allocation issue for a hybrid EH single relay network with channel and energy state uncertainties to maximize system throughput over a limited number of transmission intervals, in which sub-optimal online, optimal online and optimal offline allocation schemes were put forward. In [56], two-way FD relaying with a residual LI was studied. In [57], under the impact of imperfect CSI, the performance of a CRN was investigated. Furthermore, fault-tolerant schemes were analyzed in the presence of imperfect CSI [58]. The authors in [59] addressed a joint optimization problem over RS, subcarrier assignment, and PS ratio under the impact of imperfect CSI.

In order to conduct the optimization of throughput performance in cooperative RNs, there are a number of works carried out [60, 61, 62, 63, 64]. In particular, in [62], two-hop MIMO AF RNs with SWIPT at the multi-antenna relay were studied. Meanwhile, the impact of imperfect CSI in AF FD RN was investigated in [64], in which the optimal TS ratio was achieved numerically.

Being motivated from these works, we find that the optimal TS and PS ratios for the instantaneous rate have not been addressed carefully, so we decided to propose an optimal policy to enhance EE. Thanks to the proposed HTPSR protocol, we are able to compare the performance between AF and DF relaying protocols in case of perfect and imperfect CSI [NHS03], [NHS04].

This chapter is organized as follows: The system model is presented in Section 2 while Section 3 provides expressions for throughput, BER and optimization problems for TS and PS ratios in both AF and DF relaying schemes. We provide the numerical results in Section 4. Section 5 gives a brief conclusion for the chapter.

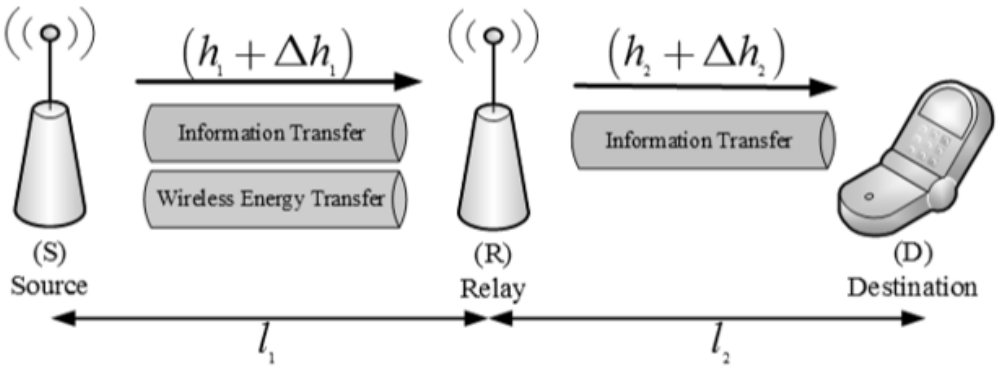

Fig. 5.1: System model

5.2 System Model

As illustrated in Fig. 5.1, a RN is considered, where S transmits data to D with the help of R. It is noted that $\widetilde{h}_1$ and $\widetilde{h}_2$ are depicted as the first hop between S and D, and the second hop between R and D, respectively. The D receives information transmitted from S in the block time, T. In particular, the communication between S and R in the first hop during αT involves EH and IT while the second time slot is responsible for IT during $(1-\alpha)T$. In terms of HTPSR protocol, α and β respectively denote the TS and PS ratios, where $\alpha \in (0,1)$, $\beta \in (0,1)$. Furthermore, R utilizes the entire received energy via EH and IT. Particularly, βP_S is used to transmit the amount of harvested energy to R while IT from S to R accounts for $(1-\beta)P_S$, where P_S is the source transmit power.

Assuming that all channels affected by Rayleigh fading, and they are also independent and identically distributed (i.i.d) from one block to another. Besides, the fading channel denoted as zero mean circularly symmetric complex Gaussian random variable, is distributed by $\widetilde{h}_1 \sim CN\left(0, \Omega_{\widetilde{h}_1}\right)$, $\widetilde{h}_2 \sim CN\left(0, \Omega_{\widetilde{h}_2}\right)$. It is noted that the distances between $S \to R$ and $R \to D$ are l_1 and l_2, respectively.

In the first hop, the fading channel, $\widetilde{h}_1$ can be expressed as in [55]

$$\widetilde{h}_1 = h_1 + \Delta h_1, \tag{5.1}$$

similarly, the fading channel, $\widetilde{h}_2$ in the second hop can be expressed as

$$\widetilde{h}_2 = h_2 + \Delta h_2, \tag{5.2}$$

where h_1, h_2 and Δh_1, Δh_2 are channel errors (CEs) and channel estimation errors (CEEs) , respectively. Meanwhile, Circularly Symmetric Complex Gaussian (CSCG) RVs are denoted by $h_1 \sim CN\left(0, \Omega_{h_1}\right)$, $h_2 \sim CN\left(0, \Omega_{h_2}\right)$, and $\Delta h_1 \sim CN\left(0, \Omega_{\Delta h_1}\right)$, $\Delta h_2 \sim CN\left(0, \Omega_{\Delta h_2}\right)$, respectively with $\Omega_{\Delta h_1} = \Omega_{\widetilde{h}_1} - \Omega_{h_1}$, and $\Omega_{\Delta h_2} = \Omega_{\widetilde{h}_2} - \Omega_{h_2}$.

In the proposed HTPSR protocol, the harvested energy depends on TS and PS ratios are expressed as

$$E_{\widetilde{h}_1}^{HTPSR} = \eta P_S \left(|h_1|^2 + \Omega_{\Delta h_1}\right) l_1^{-m} \alpha \beta T, \tag{5.3}$$

where the energy conversion efficiency is denoted by η which relies on the rectification process and the EH circuitry, $\eta \in (0, 1)$, and m stands for the path loss exponent.

At R, we compute the received power, P_R in the communication between R and D during $(1-\alpha)T$ as

$$\begin{aligned} P_R &= \frac{E_{\widetilde{h}_1}^{HTPSR}}{(1-\alpha)T} = \frac{\eta\alpha\beta P_S\left(|h_1|^2+\Omega_{\Delta h_1}\right) l_1^{-m}}{(1-\alpha)} \\ &= \varphi P_S \left(|h_1|^2 + \Omega_{\Delta h_1}\right) l_1^{-m} \end{aligned}, \tag{5.4}$$

where $\varphi = \eta\alpha\beta(1-\alpha)^{-1}$.

In AF and DF schemes, we calculate the received signal at R in the first hop as

$$y_R(k) = \sqrt{l_1^{-m}\,(1-\beta)}\,(h_1 + \Delta h_1)\, x_S(k) + n_R, \tag{5.5}$$

where we denote the data symbol for S as $x_S(k)$ at the time slot defined as k, $(k = 1, 2, ..., N)$, and it must satisfy $\mathbb{E}\left\{|x_S(k)|^2\right\} = P_S$, with AWGN denoted by n_R with zero-mean and noise variance, N_0.

In terms of AF scheme, the amplification factor, $\mathcal{G}$ processing the received signal is computed as [65]

$$\begin{aligned} \mathcal{G}^2 &= 1/\left(l_1{}^{-m}\,(1-\beta)\,P_S\left(|h_1|^2 + \Omega_{\Delta h_1}\right) + N_0\right) \\ &\approx 1/\left(l_1{}^{-m}\,(1-\beta)\,P_S\left(|h_1|^2 + \Omega_{\Delta h_1}\right)\right) \end{aligned}. \tag{5.6}$$

Therefore, the received signal at R for both AF and DF can be respectively written as

$$x_R\,(k) = \mathcal{G} y_R\,(k)\,, (\text{for AF relaying}), \tag{5.7}$$

and

$$x_R\,(k) = \frac{1}{P_S} x_S\,(k)\,, (\text{for DF relaying}). \tag{5.8}$$

Following that, the received signal at D can be given as

$$\gamma_D(k) = \sqrt{l_2^{-m} P_R}(h_2 + \Delta h_2) x_R(k) + n_D, \tag{5.9}$$

where the AWGN at D is n_D with zero mean and variance, N_0.

5.3 Performance Analysis

To give better insights into the system performance, we are going to study the performance of instantaneous rate and throughput for HD in the presence of imperfect CSI. Besides, both AF and DF are taken for comparisons in terms of perfect and imperfect CSI.

5.3.1 The calculation of SNR

Now, we are going to give expressions for the instantaneous rate for AF and DF relay schemes are given. First, let us consider the AF scheme.

A. In case AF relaying

Substituting the values of (5.5) and (5.7) into (5.9), $y_D(k)$ can be computed without the instant index time k as

$$\begin{aligned} y_D(k) = &\sqrt{(1-\beta)\,P_R l_2^{-m}}\mathcal{G}x_S\,(k)\,h_1h_2+\sqrt{(1-\beta)\,P_R l_2^{-m}}\mathcal{G}\,(h_2+\Delta h_2)\,n_R+n_D \\ &+\sqrt{(1-\beta)\,P_R l_2^{-m}}\mathcal{G}x_S\,(k)\,(h_2\Delta h_1+h_1\Delta h_2+\Delta h_1\Delta h_2). \end{aligned} \tag{5.10}$$

Based on (5.10), the end-to-end SNR at D can be computed as

$$\gamma_{AF} = \frac{|h_1|^2|h_2|^2}{|h_2|^2\mathcal{W}_1+|h_1|^2\mathcal{W}_2+\mathcal{W}_3}, \tag{5.11}$$

where $\mathcal{W}_1 = \Omega_{\Delta h_1} + \frac{N_0}{(1-\beta)l_1^{-m}P_S}$, $\mathcal{W}_2 = \Omega_{\Delta h_2}$, and $\mathcal{W}_3 = \Omega_{\Delta h_2}\Omega_{\Delta h_1} + \frac{\Omega_{\Delta h_2}N_0}{(1-\beta)l_1^{-m}P_S} + \frac{l_1^m l_2^m N_0}{\varphi P_S}$.

B. In case DF relaying

From (5.5) at R and based on (5.10) at D. The received SNRs at R and D in terms of DF scheme are respectively calculated as

$$\gamma_R = \frac{(1-\beta)\,P_S|h_1|^2}{(1-\beta)\,P_S\Omega_{\Delta h_1}+l_1^m N_0}, \tag{5.12a}$$

$$\gamma_D = \frac{|h_1|^2|h_2|^2}{\left(|h_2|^2\mathcal{Z}_1+|h_1|^2\mathcal{Z}_2+\mathcal{Z}_3\right)}, \tag{5.12b}$$

where $\mathcal{Z}_1 = \Omega_{\Delta h_1}$, $\mathcal{Z}_2 = \Omega_{\Delta h_2}$, and $\mathcal{Z}_3 = \Omega_{\Delta h_1}\Omega_{\Delta h_2} + \frac{l_1^m l_2^m}{\varphi P_S}N_0$.

Therefore, the end-to-end SNR, γ_{DF} can be given as

$$\gamma_{DF} = \min\left(\gamma_R, \gamma_D\right), \tag{5.13}$$

where γ_R and γ_D follow from (5.12a) and (5.12b).

Accordingly, the data rate achieved for AF and DF schemes can be given by

$$R_{i\in\{\mathrm{AF,DF}\}} = \log_2\left(1+\gamma_i\right). \tag{5.14}$$

Remark 5.1: In order to select the ideal values of TS and PS ratios, α and β for achieving the instantaneous rate. It is clear that the integration and the Bessel functions are helpful in the analytical expressions of ergodic capacity to obtain the closed-form expressions for the optimal TS and PS ratios. Nevertheless, we can solve this optimization issue off-line by numerically studying the optimal values, e.g., P_S, noise terms, and CEEs. Therefore, we are going to present this optimization problem in the following section.

5.3.2 Delay-Limited throughput

A. In case of AF relaying

In the delay-limited transmission mode, the throughput has a close relationship with OP, OP with a fixed source transmission rate, R_0 (bps/Hz), and the threshold value of SNR at D is $\gamma_0 = 2^{R_0} - 1$ for information decoding. In that way, OP is given by

$$\mathrm{OP}_{AF} = \Pr\left(\gamma_{\mathrm{AF}} < \gamma_0\right), \tag{5.15}$$

where the probability function is denoted by Pr(.).

It is worth noting that we are going to determine the closed-form expression for $\mathrm{OP}_{\mathrm{AF}}$ in the following Proposition 5.1. Let us first use the following theorem 5.1 to clarify the Proposition 5.1.

Theorem 5.1. We define the general SNR as

$$Y = \frac{X_1 X_2}{a_1 X_2 + a_2 X_1 + a_3}, \tag{5.16}$$

where $a_i, i \in \{1..3\}$ is constants, X_1 and X_2 are RVs with means Ω_{X_1} and Ω_{X_2}, respectively. Thus, the CDF of the exponential RVs is derived as

$$F_Y(x) \approx 1 - (\mathcal{A})^{-1}\mathcal{B} \times K_1(\mathcal{B}), \tag{5.17}$$

where $\mathcal{A} = \exp\left(x\left(\frac{a_1}{\Omega_{X_2}} + \frac{a_2}{\Omega_{X_1}}\right)\right)$, $\mathcal{B} = 2\sqrt{\frac{x(a_3 + x a_1 a_2)}{\Omega_{X_1}\Omega_{X_2}}}$.

Proof:

It is easy to derive the PDF of RV, X_1 for the Rayleigh fading channel as

$$f_{X_1}(x) \triangleq \frac{1}{\Omega_{X_1}} \exp\left(-\frac{x}{\Omega_{X_1}}\right). \tag{5.18}$$

.

Next, the CDF of Y, $F_Y(x) = \Pr(\mathrm{Y} < \mathrm{x})$ is defined as

$$F_Y(x) = \int_0^{z = x.a_2} f_{|X_1|}(z)\, dz + \int_{z = x.a_2}^{\infty} f_{|X_1|}(z) \Pr\left(1 - \exp\left(-\frac{x(a_2 z + a_3)}{(a_3 - x a_1)\Omega_{\mathrm{X_2}}}\right)\right) dz. \tag{5.19}$$

Substituting the obtained PDF of X_1 into (5.19). Thus, it can be rewritten as

$$F_Y(x) \approx 1 - \tfrac{1}{\Omega_{X_1}} \int_{y = x.a_2}^{\infty} \exp\left(-\left(\frac{y}{\Omega_{X_1}} + \frac{x(a_3 + x a_2)}{(y - x a_1)\Omega_{X_2}}\right)\right) dy, \tag{5.20}$$

where we eventually derive the result for (5.17) after some manipulations based on the expression, $\int_0^{\infty} e^{-\frac{\beta}{4x} - yx} dx = \sqrt{\frac{\beta}{y}} K_1\left(\sqrt{\beta y}\right)$ as in ([66], 3.324.1).

This ends the proof for theorem 5.1.

Proposition 5.1. Thanks to the use of theorem 5.1, the OP for AF scheme using HTPSR is computed as

$$\mathrm{OP}_{\mathrm{AF}} \approx 1 - (\mathcal{A}_{\mathrm{AF}})^{-1}\mathcal{B}_{\mathrm{AF}} \times \mathrm{K}_1\left(\mathcal{B}_{\mathrm{AF}}\right), \tag{5.21}$$

where $\mathcal{A}_{AF} = \exp\left(\gamma_0\left(\frac{\mathcal{W}_1}{\Omega_{h_2}} + \frac{\mathcal{W}_2}{\Omega_{h_1}}\right)\right)$, and $\mathcal{B}_{AF} = 2\sqrt{\gamma_0(\mathcal{W}_3 + \gamma_0\mathcal{W}_1\mathcal{W}_2)(\Omega_{h_1}\Omega_{h_2})^{-1}}$. It is noted that the channel gains of the exponential RVs, $|h_1|^2$ and $|h_2|^2$ are characterized as Ω_{h_1} and Ω_{h_2}, respectively. Now, we are going to investigate OP in DF scheme.

B. In case of DF relaying

Proposition 5.2. The system OP for DF is given by

$$\mathrm{OP}_{\mathrm{DF}}(\gamma_0) \approx 1 - \exp\left(-\frac{\psi\gamma_0}{\Omega_{\mathrm{h_1}}}\right) \times (\mathcal{A}_{DF})^{-1}\mathcal{B}_{DF} \times K_1\left(\mathcal{B}_{DF}\right), \tag{5.22}$$

where $\psi = \Omega_{\Delta h_1} + \frac{l_1^m N_0}{(1-\beta)P_S}$, $\mathcal{A}_{DF} = \exp\left(\gamma_0\left(\frac{\mathcal{Z}_1}{\Omega_{h_2}} + \frac{\mathcal{Z}_2}{\Omega_{h_1}}\right)\right)$, and $\mathcal{B}_{DF} = 2\sqrt{\frac{\gamma_0\left(\Omega_{h_1}\mathcal{Z}_3 + \gamma_0\mathcal{Z}_1\mathcal{Z}_2\right)}{\Omega_{h_1}\Omega_{h_2}}}$.

Proof:

Similarly, according to the expression of OP at D in (5.12b) for DF scheme. Using *Theorem* 5.1 in (5.17), the CDF at D can be computed as

$$F_{\gamma_D}(\gamma_0) \approx 1 - (\mathcal{A}_{DF})^{-1}\mathcal{B}_{DF} \times K_1\left(\mathcal{B}_{DF}\right), \tag{5.23}$$

where $\gamma_0 > 0$, $\mathcal{A}_{DF}$, and $\mathcal{B}_{DF}$ in (5.22).

The imperfect CSI for DF scheme, the OP at R in (5.12a) is calculated as

$$F_{\gamma_R}(\gamma_0) = 1 - \exp\left(-\frac{\psi\gamma_0}{\Omega_{h_1}}\right), \tag{5.24}$$

where the PDF of γ_R is presented as $f_{\gamma_R}(\gamma_0) = \frac{\psi}{\Omega_{h_1}}\exp\left(-\frac{\psi\gamma_0}{\Omega_{h_1}}\right)$, and ψ can be seen in (5.22).

Eventually, we have $\gamma_{DF} = \min\{\gamma_R, \gamma_D\}$, and the CDF of γ_{DF} can be derived as in Proposition 5.2.

This ends the proof for Proposition 5.2.

C. Throughput analysis

Regarding delay-limited throughput, τ_{dl} is defined as the effective communication time, $(1-\alpha)T$ leading to the given fixed transmission rate, R_0. Thus, the general expression for throughput for AF and DF schemes is defined after achieving OP as

$$\tau_i^{dl} \underset{i\in\{AF,DF\}}{=} R_0(1 - OP_i)(1-\alpha). \tag{5.25}$$

5.3.3 Delay-Tolerant transmission

In principle, in the delay-tolerant transmission mode, the code length is large compared to the block time so the code sees all the possible realizations of the channel during a code-word transmission and average channel conditions. Hence, it is possible to achieve the ergodic capacity by transmitting at a rate equal to the ergodic capacity [64]. Using the received SNR, γ_{AF} and γ_{DF} defined in (5.11) and (5.13), the expressions for ergodic capacity for AF and DF schemes are going to be derived in the following parts.

A. In case of AF relaying

Let us start with the ergodic capacity at D, C_{AF} (bps/Hz) which can be presented as

$$C_{AF} = \mathrm{E}_{|h_1|^2,|h_2|^2}\left\{\log_2\left(1+\gamma_{AF}\right)\right\}. \tag{5.26}$$

Proposition 5.3. Thus, the analytical expression for ergodic capacity is derived by

$$\begin{aligned} C_{AF} &= \tfrac{1}{\ln 2}\int_{x=0}^{\infty}\frac{1-F\left(x\right)}{\left(1+x\right)}dx \\ &\approx \tfrac{1}{\ln 2}\int_{x=0}^{\infty}\frac{\mathcal{B}_{AF}(x)\times K_1\left(\mathcal{B}_{AF}(x)\right)}{\left(1+x\right)\mathcal{A}_{AF}(x)}dx, \end{aligned} \tag{5.27}$$

where $\mathcal{A}_{AF}(x) = \exp\left(x\left(\frac{\mathcal{W}_1}{\Omega_{h_2}}+\frac{\mathcal{W}_2}{\Omega_{h_1}}\right)\right)$, $\mathcal{B}_{AF}(x) = 2\sqrt{\frac{x(\mathcal{W}_3+x\mathcal{W}_1\mathcal{W}_2)}{\Omega_{h_1}\Omega_{h_2}}}$.
Proof: Starting from utilizing the result in (5.21), the desired result can be obtained after some algebraic manipulations.

B. In case of DF relaying

Proposition 5.4. Likewise, the ergodic capacity for DF mode is depicted by

$$C_{DF} \approx \frac{1}{\ln 2}\int_{x=0}^{\infty}\frac{\exp\left(-\frac{\psi\gamma_0}{\Omega_{\mathrm{h}_1}}\right)\mathcal{B}_{DF}(x)\times K_1\left(\mathcal{B}_{DF}(x)\right)}{\left(1+x\right)\mathcal{A}_{DF}(x)}dx, \tag{5.28}$$

where $\mathcal{A}_{DF}(x) = \exp\left(x\left(\frac{\mathcal{Z}_1}{\Omega_{h_2}}+\frac{\mathcal{Z}_2}{\Omega_{h_1}}\right)\right)$, and $\mathcal{B}_{DF}(x) = 2\sqrt{\frac{x\left(\Omega_{h_1}\mathcal{Z}_3+x\mathcal{Z}_1\mathcal{Z}_2\right)}{\Omega_{h_1}\Omega_{h_2}}}$.

Proof: The proof is similar to that of Proposition 5.3 and is omitted.

C. Throughput analysis

Thanks to the expression of ergodic capacity, C_i (bps/Hz), the throughput at D is written as

$$\tau_i^{dt} \underset{i\in\{AF,DF\}}{=} \frac{(1-\alpha)T}{T}C_i = (1-\alpha)C_i. \tag{5.29}$$

5.3.4 BER consideration

In this section, expressions for the BER at D are going to provided. However, we first evaluate OP obtained in [67]. Therefore, we have

$$BER = E\left[aQ\left(\sqrt{2b\gamma}\right)\right], \tag{5.30}$$

where the Gaussian Q-Function is denoted as $Q(.)$ defined as $Q(x) = \frac{1}{\sqrt{2\pi}}\int_{x}^{\infty} e^{-\frac{t^2}{2}}dt$, and the modulation formats are defined for BPSK and QPSK as $(a,b) = (1,2)$ and $(a,b) = (1,1)$, respectively. As a consequence, the distribution function of γ is considered before the BER performance can be evaluated. Following that, we can rewrite the expression for BER obtained in (5.30) regarding OP at S by using integration as

$$BER_{i\in\{AF,DF\}} = \frac{a\sqrt{b}}{2\sqrt{\pi}}\int_{0}^{\infty}\frac{e^{-b\gamma}}{\sqrt{\gamma}}F_{\gamma_i}(\gamma)d\gamma, \tag{5.31}$$

where $F_{\gamma_i}(\gamma) = \mathrm{OP_i}(\gamma)$ for AF or DF protocol.

5.3.5 Optimization Problems

In this section, we are going to solve the optimization problem of both TS and PS ratios for AF and DF relaying protocols. Now, AF relaying protocol is considered first.

A. In case of AF relaying

Based on (5.14), the OP is given as

$$\max_{\substack{\alpha,\beta \\ \text{subject to} \quad \alpha,\beta\in(0,1)}} R_{i\in\{\mathrm{AF,DF}\}}\ . \tag{5.32}$$

In fact, the logarithmic function is a monotonically increasing function. Nevertheless, the aforementioned expressions are complex to solve, giving a closed-from expression is difficult, and the optimal instantaneous rate is a biconvex function of α and β. Therefore, the complex function above can be numerically evaluated by using the building function "NSlove"of the Mathematica software. We are going to present them in simulations.

B. In case DF relaying

Following from (5.12a) and (5.12b), we can rewrite the received SNRs as

$$\gamma_R = \frac{1}{\omega_1 + \frac{\omega_2}{(1-\beta)}}, \tag{5.33a}$$

$$\gamma_D = \frac{1}{\omega_3 + \frac{(1-\alpha)}{\alpha\beta}\omega_4}, \tag{5.33b}$$

where $\omega_1 = \frac{\Omega_{\Delta h_1}}{|h_1|^2}$, $\omega_2 = \frac{l_1^m N_0}{P_S |h_1|^2}$, $\omega_4 = \frac{l_1^m l_2^m N_0}{2\eta P_S |h_1|^2 |h_2|^2}$ and $\omega_3 = \frac{\Omega_{\Delta h_1}}{|h_1|^2} + \frac{\Omega_{\Delta h_2}}{|h_2|^2} + \frac{\Omega_{\Delta h_1}\Omega_{\Delta h_2}}{|h_1|^2 |h_2|^2}$.

The optimal α_{opt}, β_{opt} can be obtained by solving the following optimization

$$\max R_{DF} = \arg\max \gamma_{DF}(\alpha, \beta), \tag{5.34}$$

where it is subject to $0 < \alpha < 1$, $0 < \beta < 1$.

We can achieve the optimal values of the above issue analytically when $\gamma_R = \gamma_D$, so we have the following expression

$$\alpha \left[\left(\omega_1 + \frac{\omega_2}{(1-\beta)} - \omega_3 \right) \beta + \omega_4 \right] = \omega_4. \tag{5.35}$$

Now, we set the fixed value for β, so α_{opt} can be obtained as

$$\alpha_{opt} = \frac{\omega_4}{\left[\left(\omega_1 + \frac{\omega_2}{(1-\beta)} - \omega_3 \right) \beta + \omega_4 \right]}. \tag{5.36}$$

Otherwise, when α is fixed , β_{opt} is written as

$$\beta_{opt} = \frac{-b + \sqrt{b^2 - 4ac}}{2a}, \tag{5.37}$$

where $b = (\alpha\omega_1 + \alpha\omega_2 - \alpha\omega_3 + (1-\alpha)\omega_4)$, $c = (\alpha - 1)\omega_4$, and $a = \alpha(\omega_3 - \omega_1)$.

To this end, we finally achieved the the optimal values for TS and PS.

5.4 Numerical Results

In this part, we are going to provide numerical results on the throughput performance, the OP and BER under the impact of imperfect CSI. For simplicity, the simulation results follow some parameters specified in Table 5.1.

Parameters	**Values**
Transmission fixed rate, R_0	3 (bps/Hz)
Transmit power at S, P_S	1 (Joules/s)
EH efficiency, η	1
Noise variances for all nodes, $\Omega_{\Delta h_1} = \Omega_{\Delta h_2}$	0.03
PS ratios, β	0.3
TS ratios, α	0.3
Path loss exponent, m	2.7

Tab. 5.1: Main Simulation Parameters (Impact of CSI)

In Fig. 5.2 and Fig. 5.3, we present the OP in the presence of perfect CSI and imperfect CSI. It can be observed that the OP of AF is outperforms that of DF. In particular, when α and β vary from 0 to 0.9, the OP of AF and DF enjoy considerable declines, especially when α is around 0.9. Different from TS, Fig. 5.3 shows that the OP drops

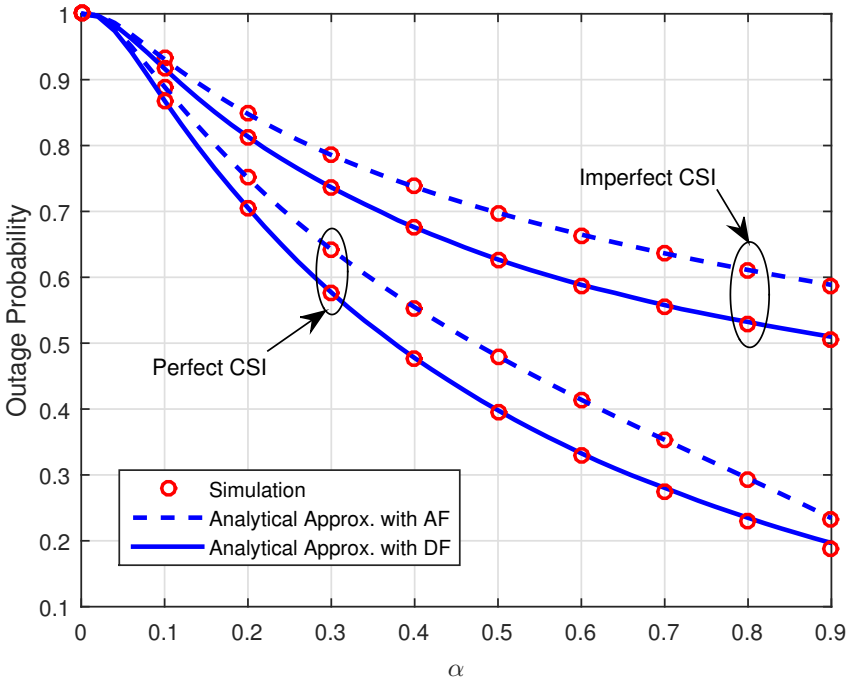

Fig. 5.2: OP of the perfect and imperfect CSI for AF and DF RNs for vs. α.

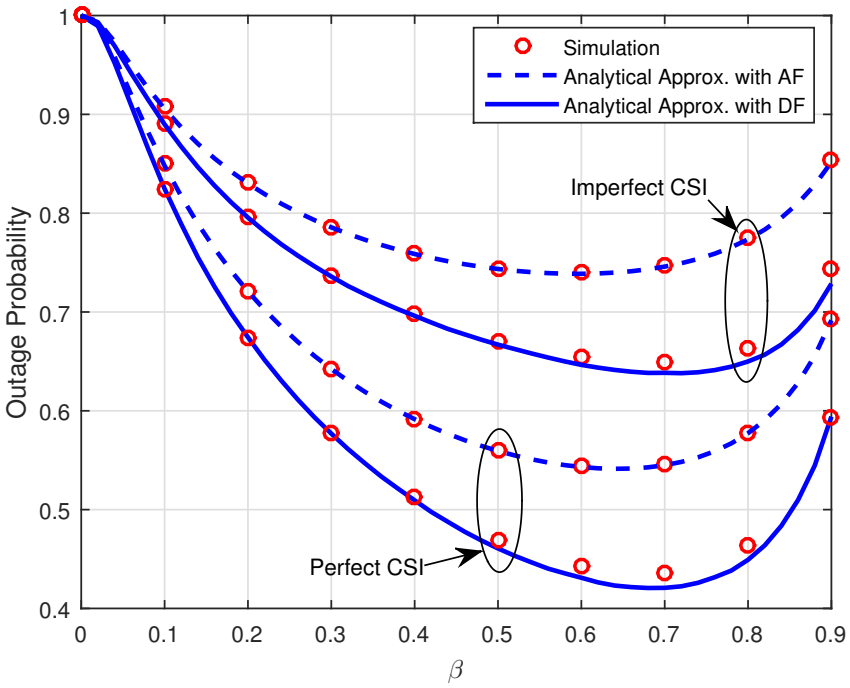

Fig. 5.3: OP of the perfect and imperfect CSI for AF and DF RNs for vs. β.

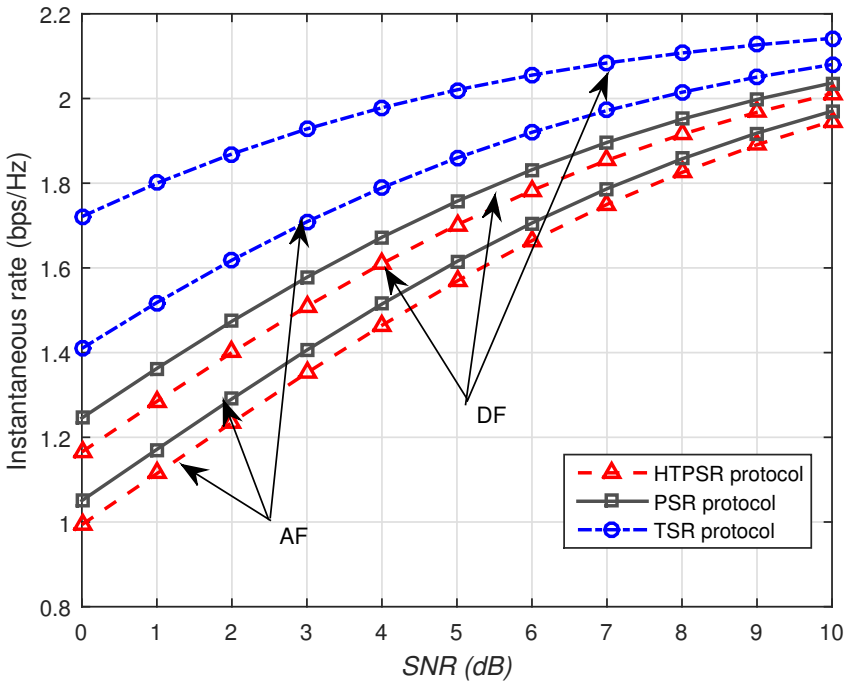

Fig. 5.4: The instantaneous rate of perfect and imperfect CSI for AF and DF RNs for different values of SNR (dB).

as β fluctuates between 0 and 0.7, since the more energy harvested at R is, the better outage performance becomes. Following that, the increase of PS from 0.7 to 0.9 leads to worse outage performance due to less power for information processing. The performance gap between imperfect CSI and perfect CSI is noticeable at approximately $\alpha = 0.9$ and $\beta = 0.7$ due to the impact of CEEs.

Fig. 5.4 presents the instantaneous rate of imperfect CSI and perfect CSI for AF and DF relaying networks for different values of SNR (dB). In this experiment, we only consider the imperfect CSI and compare the three energy harvesting protocols, namely PSR, TSR [13] with HTPSR. It can be observed that TSR is the best performance in two cases of protocols. In fact, it is worth noting that this performance depends on instantaneous values of the channel, since the transmit power from source, SNR intends to supply the energy harvesting circuit at the relay node in TSR protocol while only small fraction of such power is used for the considered protocol HTPSR. In addition, when the values of SNR increase, the system throughput in the presence of imperfect CSI of the three schemes also rise due to the contribution of SNR.

In Fig. 5.5 and Fig. 5.6, the BER of AF and DF RNs is presented. In particular, when P_S rises from 0 to 30, QPSK is better than BPSK in both AF and DF. Besides, $\sigma^2_{\Delta h_2}$ increase as the BER performance in the presence of imperfect CSI falls. Both AF and DF relaying protocols undergo the same tendency.

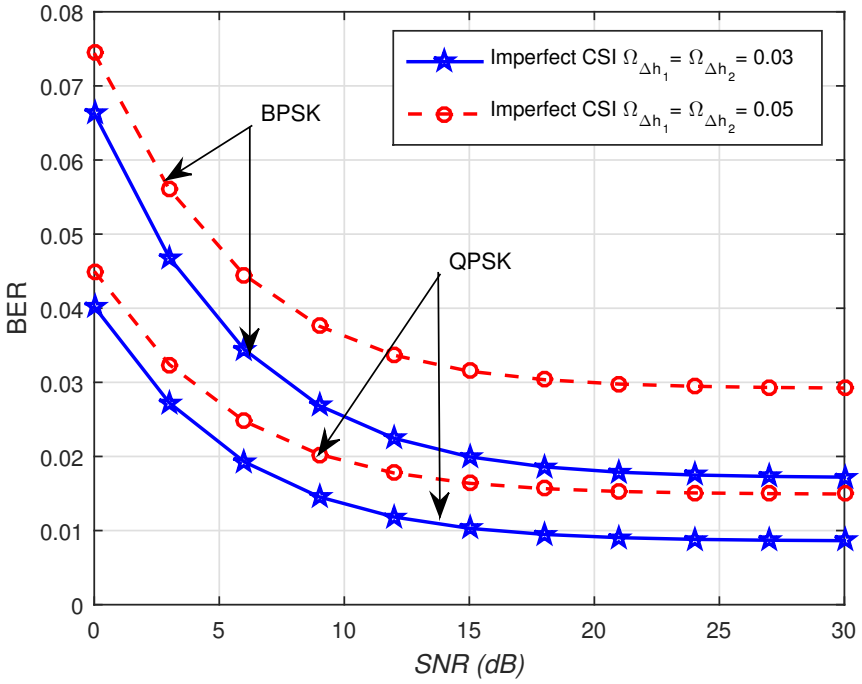

Fig. 5.5: The BER performance of AF RNs vs. various values of P_S.

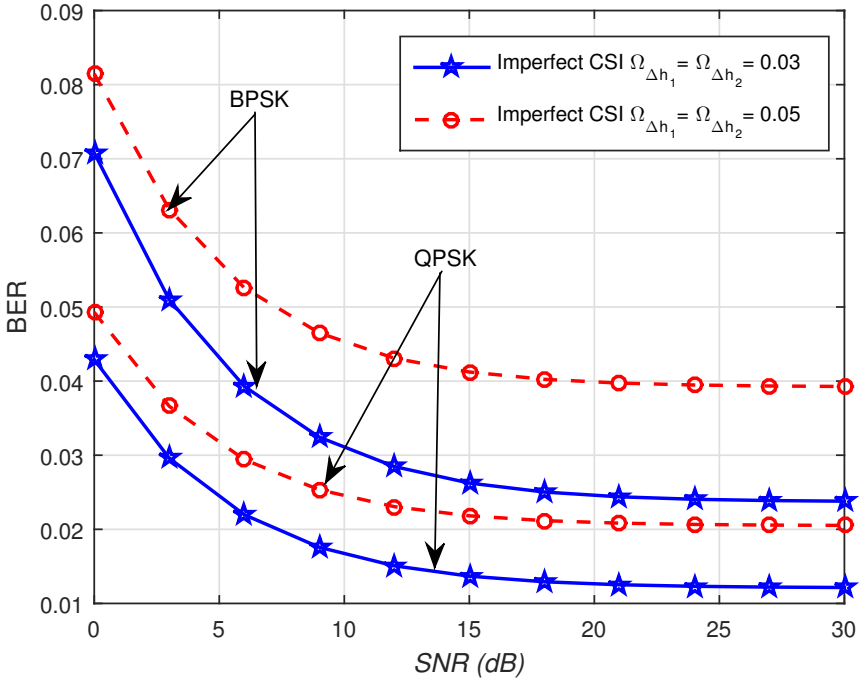

Fig. 5.6: The BER performance of DF RNs vs. various values of P_S.

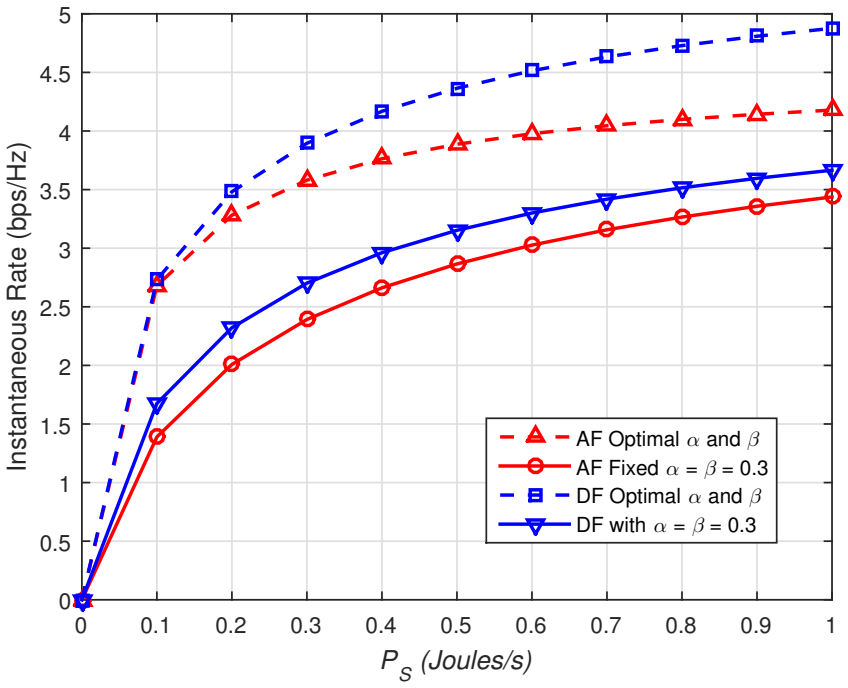

Fig. 5.7: The impact of optimal TS and PS ratios

Fig. 5.7 illustrates the instantaneous rate as a function of the transmit power at S. The instantaneous rate is proved to be superior with optimal values of α and β. It is clear that as P_S climbs from 0 to 0.6, the instantaneous rate considerably increases. Next, it sees gradually increases from 0.6 to 1. The appropriate choice of optimal values of TS and PS for the proposed HTPSR helps achieve optimal instantaneous rate.

The OP under the impact of imperfect CSI is depicted in Fig. 5.8. Regarding this simulation, we compare OP in three different cases, i.e., AF, DF relaying protocols, and an optimal power allocation (OPA) scheme proposed in [68]. In particular, we set the CCEs to 0.001, $\eta = 0.9$, $\alpha - 0.3, \beta = 0.5$, and the number of relays to $K = 1$. It is evident that outage performance of the proposed HTPSR is superior to that of OPA scheme.

In Fig. 5.9, Fig. 5.10, the impact of imperfect CSI on throughput performance in delay-limited transmission and delay-tolerant transmission mode is depicted. It can be observed that the throughput performance is degraded when imperfect CSI is available. Additionally, a comparison between three EH protocols, including HTPSR, TSR and PSR is provided, in which the pre-set values for each protocol are respectively as $\alpha = \beta = 0.2$ (HTPSR), $\alpha = 0.2, \beta = 0$ (TSR), and $\alpha = 0.5, \beta = 0.2$ (PSR). It is worth noting that PSR is better than that of other two protocols. This performance depends on the instantaneous values of the channel.

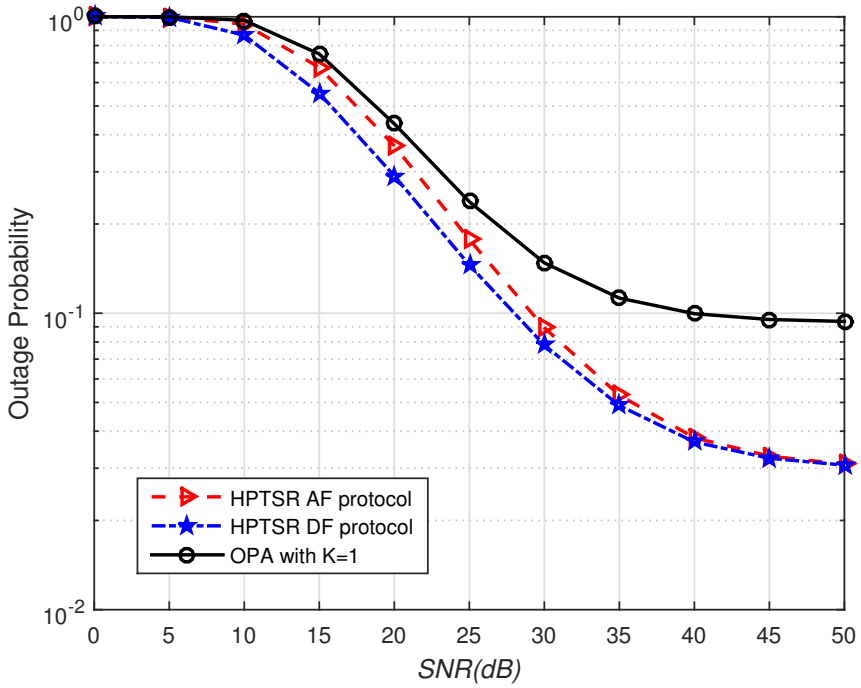

Fig. 5.8: Comparison between our model with recent work

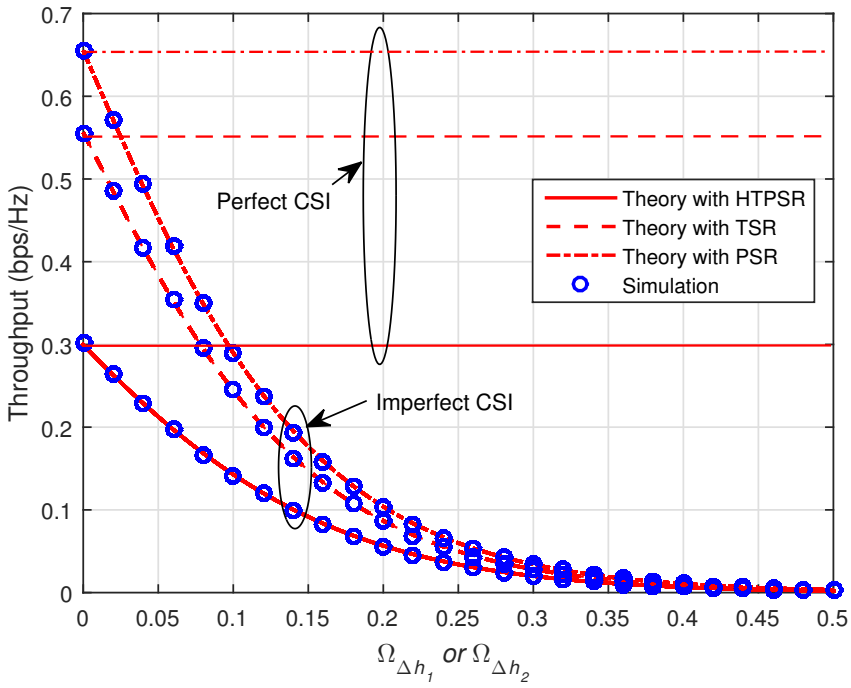

Fig. 5.9: Comparison of throughput τ for imperfect and perfect CSI in delay-limited transmission

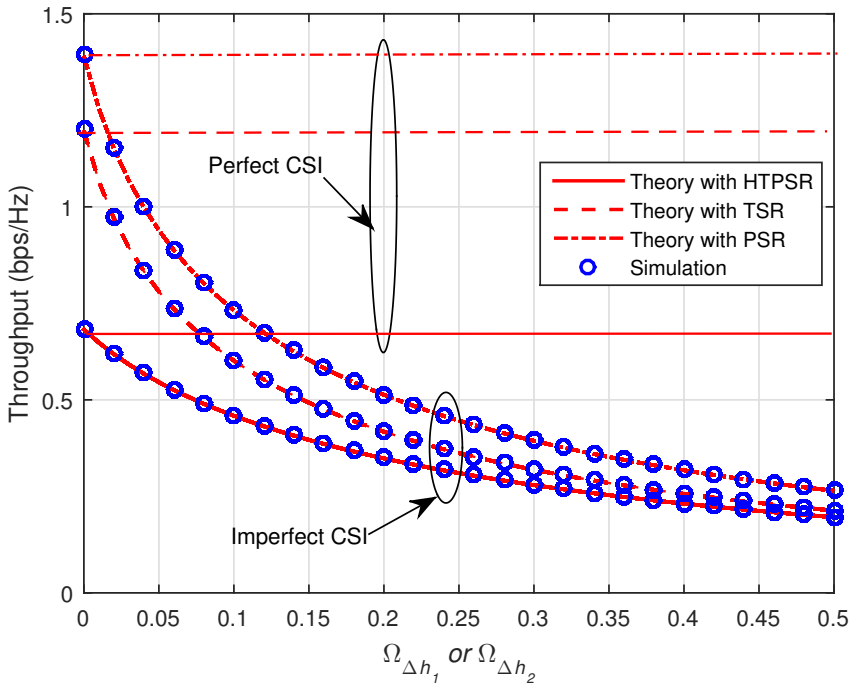

Fig. 5.10: Comparison of throughput, τ for imperfect and perfect CSI in delay-tolerant transmission

5.5 Summary

In this chapter, we studied both AF and DF RNs under the impact of imperfect CSI. The system is determined by the harvested power for AF and DF RNs. The analytical expressions for achievable throughput, BER and the impact on imperfect CSI on AF and DF RNs were obtained. Thanks to the numerical analysis, it is noted that AF relaying performs worse than that of DF relaying in terms of throughput. In particular, the best instantaneous rate was achieved for HTPSR with optimal values of TS and PS ratios. Interestingly, comparisons between the proposed HTPSR protocol with TSR and PSR protocols in simulations were also given.

6 THE IMPACT OF HWIS ON COGNITIVE D2D COMMUNICATION

This chapter studies the impact of HWIs on the cognitive EH D2D communication underlaying cellular network with of two communication types, i.e., multi-hop D2D and P2P. Closed-form expressions for the STP, average EE and SE were provided, and the optimization problem of TS and PS ratios was solved using a genetic algorithm (GA)-based optimization algorithm. We obtain the simulation results to verify the comparisons between AF and DF schemes, where DF outperforms AF in every performance metrics. We can ensure the STP although HWIs are available at all nodes of the system [NHS05].

6.1 Motivation

In principle, D2D communication is considered as a promosing technology [69]. For example, the authors in [70], [71] showed that the total power consumption was drastically reduced because of grouping mobile devices together in multi-hop D2D networks, while they satisfied with the minimum rate for each device. Apart from that, the improvement of throughput in D2D-aided underlaying cellular networks was discussed in [72], in which D2D devices can operate in FD mode to transmit and receive information simultaneously in the same frequency band.

Regarding the distortions stemming from HWIs, several works can be mentioned. In particular, a FD RN was examined in [73], where a FD relay is deployed to assist D2D pairs in direct communicating with each other. In [74], the authors focused on the outage performance of multi-relay DF cooperative RNs in the presence of HWIs, where RF-EH technique was implemented to combat energy constraints at R nodes.

Based on our previous works [11, 75, 76, 77] which considered the impact of HWIs on particular nodes. In particular, we respectively studied the impact of HWIs in AF using TSR protocol and PSR protocol in [75] and [76], while the work [77] examine DF scheme using TSR protocol. It is noted that only a few investigations have been carried out on the impact of HWIs with regards to multi-hop D2D communications. In this chapter, we are going to obtain the closed-form expressions for the average EE and SE to quantify the energy consumption when all nodes are under the impact of HWIs. Besides, comparisons between AF and DF schemes are given, and we solve the optimization problem of TS and PS ratios by using (GA)-based optimization algorithm. The most important focus of this chapter is to optimize the STP.

We organize this chapter as follows: Section 2 presents the system model. Meanwhile, the system performance is analysed Section 3. Section 4 provides numerical and simulation results with detailed analysis and comparisons. A conclusion for the chapter is drawn in Section 5.

6.2 System Model

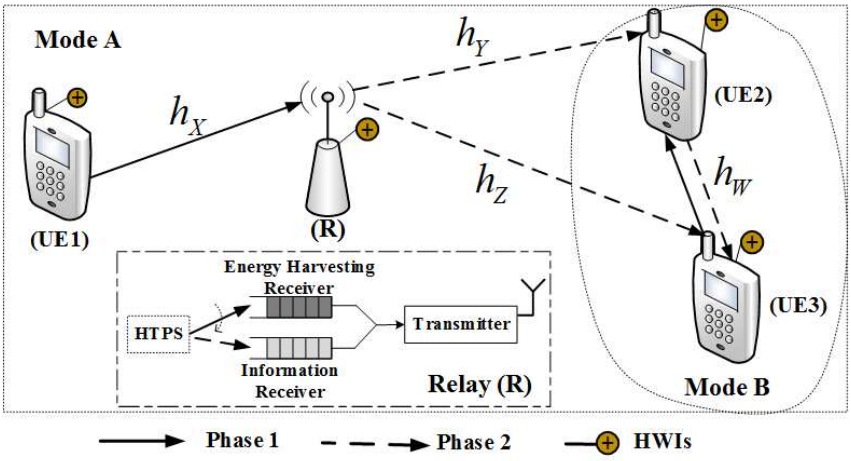

Fig. 6.1: System model

In Fig. 6.1, we provide a cognitive D2D communication underlaying a cellular network, where two different modes are presented including Mode A being considered as a multi-hop D2D communication and Mode B being a one-hop P2P wireless communication. In particular, Mode A consists of two PU equipments (i.e. UE1 and UE2) communicating with each other via a EH R. Meanwhile, Mode B describes the direct information exchange between UE2 and UE3. It is noted that R can also transfer secondary information to UE3. This system operates in HD mode, and a single antenna is equipped at each UE.

The communication model in Mode A comprises two phases. In particular, in phase 1, UE1 transmits the information to R. Then, R exploits the harvested energy to broadcast resulting signals as well as the information intended to UE2 and UE3 in phase 2. It is noted that UE3 can receive signals to conduct interference cancellation in phase 2. In case of mode B, UE2 and UE3 will exchange information in two time slots.

The maximum threshold of the transmit power and the circuit power for UEs denoted as E_{Di}, E_{Ci} with $i = 1, 2, 3$ are assumed to be the same. For simplicity, we denote $E_{Di} = E_D$, $E_{Ci} = E_C$. Note that the transmit power of R is denoted as E_R. Besides that, n_0 is the AWGN with mean power, N_0.

The channel gains are denoted as h_X, h_Y, h_Z for the links from UE1 to R, and R to UE2, UE3, respectively, while the channel gains for P2P communication is h_W. In addition, r_k is the distances for the aforementioned links, where $k \in \{X, Y, Z, W\}$.

In addition, the path loss model denoted as PL_k is defined by $PL_k = 1/\phi r_k^m$ with m being the path-loss exponent, and the path-loss constant is represented by ϕ as in [17]. All channel gains between two nodes are modelled as Rayleigh fading channels with free space propagation path loss. In terms of the channel gain coefficient, we have $|h_k|^2 = |k|^2 PL_k$, where k is the complex Gaussian distributed RVs to model fading phenomena with zero

mean and variances, $\Omega_k \sim CN(0,1)$.

In this chapter, HTPSR is deployed T being the time block, where the portion, $\alpha_1 T$ is used for EH at R with E_D. Signals transmitted to R from UE1 is divided into two parts. In particular, $\alpha_2 T$, βE_D is used for EH at R while $(1-\beta)E_D$ is used for IT. Note that, the residual fraction, $(T - \alpha_1 T - \alpha_2 T)$ is used for broadcasting signals from R to UE2, UE3 with power allocation being λ and $(1-\lambda)$, respectively. Note that PSR protocol is a special case of HTPSR when $\alpha_1 = 0$ and $\alpha_2 = 0.5$, while TSR protocol is a special case when $\beta = 0$ and $\alpha_2 = 0.5 \times (1-\alpha_1)$.

Since all nodes are assumed to suffer from HWIs [78] so we represent the practical transceiver impairments at UEs as x in the $a \to b$ link, while the HWIs of receivers degrade the during the reception phase. HI_a and HI_b are denoted as the aggregate distortions degrading the $a \to b$ link with zero mean variance $HI_a \sim CN\left(0, \kappa_a |h|^2 E_D\right)$, $HI_b \sim CN\left(0, \kappa_b |h|^2 E_D\right)$, respectively, and κ_a, κ_b are the levels of HWIs at HI_a and HI_b. Thus, the received signal can be expressed as

$$\begin{aligned} y_b &= \sqrt{E_D} hx + HI_a + HI_b + n_0 \\ &= \sqrt{E_D} hx + HI_{ab} + n_0 \end{aligned}, \tag{6.1}$$

where the channel gain for the $a \to b$ link is h, and an aggregate distortion at the receiver b is denoted as HI_{ab} with aggregate distortion power $HI_{ab} \sim CN\left(0, \kappa |h|^2 E_D\right)$, where $\kappa \triangleq \kappa_a + \kappa_b$ is the aggregate impairment level during the information processing phase.

Hence, the distortion noise stemming from HWIs at R is represented by HI_1 with variance $HI_1 \sim \mathrm{CN}\left(0, \kappa \mathrm{E_D PL_X} |\mathrm{X}|^2\right)$, while the corresponding distortion noise caused by HWIs at UE2, UE3 are denoted by HI_2, HI_3 with variance $HI_2 \sim CN\left(0, \kappa\lambda E_R |Y|^2 PL_Y\right)$, $HI_3 \sim CN\left(0, \kappa(1-\lambda) E_R |Z|^2 PL_Z\right)$, respectively.

6.3 Performance Analysis

In this section, we are going to study the STP, the EE and SE in the presence HWIs. Besides that, comparisons between AF and DF scheme are evaluated in multi-hop D2D communication and P2P communication, and we also derive closed-form expressions for each aforementioned factor. Eventually, we are going to solve the optimization problem of TS and PS ratios with the help of GA-based algorithm.

6.3.1 Energy harvesting and information transmission under the impact of HWIs

Mode A: Multi-hop cognitive D2D wireless communication

In this part, the impact of HWIs considering HTPSR protocol is going to discussed. Let us first conisder the first phase.

A. Phase 1

Now, the amount of energy harvested at R is given as

$$E_h = \eta E_D |X|^2 PL_X \left(\alpha_1 + \alpha_2 \beta\right) T, \tag{6.2}$$

where η is the energy conversion efficiency and $\eta \in (0, 1]$.

Therefore, the transmit power of R is expressed as

$$E_R = \frac{E_h}{(1 - \alpha_1 - \alpha_2) T} = \frac{\eta \left(\alpha_1 + \alpha_2 \beta\right) E_D PL_X |X|^2}{1 - \alpha_1 - \alpha_2}. \tag{6.3}$$

Following that, we calculate the received data at R as

$$y_1 = \sqrt{(1 - \beta) E_D} h_X x_1 + n_0 + HI_1, \tag{6.4}$$

where we denote x_1 as the normalized data signal from UE1 satisfying $\mathbb{E}\left\{|x_1|^2\right\} = 1$.

It is noted that R splits the harvested power into two parts, λE_R is used for transmitting data to UE2 while $(1 - \lambda) E_R$ is for forwarding signals to UE3. Now, we are going to consider both AF and DF transmission scheme.

Regarding DF relaying scheme, the transmitted signal at R, x_R is given by

$$x_R = \left(\sqrt{\lambda E_R} x_2 + \sqrt{(1 - \lambda) E_R} x_3\right), \tag{6.5}$$

where the power unit of the transmitted information for UE2 and UE3 is represented as x_2, x_3, respectively, which satisfy $\mathbb{E}\left\{|x_2|^2\right\} = 1$, and $\mathbb{E}\left\{|x_3|^2\right\} = 1$.

In AF scheme, the transmitted signal at R, x_R can be expressed as

$$x_R = G\sqrt{\lambda E_R} y_1 + \sqrt{(1 - \lambda) E_R} x_3, \tag{6.6}$$

where the amplification factor at R [79] is calculated as
$G = \sqrt{\left((1 - \beta) E_D |X|^2 PL_X + \Omega_0 + \kappa E_D |X|^2 PL_X\right)^{-1}} \approx \sqrt{\left((1 - \beta + \kappa) E_D |X|^2 PL_X\right)^{-1}}$.

Remark 6.1. It is noted that the power allocation, λ is the primary concern, due to the importance of balancing the received information at UE2 and UE3. Therefore, to maintain the quality of UE2 at an acceptable level, as λ increases, the amount of signal received at UE3 drops. This scenario is going to be explained in Remark 6.3.2.

B. Phase 2

Considering the IT process between R and UE2, we compute the received signal at UE2 as

$$y_2 = h_Y x_R + n_0 + HI_2, \tag{6.7}$$

and we similar derive the expression for UE3 as

$$y_3 = h_Z x_R + n_0 + HI_3. \tag{6.8}$$

Mode B: P2P Wireless Communication

In this section, the P2P communication between UE2 and UE3 happens within two time slots. It is assumed that the same signal is received at UE2 and UE3 which is written as

$$y_4 = \sqrt{E_D} h_W x_4 + n_0 + HI_4, \tag{6.9}$$

where the transmitted data from UE2 to UE3 and vice versa is represented as x_4, and it must satisfy $\mathbb{E}\left\{|x_4|^2\right\} = 1$, and the distortion noise at UE2 and UE3 is HI_4, where $\Omega_4 \sim CN\left(0, \kappa E_D |W|^2 PL_W\right)$. Besides, $PL_W = (\phi r_W^m)^{-1}$.

6.3.2 The end-to-end signal-to-noise-plus-distortion ratio (SNDR)

In this part, we investigate the end-to-end signal-to-noise-plus-distortion ratio (SNDR) , γ, where $\gamma = \mathbb{E}\left\{|signal|^2\right\} / \mathbb{E}\left\{|\text{overall noise}|^2\right\}$ for AF and DF scheme. Now, AF scheme is going to examined first.

A. AF relaying

Replacing (6.3), (6.4) into (6.6), and then combining with (6.7), we express the end-to-end SNDR at UE2 when UE2 treats x_3 as interference and later decodes the primary information, x_1 as

$$\gamma_1^{AF} = \frac{\tau_{1,a}|X|^2|Y|^2}{\tau_{1,b}|X|^2|Y|^2 + \tau_{1,c}|Y|^2 + \tau_0}, \tag{6.10}$$

where $\delta_1 = \kappa\lambda + \kappa\lambda(1-\beta+\kappa) + (1-\lambda)(1-\beta+\kappa)$, $\tau_0 = \frac{(1-\beta+\kappa)(1-\alpha_1-\alpha_2)}{\eta(\alpha_1+\alpha_2\beta)}$, and

$$\begin{cases} \tau_{1,a} = \frac{E_D}{N_0}(1-\beta)\lambda PL_X PL_Y \\ \tau_{1,b} = \frac{E_D}{N_0}\delta_1 PL_X PL_Y \\ \tau_{1,c} = \lambda PL_Y. \end{cases}$$

Similarly, substituting (6.3), (6.4), and (6.6) into (6.8), the end-to-end SNDR at UE3 when UE3 treats x_1 as interference and later decodes the secondary information, x_3 is written as

$$\gamma_2^{AF} = \frac{\tau_{2,a}|X|^2|Z|^2}{\tau_{2,b}|X|^2|Z|^2 + \tau_{2,c}|Z|^2 + \tau_0}, \tag{6.11}$$

where we already mentioned $\delta_2 = \kappa\lambda + \kappa(1-\lambda)(1-\beta+\kappa) + \lambda(1-\beta-\kappa) + \kappa$, τ_0 in the above expression, and

$$\begin{cases} \tau_{2,a} = \frac{E_D}{N_0}(1-\beta)(1-\lambda)PL_X PL_Z \\ \tau_{2,b} = \frac{E_D}{N_0}\delta_2 L_X PL_Z \\ \tau_{2,c} = \lambda PL_Z. \end{cases}$$

As a consequence, we obtain the achievable data rate at UE2 and UE3 as

$$r_i^{AF} \underset{i\in\{1,2\}}{=} \frac{B}{2}\log_2\left(1+\gamma_i^{AF}\right), \tag{6.12}$$

where the channel bandwidth is B.

Remark 6.2. To clarify Remark 6.1, we derive the end-to-end SNDR at UE2 to satisfy the QoS. In particular, when secondary signals are treated as interference, we can easily derive the desirable expression from (6.10) if $E_D \to \infty$ in case all parameters is fixed, $\lim_{E_D\to\infty}\gamma_1^{AF} = \lambda/(1-\lambda)$. However, due to the achievement of the end-to-end SNDR at UE3 (6.11), primary signals are considered as interference, where if $E_D \to \infty$, $\lim_{E_D\to\infty}\gamma_2^{AF} = (1-\lambda)/\lambda$. We are going to give simulation results to explain these phenomena.

B. DF relaying

Similarly, regarding DF scheme, the end-to-end SNDR at both UE2 and UE3 can be written as

$$\gamma_i^{DF} \underset{i\in\{1,2\}}{=} \min\left\{\gamma_{i,a}^{DF}, \gamma_{i,b}^{DF}\right\}, \tag{6.13}$$

where the instantaneous SNDR at R, UE2, and UE3 can be computed, respectively based on (6.4), (6.7) and (6.8) as follows

$$\begin{cases} \gamma_{1,a}^{DF} = \gamma_{2,a}^{DF} = \frac{(1-\beta)\frac{E_D}{N_0}PL_X|X|^2}{1+\kappa\frac{E_D}{\Omega_0}PL_X|X|^2} \\ \gamma_{1,b}^{DF} = \frac{\psi_{1,a}|X|^2|Y|^2}{\psi_{1,b}|X|^2|Y|^2+\psi_0} \\ \gamma_{2,b}^{DF} = \frac{\psi_{2,a}|X|^2|Z|^2}{\psi_{2,b}|X|^2|Z|^2+\psi_0} \end{cases},$$

and $\psi_0 = \frac{(1-\alpha_1-\alpha_2)}{\eta(\alpha_1+\alpha_2\beta)}$, $\psi_{1,a} = \frac{E_D}{N_0}\lambda PL_X PL_Y$, $\psi_{2,a} = \frac{E_D}{N_0}(1-\lambda)PL_X PL_Z$, $\psi_{1,b} = \frac{E_D}{N_0}(\kappa\lambda+1-\lambda)PL_X PL_Y$, $\psi_{2,b} = \frac{E_D}{N_0}(\kappa(1-\lambda)+\lambda)PL_X PL_Z$.

Therefore, the transmission rate for DF protocol is given by

$$r_i^{DF} \underset{i\in\{1,2\}}{=} \frac{B}{2}\log_2\left(1+\gamma_i^{DF}\right). \tag{6.14}$$

C. P2P communication

In this part, we are going to study the SNDR under the impact of HWIs in P2P communication as follows

$$\gamma_3^{PP} = \frac{\frac{E_D}{\Omega_0}PL_W|W|^2}{1+\kappa\frac{E_D}{\Omega_0}PL_W|W|^2}. \tag{6.15}$$

6.3.3 Successful transmission probability

In this section, we represent the STP as the probability that a receiver is able to receive packets successfully in the up-link in a time slot. Considering the STP in the one hop P2P communication, packets are successfully received if the SNDR is higher than its threshold, Γ_D, $\Pr(\gamma \geq \Gamma_D)$. Therefore, UE2 and UE3 will receive a negative feedback, and the packets will be put first in the queue for retransmission. Hence, we derive the

STP for P2P communication as

$$\begin{aligned}\Pr\left(\gamma_3^{PP} \geq \Gamma_D\right) &= \Pr\left(\frac{\frac{E_D}{\Omega_0} PL_W |W|^2}{1+\kappa \frac{E_D}{\Omega_0} PL_W |W|^2} \geq \Gamma_D\right) \\ &= 1 - \Pr\left(\frac{\frac{E_D}{\Omega_0} PL_W |W|^2}{1+\kappa \frac{E_D}{\Omega_0} PL_W |W|^2} < \Gamma_D\right) \cdot \\ &= e^{-\frac{\Omega_0 \Gamma_D}{\Omega_W E_D PL_W (1-\kappa\Gamma_D)}}\end{aligned} \tag{6.16}$$

In terms of multi-hop D2D communication in the presence of HWIs, expressions for STP with the large scale path-loss and small scale Rayleigh fading at UE2 and UE3 in AF and DF scheme are going to be obtained in *Proposition* 6.1 and *Proposition* 6.2, respectively.

Proposition 6.1. Thus, the STP at UE2 and UE3 in AF scheme in case $\Gamma_D \geq \tau_{i,a}/\tau_{i,b}$ is given by

$$\Pr\left(\gamma_i^{AF} \geq \Gamma_D\right) \underset{i\in\{1,2\}}{=} 1. \tag{6.17}$$

Otherwise, in case $\Gamma_D < \tau_{i,a}/\tau_{i,b}$, the STP at UE2 and UE3 is derived as

$$\Pr\left(\gamma_i^{AF} \geq \Gamma_D\right) \underset{i\in\{1,2\}}{=} 2e^{-\omega_i^{AF}} \sqrt{\vartheta_i^{AF}} K_1\left(2\sqrt{\vartheta_i^{AF}}\right), \tag{6.18}$$

where $\omega_i^{AF} = \frac{\Gamma_D \tau_{i,c}}{\Omega_X\left(\tau_{i,a} - \Gamma_D \tau_{i,b}\right)}$, and $\vartheta_i^{AF} = \frac{\Gamma_D \tau_0}{\Omega_X \Omega_Y\left(\tau_{i,a} - \Gamma_D \tau_{i,b}\right)}$.

Proof: Considering AF scheme, the general SNDR for both UE2 and UE3 can be obtained as

$$\gamma_i^{AF} = \frac{aXY}{bXY + cY + d}, \tag{6.19}$$

where constant values are a, b, c, d, and the exponential RVs, i.e. X, Y are independent with mean, Ω_X and Ω_Y, respectively.

Following from (6.19), we calculate the CDF of SNDR as

$$\begin{aligned}\Pr\left(\gamma_i^{AF} < \Gamma_D\right) &= \Pr\left(X < \tfrac{\Gamma_D(cY+d)}{Y(a-\Gamma_D b)}\right) \\ &= \tfrac{1}{\Omega_Y} \int_{y=0}^{\infty} \left(1 - e^{-\frac{\Gamma_D(cy+d)}{\Omega_X y(a-\Gamma_D b)}}\right) e^{-\frac{y}{\Omega_Y}} dy \\ &= 1 - 2e^{-\frac{\Gamma_D c}{\Omega_X(a-\Gamma_D b)}} \sqrt{\frac{\Gamma_D d}{\Omega_X \Omega_Y (a-\Gamma_D b)}} K_1\left(2\sqrt{\frac{\Gamma_D d}{\Omega_X \Omega_Y (a-\Gamma_D b)}}\right)\end{aligned} \quad , \tag{6.20}$$

where the above expression is obtained thanks to the use of [[66], 3.324.1] under the condition, $\Gamma_D < \tau_{i,a}/\tau_{i,b}$. On the contrary, if $\Gamma_D \geq \tau_{i,a}/\tau_{i,b}$, $\Pr\left(X < \frac{\Gamma_D(cY+d)}{Y(a-\Gamma_D b)}\right) = 1$ since the probability is higher than the negative values, and it can be equal to 1.

To this point, the STP at UE2 can be written as

$$\Pr\left(\gamma_i^{AF} \geq \Gamma_D\right) = 2e^{-\frac{\Gamma_D c}{\Omega_X(a-\Gamma_D b)}} \sqrt{\frac{\Gamma_D d}{\Omega_X \Omega_Y (a-\Gamma_D b)}} K_1\left(2\sqrt{\frac{\Gamma_D d}{\Omega_X \Omega_Y (a-\Gamma_D b)}}\right) \cdot \tag{6.21}$$

This ends the proof for Proposition 6.1.

Proposition 6.2. In case of DF, the STP at UE2 and UE3 can be similarly given by

$$\Pr\left(\gamma_i^{DF} \geq \Gamma_D\right) \underset{i\in\{1,2\}}{=} 2e^{-\omega_i^{DF}}\sqrt{\vartheta_i^{DF}}K_1\left(2\sqrt{\vartheta_i^{DF}}\right), \tag{6.22}$$

where $\omega_i^{DF} = \frac{\Gamma_D\Omega_0}{\Omega_X E_D PL_X((1-\beta)-\Gamma_D\kappa)}$, $\vartheta_i^{DF} = \frac{\Gamma_D\psi_0}{\Omega_X\Omega_Z\left(\psi_{i,a}-\Gamma_D\psi_{i,b}\right)}$.

proof: We first follow from (6.4), so the CDF of the instantaneous SNDR from UE1 to R can be computed by

$$\begin{aligned}\Pr(\gamma_{ia}^{DF} < \Gamma_D) &= \Pr\left(\frac{(1-\beta)\frac{E_D}{\Omega_0}PL_X|X|^2}{1+\kappa\frac{E_D}{\Omega_0}PL_X|X|^2} < \Gamma_D\right) \\ &= 1 - e^{-\frac{\Gamma_D\Omega_0}{\Omega_X E_D PL_X\left((1-\beta)-\kappa\Gamma_D\right)}}\end{aligned}. \tag{6.23}$$

Next, based on (6.23), the STP in the first hop can be written by

$$\Pr\left(\gamma_{ia}^{DF} \geq \Gamma_D\right) = e^{-\frac{\Gamma_D\Omega_0}{\Omega_X E_D PL_X\left((1-\beta)-\Gamma_D\kappa\right)}}. \tag{6.24}$$

If $\Gamma_D < \psi_{i,a}/\psi_{i,b}$, the STP of the instantaneous SNDR from R to UE2, UE3 in the second hop can be computed based on (6.7), (6.8) as

$$\begin{aligned}\Pr(\gamma_{ib}^{DF} \geq \Gamma_D) &= \Pr\left(\tfrac{\psi_{i,a}XY}{\psi_{i,b}XY+\psi_0} \geq \Gamma_D\right) \\ &= 1 - \Pr\left(\tfrac{\psi_{i,a}XY}{\psi_{i,b}XY+\psi_0} < \Gamma_D\right) \\ &= \tfrac{1}{\Omega_Y}\int_{y=0}^{\infty}\left(e^{-\frac{1}{y}\left(\frac{\Gamma_D\psi_0}{\Omega_X\left(\psi_{i,a}-\Gamma_D\psi_{i,b}\right)}\right)}\right)e^{-\frac{y}{\Omega_Y}}dy \\ &= 2\sqrt{\frac{\Gamma_D\psi_0}{\Omega_X\Omega_Y\left(\psi_{i,a}-\Gamma_D\psi_{i,b}\right)}}K_1\left(2\sqrt{\frac{\Gamma_D\psi_0}{\Omega_X\Omega_Y\left(\psi_{i,a}-\Gamma_D\psi_{i,b}\right)}}\right).\end{aligned} \tag{6.25}$$

Otherwise, if $\Gamma_D \geq \psi_{i,a}/\psi_{i,b}$, then $\Pr\left(\frac{\psi_{i,a}XY}{\psi_{i,b}XY+\psi_0} \geq \Gamma_D\right) = 0$.

Finally, by denoting the end-to-end SNDR at UE2, UE3 in DF scheme as $\gamma_i^{DF} = min(\gamma_{ia}^{DF}, \gamma_{ib}^{DF})$ with $i \in \{1,2\}$, the STP of γ_i^{DF} can be given by

$$\Pr(\gamma_i^{DF} \geq \Gamma_D) = \Pr(\gamma_{ia}^{DF} \geq \Gamma_D) \times \Pr(\gamma_{ib}^{DF} \geq \Gamma_D). \tag{6.26}$$

Substituting (6.24), (6.25) into (6.26), this ends the proof for Proposition 6.2.

Remark 6.3. The joint optimal values of TS and PS ratios can optimize STP which is difficult to evaluate in terms of the STP with Bessel function for maximum transmission power, distances, power allocation and HWIs level, etc. Since the above optimization problem is non-convex, a genetic algorithm (GA)-based optimization algorithm is going to be used in Section 6.3.5.

6.3.4 Average energy efficiency and average spectral efficiency

In this part, expressions for average EE and average SE. Note that EE is defined as the average transmission rate under unit-energy consumption. In order to achieve energy-efficient communication, both the transmission power and the circuit power can be examined [80].

Proposition 6.3. We derive the expressions for the average EE and average SE, respectively in AF scheme as

$$\begin{aligned} ee_i^{AF} &= \mathbb{E}\left\{\frac{B\log_2\left(1+\gamma_i^{AF}\right)}{2E_{sum}}\right\} \\ &= \frac{B}{2E_{sum}} \int_{x=0}^{\tau_{i,a}/\tau_{i,b}} \left(M_i^{AF}+N_i^{AF}\right)\log_2\left(1+x\right)dx \end{aligned}, \tag{6.27a}$$

and

$$\begin{aligned} se_i^{AF} &= \mathbb{E}\left\{\frac{B\log_2\left(1+\gamma_i^{AF}\right)}{2B}\right\} \\ &= \frac{1}{2} \int_{x=0}^{\tau_{i,a}/\tau_{i,b}} \left(M_i^{AF}+N_i^{AF}\right)\log_2\left(1+x\right)dx \end{aligned}, \tag{6.27b}$$

where $M_i^{AF} = \frac{2\tau_{i,a}e^{-\omega_i^{AF}}\vartheta_i^{AF}K_0\left(2\sqrt{\vartheta_i^{AF}}\right)}{x\left(\tau_{i,a}-x\tau_{i,b}\right)}$, $N_i^{AF} = \frac{2\tau_{i,a}\omega_i^{AF}e^{-\omega_i^{AF}}\sqrt{\vartheta_i^{AF}}K_1\left(2\sqrt{\vartheta_i^{AF}}\right)}{x\left(\tau_{i,a}-x\tau_{i,b}\right)}$, and the total power consumption of Mode A is defined as $E_{sum} = 2E_D + 2E_C + E_R$.

Proof: Based on Proposition 6.1, the CDF of SNDR at UE2, UE3 in AF scheme is given by

$$F_{\gamma_i^{AF}}(x) = 1 - 2e^{-\omega_i^{AF}}\sqrt{\vartheta_i^{AF}}K_1\left(2\sqrt{\vartheta_i^{AF}}\right), \tag{6.28}$$

where $\vartheta_i^{AF} = \frac{\tau_0 x}{\Omega_X\Omega_Y\left(\tau_{i,a}-x\tau_{i,b}\right)}$, $\omega_i^{AF} = \frac{x\tau_{i,c}}{\Omega_X\left(\tau_{i,a}-x\tau_{i,b}\right)}$.

The derivative of $F_{\gamma_i^{AF}}(x)$ with respect to x helps us derive the PDF of γ_i^{AF} as

$$\begin{aligned} f_{\gamma_i^{AF}}(x) &= \frac{\partial}{\partial(x)}F_{\gamma_i^{AF}}(x) \\ &= M_i^{AF} + N_i^{AF} \end{aligned}, \tag{6.29}$$

where $M_i^{AF} = \frac{2\tau_{i,a}e^{-\omega_i^{AF}}\vartheta_i^{AF}K_0\left(2\sqrt{\vartheta_i^{AF}}\right)}{x\left(\tau_{i,a}-x\tau_{i,b}\right)}$, $N_i^{AF} = \frac{2\tau_{i,a}\omega_i^{AF}e^{-\omega_i^{AF}}\sqrt{\vartheta_i^{AF}}K_1\left(2\sqrt{\vartheta_i^{AF}}\right)}{x\left(\tau_{i,a}-x\tau_{i,b}\right)}$, and we derive the expression above by using the property of Bessel function in [[66], 8.486.18].

Thus, we give the closed-form expression for the average EE as

$$\begin{aligned} \mathbb{E}\left\{\log_2\left(1+\gamma_i^{AF}\right)\right\} &= \int_{x=0}^{\tau_{i,a}/\tau_{i,b}} f_{\gamma_i^{AF}}(x)\log_2\left(1+x\right)dx \\ &= \int_{x=0}^{\tau_{i,a}/\tau_{i,b}} \left(M_i^{AF}+N_i^{AF}\right)\log_2\left(1+x\right)dx \end{aligned}. \tag{6.30}$$

This proof is provided to prove Proposition 6.3.

Similar to **Proposition** 6.3, we similar compute the closed-form average EE and average SE in Mode A using DF scheme as

$$\begin{aligned} ee_i^{DF} &= \mathbb{E}\left\{\frac{B\log_2\left(1+\gamma_i^{DF}\right)}{2E_{sum}}\right\} \\ &= \frac{B}{2E_{sum}} \int_{x=0}^{\psi_{i,a}/\psi_{i,b}} \left(M_i^{DF}+N_i^{DF}\right)\log_2\left(1+x\right)dx \end{aligned}, \tag{6.31a}$$

and

$$\begin{aligned} se_i^{DF} &= \mathbb{E}\left\{\frac{B\log_2\left(1+\gamma_i^{DF}\right)}{2B}\right\} \\ &= \frac{1}{2}\int_{x=0}^{\psi_{i,a}/\psi_{i,b}} \left(M_i^{DF}+N_i^{DF}\right)\log_2\left(1+x\right)dx \end{aligned}, \tag{6.31b}$$

where $M_i^{DF} = \frac{2\psi_{i,a}e^{-\omega_i^{AF}}\vartheta_i^{AF}K_0\left(2\sqrt{\vartheta_i^{DF}}\right)}{x\left(\psi_{i,a}-x\psi_{i,b}\right)}$, $N_i^{DF} = \frac{2(1-\beta)\omega_i^{DF}e^{-\omega_i^{DF}}\sqrt{\vartheta_i^{DF}}K_1\left(2\sqrt{\vartheta_i^{DF}}\right)}{x\left(\psi_{i,a}-x\psi_{i,b}\right)}$.

Meanwhile, in case $\Gamma_D < 1/\kappa$ and the sum of the transmit power and the circuit power is defined as $P_{sum} = 2E_D + 2E_C$, the expressions for both average EE and average SE in P2P communication can be given by

$$\begin{aligned} ee_3^{PP} &= 2\times\mathbb{E}\left\{\frac{B\log_2\left(1+\gamma_3^{PP}\right)}{2P_{sum}}\right\} \\ &= \frac{B}{P_{sum}\ln 2}\int_{x=0}^{1/\kappa} e^{-\frac{\Omega_0 x}{\Omega_W E_D PL_W(1-\kappa x)}}(1+x)^{-1}dx \end{aligned}, \tag{6.32a}$$

and

$$\begin{aligned} se_3^{PP} &= 2\times\mathbb{E}\left\{\frac{B\log_2\left(1+\gamma_3^{PP}\right)}{2B}\right\} \\ &= \frac{1}{\ln 2}\int_{x=0}^{1/\kappa} e^{-\frac{\Omega_0 x}{\Omega_W E_D PL_W(1-\kappa x)}}(1+x)^{-1}dx \end{aligned}. \tag{6.32b}$$

6.3.5 Optimization problem

In terms of the HTPS relaying protocol, the optimization problem of TS and PS ratios are going to be solved to optimize the STP. Thus, it can be overall obtained as

$$\max_{\alpha_1,\alpha_2,\beta}\left\{2e^{-\omega_i^j}\sqrt{\vartheta_i^j}K_1\left(2\sqrt{\vartheta_i^j}\right)\right\}, \tag{6.33}$$

where the expression is subject to $\alpha_1, \alpha_2, \beta \in (0, 1]$, and ω_i^j, ϑ_i^j were defined in **Proposition** 6.1 and **Proposition** 6.2, respectively, $i \in \{1, 2\}, j \in \{AF, DF\}$.

Because the expression (6.33) is a non-convex function, a genetic algorithm (GA)-based optimization algorithm is applied to obtain the optimal values of TS and PS to maximize the STP which is explained in details as follows:

Definition 6.3.5: The generation of a random population is defined as a set of chromosomes which comprises a group of genes, and it is assumed to contain the optimal values for the considered variables [81]. Since the chromosome is against an objective function, the fitness of each one is determined. Only best chromosomes can exchange information (via crossover or mutation) to produce offspring chromosomes so that simulations for the natural survival of the fittest process can be provided. If offspring solutions are more feasible than weak population members, they are going to be investigated and used for population evolution. The process continues for many generations to find a best-fit (near-optimum) solution. Parameters, i.e., the number of generations, population size, crossover rate, and mutation rate affect the performance of GAs [82, 83].

TS and PS denoted as α and β are considered as genes, a chromosome is created by combining α and β. To obtain each chromosome's fitness, objective function in (6.33) is used. H_{max} denotes the optimal solution of the t-th generation, and the predefined precision with constraint tolerance of GA is denoted by ϵ. Thus, all the steps of the GA-based optimization algorithm 1 can be summarized as follows:

Algoritmus 1: GA-based Optimization Algorithm

Input : N as the number of generations, constraint tolerance, ϵ, and mutation probability, p_m

Output: H_{max} with joint optimal TS and PS

Step 1: *Generate random population for P solutions (chromosomes)*;

Step 2: foreach *individual* $t \leftarrow 1$ **to** P **do**
fitness (t) is evaluated by objective function in formula (6.33);
if $(H_{max}(t) - H_{max}(t-1)) < \epsilon$ **then** the algorithm will stop;
else go back to Step 3;

Step 3: for $t \leftarrow 1$ **to** N **do**
An operation is selected randomly (i.e. crossover or mutation);
if *crossover is chosen* **then**
use Roulette wheel selection to Select two parents at random t_a and t_b;
Generate on offspring t_c = crossover(t_a and t_b);
else *mutation is chosen*;
Select one chromosome randomly, t with mutation probability, p_m;
Note that generate mutation results in the production of a new group of TS and PS which is similar to an offspring, where t_c = mutate(t);
End if;
The fitness of the offspring, t_c is Calculated;
if t_c *is better than the worst chromosome* **then**
Update the worst chromosome by t_c;
Replace $t = t + 1$,
end
return to Step 2;

As a result, the use of a genetic algorithm (GA)-based optimization helps us achieve the joint optimal TS and PS ratios to guarantee the best STP.

6.4 Numerical Results

In this section, simulations are provided to prove the analytical expressions and evaluate the impact of HWIs on the STP and average EE and average SE, where we compare AF and DF in both communications. Besides, the joint optimization of TS and PS is solved. For simplicity, we summarize all the primary parameters and default values in Table 6.1

Parameter	**Values**
Circuit power at UEi, E_C	100 W
Channel bandwidth, B	10 Mhz
Path loss for all links in the system, PL_k, $k \in [X, Y, Z, W]$	$(148 + 40\log_{10}(r_k))^{-1}$ dB
Thermal noise density, N_0	-174 dBm/Hz
Energy conversion efficiency, η	1
TS and PS ratios, $\alpha_1 = \alpha_2 = \beta$	0.1
Power allocation, λ	0.7
Hardware impairments level, κ	0.15
SNDR threshold at UE2, Γ_D	3 dB
SNDR threshold at UE3 , Γ_D	1 dB

Tab. 6.1: Main Simulation Parameters (Impact of HWIs)

which are used when UE1, R and UE2 are located at $(0, 0)$, $(0.5, 0)$, and $(1, 0)$ on the X-Y plane, respectively while UE3 is located at $(1, 0.5)$. The simulation results are averaged over 10^5 channel realizations.

A. STP vs. the maximum transmission, E_D at UE2 and UE3

In Fig. 6.2 and Fig. 6.3, the STP is illustrated as a function of the maximum transmission, E_D at UE2 and UE3, where AF and DF scheme are compared with each other using the proposed HTPSR and TSR under the impact HWIs. We can observe that more E_D results in better STP, DF scheme outperforms AF scheme, where HTPSR relaying protocol is better than TSR in terms of STP. Besides, UE2 is much better than UE3 without spectrum sharing, e.g., when $E_D = 10dB$, the STP at UE2 is approximately 0.55 and 0.72 for AF and DF, respectively, while the STP at UE3 is at around 0.48 and 0.59 for AF and DF, respectively.

B. Successful transmission probability vs. HWIs levels, κ at UE2 and UE3

The STP with HWIs for AF and DF schemes is presented in Fig. 6.4 and Fig. 6.5. The impact of HWIs on the STP is obvious, as κ increases the STP is degraded, where the STP in AF scheme drops remarkably when $E_D = 5dB$.

C. Average EE and average SE at UE2 and UE3 vs. E_D

In Fig. 6.6 and Fig. 6.7, the average EE and average SE at UE2 are considered as a function of E_D (W). We can observe that the average EE rises as E_D increases before dropping gradually when E_D reaches approximately 0.2, since E_D rises, E_{sum} increases while the average SE is linear. In particular, two different levels of HWIs, $\kappa = 0.15$,

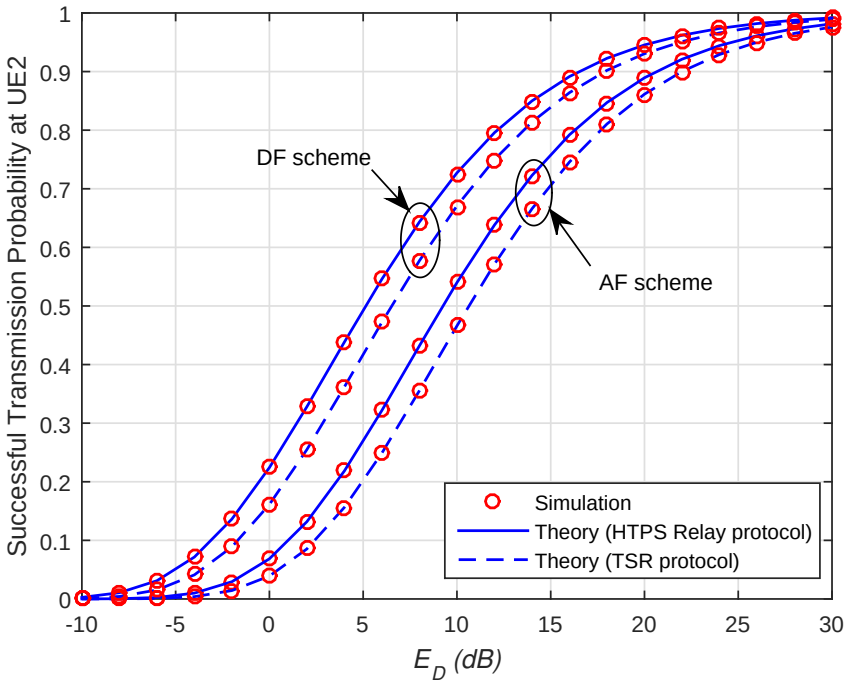

Fig. 6.2: STP versus E_D (dB) at UE2.

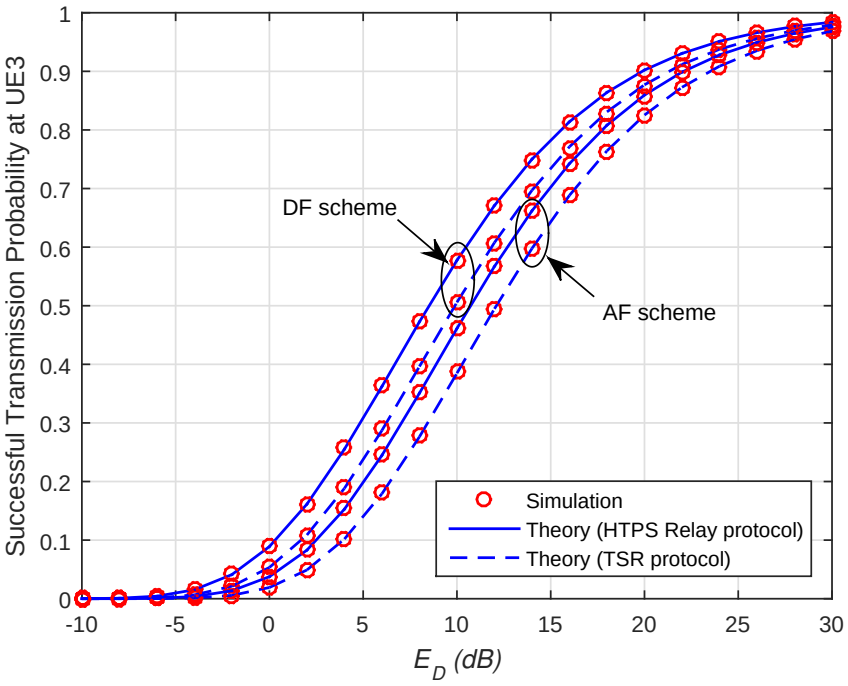

Fig. 6.3: STP versus E_D (dB) at UE3.

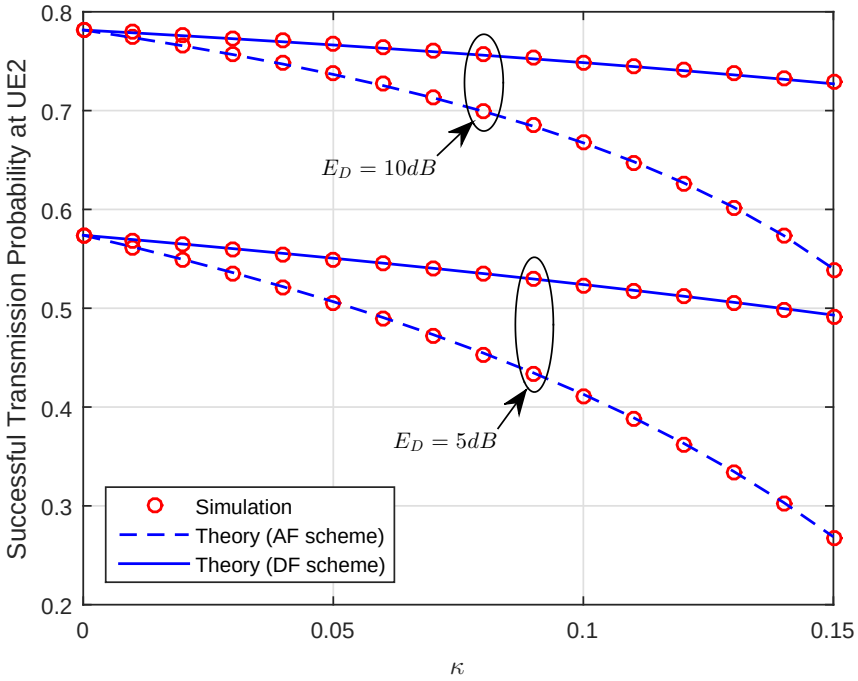

Fig. 6.4: STP versus HWIs level, κ with $E_D = 10dB$ and $E_D = 5dB$ at UE2.

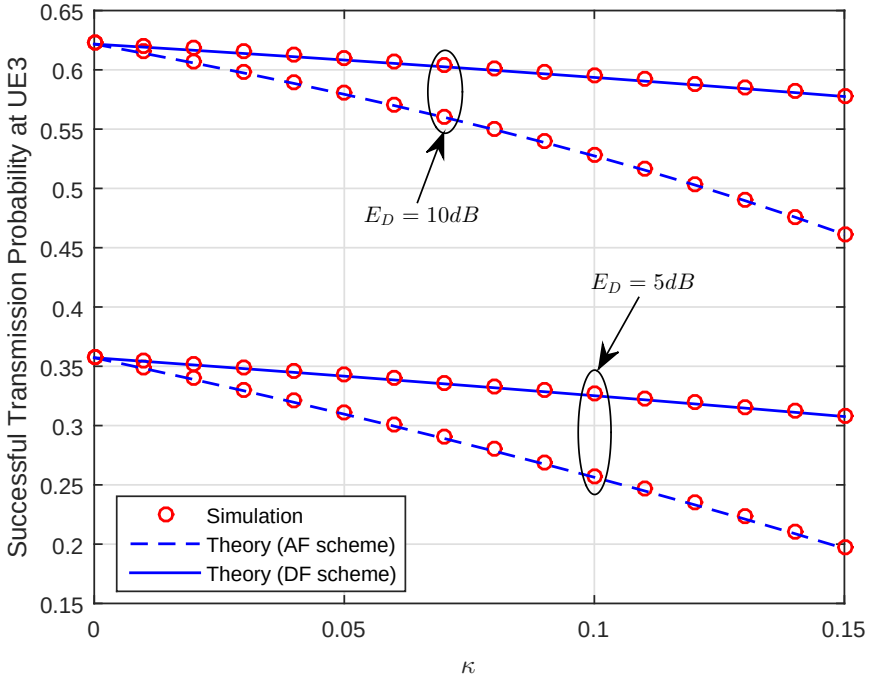

Fig. 6.5: STP versus HWIs level, κ with $E_D = 10dB$ or $E_D = 5dB$ at UE3.

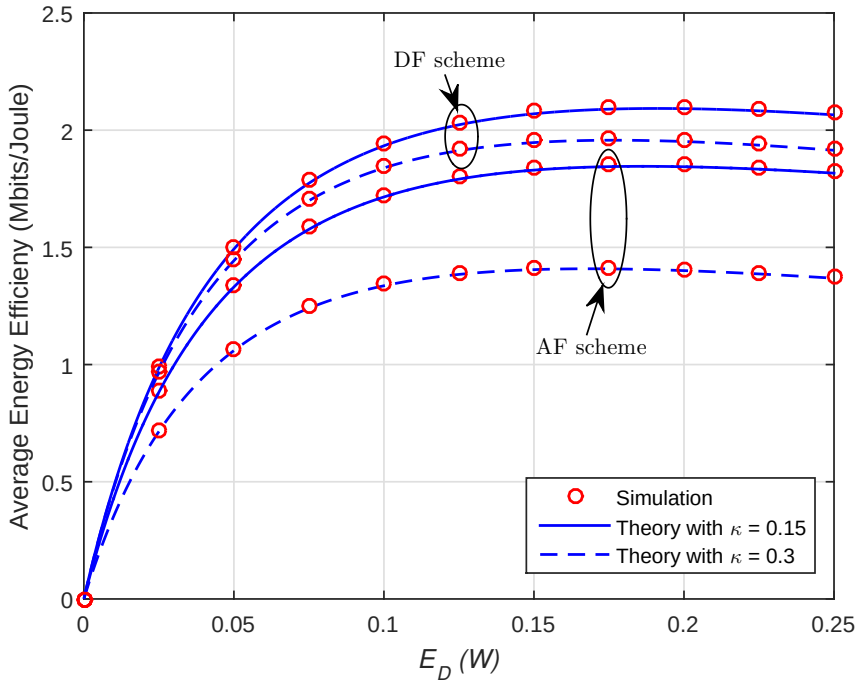

Fig. 6.6: Average EE versus E_D (W) at UE2.

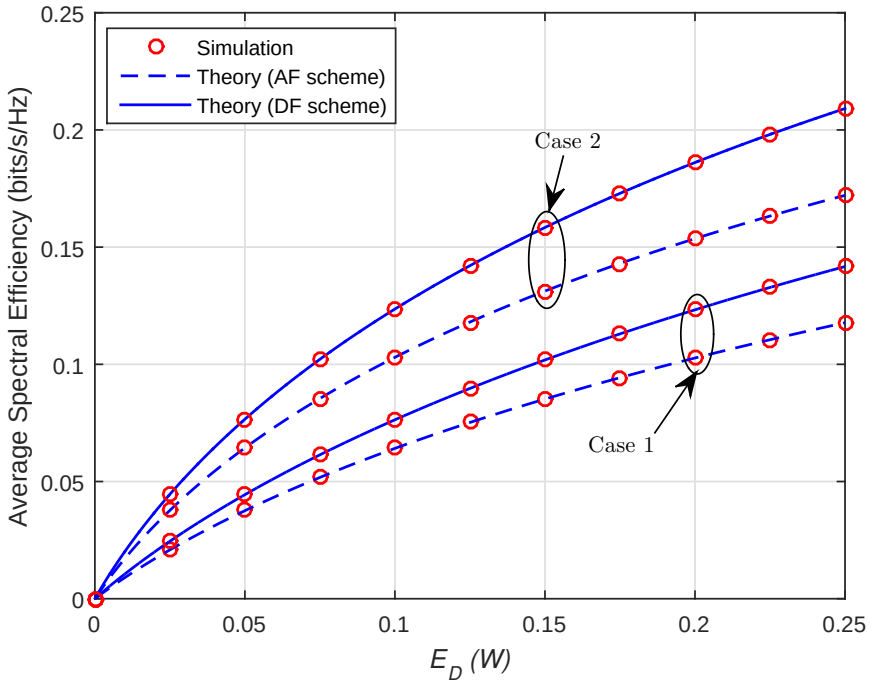

Fig. 6.7: Average SE versus E_D(W) in Case 1 and Case 2 at UE2.

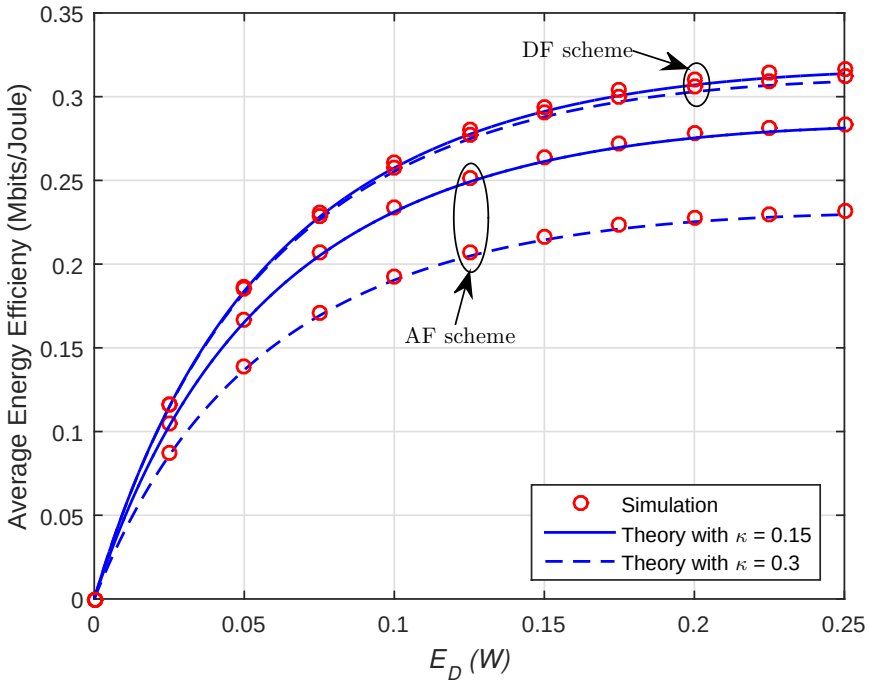

Fig. 6.8: Average EE versus E_D(W) at UE3.

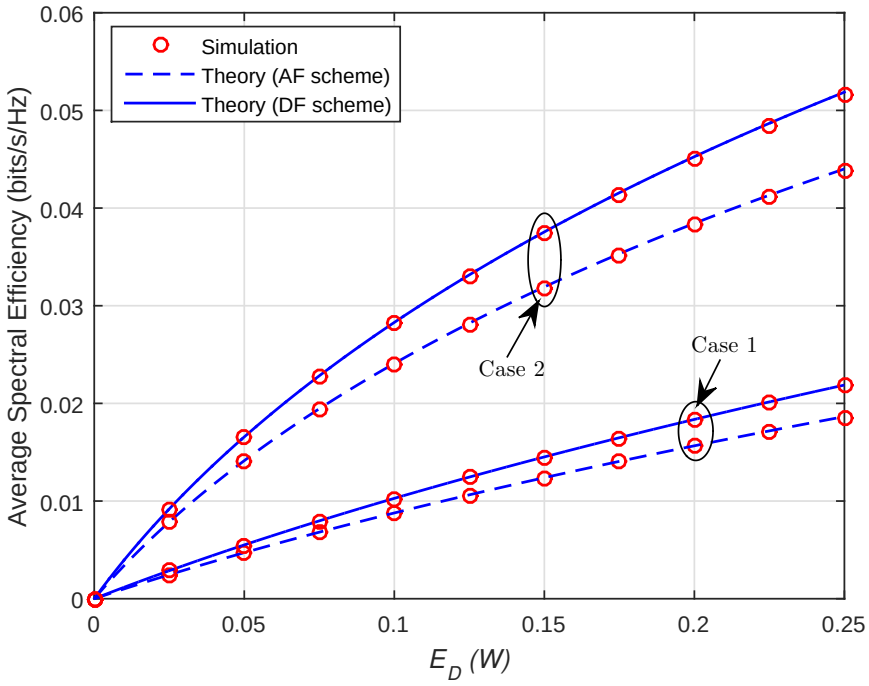

Fig. 6.9: Average SE versus E_D(W) in Case 1 and Case 2 at UE3.

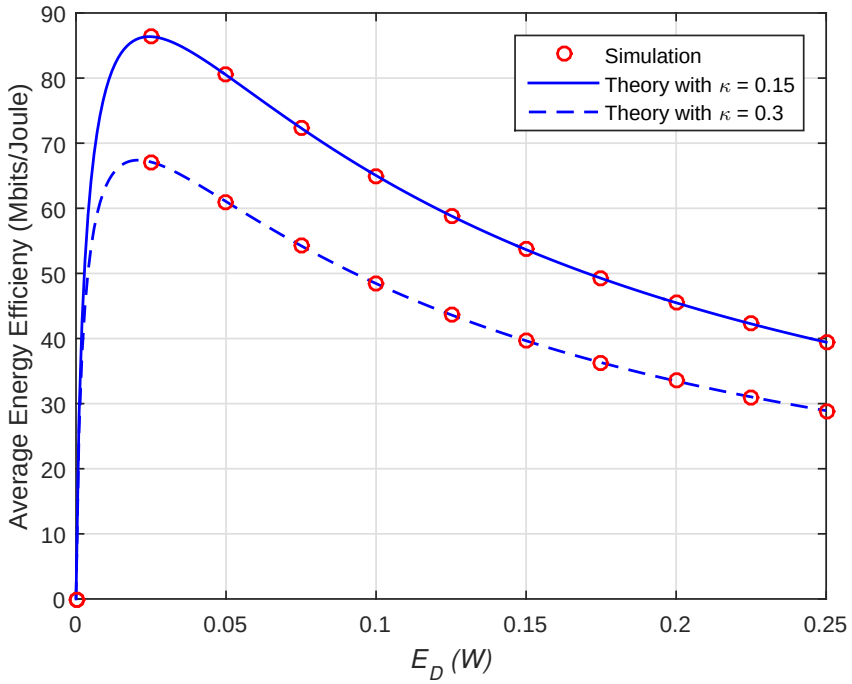

Fig. 6.10: Average EE versus E_D(W) in P2P communication under the impact of HWIs.

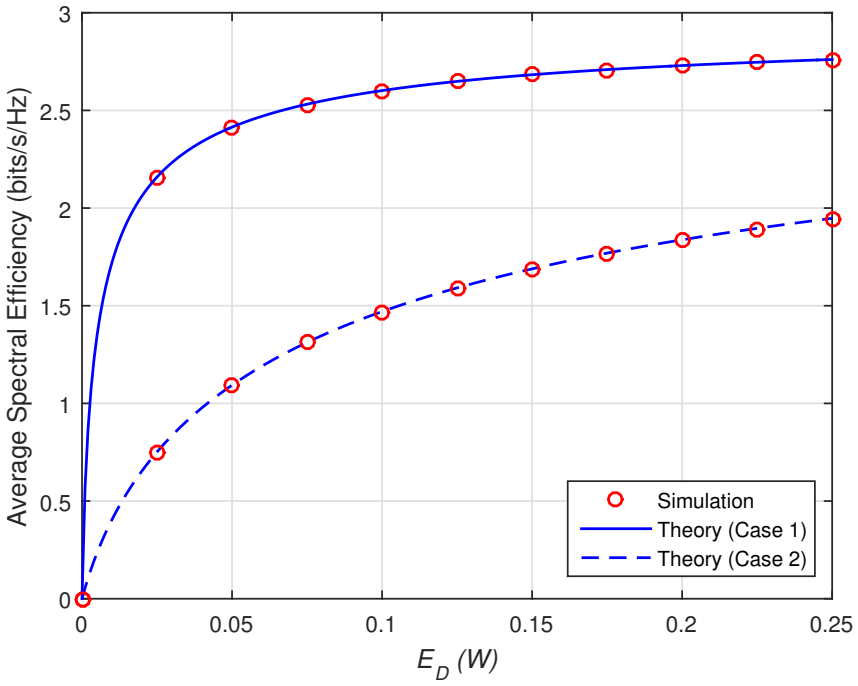

Fig. 6.11: Average SE versus E_D(W) in P2P communication under the impact of HWIs

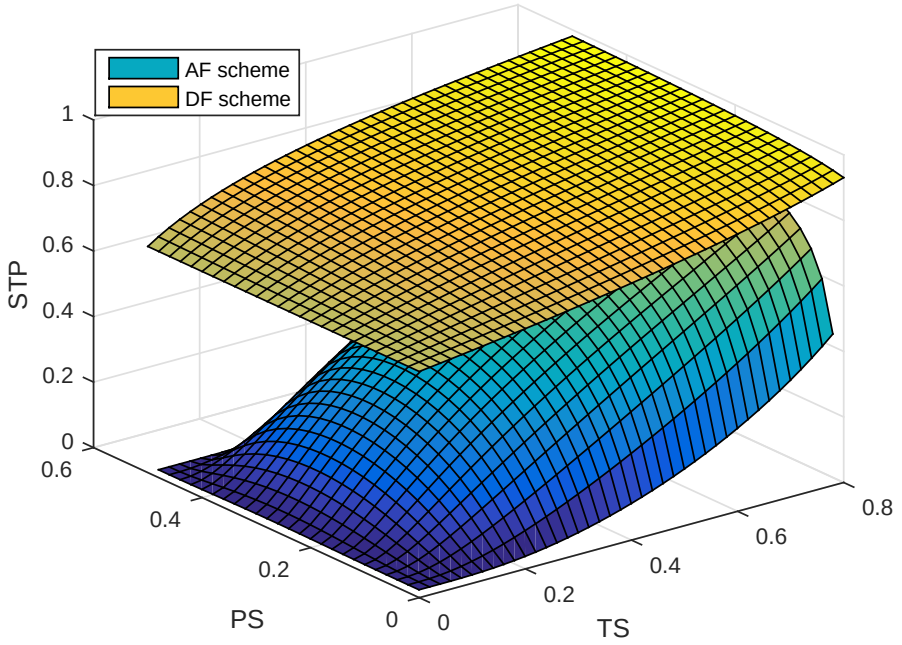

Fig. 6.12: STP versus TS and PS at UE2

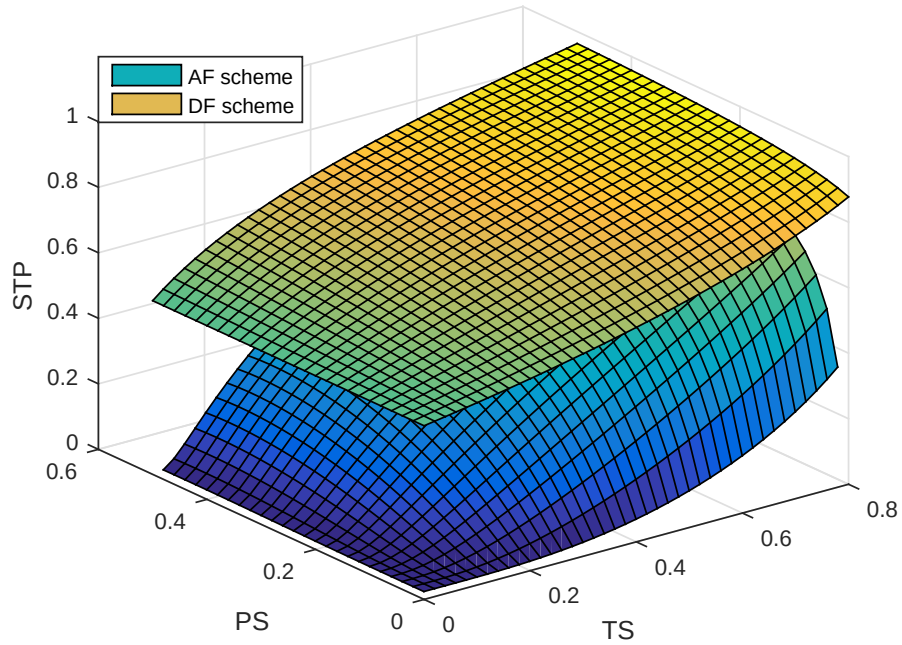

Fig. 6.13: STP versus TS and PS at UE3

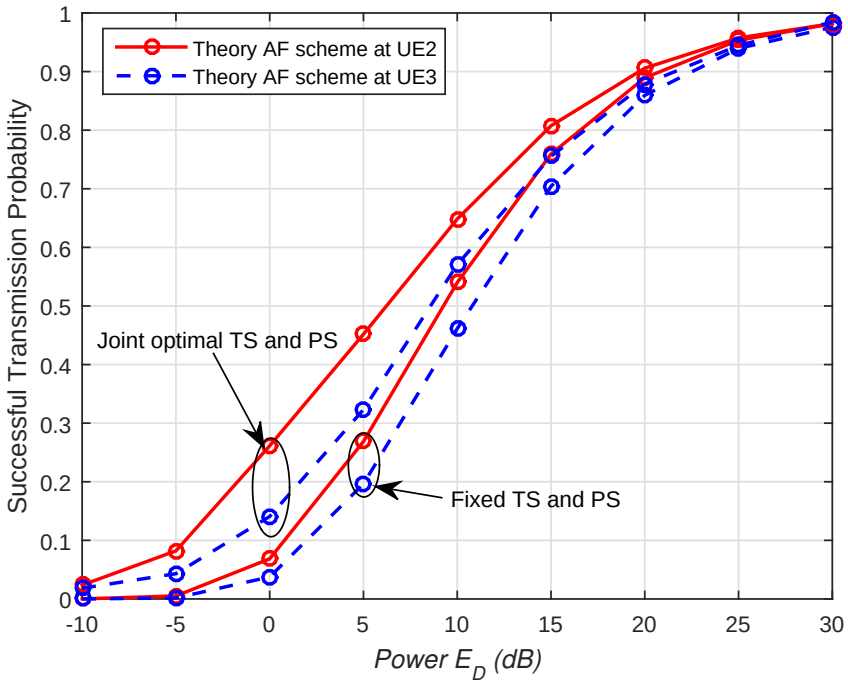

Fig. 6.14: STP versus E_D(dB) in AF scheme

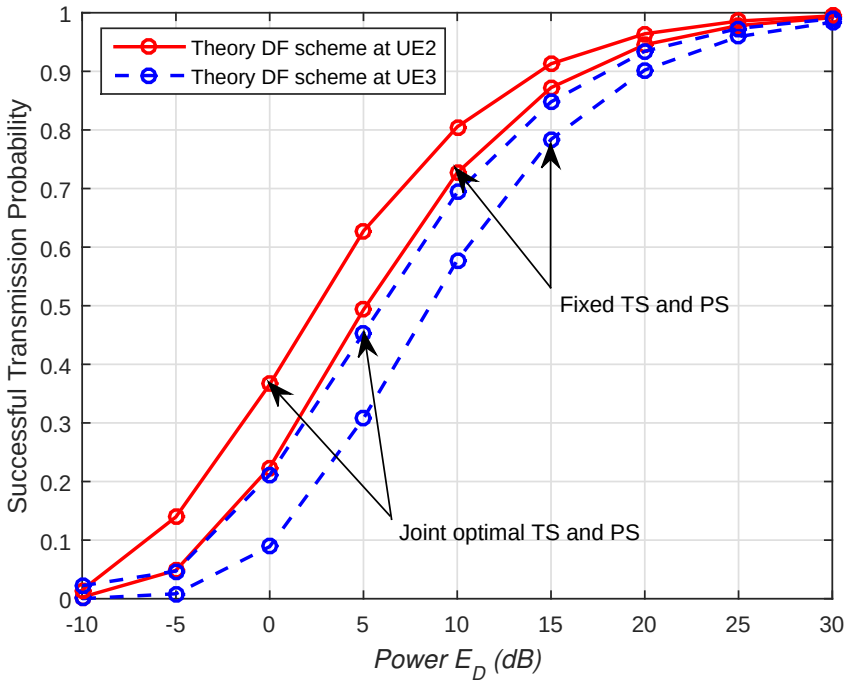

Fig. 6.15: STP versus E_D(dB) in DF scheme

$\kappa = 0.3$ are presented in Fig. 6.6, where the average EE is degraded considerably, e.g., when $\kappa = 0.3$, the average EE falls dramatically. Nevertheless, the locations of R in two cases, including Case 1: $(0.5, 0)$ and Case 2: $(0.3, 0)$ are spotted in Fig. 6.7, where Case 2 enjoys better SE, due to the close distance between UE2 and R, leading to better SE. Furthermore, the similar trends at UE3 are seen in Fig. 6.8 and Fig. 6.9, the average EE falls as E_D rises while the average SE increases, where the performance gap between Case 1 and Case 2 is clear when the nearer the communication between R and UE3 is, the better SE is achieved.

D. Average EE and average SE vs. E_D in the P2P communication

Fig. 6.10 shows the average EE and average SE as functions of E_D in P2P communication in case the distance between UE2 and UE3 is set to 5 Km. Meanwhile, Fig. 6.11 compares 2 cases of the distance between the two nodes, including Case 1: 5 km and Case 2: 10 km, respectively. It is easy to see that the EE first increases along with SE. After hitting the highest level ($\kappa = 0.15$) and ($\kappa = 0.3$), it drops when average SE increases. It is evident that $\kappa = 0.15$ shows SE is not affected much by HWIs, so it increases rapidly compared to the scenario when $\kappa = 0.3$.

E. Time switching and power splitting ratios under HWis at UE2 and UE3

In Fig. 6.12 and Fig. 6.13, visual results under different TS and PS ratios for UE2 and UE3 under the impact of HWIs are presented. The STP in case of HTPSR achieves its optimal values when the joint values of TS and PS varies between 0 and 0.7, 0 and 0.4, respectively with $E_D = 10dB$ and $\kappa = 0.15$.

F. The joint optimal value of α and β vs. E_D at UE2 and UE3

The optimization problem achieved in Section 6.3.5 can be presented in Fig. 6.14 and Fig. 6.15. In particular, we set the number of generations, constraint tolerance, and mutation probability as $N = 100$, $\epsilon = 10^{-5}$, and $p_m = 0.05$, respectively. The joint optimization is compared with the fixed values of TS and PS ratios with $\alpha_1 = \alpha_2 = \beta = 0.1$ at UE2 and UE3 in AF and DF scheme. We observe upward trends for all curves as E_D increases, because the higher E_D means larger SDNR, which increases the STP. In addition, the performance gain of the joint optimized TS and PS achieves maximum value when E_D reaches approximately 25dB.

6.5 Summary

In this paper, the impact of HWIs on the cognitive EH D2D communication underlaying cellular network consisting of two communication types, i.e., multi-hop D2D and P2P was discussed. Closed-form expressions for the STP, average EE and SE were derived, and

we solved the optimization problem of TS and PS ratios thanks to the deployment of a genetic algorithm (GA)-based optimization algorithm. With the simulation results, DF outperforms AF in terms of every performance metrics. The STP is guaranteed regardless of the existence of HWIs at all nodes.

7 TIME SLOTS IN TWO-WAY RELAYING NETWORKS

In this chapter, we study the performance of our two proposed PTSTW and PTSTH protocols for 2TS and 3TS. We provide expressions for OP, the optimization of throughput is also given. In particular, the throughput performance is studied in delay-limited and delay-tolerant transmission mode, where PTSTW outperforms PTSTH. In addition, delay-tolerant throughput is superior to the delay-limited throughput. We try to optimize TS and PS ratios to enhance the performance of the proposed schemes. It is evident from the simulation results that the placement of the relay node helps boosts the system performance [NHS06], [NHS07].

7.1 Motivation

To improve system bandwidth utilization, the two-way transmission mode was introduced in RNs. In particular, there are investigations carried out on bidirectional communication with helping of EH-assisted nodes. Combining AF and two-way transmission is also popular model in field of wireless technology. Regarding applications of AF two-way relay networks in green communication for 5G, the OP and ergodic capacity were analysed with PS receiver architecture protocol in [84]. Meanwhile, the authors in [32] proposed flexible policies for WPT to select the most appropriate S nodes for IT in TS and PS protocols. In [85], the source power, TS and PS ratios were jointly optimized to achieve the optimal sum rate. In addition, in [3], TWRN under the impact of HWIs was put forward, and the closed-form expression for throughput was derived to evaluate the trade-off between throughput and TS-PS ratios. In [33], the authors deployed TSR protocol for EH TWRNs. However, the time-slot processing problems should be focused on to have a nice balance between EH and IT.

Motivated from the aforementioned works, we come up with two EH relaying protocols, including PTSTW and PTSTH based on the proposed HTPSR protocol. They can help balance TS and PS ratios.

We organize this chapter as follows: the system model is presented in Section 2. Meanwhile, the SNR of the two proposed schemes, including 2TS and 3TS in TWRN is studied Section 3. Next, we obtain the expression for OP and throughput in Section 4. Section 5 provides simulation results. Eventually, we write a brief a conclusion for this chapter in Section 6.

7.2 System Model

In Fig. 7.1, we take a HD AF TWRN consisting of two S nodes, A and B into consideration. In the communication process, an EH R is deployed to assist the communication between the two nodes. It is noted that a single antenna is equipped at each node. In particular,

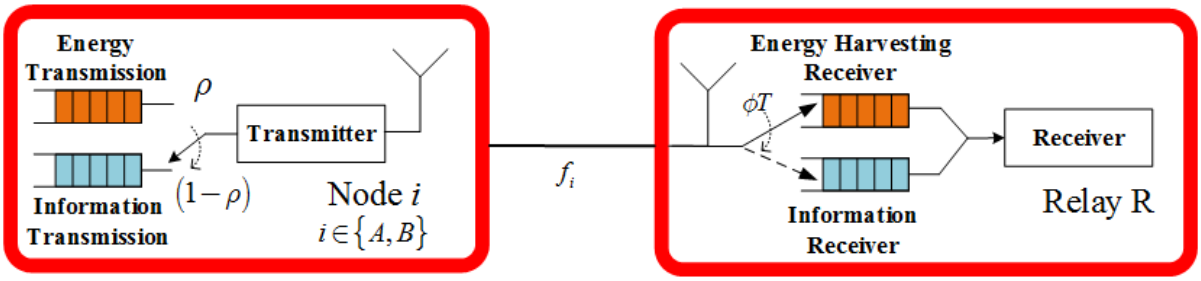

Fig. 7.1: The structure of PS and TS protocol for each pair of S-R

[2 Time Slot]

Phase 1		Phase 2
(ρP) EH at (R) from (A) and (B)	$((1-\rho)P)$ Information Transmission (IT) (A) → (R), (B) → (R)	Information Transmission (R) → (A) (R) → (B)
ϕT	$(1-\phi)T/2$	$(1-\phi)T/2$

[3 Time Slot]

Phase 1		Phase 2		Phase 3
(ρP) EH at (R) from (A)	$((1-\rho)P)$ IT (A) → (R)	(ρP) EH at (R) from (B)	$((1-\rho)P)$ IT (B) → (R)	Information Transmission (R) → (A) (R) → (B)
$\phi T/2$	$(1-\phi)T/3$	$\phi T/2$	$(1-\phi)T/3$	$(1-\phi)T/3$

T

Fig. 7.2: PTSTW and PTSTH protocols for 2TS and 3TS transmission scheme.

the transmit power at S node, i is denoted as P_i to transmit the data symbol x_j, where $i, j \in \{A, B\}$ and $i \neq j$. The Rayleigh fading channel between i and R is represented by $f_i \sim CN(0, \Omega_i)$, and the noise term is distributed by AWGN at $n_i \sim CN(0, \sigma_i^2)$, at R $n_R \sim CN(0, \sigma_R^2)$.

We describe how TS and PS function in this chapter in Fig. 7.1. In particular, the transmit power, ρP is used to transfer EH to R while $(1-\rho)\,P$ is responsible for IT from S nodes to R.

In Fig. 7.2, we clarify the TS coefficient of the proposed protocols, where the block time is T, and ϕT is allocated for R for EH from both S nodes while the remaining time, $(1-\phi)\,T$ is utilized for IT. Regarding EH time, ϕT is divided into two equal durations for 3TS scheme and each duration, $\phi T/2$ while ϕT is used for EH in 2TS scheme. The IT time $(1-\phi)\,T$ is divided into two equal durations for 2TS, and three durations for 3TS, and each duration $(1-\phi)\,T/2$ and $(1-\phi)\,T/3$, respectively. A and B node transfer its data to R in the first $(1-\phi)\,T/2$ of 2TS, and A (or B) transmits its information to R during the first two $(1-\phi)\,T/3$ durations of 3TS. Besides, R broadcasts to the two

S nodes in the remaining time. When information is received at either node, it is then decoded based on the knowledge of CSI.

In our proposed protocols, the power allocation, ρ, which is used to process the transmit signal, x_C, can be written as

$$x_C \underset{i\in\{A,B\}}{=} \sqrt{\rho}P_i x_E + \sqrt{(1-\rho)}P_i x_i, \tag{7.1}$$

where x_E describes the energy capability while x_i represents the IT process which satisfy $E\left\{|x_E|^2\right\} = 1$, $E\left\{|x_i|^2\right\} = 1$, respectively and $i \in \{A, B\}$.

The distances of $R \to i$ or $R \to j$ are denoted as $d_{R,i}$ or $d_{R,j}$ while m is denoted as the path loss exponent. The location allocation of R is presented by ϵ, in which each hop is $i \to R$ and $j \to R$ with d_{ij} being the distance of i node and j node. Therefore, we can obtain

$$d_{R,j} = \epsilon d_{R,i}, \tag{7.2}$$

then we have

$$\frac{d_{R,A}}{d_{AB}} = \frac{1}{1+\epsilon} \quad and \quad \frac{d_{R,B}}{d_{AB}} = \frac{\epsilon}{1+\varepsilon}. \tag{7.3}$$

7.3 SNR in two schemes of bidirectional relaying

In Fig. 7.2, we represent 2TS in its phase 1 of the transmission process, and phase 1 and phase 2 of 3TS for i to transfer power and information to R, respectively. In addition, the remaining phase of both time slots is used for R to transfer the received data to node i.

It is evident that there is a trade-off between the amount of power transferred and information decoding. Therefore, we are going to HTPSR which is computed in one-way RNs as below

$$E_{h,i}^{HTPSR} = \lambda\eta P_i d_{R,i}^{-m}\rho|f_i|^2, \tag{7.4}$$

where $0 < \eta < 1$ denotes energy conversion efficiency which depends on the quality of power collection circuits, $\lambda = \phi T$ (for PTSTW protocol), and $\lambda = \phi T/2$ (for PTSTH protocol).

However, in TWRNs, we can calculate the transmitted power from R as

$$P_R^{PTSTW} = \frac{\left(E_{h,A}^{PTSR} + E_{h,B}^{PTSR}\right)}{(1-\phi)T/2} = \frac{2\eta\phi\rho}{(1-\phi)}\left(\sum_{\substack{\{i,j\}\in\{A,B\}\\ i\neq j}} \frac{P_i}{d_{R,i}^m}|f_i|^2\right), \tag{7.5}$$

and

$$P_R^{PTSTH} = \frac{\left(E_{h,A}^{PTSR} + E_{h,B}^{PTSR}\right)}{(1-\phi)\,T/3} = \frac{3\eta\phi\rho}{2\,(1-\phi)}\left(\sum_{\substack{\{i,j\}\in\{A,B\}\\ i\neq j}} \frac{P_i}{d_{R,i}^m}|f_i|^2\alpha_j^2\right), \tag{7.6}$$

where the power allocation, α_A and α_B must satisfy the condition, $\alpha_A^2 + \alpha_B^2 = 1$.

7.3.1 Power splitting-based and time switching-based 2TS relaying protocol (PTSTW)

Regarding this protocol, phase 1 describes the communication between both A and B and R. As a result, data is amplified and forwarded to the two S nodes in phase 2. Therefore, the received signal in phase 1 can be given as

$$y_{R}^{PTSTW} = \sqrt{\frac{P_A}{d_{R,A}^m}} f_A x_A + \sqrt{\frac{P_B}{d_{R,B}^m}} f_B x_B + n_R. \tag{7.7}$$

The received signal is used for IT in phase 2, R broadcasts signals to two S nodes. Hence, the transmitted signal can be calculated by

$$x_{R}^{PTSTW} = G^{PTSTW} \sqrt{P_{R}^{PTSTW}} \left(\sqrt{1-\rho} y_{R}^{PTSTW} \right), \tag{7.8}$$

where the amplification factor is G^{PTSTW} which is random in the presence of immediate CSI. In order to restrict the instantaneous transmit power, statistical noise should be at high SNR.

The energy constraint, G^{PTSTW} of R can be computed as

$$\left(G^{PTSTW} \right)^2 \approx \left((1-\rho) \left(\frac{P_A}{d_{R,A}^m} |f_A|^2 + \frac{P_B}{d_{R,B}^m} |f_B|^2 \right) \right)^{-1}, \tag{7.9}$$

where $\sigma_R^2 \approx 0$ is at high SNR. The received signal in phase 2 at two S nodes can be expressed as

$$y_{i}^{PTSTW} = f_i x_{R}^{PTSTW} + n_i. \tag{7.10}$$

It is noted that due to the knowledge of the received channel, SI can be eliminated. Therefore, we can obtain the expression obtained in (7.10) again by

$$\begin{aligned} y_{i}^{PTSTW} = & \underbrace{\sqrt{1-\rho} \sqrt{\frac{P_j}{d_{R,j}^m}} \sqrt{P_{R}^{PTSTW}} G^{PTSTW} f_i f_j x_j}_{signal} \\ & + \underbrace{\sqrt{P_{R}^{PTSTW}} G^{PTSTW} f_i n_R + n_i}_{noise} \end{aligned} \tag{7.11}$$

where $i, j \in \{A, B\}$ and $i \neq j$.

Lemma 7.1. Based on $\gamma_i^{PTSTW} = \frac{E(signal)^2}{E(noise)^2}$, replacing (7.3),(7.5), (7.9) into (7.11), the SNRs at A and B node can be given as

$$\gamma_{A}^{PTSTW} = \left(\frac{1+\varepsilon}{\varepsilon d_{AB}} \right)^m \frac{P_B (1-\rho) |f_A|^2 |f_B|^2}{\left(|f_A|^2 \sigma_R^2 + \frac{(1-\rho)(1-\phi)\sigma_A^2}{2\eta\phi\rho} \right)}, \tag{7.12a}$$

and

$$\gamma_{B}^{PTSTW} = \left(\frac{1+\varepsilon}{d_{AB}} \right)^m \frac{P_A (1-\rho) |f_A|^2 |f_B|^2}{\left(|f_B|^2 \sigma_R^2 + \frac{(1-\rho)(1-\phi)\sigma_B^2}{2\eta\phi\rho} \right)}. \tag{7.12b}$$

7.3.2 Power splitting-based and time switching-based 3TS relaying protocol (PTSTH)

With this proposed protocol, the received signal at R is presented by

$$y_{R,i}^{PTSTH} = \sqrt{\frac{P_i}{d_{R,i}^m}} f_i x_i + n_{R,i}, \tag{7.13}$$

where the AWGN term can be defined as $n_{R,i} = n_{R,j} = n_R$, and $n_R \sim CN(0, \sigma_R^2)$.

Next, the transmitted signal at R is written as

$$x_R^{PTSTH} = G^{PTSTH} \sqrt{P_R^{PTSTH}} \sum_{\substack{\{i,j\}\in\{A,B\} \\ i\neq j}} \left(\alpha_j \sqrt{(1-\rho)} y_i^{PTSTH} \right). \tag{7.14}$$

Similarly, the energy constraint, G^{PTSTH} of R in this protocol is given as

$$\left(G^{PTSTH}\right)^2 \approx \left(\sum_{\substack{\{i,j\}\in\{A,B\} \\ i\neq j}} \left(\frac{P_i}{d_{R,i}^m} (1-\rho) \alpha_j^2 |f_i|^2 \right) \right)^{-1}. \tag{7.15}$$

In phase 3, the received signal at A and B is computed by

$$\begin{aligned} y_i^{PTSTH} &= f_i x_R^{PTSTH} + n_i \\ &= \sum_{\substack{\{i,j\}\in\{A,B\} \\ i\neq j}} \left(\alpha_j \sqrt{(1-\rho)} \sqrt{\frac{P_i}{d_{R,i}^m}} f_i x_i + \alpha_j n_R \right) \sqrt{P_R^{PTSTH}} G^{PTSTH} f_i + n_i \ , \end{aligned} \tag{7.16}$$

As in (7.11), we write the received signal at A and B as

$$\begin{aligned} y_i^{PTSTH} = &\left(\underbrace{f_i \sqrt{P_R^{PTSTH}} G^{PTSTH} \alpha_i \sqrt{(1-\rho)} \sqrt{\frac{P_j}{d_{R,j}^m}} f_j x_j}_{signal} \right) \\ &+ \underbrace{\left(f_i \sqrt{P_R^{PTSTH}} G^{PTSTH} \left(\alpha_j + \alpha_i\right) n_R + n_i \right)}_{noise}. \end{aligned} \tag{7.17}$$

According to *Lemma* 7.1, the SNRs at A and B are expressed as

$$\gamma_i^{PTSTH} = \frac{1}{d_{R,j}^m} \left(\frac{\alpha_i^2 (1-\rho) P_j P_R^{PTSTH} \left(G^{PTSTH}\right)^2 |f_i|^2 |f_j|^2}{(1-\rho) P_R^{PTSTH} (G^{PTSTH})^2 \sigma_R^2 |f_i|^2 + \sigma_i^2} \right). \tag{7.18}$$

Substituting (7.3), (7.6) and (7.15) into (7.18), the output SNRs at A and B are written as

$$\gamma_A^{PTSTH} = \left(\frac{1+\varepsilon}{\varepsilon d_{AB}} \right)^m \left(\frac{\alpha_A^2 (1-\rho) P_B |f_A|^2 |f_B|^2}{|f_A|^2 \sigma_R^2 + \frac{2(1-\phi)(1-\rho)\sigma_A^2}{3\eta\phi\rho}} \right), \tag{7.19a}$$

and

$$\gamma_B^{PTSTH} = \left(\frac{1+\varepsilon}{d_{AB}} \right)^m \left(\frac{\alpha_B^2 (1-\rho) P_A |f_A|^2 |f_B|^2}{|f_B|^2 \sigma_R^2 + \frac{2(1-\phi)(1-\rho)\sigma_B^2}{3\eta\phi\rho}} \right). \tag{7.19b}$$

7.4 Performance Analysis

In this section, we are going to derive expressions for OP and throughput for 2TS and 3TS in the proposed protocols. In principle, thanks to achievements SNR expressions, the transmission rate at A and B is calculated by

$$R_i^{PTSTx} = \frac{1}{u}\log_2(1+\gamma_i^{PTSTx}), \tag{7.20}$$

where $i \in \{A, B\}$ and $\begin{cases} x = W, u = 2 \\ x = H, u = 3 \end{cases}$.

7.4.1 Outage Probability

In such TWRNs, OP is defined as a probability when SNR is less than the threshold values of SNR. OP is used to measure the quality of communication links. Therefore, the OP in this chapter can be expressed by

$$\begin{aligned} OP^{PTSTx} &= Pr\left(R_A < R_{A,0}^{PTSTx}, \text{or} \quad R_B < R_{B,0}^{PTSTx}\right) \\ OP^{PTSTx} &= Pr\left(\gamma_A < \gamma_{A,0}^{PTSTx}, \text{or} \quad \gamma_B < \gamma_{B,0}^{PTSTx}\right) \\ &= Pr\left(\gamma_A < \gamma_{A,0}^{PTSTx}\right) + Pr\left(\gamma_B < \gamma_{B,0}^{PTSTx}\right) \\ &\quad -Pr\left(\gamma_A < \gamma_{A,0}^{PTSTx} \quad \text{and} \quad \gamma_B < \gamma_{B,0}^{PTSTx}\right) \\ &\approx OP_A^{PTSTx} + OP_B^{PTSTx} - OP_A^{PTSTx} OP_B^{PTSTx}, \end{aligned} \tag{7.21}$$

where $\gamma_{i,0}^{PTSTx} = 2^{uR_{i,0}^{PTSTx}} - 1$, and $R_{i,0}^{PTSTx}$ denotes the target rate of A and B.

Proposition 7.1. The OP at A and B is expressed by

$$OP_A^{PTSTx} = F_{\gamma_A}^{PTSTx}\left(\gamma_{A,0}^{PTSTx}\right) = 1 - 2\exp\left(-\frac{\varepsilon^m U_1^{PTSTx}\gamma_{A,0}^{PTSTx}}{U_2^{PTSTx}\Omega_A}\right)\mu_A K_1\left(2\mu_A\right), \tag{7.22a}$$

and

$$OP_B^{PTSTx} = F_{\gamma_B}^{PTSTx}\left(\gamma_{B,0}^{PTSTx}\right) = 1 - 2\exp\left(-\frac{U_1^{PTSTx}\gamma_{B,0}^{PTSTx}}{U_2^{PTSTx}\Omega_B}\right)\mu_B K_1\left(2\mu_B\right), \tag{7.22b}$$

where

$$\begin{aligned} &U_1^{PTSTx} = (d_{AB})^m\sigma_R^2,\ U_2^{PTSTx} = l\,(1-\rho)\,(1+\varepsilon)^m,\ U_3^{PTSTx} = v\frac{(1-\rho)(1-\phi)(d_{AB})^m}{\eta\phi\rho}, \\ &\text{for node A:} \quad \mu_A = \sqrt{\frac{\varepsilon^m U_3^{PTSTx}}{U_2^{PTSTx}\Omega_A\Omega_B}\gamma_{A,0}^{PTSTx}}, \quad \begin{cases} x = W, l = P_B, v = \sigma_A^2/2 \\ x = H, l = \alpha_A^2 P_B, v = 2\sigma_A^2/3 \end{cases} \\ &\text{for node B:} \quad \mu_B = \sqrt{\frac{U_3^{PTSTx}}{U_2^{PTSTx}\Omega_A\Omega_B}\gamma_{B,0}^{PTSTx}}, \quad \begin{cases} x = W, l = P_A, v = \sigma_B^2/2 \\ x = H, l = \alpha_B^2 P_A, v = 2\sigma_B^2/3 \end{cases} \end{aligned}$$

Proof: See in Appendix B.

Substituting (7.22) into (7.21), the OP of the two S nodes can be approximated as

$$OP^{PTSTx} \approx 2 - \left(\Upsilon_A^{PTSTx} + \Upsilon_B^{PTSTx}\right) - \left[\left(1 - \Upsilon_A^{PTSTx}\right) \times \left(1 - \Upsilon_B^{PTSTx}\right)\right], \tag{7.23}$$

where $\Upsilon_A^{PTSTx} = \exp\left(-\varepsilon^m \frac{U_1^{PTSTx}\gamma_{A,0}^{PTSTx}}{U_2^{PTSTx}\Omega_A}\right) 2\mu_A K_1(2\mu_A)$ and
$\Upsilon_B^{PTSTx} = \exp\left(-\frac{U_1^{PTSTx}\gamma_{B,0}^{PTSTx}}{U_2^{PTSTx}\Omega_B}\right) 2\mu_B K_1(2\mu_B)$.

In order to find the approximation expression, we should derive the upper and lower bound of the OP at A and B for the transmission schemes as below

$$\begin{aligned} &OP^{PTSTx} \le \min\left(1, \Pr\left(\gamma_A^{PTSTx} < \gamma_{A,0}^{PTSTx}\right) + \Pr\left(\gamma_B < \gamma_{B,0}^{PTSTx}\right)\right) = P_{out,up}^{PTSTx}, \\ &\text{and} \\ &OP_{low}^{PTSTx} = \max\left(\Pr\left(\gamma_A^{PTSTx} < \gamma_{A,0}^{PTSTx}\right), \Pr\left(\gamma_B^{PTSTx} < \gamma_{B,0}^{PTSTx}\right)\right) \le OP^{PTSTx}, \end{aligned} \tag{7.24}$$

where $\Pr\left(\gamma_i^{PTSTx} < \gamma_{i,0}^{PTSTx}\right) = P_{out,i}^{PTSTx}$ and $i \in \{A, B\}$, $x \in \{W, H\}$.

7.4.2 Throughput Analysis

In this part, two transmission modes are derived, including delay-limited transmission and delay-tolerant transmission.

A. Delay-limited transmission

Here, the throughput in this case is evaluated by the knowledge of OP in case the source transmission rate is fixed as R_0^{PTSTx} (bps/Hz), where $R_0^{PTSTx} = \frac{1}{2}\log_2\left(1 + \gamma_0^{PTSTx}\right)$ with γ_0^{PTSTx} being the threshold SNRs.

Therefore, the throughput is calculated by

$$\tau_{DL}^{PTSTx} = \frac{(1-\phi)}{u}(1 - OP^{PTSTx})R_0^{PTSTx}, \tag{7.25}$$

where the 2TS or 3TS TWRN is defined by $u = 2$ or $u = 3$, respectively.

B. Delay-tolerant transmission

Regarding the delay-tolerant throughput, S transmits data at a fixed rate set below the ergodic capacity. Hence, we compute the ergodic capacity as

$$\begin{aligned} \tau_{DT}^{PTSTx} &= \tfrac{1}{2}\tfrac{(1-\varphi)T}{uT}\left(E\left\{\log_2\left(1+\gamma_A^{PTSTx}\right)\right\} + E\left\{\log_2\left(1+\gamma_B^{PTSTx}\right)\right\}\right) \\ &= \tfrac{1}{2}\tfrac{(1-\varphi)}{u\ln 2}\int_{z=0}^{\infty}\left(\chi_A^{PTSTx} + \chi_B^{PTSTx}\right)(1+z)^{-1}dz, \end{aligned} \tag{7.26}$$

where $\chi_A^{PTSTx} = \exp\left(-\varepsilon^m \frac{U_1^{PTSTx} z}{U_2^{PTSTx}\Omega_A}\right)\mu_1 K_1(\mu_1)$, $\mu_1 = \sqrt{4\varepsilon^m \frac{U_3^{PTSTx}}{U_2^{PTSTx}\Omega_A\Omega_B} z}$ and $\chi_B^{PTSTx} = \exp\left(-\frac{U_1^{PTSTx} z}{U_2^{PTSTx}\Omega_B}\right)\mu_2 K_1(\mu_2)$, $\mu_2 = \sqrt{4\frac{U_3^{PTSTx}}{U_2^{PTSTx}\Omega_A\Omega_B} z}$.

Remark 7.2. It is noted that the obtained expressions for OP and throughput are based on the joint of TS and PS ratios, ϕ and ρ. Nevertheless, to provide closed-form expressions of optimal TS and PS ratios is complication. Therefore, we are going to find the

optimal values of ϕ and ρ by numerical methodology. In addition, the throughput performance is dependent on the position allocation of R. Similarly, the findings of optimal location cannot be solved in closed-form expressions, and the optimal allocation can then be calculated through simulations.

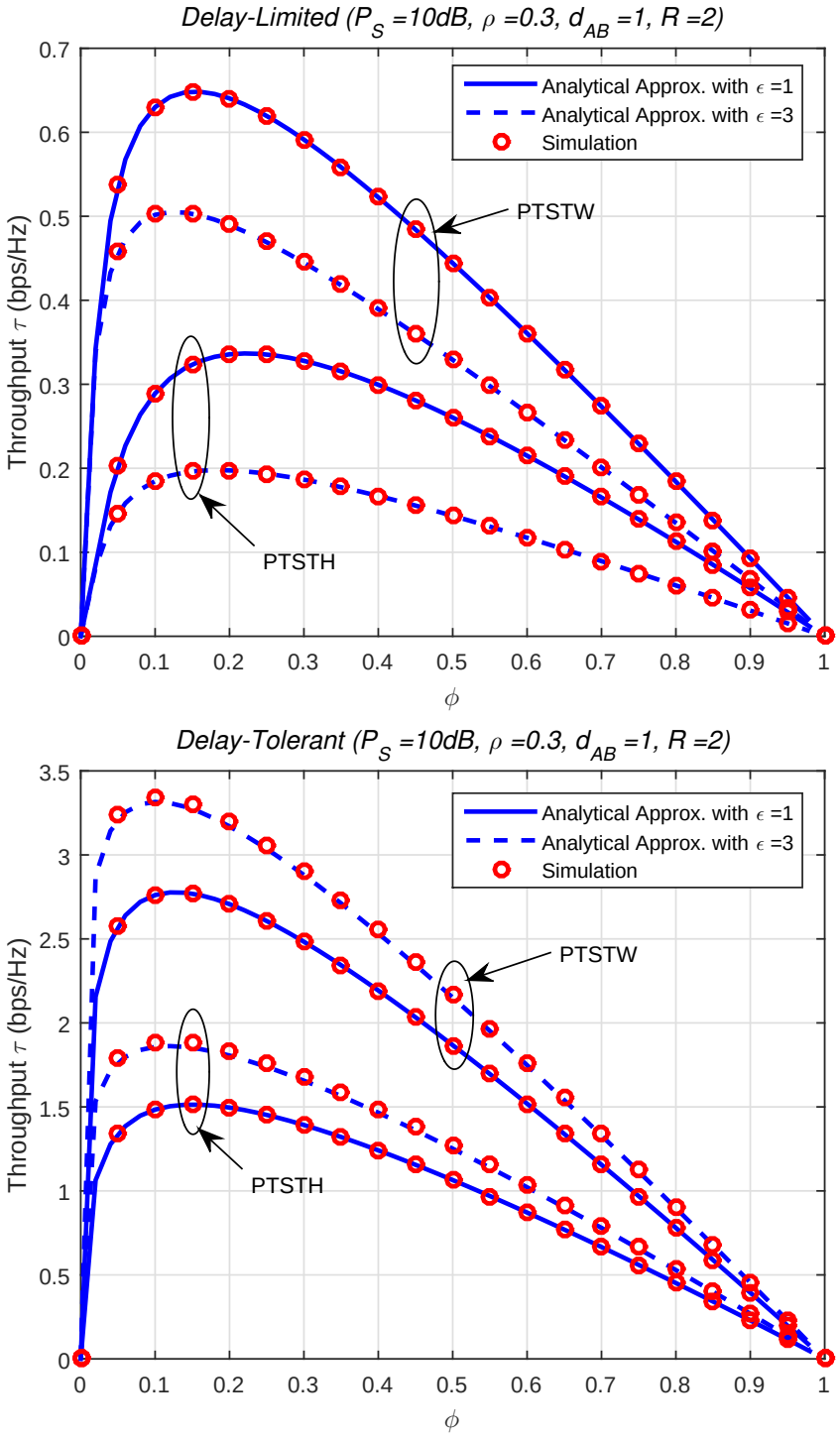

Fig. 7.3: Throughput τ at destination node in delay-limited and delay-tolerant modes vs. ϕ

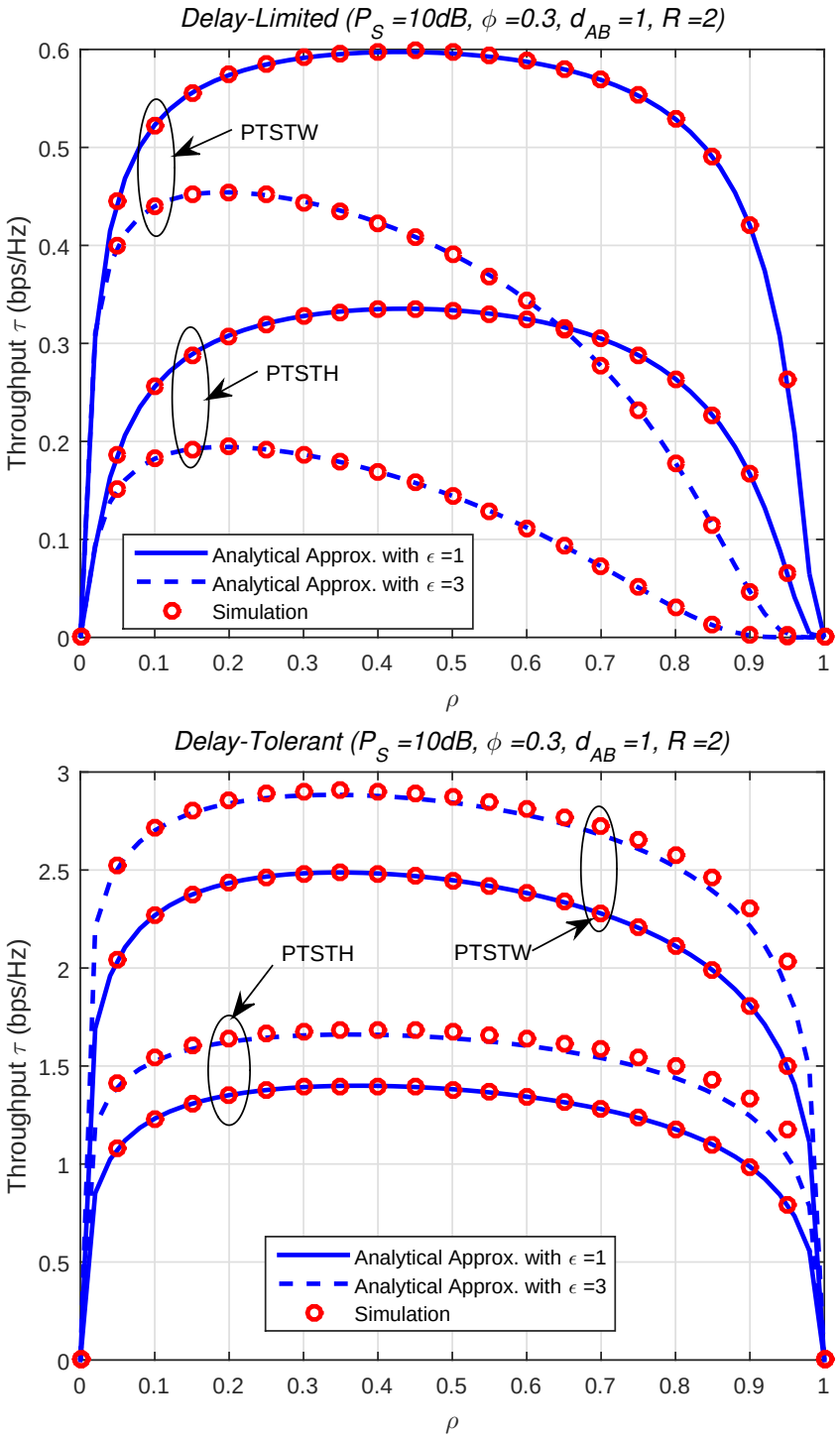

Fig. 7.4: Throughput τ at destination node in delay-limited and delay-tolerant mode with different ρ

7.5 Numerical results

In this section, we are going to achieve the optimal value of throughput relying on ρ and ϕ in the proposed protocols based on HPTSR protocol, including PTSTW and PTSTH in delay-limited and delay-tolerant transmission modes. The simulation results follow some parameters specified in Table 7.1.

Parameters	**Values**
Power transmission, P_S	10(dB)
Energy conversion efficiency, η	1
TS ratios, ϕ	0.3
PS ratio, ρ	0.3
Distance of A-B, d_{AB}	1
The location allocation, ϵ	1
SNR threshold, R	2

Tab. 7.1: Main Simulation Parameters (TS in Two-way)

We consider ϕ to achieve the optimal throughput in Fig. 7.3. It is clear that as ϕ increases from 0 to approximate 0.2 throughput dramatically rises. However, as ϕ exceeds its optimal value, the throughput drops because of the trade-off between IT and EH. In particular, the delay-limited throughput is outperformed by the delay-tolerant throughput, because we assume the delay time to be zero for delay-tolerant mode. Besides, the delay-limited throughput for PTSTW and PTSTH with $\epsilon = 1$ is greater than that of $\epsilon = 3$, while the delay-tolerant throughput with $\epsilon = 1$ is less than that of $\epsilon = 3$. Besides, the throughput of PTSTW outperforms that of PTSTH because the amount of time used for information processing in PTSTW is huge which leads to higher throughput compared to PTSTH.

In Fig. 7.4, we can see that the delay-limited throughput is worse than delay-tolerant throughput. In addition, the value of throughput with $\epsilon = 1$ and $\epsilon = 3$ in two modes have the similar trends as shown in Fig.7.3. Throughput increases significantly when ρ rises from 0 to its optimal value, later dropping when ρ reaches its optimal factor.

The OP in delay-limited mode is presented in Fig. 7.5. In particular, the OP of PTSTW is worse than PTSTH. Furthermore, HTPSR protocol enjoys better outage performance than TSR, since the transmit power at S supplies the EH circuit at R in TSR protocol while only small fraction of such power is used for the proposed protocols based on HPTSR, e.g., PTSTW, and PTSTH.

The OP of PTSTH protocol is illustrated in Fig. 7.6, where it is proved to be better than PTSTW in delay-limited mode. In addition, they both see similar trends. It is noted that when m rises, the OP drops, and outage probability increases as a function of ϵ. As a consequence, the impact of location of each node has an impact on the system performance.

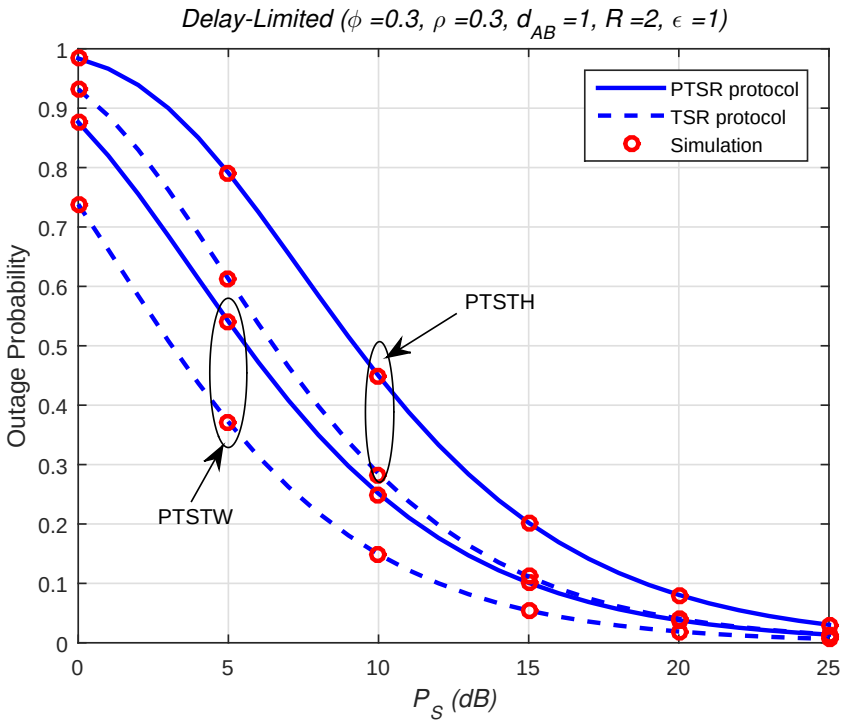

Fig. 7.5: OP at destination node in delay-limited mode vs. P_S (dB)

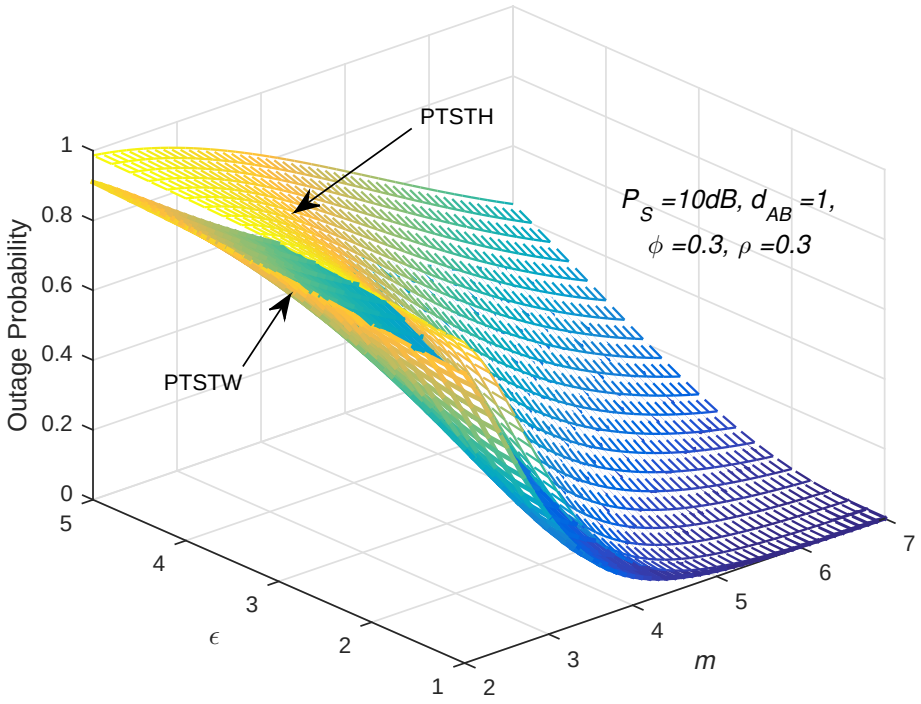

Fig. 7.6: Optimal OP of delay-limited mode vs. ϵ and m.

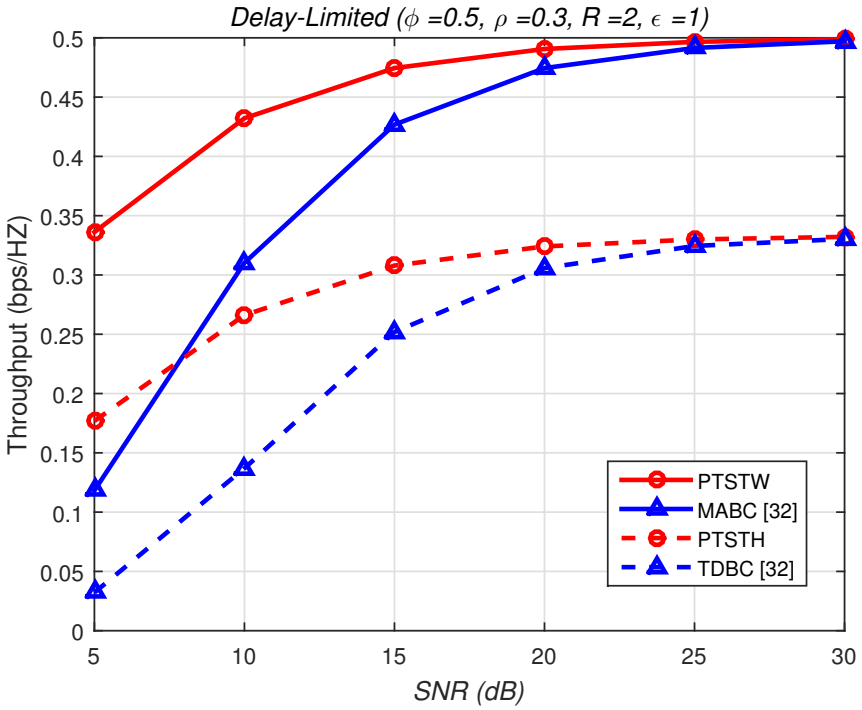

Fig. 7.7: A comparison between the proposed protocols and existing protocols.

We compare our proposed protocols with existing ones in Fig. 7.7. In particular, the OP of PTSTH and PTSTW are superior to time division broadcast and multiple access broadcast in [32] at low SNR. It is worth nothing that the similar throughput performance of these protocols can be seen when SNR reaches 30 dB, because the optimal values of TS and PS ratios are found to achieve the optimal throughput.

7.6 Summary

In this chapter, we introduced and evaluated the performance of PTSTW and PTSTH relaying protocols for 2TS and 3TS. To analyse the system performance, expressions of OP and optimal throughput were obtained. In particular, we provide numerical results to prove the throughput of PTSTW outperforms that of PTSTH. In addition, the throughput of the delay-limited mode is way lower compared to that of the delay-tolerant mode. The performance improvements of the proposed schemes can be done by optimizing TS and PS ratios. Last but not least, the appropriate placement of R can contribute to better the system performance.

8 RELAY SELECTION FOR SWIPT: PERFORMANCE ANALYSIS OF OPTIMIZATION PROBLEMS AND THE TRADE-OFF BETWEEN ERGODIC CAPACITY AND EH

In this chapter, optimal RS in a multi-relay cooperative RN is going to addressed. Our main target is to solve the optimization problem of TS and PS ratios and obtain the expressions for OP and throughput in delay-restricted and delay-tolerant modes. Besides, we apply the proposed HTPSR to study the trade-off between ergodic capacity and average EH [NHS08].

8.1 Motivation

In principle, a trade-off between the quality of IT and EH exists when it comes to RS. Due to the implementation of multiple relays, we can greatly improve SE, because more than one relay nodes are selected for IT, while RS based on the instantaneous CSI is a well-established strategy with conventional relay nodes.

In terms of optimal RS, there are a number works carried out on this research area. In particular, the work in [86] focused on the physical-layer security in AF and DF relaying networks RNs, where AF and DF optimal RS policies were proposed to enhance security and avoid being eavesdropped. In [87], an energy-aware optimal RS was proposed, where they selected optimal relays based on the energy consumption. Besides, the work in [88] designed an optimal RS scheme with less outage probability, while they approximated the expressions for OP at high SNR in [13]. The work in [89] studied opportunistic multiple RS schemes with both FD and HD scheme for both EH and non-EH in decode-and-forward (DF) relaying mode

Motivated from state-of-the-art works, it is clear that there are a few works focusing on ergodic capacity and the optimization of RS in EH multi-relay cooperative RNs. We learn that there are a few works on the trade-off between ergodic capacity and the average EH, so we are going to study it in this chapter.

We organize this chapter as follows: Section 2 presents the system model, while the system performance is studied in Section 3. We provide the simulation results in Section 4. Section 5 gives us a brief conclusion for the chapter.

8.2 System Model

In Fig. 8.1, we study a multi-relay RN which has a S, a cluster of relays, (R_i) with $i \in \{1, 2, ..., N\}$ denoted as N AF intermediate relays in HD mode and a D. It is noted that ith R depends on external charging via RF-EH. Besides, P_S and P_R are the transmit powers at S and ith R, respectively. We denote the distances from S to ith R and ith R

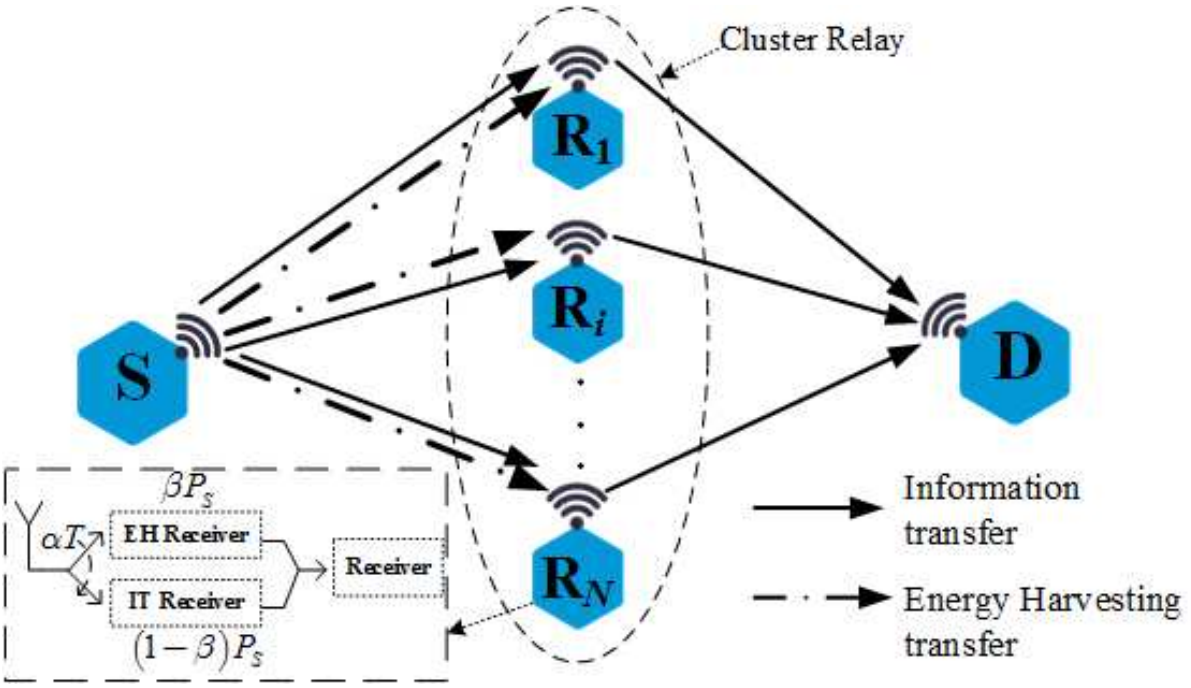

Fig. 8.1: The system model

to D as l_1 and l_2, respectively while m is the path loss exponent. Furthermore, n_r and n_d are the zero mean AWGN at ith R and D with zero mean and variance N_0, respectively.

Considering the system channels, we represent h_S and h_D as quasi-static block-fading and frequency non-selective parameters from S to ith R and from the ith R to D, respectively. These channels are constant over the block time T, and $|h_S|^2$, $|h_D|^2$ are i.i.d. following a Rayleigh distribution and exponential RVs with mean Ω_S and Ω_D, respectively. Nonetheless, CSI is assumed to be available at D when considering IT, and we study the long-term SE, where R with best statistical CSI is selected with the control unit.

In this chapter, we use the proposed HTPR to study EH. In particular, T is the block time for information being transmitted from S to D, so αT is the EH ratio. Meanwhile, the transmission signal from S is split into two parts, where ith R harvests energy from the received signal with the power ratio, β. Particularly, a part of power at S, βP_S is used for EH while the portion, $(1-\beta)P_S$ belongs to IT from S to ith R, and the remaining, $(T-\alpha T)$ is used for IT from ith R to D. It is noted that $\alpha, \beta \in [0, 1]$. Nevertheless, because of the implementation of multiple relays in signal transmission, D can receive multiple similar blocks of the signal. This makes the synchronization become complicated [90]. Since deploying one relay in IT may not be reasonable, we are going to discuss the single RS mode thoroughly in the following section.

For simplicity, primary symbols used in this paper are listed in Table. 8.1.

Tab. 8.1: List of the symbol meanings

Symbols	**Meanings**
l_1	The distance between S and ith R.
l_2	The distance between ith R and D.
h_S	The Rayleigh fading channel between S and the ith R node with mean Ω_S.
h_D	The Rayleigh fading channel between the i^{th} R and D node with mean Ω_D.
P_S	The transmission power from S to ith R.
P_R	The transmission power from ith R to D.
αT	The amount of time used for EH.
$(T-\alpha T)$	The amount of time used for IT.
βP_S	The power splitting ratio in EH.
$(1-\beta)P_S$	The information received at i^{th} R.

8.3 Performance Analysis

In this chapter, we first obtain preliminary analytical results, contributing to the comprehensive understandings on the study of a single relay. Besides, we also study the average end-to-end SNR, optimal RS, and the system performance in multi-relay mode in this section.

8.3.1 HTPR Protocol for Single Relay-Assisted Transmission

In this part, we take the average end-to-end SNR and the OP into consideration when only one relay is deployed which is taken from N relays. Hence, we can solve the joint optimization of α and β.

First, the sampled baseband signal, y_R is written by

$$y_R = \sqrt{l_1^{-m}(1-\beta)P_S}h_S z_S + n_R, \tag{8.1}$$

where the information transmitted to ith R is z_S which satisfies $\mathbb{E}\left\{|z_S|^2\right\} = 1$.

In addition, we can obtain the same expression in case of the proposed HTPSR protocol as

$$E_h^{HTPR} = \eta P_S l_1^{-m}\alpha\beta T|h_S|^2. \tag{8.2}$$

When ith R transmits the amplified signal using the received energy within $(T-\alpha T)$, the transmit power at ith R can be expressed by

$$P_R = \frac{E_h^{HTPR}}{(1-\alpha)T} = \frac{\eta\alpha\beta}{(1-\alpha)l_1^m}P_S|h_S|^2. \tag{8.3}$$

Regarding AF protocol, we can compute the input signal at ith R as

$$z_R = G\sqrt{P_R}y_R, \tag{8.4}$$

where the power coefficient at ith R in the presence of CSI can be written by

$$G^{-1} = \sqrt{(1-\beta)\, l_1^{-m} P_S |h_S|^2 + N_0}. \tag{8.5}$$

The received signal at D, y_D is given by

$$y_D = \sqrt{l_2^{-m}} h_D z_R + n_D. \tag{8.6}$$

Hence, substituting (8.1), (8.4) into (8.6), the expression for y_D can rewritten as

$$y_D = \underbrace{\left(l_2^{-m} G \sqrt{P_R} \sqrt{l_1^{-m}(1-\beta) P_S} h_S h_D z_S \right)}_{\text{Signal}} + \underbrace{\left(l_2^{-m} G \sqrt{P_R} h_D n_R + n_D \right)}_{\text{Noise}}. \tag{8.7}$$

To evaluate RS, we decided study the average end-to-end SNR, OP and throughput. Therefore, by replacing (8.3), (8.5) into (8.7), we obtain the expression for the average end-to-end SNR at D as

$$\gamma_D = \frac{\frac{\eta\alpha\beta(1-\beta)}{(1-\alpha)} P_S^2 X^2 Y}{\frac{\eta\alpha\beta}{(1-\alpha)} l_1^m P_S N_0 XY + l_1^m l_2^m (1-\beta) P_S N_0 X + l_1^{2m} l_2^m N_0 N_0}, \tag{8.8}$$

where $X = |h_S|^2$, $Y = |h_D|^2$.

Therefore, the data transmission rate is derived as follows

$$R = B(1-\alpha) \log_2 \{1 + \gamma_D\}. \tag{8.9}$$

8.3.2 The CDF and PDF of the average SNR

Proposition 8.1. The approximation of CDF of the average end-to-end at high SNR at D can be done by

$$F_{\gamma_D}(x) \approx 1 - 2\exp\left(-\frac{\mathcal{A}}{\mathcal{B}\Omega_S}\right) \sqrt{\frac{\mathcal{C}}{\mathcal{B}\Omega_S\Omega_D}} K_1\left(2\sqrt{\frac{\mathcal{C}}{\mathcal{B}\Omega_S\Omega_D}}\right), \tag{8.10}$$

where $\mathcal{A} = \frac{\eta\alpha\beta}{(1-\alpha)} P_S N_0 x$, $\mathcal{B} = \frac{\eta\alpha\beta(1-\beta)}{(1-\alpha)} P_S^2$, and $\mathcal{C} = l_1^m l_2^m (1-\beta) P_S N_0 x$.

Proof: See appendix C.

Remark 8.1. It is noted that we set the fixed values for P_S, η, l_1, l_2, N_0, X and Y to 1, so some assumptions can be made: i) When ($\alpha \to 0$, β is fixed) and ($\beta \to 0$, α is fixed), the performance is worse in terms of all aspects, particularly $\gamma_D \to 0$, which is presented in (8.8), makes the OP goes to 1, and the throughput goes to 0, since the communication between R and D is impossible due to no energy harvested at R, ($E_h^{HTPR} \to 0$). ii) While high values of ($\beta \to 1$) provide the energy harvester with more input signal, the signal power is affected, particularly $\gamma_D \to 0$ which makes the OP and throughput go to 1 and 0, respectively. iii) In case ($\alpha \to 1$), we achieve the best average end-to-end SNR at approximately 1 defined by $\lim_{\alpha\to 1}\gamma_D = \frac{(1-\beta)P_S X}{N_0 l_1^m}$, and the OP can be expressed as $1 - \exp\left(-\frac{x N_0 l_1^m}{(1-\beta)P_S\Omega_X}\right)$, in which the SNR threshold value is x. Besides, when ($\alpha \to 1$) or

($\beta \to 1$) at the same time, the throughput performance turns worse because R harvests energy during the whole block time T, and the signal is transmitted to D infinitesimally with large power, which we are going to be proved with simulation results.

Proposition 8.2. The expression, (8.10) is taken derivative with respect to x, so we can approximate the PDF of RV at SNR as

$$f_{\gamma_D}(x) \approx \frac{2\mathcal{C}\exp\left(-\frac{\mathcal{A}}{\mathcal{B}\Omega_S}\right)K_0\left(2\mathcal{D}\right)}{\mathcal{B}\Omega_S\Omega_D x} + \frac{2\mathcal{A}\mathcal{D}\exp\left(-\frac{\mathcal{A}}{\mathcal{B}\Omega_S}\right)K_1\left(2\mathcal{D}\right)}{\mathcal{B}\Omega_S x}, \tag{8.11}$$

where we mentioned $\mathcal{A}$, $\mathcal{B}$, $\mathcal{C}$ above, and $\mathcal{D} = \sqrt{\mathcal{C}(\mathcal{B}\Omega_S\Omega_D)^{-1}}$.
Proof: The CDF of the average end-to-end SNR at D, $F_{\gamma_D}(x)$ can be computed as

$$\begin{aligned} F_{\gamma_D}(x) &= Pr\left(\gamma_D < x\right) \\ &= 1 - \frac{1}{\Omega_S}\int\limits_{y=Q_4/Q_3}^{\infty} e^{-\left(\frac{y}{\Omega_S} + \frac{Q_1 y + Q_2}{(Q_3 y^2 - Q_4 y)\Omega_D}\right)} dy \ , \end{aligned} \tag{8.12}$$

where $Q_1 = l_1^m l_2^m \left(1-\beta\right) P_S N_0 x$, $Q_2 = l_1^{2m} l_2^m N_0 N_0 x$, $Q_3 = \frac{\eta\alpha\beta(1-\beta)}{(1-\alpha)} P_S^2$, and $Q_4 = \frac{\eta\alpha\beta}{(1-\alpha)} P_S N_0 x$.

Meanwhile, the PDF of γ_D with respect to x is expressed as

$$\begin{aligned} f_{\gamma_D}(x) &= \frac{\partial F_{\gamma_D}(x)}{\partial x} \\ &= \frac{1}{\Omega_S x}\int\limits_{y=Q_4/Q_3}^{\infty} \left(\frac{\left(Q_1 y + Q_2\right) Q_3 y^2}{\left(Q_3 y^2 - Q_4 y\right)^2 \Omega_D}\right) e^{-\left(\frac{y}{\Omega_S} + \frac{Q_1 y + Q_2}{(Q_3 x^2 - Q_4 y)\Omega_D}\right)} dy. \end{aligned} \tag{8.13}$$

To this point, the integration (8.13) cannot be simplified while the CDF can be applied at high SNR approximation mentioned in Appendix C. Therefore, we decided to use Bessel function ([66], 8.486.18) and the approximated value of the CDF of γ_D, the derivative of PDF with respect to x can be rewritten by

$$f_{\gamma_D}(x) \approx \frac{2}{xQ_3\exp\left(\frac{Q_4}{Q_3\Omega_S}\right)} \times \left(\frac{Q_4\sqrt{\frac{Q_1}{Q_3\Omega_S\Omega_D}}K_1\left(2\sqrt{\frac{Q_1}{Q_3\Omega_S\Omega_D}}\right)}{\Omega_S} + \frac{Q_1 K_0\left(2\sqrt{\frac{Q_1}{Q_3\Omega_S\Omega_D}}\right)}{\Omega_S\Omega_D}\right) . \tag{8.14}$$

This ends the proof for Proposition 8.2.

8.3.3 Optimal relay selection

In this section, RS is deployed in a centralized manner, where a central unit (CU) selects the best relay for a each transmission frame. In other words, the selected relay must satisfy the total transmitted energy to ith R and maximize IT to D.

A. Relay selection optimizing the average SNR at D

In this part, the joint optimization of TS and PS ratios can be done by using a robust algorithm so-called Alternate Convex Search [90], second derivatives and Hessian matrices.

In Table. 8.2, we present the joint optimization α and β, where we optimize the variables of an active block while other blocks are fixed [90]. Meanwhile, defining the stop criterion has several ways in the final step of the algorithm. For example, the absolute values of these functions are considered. Different function values are used as the criteria standard.

Theorem 8.1. This is how the convex is defined.

We set $A \subseteq R^n$ as a convex open set and $f : A \to R$. It is assumed that for all $x \in A$, $\frac{\partial^2 f}{\partial x^2}$ is considered as the positive semi-definite.

Theorem 8.2. By using both the Hessian matrix denoted as $M(x)$ in *Theorem* 8.1, the following functions should be considered:

1. When $\frac{\delta f}{\delta x} = 0$ and $M(x)$ is positive definite, f has a strict local minimum at x.
2. When $\frac{\delta f}{\delta x} = 0$ and $M(x)$ is negative definite, f has a strict local maximum at x.
3. When $\frac{\delta f}{\delta x} = 0$ and $M(x)$ has positive and negative eigenvalues, f does not have neither a local minimum nor a local maximum at x, since f has a saddle point at x.

Tab. 8.2: Optimal algorithm to solve the joint optimization of α and β

	$H(\alpha, \beta)$ is first used to represent the objective optimization while we use E and F to denote the set of α and β.
Step 1:	Then, the biconvex set of α and β is denoted as $B = E \times F$, where a random starting point, $x_0 = (\alpha_0, \beta_0)$ can be selected, and we set i to 0.
Step 2:	If α_i is fixed, the convex optimization problem is solved as: $\min\{H(\alpha_i, \beta), \beta \in B_{\alpha_i}\}$. If an optimal point $\beta^* \in B_{\alpha_i}$ exists, set $\beta_{i+1} = \beta^*$ or the algorithm stops here.
Step 3:	If β_{i+1} is fixed, we solve the convex optimization problem as: $\min\{H(\alpha, \beta_{i+1}), \alpha \in B_{\beta_{i+1}}\}$. In case the existence of the optimal point $\alpha^* \in B_{\beta_{i+1}}$, the algorithm stops or we need to set $\alpha_{i+1} = \alpha^*$.
Step 4:	In case $(\alpha_{i+1}, \beta_{i+1})$ achieves a stopping criterion, then stop or increase i by 1 and return to step 2.

Remark 8.2. Let us denote $B \subseteq X \times Y$, where $X \subseteq R^n$ and $Y \subseteq R^m$ stand for the two independent non-empty convex sets. Therefore, x and y of B are expressed by

$$B_x := \{y \in Y : (x, y) \in B\},$$
$$B_y := \{x \in Y : (x, y) \in B\}.$$

In case B_x is convex for every fixed $x \in X$, and B_y is convex for every fixed $y \in Y$, we express the set $B \subseteq X \times Y$ as a biconvex set similar to the one in [91].

Therefore, the optimal RS at high SNR at D is R_k, where if $k = i$, $i = 1, ..., N$, ith R

is selected. Hence, we examine the optimization problem for IT as

$$\begin{aligned} & k = \arg\max \gamma_D. \\ & \text{subject to} \begin{cases} 0 < \alpha \leq 1 \\ 0 < \beta \leq 1 \end{cases} \end{aligned} \tag{8.15}$$

Thanks to (8.15), the logarithmic function is a monotonically increasing function of its arguments, the following expression is as follows

$$\begin{aligned} & \min_{\alpha,\beta} \tfrac{1}{\gamma_D} = \tfrac{\varphi_1}{(1-\beta)} + \tfrac{(1-\alpha)\varphi_2}{\alpha\beta} + \tfrac{(1-\alpha)\varphi_3}{(1-\beta)\alpha\beta}, \\ & \text{subject to} \begin{cases} 0 < \alpha \leq 1 \\ 0 < \beta \leq 1 \end{cases} \end{aligned} \tag{8.16}$$

where $\varphi_1 = \frac{l_1^m N_0}{|h_S|^2 P_S}$, $\varphi_2 = \frac{l_1^m l_2^m N_0}{\eta |h_S|^2 |h_D|^2 P_S}$, and $\varphi_3 = \frac{l_1^{2m} l_2^m N_0 N_0}{\eta X^2 |h_D|^2 P_S^2}$.

Following that, we represent the objective optimization of (8.16) by $F(\alpha, \beta)$. With the second partial derivative of $F(\alpha, \beta)$ with respect to β while α is fixed, we have

$$\frac{\partial^2 F(\alpha,\beta)}{\partial \beta^2} = \frac{2(1-\alpha)(\varphi_2 + \varphi_3)}{\alpha\beta^3} + \frac{2(\varphi_1\alpha + (1-\alpha)\varphi_3)}{\alpha(1-\beta)^3}. \tag{8.17}$$

The expression, $\frac{\partial^2 F(\alpha,\beta)}{\partial \beta^2}$ is obviously positive. Therefore, $F(\alpha, \beta)$ is convex in β.

Next, the second partial derivative of $F(\beta, \alpha)$ with respect to α while β is fixed. Therefore, we have

$$\frac{\partial^2 F(\alpha,\beta)}{\partial \alpha^2} = \frac{2\varphi_2}{\alpha^3\beta} + \frac{2\varphi_3}{(1-\beta)\alpha^3\beta}. \tag{8.18}$$

Likewise, the value of $\frac{\partial^2 F(\alpha,\beta)}{\partial \alpha^2}$ is always positive. As a result, $F(\beta, \alpha)$ is convex in α. Besides, the Hessian matrix $\frac{\partial^2 F(\alpha,\beta)}{\partial \alpha^2}\frac{\partial^2 F(\alpha,\beta)}{\partial \beta^2} - \left[\frac{\partial^2 F(\alpha,\beta)}{\partial \alpha \partial \beta}\right]^2$ is positive.

Consequently, using the partial optimum with the algorithm described in Table. 8.2, we finally achieve a partial optimal point, (α, β) from (8.16).

B. Relay selection optimizing the harvested energy at R

From (8.2), we use R_λ to denote optimal RS of the amount of energy harvested at R, where $\lambda = \text{i}$, $i = 1, ..., N$ if ith R is selected. Therefore, we have

$$\lambda = \arg\max E_h^{HTPR}. \tag{8.19}$$

Hence, the minimum average energy harvested at the selected relay can be expressed by

$$E_{\min}^{HTPR} = \eta P_S l_1^{-m} \alpha\beta T \Omega_S. \tag{8.20}$$

Meanwhile, the maximum average energy harvested at N is computed by

$$E_{\max}^{HTPR} = \sum\nolimits_{i=1}^{N} \frac{\eta P_S l_1^{-m} \alpha\beta T \Omega_S}{i}. \tag{8.21}$$

Remark 8.3. In principle, RS is applied to satisfy the balance between IT and EH, so we use a technique called Time-Sharing selection method (TSM) which is a simplistic selection method, or the CU selects R_k or R_λ in a pseudo-random fashion. We are going to examine these methods in Section 8.3.5.

8.3.4 Performance analysis for multi-relay selection

To this point, we are going to give expressions for OP, ergodic capacity and throughput in case multiple-relay mode.

A. Delay-Restricted Transmission Mode

In the delay-restricted transmission mode, we obtain the expression for the OP at D with ith R as $P_{out,i} = Pr(\gamma_D < \gamma_0)$, where the expression for $P_{out,i} = F_{\gamma_D}(\gamma_0)$ can be derived in **Proposition** 8.1.

Using the order statistics, when channels are independent, the OP at D for RS can be given as

$$\begin{aligned} P_{out} &= P_{out,1} \times ... \times P_{out,i} \times P_{out,N} \\ &= \prod_{i=1}^{N} F_{\gamma_D}(\gamma_0) \\ &\approx [F_{\gamma_D}(\gamma_0)]^N \end{aligned} . \tag{8.22}$$

We see that the OP derived in (8.22) is a function of α, it decreases as α climbs from 0 to 1. Hence, the throughput at D, τ_{DR} in delay-restricted mode can be written by

$$\tau_{DR} = (1-\alpha)(1-P_{out})R_0. \tag{8.23}$$

B. Delay-Tolerant Transmission

Here, we compute the ergodic capacity for the received SNR at D by

$$C = E_{|h_S|^2,|h_D|^2}\{\log_2(1+\gamma_D)\}. \tag{8.24}$$

Proposition 8.3. The ergodic capacity at D can be expressed as

$$C = \int_{x=0}^{\infty} f_{\gamma_D}(x)\log_2(1+x)dx. \tag{8.25}$$

Thanks to **Proposition** 8.2, we approximate the ergodic capacity at high SNR as

$$\begin{aligned} C \approx &\int_{x=0}^{\infty} \frac{2\mathcal{C}\exp\left(-\frac{\mathcal{A}}{\mathcal{B}\Omega_S}\right)K_0(2\mathcal{D})}{\mathcal{B}\Omega_{h_S}\Omega_D x}\log_2(1+x)\,dx \\ &+\int_{x=0}^{\infty} \frac{2\mathcal{A}\mathcal{D}\exp\left(-\frac{\mathcal{A}}{\mathcal{B}\Omega_S}\right)K_1(2\mathcal{D})}{\mathcal{B}\Omega_S x}\log_2(1+x)\,dx \end{aligned} , \tag{8.26}$$

where we already defined the constants, $\mathcal{A}$, $\mathcal{B}$, $\mathcal{C}$ and $\mathcal{D}$ in (8.10) and (8.11).

To this end, the ergodic capacity for the network is

$$\begin{aligned} C &= N \int_0^\infty \left[F_{\gamma_D}(x)\right]^{N-1} f_{\gamma_D}(x) \log_2(1+x)\, dx \\ &\approx N \int_0^\infty \left[F_{\gamma_D}(x)\right]^{N-1} (\mathcal{Z}_1 + \mathcal{Z}_2) \log_2(1+x)\, dx \end{aligned}, \tag{8.27}$$

where $\mathcal{Z}_1 = \frac{2\mathcal{C}\exp\left(-\frac{\mathcal{A}}{\mathcal{B}\Omega_S}\right)K_0(2\mathcal{D})}{\mathcal{B}\Omega_S\Omega_D x}$, $\mathcal{Z}_2 = \frac{2\mathcal{A}\mathcal{D}\exp\left(-\frac{\mathcal{A}}{\mathcal{B}\Omega_S}\right)K_1(2\mathcal{D})}{\mathcal{B}\Omega_S x}$, and the PDF of the average end-to-end SNR in case of multi-relay mode is solved by taking partial derivative of the CDF from (8.12) with respect to x.

We assume that if IT is at a fixed rate equal to the ergodic capacity, and the throughput, τ_{DT} at D with αT relying on the successful IT time, $(1-\alpha)T$ can be expressed as

$$\tau_{DT} = \frac{(1-\alpha)T}{T} C = (1-\alpha)C. \tag{8.28}$$

Remark 8.4. It is worth noting that the ergodic capacity derived in (8.24) is the function of α, it increases when α rises from 0 to 1. If α is larger, more energy is transmitted, leading to better ergodic capacity. Nevertheless, the block time, $(1-\alpha)\,T$ falls as α climbs. Hence, the trade-off between ergodic capacity and the average EH is going to be studied in the following section, where the average EH and the ergodic capacity are regarded as the reference for metric (x) and the cost metric (y) [92], respectively.

8.3.5 Trade-off between ergodic capacity and average energy harvesting

In this part, the trade-off between the average EH at ith R and ergodic capacity is considered. In particular, TSM is applied, where δ represents the proportion of transmission frames for optimal IT and the harvested energy. For example, R_k is selected with the probability, δ while R_λ is selected with the probability, $1-\delta$.

From (8.20) and (8.21), if $\delta = k$ then $E_{\min}^{HTPR}$ is activated. In contrast, in case $\delta = \lambda$, $E_{\max}^{HTPR}$ is activated. Hence, by applying TSM, the average EH at ith R is given by

$$E_{TSM}^{HTPR} = \delta E_{\min}^{HTPR} + (1-\delta)\, E_{\max}^{HTPR}. \tag{8.29}$$

By solving (8.29) with respect to δ, we have

$$\delta = \frac{E_{TSM}^{HTPR} - \sum_i^N \eta P_S l_1^{-m} \alpha\beta\Omega_S i^{-1}}{\eta P_S l_1^{-m} \alpha\beta\Omega_S \left(1 - \sum_i^N i^{-1}\right)}. \tag{8.30}$$

In addition, we represent the minimum and maximum ergodic capacity of TSM for IT as C_{min} obtained in (8.26) for the time frames when $\delta = \lambda$ and C_{max} derived in (8.27) for the time frames where $\delta = k$, respectively. As a consequence, using (8.30), the ergodic

capacity can be expressed as a function of the average EH, E_{TSM}^{HTPR} at ith R as

$$\begin{aligned} C_{TSM} &= \delta C_{max} + (1-\delta)\, C_{min} \\ &= \frac{E_{TSM}^{HTPR} - \sum_i^N \eta P_S l_1^{-m} \alpha\beta\Omega_S i^{-1}}{\eta P_S l_1^{-m} \alpha\beta\Omega_S \left(1 - \sum_i^N i^{-1}\right)} C_{max} \\ &\quad + \left(1 - \frac{E_{TSM}^{HTPR} - \sum_i^N \eta P_S l_1^{-m} \alpha\beta\Omega_S i^{-1}}{\eta P_S l_1^{-m} \alpha\beta\Omega_S \left(1 - \sum_i^N i^{-1}\right)}\right) C_{min}. \end{aligned} \tag{8.31}$$

8.4 Numerical Results

In this section, simulations on the throughput, transmission rate and ergodic capacity are given. In addition, the analytical results are also provided to evaluate the trade-off between ergodic capacity and the average EH by deploying TSM. The simulation results are averaged over 10^5 channel realizations following the Rayleigh fading channels. Regarding the distances, we normalize l_1 and $l_2 = 2 - l_1$ to unit value. Meanwhile, the mean values, Ω_S and Ω_D of the exponential RVs, $|h_S|^2$ and $|h_D|^2$ are set to 1. The simulation results follow some parameters specified in Table 8.3

Parameters	**Values**
Number relays, N	3
Power transmission, P_S	1(dB)
Energy conversion efficiency, η	1
The path loss exponent, m	2.7
The SNR threshold, R_0	3(bps/Hz)
The zero mean AWGN, N_0	0.01
The distances, $l_1 = l_2$	1

Tab. 8.3: Main Simulation Parameters (RS for SWIPT)

The impact of α and β on EH in delay-restricted mode is presented in Fig. 8.2 and Fig. 8.3. We see that the optimal throughput is a function of to the number of relays. In particular, tthe throughput changes thanks to the change of N, e.g., 1 to 5. It is clear that for each value of N, α and throughput increase significantly, e.g., α rises from 0 to 0.3. However, as α falls, the throughput begins falling. Meanwhile, the throughput increases dramatically when β climbs from 0 to 0.3 before falling at the end values of β, ranging from 0.8 to 1.

We present the delay-tolerant throughput with α and β as a function of N in Fig. 8.4 and Fig. 8.5. The throughput reaches its optimal values as α increases from 0 to 0.2. It is clear that throughput in delay-tolerant mode outperforms that of delay-restricted mode, since the time delay in delay-tolerant mode is set to zero. Meanwhile, the delay-tolerant throughput is superior to the delay-restricted throughput, where for every values of N, the optimal throughput is achieved as β rises from 0 to 0.6, but it decreases in the remaining values of β. It is worth noting that while $\alpha \to 0$, $\beta \to 0$, $\gamma_D \to 0$, the OP

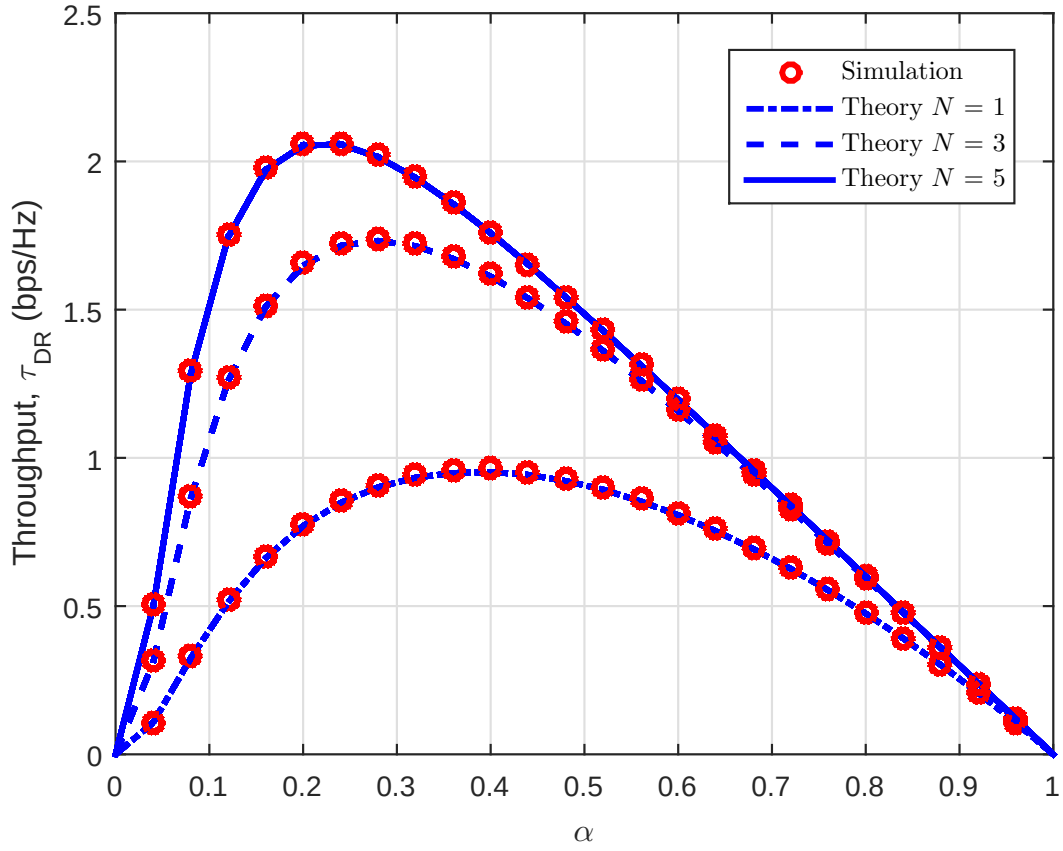

Fig. 8.2: Throughput at D with α in delay-Restricted mode with $\beta = 0.3$

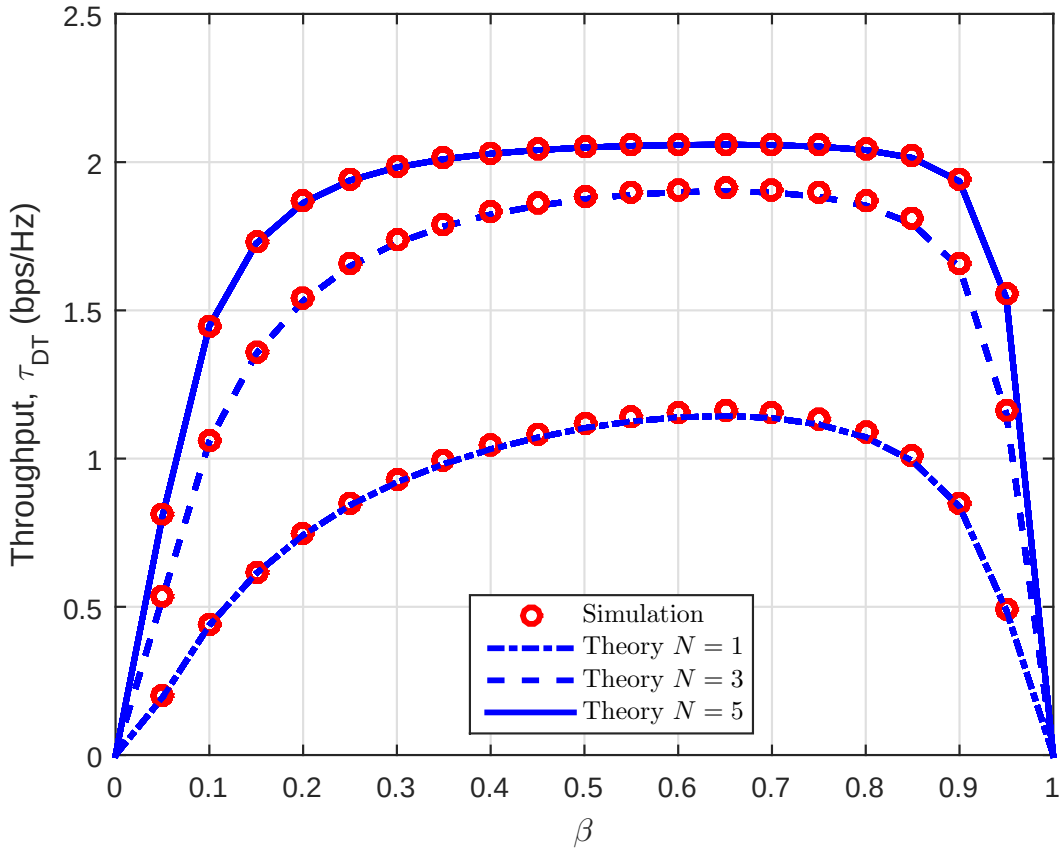

Fig. 8.3: Throughput at D with β in delay-Restricted mode with $\alpha = 0.3$

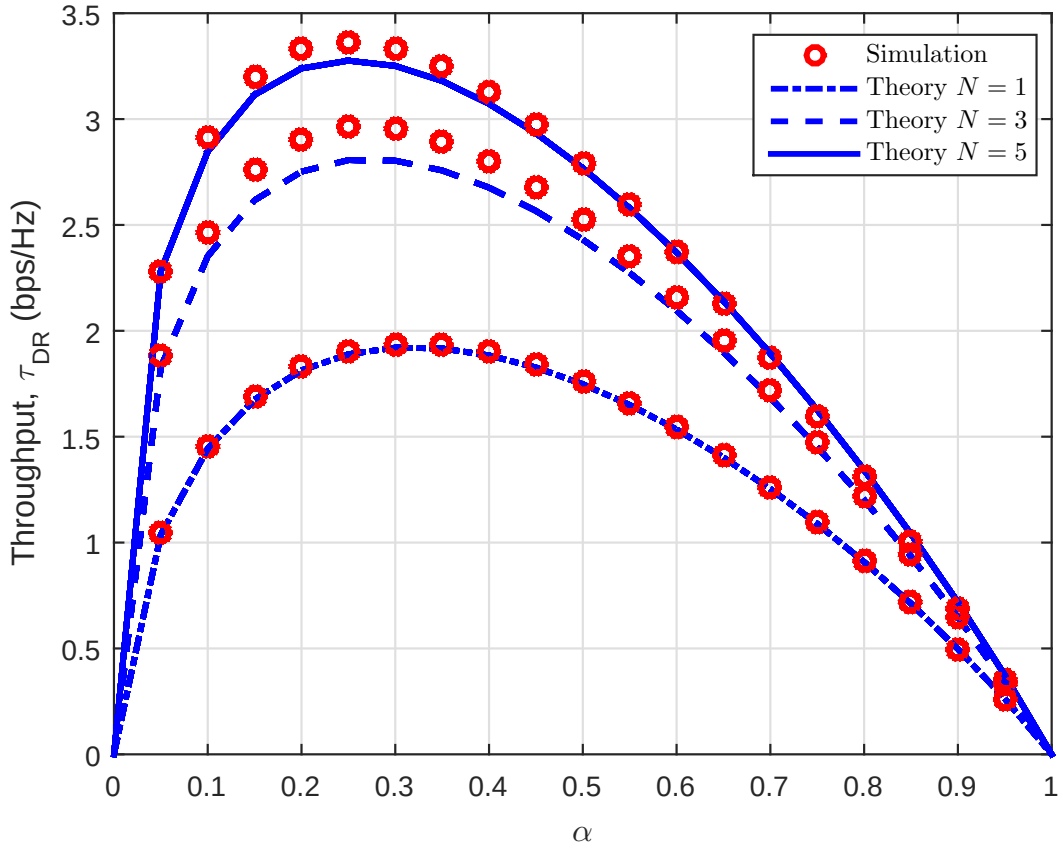

Fig. 8.4: Throughput at D with α in delay-tolerant mode with fixed $\beta = 0.3$

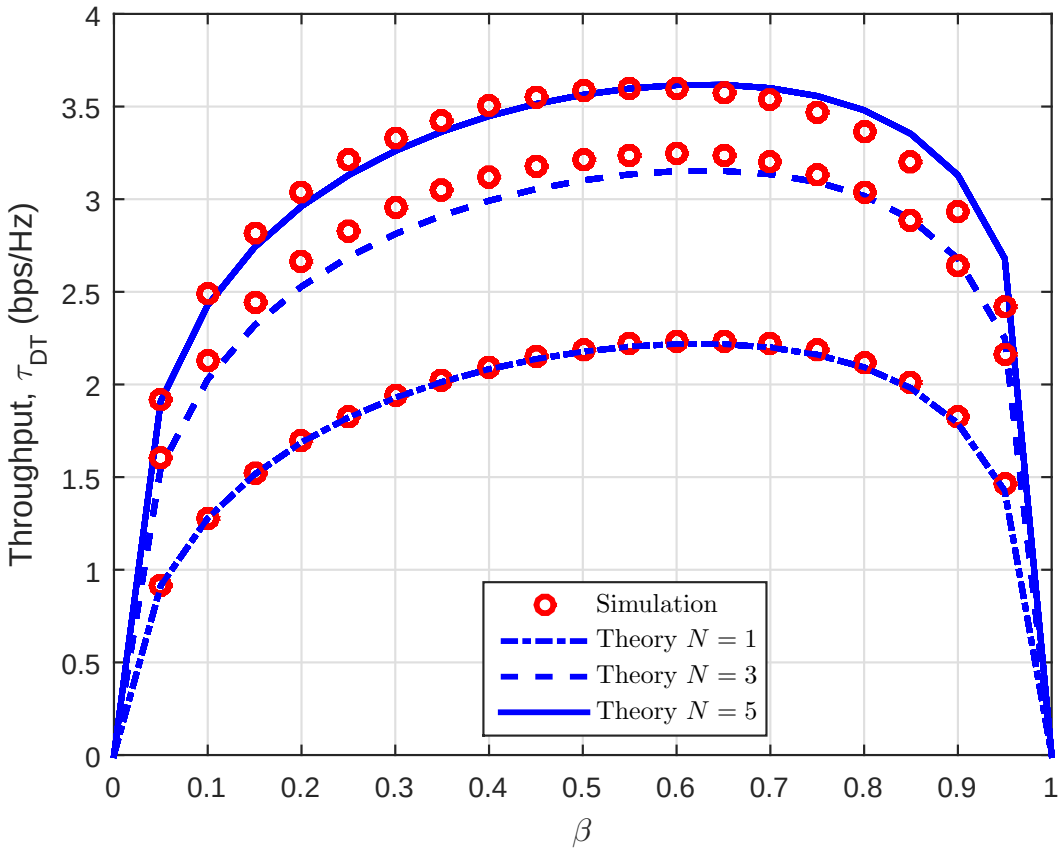

Fig. 8.5: Throughput at D with β in delay-Tolerant mode with fixed $\alpha = 0.3$

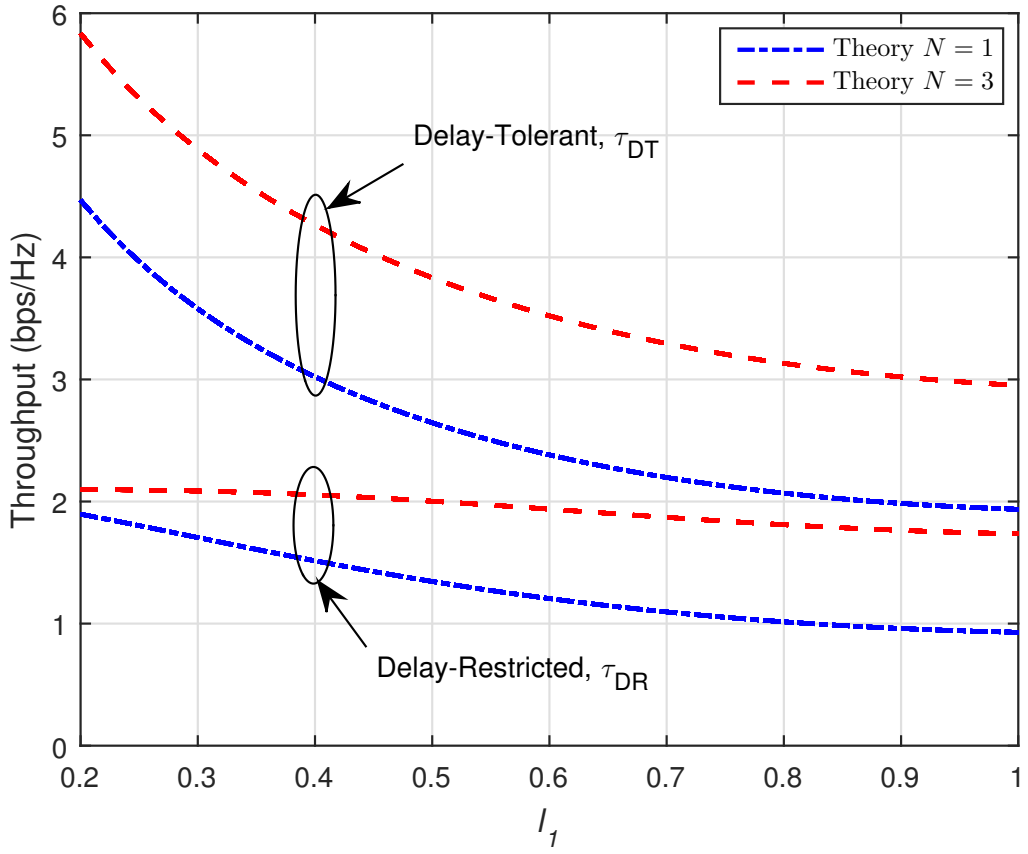

Fig. 8.6: Throughput at D in Delay-restricted and Delay-tolerant transmission mode within l_1

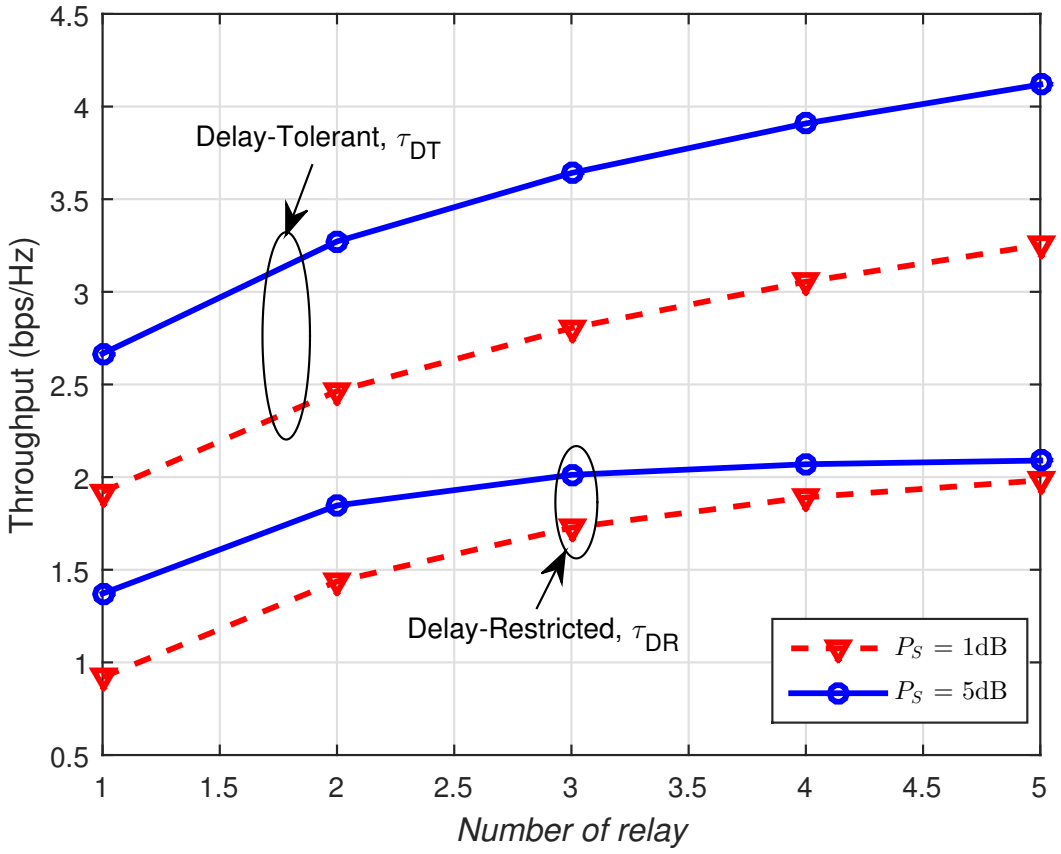

Fig. 8.7: Throughput versus N relays for different P_S

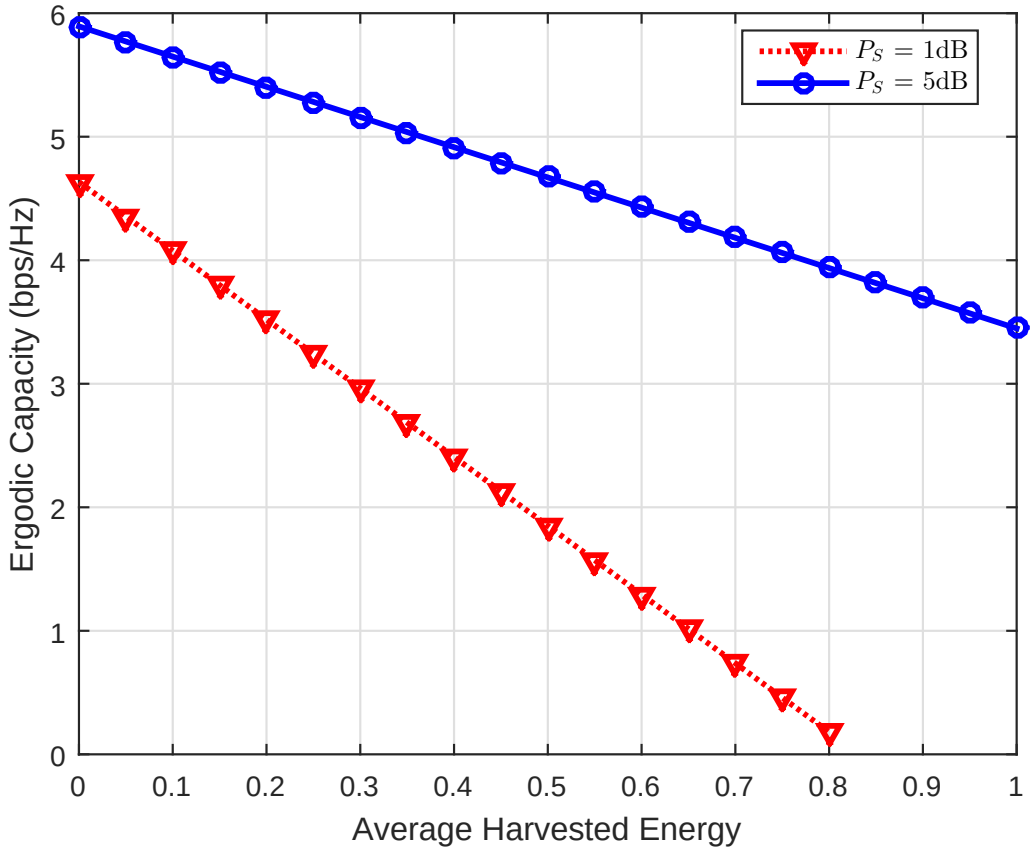

Fig. 8.8: The trade-off between average EH and ergodic capacity with $N = 3$

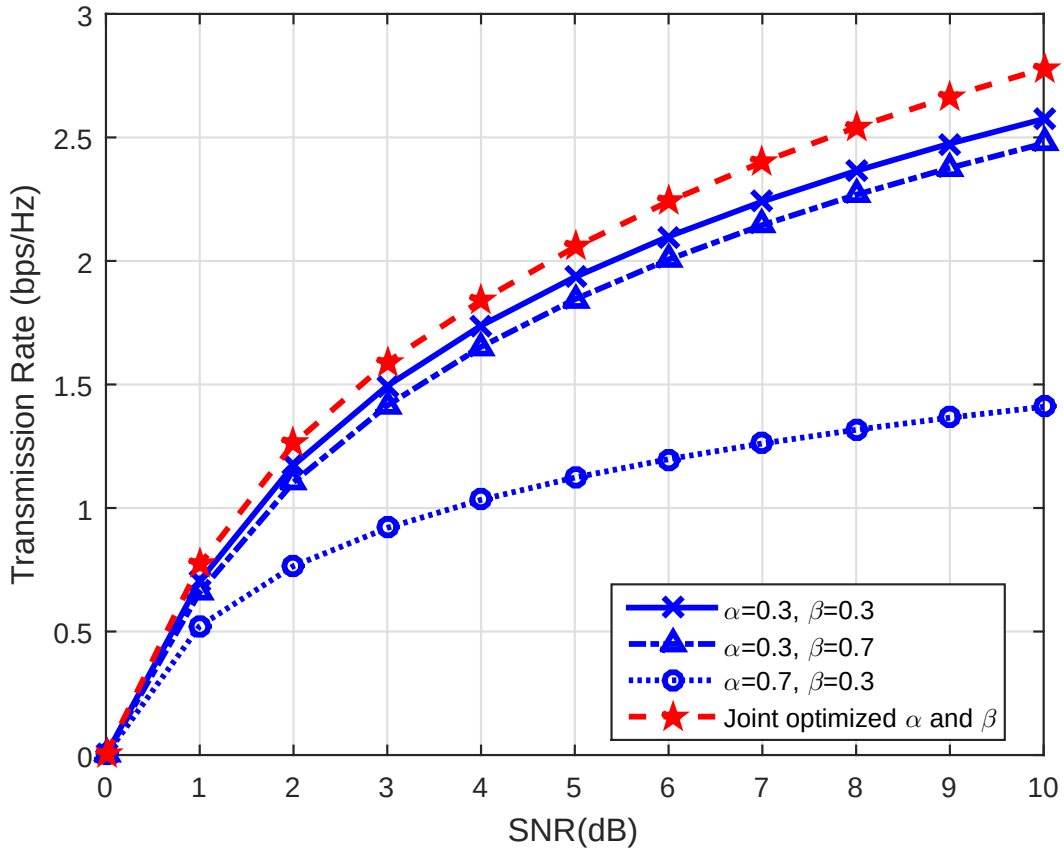

Fig. 8.9: Joint optimal values of α and β with $N = 1$

goes to 1 and the throughput goes to 0. In contrast, the high end-to-end SNR is valid when $\alpha \to 1$, in this case, the OPy goes to 0.1101 leading to worse throughput (0,1068). Similarly, in case $\beta \to 1$, the OP goes to approximately 1 (0,8209), and the throughput goes to approximately 0 (0,3760) in delay-restricted mode.

In Fig. 8.6, throughput drops as l_1 rises, $l_2 = 2 - l_1$. In particular, the distance between S and ith R increases, e.g., $N = 1$ and $N = 3$, the energy harvested and the received signal at ith R drop because of the path loss. So, throughput falls dramatically since the received signal at D is weak. However, the throughput gap is much different when we change the number of relays, e.g., $N = 1$ to $N = 3$. Due to the near distance between ith R and D, less energy is harvested to serve for reliable communication.

The throughput is presented in Fig. 8.7 in both delay-restricted and delay-tolerant modes for different number of relays, where we set the source transmission power, $P_S =$ 1dB and $P_S = 5$dB. At first glance, the system performance metrics enjoy upward trends as N increases. It is obvious that delay-tolerant throughput is better when $P_S = 5$dB, and it rises significantly because more energy is harvested at ith R.

In Fig. 8.8, we show the trade-off between ergodic capacity and average EH at ith R. The performance of the TSM is evaluated versus the average harvested energy. We see that TSM contributes to a linear trade-off. The ergodic capacity decreases as the average harvested energy rises. Besides, when the harvested energy rises, e.g., to approximately (0.8) (bps/Hz), the ergodic capacity dramatically drops.

In Fig. 8.9, we prove the considered optimization problem. It can be observed that all curves go up as SNR rises, which accordingly lead to better data rate. In practice, the EH RNs can be enhanced with the optimization of α when we can select the best end-to-end SNR for a given EH time, αT. In Fig. 8.9, the role of α influences the transmission rate, e.g., when $\beta = 0.3$, the solid curve outperforms the dot curve with $\alpha = 0.3$ or $\alpha = 0.7$, respectively. Besides, when $\alpha = 0.3$, the solid curve is better than the dash curve with $\beta = 0.3$ or $\beta = 0.7$, respectively. On the other hand, if the values of α are higher than the optimal values of α, more time is spent on EH, and less time is available for IT. Thanks to the proposed joint optimization of α and β, the instantaneous transmission rate reaches its optimal value. Interestingly, the joint optimal values of α and β outperform the two pre-set random values.

8.5 Summary

In this chapter, we studied optimal RS in a multi-relay cooperative RN. We tried to solve the optimization problem between TS and PS ratios and derived the expressions for OP and throughput in delay-restricted and delay-tolerant modes. In addition, we also studied the trade-off between ergodic capacity and average EH using the proposed HTPSR protocol. Thanks to the numerical results, the system throughput was significantly improved when RS is applied at high SNR, where the delay-tolerant throughput outperforms

that the delay-restricted throughput. In addition, we observed the improvement in the transmission data rate with the joint optimal TS and PS ratios.

9 HYBRID FD/HD RS SCHEME WITH OPTIMAL POWER UNDER INDIVIDUAL POWER CONSTRAINTS AND EH

In this chapter, we extend the work in the previous chapter on the optimal RS. Particularly, we evaluate OP at high SNR in three new proposed RS schemes, i.e. HDMRC and FDJD and HTS to reduce the impact of SI. In addition, we propose two optimal power supply policies, namely OPIPC and OPEHA which are used to analyse the proposed RS schemes. We try to derive closed-form expressions and asymptotic results for OP to prove the correctness of the system. This system's EE is improved thanks to the proposed power consumption model. According to the numerical results, HTS scheme outperforms HDMRC and FDJD in terms of OP [NHS09].

9.1 Motivation

In principle, HD and FD relaying schemes contribute to the loss of SE and the SI. Thus, adaptive relaying schemes have attracted much research interest since they can switch between HD and FD without spectrum sharing. Thanks to the implementation of hybrid relaying techniques, we can clearly see the impact of SI on HD relaying mode which accordingly degrades the e2e symbol rate while the residual SI impairs the performance of FD mode regardless of cancellation process.

In fact, the presence of SI has a detrimental impact on FD wireless systems FD [93, 94, 95, NHS07, 96, 97, 98]. In [93], the authors proposed an optimal RS scheme to maximize SINR, while RS in FD RNs under the impact of multi-path fading was studied in [94]. Different from [99], the work in [95] analysed the secrecy OP under the impact of an eavesdropper in cooperative RNs with RS schemes. In addition, opportunistic RS schemes with EH and without EH in both FD and HD were discussed in [NHS07], while the work in [96] considered the SNR, OP and the average channel capacity. In [97], RS was investigated in multi-relay FD systems under the multi-path fading conditions.

However, network lifetime and the power saving are two concerns in low-power wireless networks, so power efficiency should be paid more attention [100, 101, 102, 103]. In particular, the authors in [103] evaluated a hybrid wireless network, in which the amount of successful data transmission and the network lifetime at MUs were studied.

In order to take advantage of both FD and HD, hybrid relaying techniques actively switching between HD and FD have been addressed in several works, [98], [104] and [105]. In particular, the selection of relaying mode and the transmit power adaptation were combined to maximize SE in [104]. Despite optimal RS schemes proposed in FD and HD in [98], the combination of the direct link and relay links [105] has not been addressed. In [106], four hybrid relaying modes were proposed thanks to an integrated model, and the authors developed a joint RS mode and a power allocation algorithm, where a hybrid relaying scheme was proposed to prove that FD outperforms HD mode

in terms of throughput performance. These works motivated us to conduct this extended work.

We organize this chapter as follows: The system performance is analysed in Section 3, in which we derive the expressions for OP for the three considered RS schemes for the two power supply policies, and the power consumption model for each RS scheme is given. In Section 4, numerical and simulation results are provided. Finally, a brief conclusion is drawn in Section 5.

9.2 System Model

In Fig. 9.1, a multi-relay cooperative network is considered, in which there are a source node (S) communicating with a destination node (D) via a cluster of N relays denoted by (R_i) with $1 \leq i \leq N$ operating in decode-and-forward (DF) transmission mode. In our system model, each node is equipped with a single antenna while relay nodes are equipped with two antennas (i.e. a transmit antenna and a receive antenna) operating in full-duplex (FD) transmission mode.In principle, we focus on the coverage extension scenario, where the direct communication between S and D is not strong, so relay nodes are deployed to assist other nodes in the system without utilizing their data.

In terms of system channels, we denote h_X, h_Y and h_Z as the channel coefficients of the S–R_i link (first hop), the R_i–D link (second hop) and the S–D link (direct channel), respectively. Meanwhile, h_W is denoted as the channel coefficient of the self-interference (SI) link, where it is assumed that the transmit and receive antennas suffer from the scattering component while the specular component is greatly weakened due to the deployment of passive and active SI cancellation methods in case FD is deployed. Further to this, the received signal is compromised by additive white Gaussian noise (AWGN), N_0. It is noted that all links undergo Rayleigh fading channels over independent and identically distributed (i.i.d), in which we assume that all channel coefficients are constant in each data transmission block but independently fluctuate from one block to another. As a result, the channel coefficient, h_A with $A \in \{X, Y, Z, W\}$ is modeled as a zero-mean, independent and circularly symmetric complex Gaussian random value (RV) with variance, $\Omega_A = \mathbb{E}\left\{|h_A|^2\right\}$. Furthermore, the channel power gain of h_A is denoted as $|A| = |h_A|^2$ following an exponential distribution with the mean value, Ω_A. It is worth noting that P_S and P_{R_i} are respectively the maximum allowed transmit powers at S and $i-$th R, since the system's total energy consumption is more practically trivial compared to each pre-set transmitter's power.

It is worth noting that the communication from S to D can be assisted by the best selected relay in each time slot, $(R_i \in N)$. Most importantly, the benefits of RS have caught much attention in a number of new wireless networks in terms of evaluating OP. Therefore, let us begin with the generalized case in single relay mode.

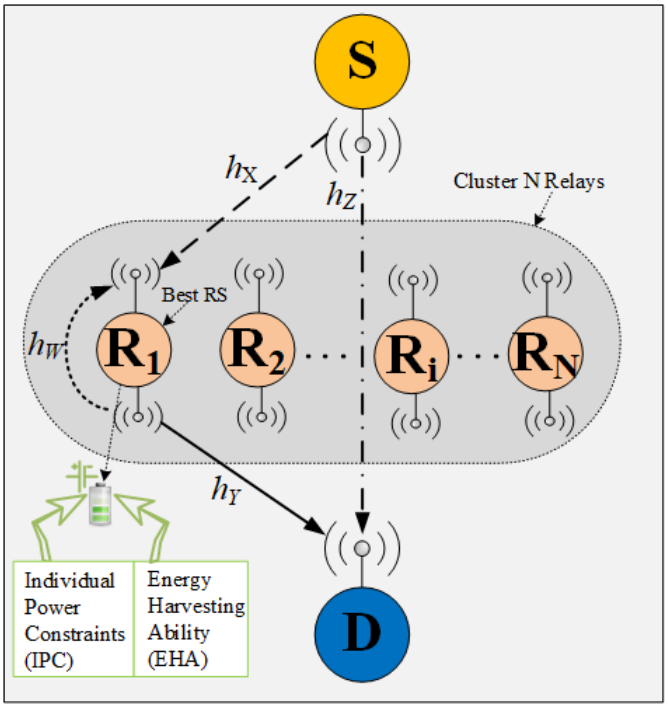

Fig. 9.1: The desired-signal links respectively stand for the dash line, solid line, and dash-dot line while the interference link is denoted by the half dash line.

In practice, the antenna noise power is not noticeable than the baseband noise power in most practical baseband circuits. For simplicity, we assume that the antenna noise power is zero [107], so the high instantaneous signal-to-noise ratio (SNR) for FD in the presence of SI and HD without SI can be approximated as

$$\Gamma_{SR_i} = \begin{cases} \frac{P_S|X|}{P_{R_i}|W|+N_0} \approx \frac{P_S|X|}{P_{R_i}|W|}, & \text{for FD} \\ \frac{P_S|X|}{N_0} \approx P_S|X|, & \text{for HD} \end{cases}. \tag{9.1}$$

The equivalent instantaneous received SNR at D is given by

$$\Gamma_{R_iD} = P_{R_i}|Y|/N_0 + P_S|Z|/N_0. \tag{9.2}$$

The overall end-to-end (e2e) SNR deploying DF protocol can be computed by

$$\Gamma_{eq,i} = \min_{i:R_i \in N} \{\Gamma_{SR_i}, \Gamma_{R_iD}\}. \tag{9.3}$$

9.3 Performance analysis

In this section, we derive exact and approximate closed-form expressions for outage probability (OP) in multi-relay mode. In addition, opportunistic relay selection (RS) schemes are evaluated for the proposed power supply policies.

9.3.1 Outage Probability

Regarding the two proposed optimal RS schemes, FDJD and HDMRC based on the statistical channel state information (CSI), the instantaneous e2e capacity is given by

$$C_i^j \underset{\substack{i:R_i\in N \\ j\in\{FDJD,HDMRC\}}}{=} \mu B \log_2\left(1+\Gamma_{eq,i}\right), \tag{9.4}$$

where $\mu = 1$ or $\mu = \frac{1}{2}$ due to the switching between FDJD and HDMRC RS scheme.

Remark 9.1. All fading channels are independent in each block, and the fading gain, h_Z of the S–D link is trivial compared to that of h_Y of the R_i–D link, i.e., $\mathbb{E}\{|Z|\} < \mathbb{E}\{|Y|\}$.

Furthermore, each variable corresponds with the instantaneous SNR, where the single-hop transmission is carried out over the distinct fading channels to maximize spectral efficiency (SE) and energy efficiency (EE), since the relay with the best statistical CSI is selected by the control unit to guarantee the Quality of Service (QoS). It is clear that the source transmit power, P_S monotonically increases along with $\Gamma_{eq,i}$. Besides that, the SNR in the (S–R_i) link increases as P_{R_i} declines and vice versa. Similarly, the same situation happens when SNR in the (R_i–D) link climbs as a function of P_{R_i}. Hence, OPIPC and OPEHA are going to comprehensively evaluated in the following section.

It is noted that OP is less than a pre-set value SE, R_0 (bits/s/Hz), where $R_0 = \log_2\{1+\Gamma_1\}$ or $R_0 = \frac{1}{2}\log_2\{1+\Gamma_2\}$, and Γ_1, Γ_2 are the target SNR thresholds for FDJD and HDMRC, respectively. The OP for the strongest bottleneck link depends on the selection of $i-$th relay which is defined as $OP^j = \Pr\left(C_i^j < R_0\right)$, $j \in \{FDJD, HDMRC\}$, since the OP for N relays can be expressed in *Theorem* 9.1.

Theorem 9.1. The OP in multi-relay mode can be written symmetrically due to the selection of R_i as

$$\begin{aligned} OP &= \Pr\left(C_1^j < R_0, ..., C_i^j < R_0, ..., C_N^j < R_0\right) \\ &= \prod_{i=1}^{N} \Pr\left(C_i^j < R_0\right) \\ &= \left[\Pr\left(C_i^j < R_0\right)\right]^N. \end{aligned} \tag{9.5}$$

In the following sections, we are going to study OP in different RS schemes for the two proposed power supply policies.

9.3.2 RS Schemes for Full-Duplex relaying deploying joint decoding (FDJD)

In this section, we are going to study proposed RS schemes for the two proposed power supply policies based on the instantaneous SE. Let us first evaluate FDJD, the max-min RS under the impact of SI is considered. It is noted that this scheme depends on the selection of the strongest bottleneck link, where the best e2e SNR link and the SI are evaluated to select the best relay which can be given as

$$l = \arg\max_{i:R_i\in N} \min\left\{\frac{P_S|X|}{P_{R_i}|W|}, \frac{P_{R_i}|Y|}{N_0} + \frac{P_S|Z|}{N_0}\right\}. \tag{9.6}$$

Here, we express the instantaneous e2e capacity as

$$C_l^{FDJD} = \log_2\left(1 + \Gamma_{eq,l}\right), \tag{9.7}$$

where $\Gamma_{eq,l}$ is the instantaneous SNR at D via l-th R as in (9.3).

A. Optimal power under the individual power constrains (OPIPC)

Let us define OPIPC as

$$\left(P_S^*, P_{R_l}^*\right) = \arg \max_{(P_S, P_{R_l})} \left(C_l^{FDJD}\right), \tag{9.8}$$

where the average optimal transmit powers at S and $l-$th R are denoted by P_S^*, $P_{R_l}^*$, respectively.

We assume that the maximum transmit power, $P_S^* = 1$ is used for coverage extension, so we first solve the following expression to express OPIPC later as

$$\begin{cases} \frac{P_S^*|X|}{P_{R_l}^*|W|} = \frac{P_{R_l}^*|Y|}{N_0} + \frac{P_S^*|Z|}{N_0} \\ P_S^* = 1, \end{cases} , 0 \leq \left(P_S^*, P_{R_l}^*\right) \leq 1 \tag{9.9}$$

Based on (9.9), the long-term SE and the R_l with the best CSI are used to obtain the average optimal transmit power at l-th R. Therefore, the average optimal transmit power at l-th R can be written after algebraic manipulations as

$$P_{R_l}^* = \min\left\{P_S^*, \frac{|Z|}{2|Y|}\left[-1 + \sqrt{1 + 4N_0\frac{|X||Y|}{|W|(|Z|)^2}}\right]\right\}. \tag{9.10}$$

In fact, we can rewrite the expression (9.10) as

$$P_{R_l}^* = \min\left\{P_S^*, \frac{\Omega_Z}{2\Omega_Y}\left[-1 + \sqrt{1 + \frac{4N_0\Omega_X\Omega_Y}{\Omega_W(\Omega_Z)^2}}\right]\right\}. \tag{9.11}$$

Proposition 9.1. Following from *Theorem* 9.1, we obtain the exact closed-form expression for OP for OPIPC policy at high SNR as

$$OP_{IPC}^{FDJD}\left(\Gamma_1\right) = \left[1 - \left(\Theta_1 \times \Theta_2\right)\right]^N, \tag{9.12}$$

where $\Theta_1 = \frac{P_S\Omega_X}{P_{R_l}\Omega_W\Gamma_1 + P_S\Omega_X}$, $\Theta_2 = \frac{P_S\Omega_Z \mathrm{e}^{-\frac{N_0\Gamma_1}{P_S\Omega_Z}} - P_{R_l}\Omega_Y \mathrm{e}^{-\frac{N_0\Gamma_1}{P_{R_l}\Omega_Y}}}{P_S\Omega_Z - P_{R_l}\Omega_Y}$, and the definition of the target SNR threshold for FDJD is $\Gamma_1 = 2^{R_0} - 1$.

Proof: The proof for **Proposition** 9.1 can be seen in Appendix D.1.

B. Optimal power with energy harvesting ability (OPEHA)

Regarding this policy, R nodes have EH capacity based on the principles of TSR protocol without fixed power supplies [13]. In principle, the fraction used for EH and IT from S to R_i link in the first hop is αT while the remaining block time, $(1-\alpha)\,T$ is for IT from R_i to D, where each period of IT from S to D is $0 < \alpha \leq 1$.

Therefore, we express the transmit power at l-th R during $(1-\alpha)\,T$ as

$$P_{R_l} = \frac{E_h}{(1-\alpha)\,T} = \rho_l P_S |X|, \tag{9.13}$$

where we define the harvested energy at l-th R as $E_h = \eta\alpha P_S |X| T$.

Following from (9.1), (9.2), (9.13), we rewrite the e2e high SNR for OPEHA policy (9.3) as

$$\Gamma_{eq,l} = \min\left\{\frac{1}{\rho_l\,|W|}, \rho_l \frac{P_S}{N_0}\,|X|\,|Y| + \frac{P_S}{N_0}\,|Z|\right\}. \tag{9.14}$$

Therefore, the following expression must be solved to maximize the e2e high SNR as

$$\frac{1-\alpha_l^*}{\eta\alpha_l^*\,|W|} = \frac{\eta\alpha_l^*}{1-\alpha_l^*}\frac{P_S}{N_0}\,|X|\,|Y| + \frac{P_S}{N_0}\,|Z|\,, \tag{9.15}$$

where we define α_l^* as the optimal TS ratio at R_l.

Following from *Remark* 9.1, the above expression must be solved first to achieve α_l^* for OPEHA policy. Thus, we have

$$\alpha_l^* = \left[\frac{2\eta\Omega_X\Omega_Y}{\sqrt{\left(\Omega_Z\right)^2 + \frac{4N_0}{P_S}\frac{\Omega_X\Omega_Y}{\Omega_W}} - \Omega_Z} + 1\right]^{-1}. \tag{9.16}$$

Proposition 9.2. Similar to **Proposition** 9.1, the exact closed-form OP for this policy be expressed as

$$OP_{EHA}^{FDJD}(\Gamma_1) = \left[1 - (\Theta_1 \times \Theta_2)\right]^N, \tag{9.17}$$

where $\Theta_1 = e^{-\left(\frac{N_0\Gamma_1}{P_S\Omega_Z}\right)}\left(1 - e^{\left(-\frac{1}{\rho_l\Gamma_1\Omega_W}\right)}\right)$,

and $\Theta_2 = \left(1 + \frac{2N_0}{P_S\Omega_Z}\int_{x=0}^{\sqrt{\Gamma_1}} x e^{\left(\frac{x^2N_0}{P_S\Omega_Z}\right)}\sqrt{\frac{4x^2}{\rho_l P_S\Omega_X\Omega_Y}}K_1\left(\sqrt{\frac{4x^2}{\rho_l P_S\Omega_X\Omega_Y}}\right)dx\right)$.

Proof: The proof for **Proposition** 9.2 is given in Appendix D.2.

9.3.3 RS Schemes for Half-Duplex relaying deploying maximal ratio combine (HDMRC)

Different from FDJD RS scheme, the best relay node is selected without the knowledge of SI based on the max-min RS without the impact of SI in HDMRC. Regarding the best e2e link, we select k-th relay by

$$k = \arg\max_{i:R_i\in N} \min\left\{P_S|X|, \frac{P_{R_i}|Y|}{N_0} + \frac{P_S|Z|}{N_0}\right\}. \tag{9.18}$$

The instantaneous e2e of HDMRC RS scheme is computed by

$$C_k^{HDMRC} = \frac{1}{2}\log_2\left(1+\Gamma_{eq,k}\right), \tag{9.19}$$

where the instantaneous e2e SNR at D is denoted as $\Gamma_{eq,k}$, when the best relay, R_k is selected.

A. Optimal power under individual power constrains (OPIPC)

Proposition 9.3. In terms of OPIPC, we obtain the exact closed-form expression for OP in the e2e high SNR based on (9.12) as

$$\Theta_1 = e^{-\frac{\Gamma_2}{P_S\Omega_X}}, \tag{9.20a}$$

and

$$\Theta_2 = \frac{P_S\Omega_Z \mathrm{e}^{-\frac{N_0\Gamma_2}{P_S\Omega_Z}} - P_{R_k}\Omega_Y \mathrm{e}^{-\frac{N_0\Gamma_2}{P_{R_k}\Omega_Y}}}{P_S\Omega_Y - P_{R_k}\Omega_Z}, \tag{9.20b}$$

where the target SNR threshold for HDMRC is $\Gamma_2 = 2^{2R_0}-1$, and the average transmit power at k-th R is obtained following from (9.11) as $P_{R_k} = \min\left\{P_S, \frac{(N_0\Omega_X-\Omega_Z)}{\Omega_Y}\right\}$.
Proof: We present the proof for **Proposition** 9.1 similarly in Appendix D.1. However, thanks to SI cancellation process at k-th R, the CDF of the first branch at high SNR, Γ_{SR_k} at k-th R is now updated as $F_{\Gamma_{SR_k}}(\Gamma_2) \triangleq \Pr\left(P_S|X| \le \Gamma_2\right) = 1 - e^{-\frac{\Gamma_2}{P_S\Omega_X}}$.

B. Optimal power with energy harvesting ability (OPEHA)

Proposition 9.4. Similarly, we derive the exact closed-form expression for OP for OPEHA at high SNR can be computed using (9.17) as

$$\Theta_1 = e^{-\left(\frac{N_0\Omega_X+\Omega_Z}{P_S\Omega_X\Omega_Z}\right)\Gamma_2}, \tag{9.21a}$$

and

$$\Theta_2 = 1 + \frac{2N_0}{P_S\Omega_Z}\int_{x=0}^{\sqrt{\Gamma_2}} xe^{\left(\frac{x^2N_0}{P_S\Omega_Z}\right)}\sqrt{\frac{4x^2}{\rho_k P_S\Omega_X\Omega_Y}}K_1\left(\sqrt{\frac{4x^2}{\rho_k P_S\Omega_X\Omega_Y}}\right)dx, \tag{9.21b}$$

where since we obtained the optimal TS ratio in (9.16), we can similarly express it for OPEHA policy as $\alpha_k^* = \left[1+\frac{\eta\Omega_X\Omega_Y}{N_0\Omega_X-\Omega_Z}\right]^{-1}$.
Proof: We omit the detailed proof for the above expression due to similar steps provided in Appendix D.2.

9.3.4 RS schemes Hybrid FD/HD relaying transmission scheme (HTS)

In fact, both FDJD and HDMRC suffer from zero diversity gain because of the nature of FD transmission and the impact of SI. Therefore, we come up with an adaptive RS

policy called HTS to overcome these situations which is able to switch between FD and HD relaying.

It is noted that the proposal of an efficient RS scheme is important, where HTS activates the h-th relay to enjoy the best outage performance. However, the following condition must be satisfied

$$h \underset{m\in\{IPC,EHA\}}{=} \arg\max_{i:R_i\in N} \max\left\{C_{m,i}^{FDJD}, C_{m,i}^{HDMRC}\right\}. \tag{9.22}$$

Theorem 9.2. Therefore, the OP in HTS in both OPIPC and OPEHA can be respectively expressed by

$$\begin{aligned} OP_m^{HTS} &\underset{m\in\{IPC,EHA\}}{=} \Pr\left\{\max\left\{C_m^{FDJD}, C_m^{HDMRC}\right\} < R_0\right\} \\ &\underset{m\in\{IPC,EHA\}}{=} \Pr\left\{C_m^{FDJD} < R_0, C_m^{HDMRC} < R_0\right\}. \end{aligned} \tag{9.23}$$

Remark 9.2. It is interesting that HTS scheme helps the system select the suitable duplexing mode with better transmission efficiency at R nodes. In this scheme, we can achieve the better outage performance than other RS schemes without being degraded by zero-diversity. Besides, when an outage event exists, the best relay is selected with the maximum information rate in case we set the system below the target SE, R_0. In other words, we express the maximum instantaneous capacity in FDJD and HDMRC in (9.7) and (9.19), respectively.

Please note that we are going to obtain the closed-form expression for OP in *Theorem* 9.3, **Proposition** 9.5 and **Proposition** 9.6 later. Now, the following lemmas are used to explain the proof of these propositions. *Lemma* 9.1 is considered first.

Lemma 9.1. We define $a_1 > 0$, $a_2 > 0$, $\tau_1 > 0$ and $\tau_2 \in [0,\infty]$. The probability of the intersection of events, i.e., $[a_1|Y| + a_2|Z| \le \tau_1]$ and $[|Y| \le \tau_2]$ denoted by $\Upsilon_1(a_1,a_2,\tau_1,\tau_2)$ can be written as

$$\begin{aligned} &\Upsilon_1(a_1,a_2,\tau_1,\tau_2) \\ &= \begin{cases} 1 - e^{-\frac{\tau_0}{\Omega_Y}} - \frac{\tau_0}{\Omega_Y} e^{-\left(\frac{\tau_1}{a_2\Omega_Z}\right)}, & \text{if} \quad a_2|Z| - a_1|Y| = 0 \\ 1 - e^{-\frac{\tau_0}{\Omega_Y}} - \frac{1}{\Omega_Y}\left(\frac{1}{\Omega_Y} - \frac{a_1}{a_2\Omega_Z}\right)^{-1} e^{-\frac{\tau_1}{a_2\Omega_Z}} \left(1 - e^{-\left(\frac{1}{\Omega_Y} - \frac{a_1}{a_2\Omega_Z}\right)\tau_0}\right), & \text{otherwise} \end{cases}, \end{aligned} \tag{9.24}$$

where $\tau_0 = \min\left\{\tau_2, a_1^{-1}\tau_1\right\}$. Particularly, if $\tau_2 = \infty$, $\Pr([a_1|Y| + a_2|Z| \le \tau_1]) = \Upsilon_1\left(a_1,a_2,\tau_1,a_1^{-1}\tau_1\right)$.

Proof: We define the transformation, $\{|Y|,|Z|\} \to \{U,V\}$ as $\{U = |Y|, V = a_1|Y| + a_2|Z|\}$. Thus, the Jacobian determinant of its inverse transformation is a_2^{-1}. Thus, the probability $\Pr([V \le \tau_1],[U \le \tau_2])$ is expressed as

$$\begin{aligned} \Upsilon_1(a_1,a_2,\tau_1,\tau_2) &= \int_0^{\tau_0}\left(\int_0^{\tau_1} \frac{1}{a_2} f_{|Y|}(u) f_{|Z|}\left(\frac{1}{a_2}(v - a_1u)\right) dv\right) du \\ &= \int_0^{\tau_0}\left(\int_0^{\frac{1}{a_2}(\tau_1 - a_1u)} f_{|Y|}(u) f_{|Z|}(t)\, dt\right) du \\ &= \int_0^{\tau_0} f_{|Y|}(u) F_{|Z|}\left(\frac{1}{a_2}(\tau_1 - a_1u)\right) du, \end{aligned} \tag{9.25}$$

where τ_0 is defined in *Lemma* 9.1. After some algebraic manipulations, the useful expression (9.24) is derived which ends the proof for *Lemma* 9.1.

Lemma 9.2. We assume $\alpha \in (0,\infty]$, and $A,B,C > 0$. Besides, $\mathcal{J}^{(p)}(\alpha,A,B,C) = \int_0^{\alpha} \frac{x}{-x+A} \exp\left(-\left(Bx+Cx^{-1}\right)\right) dx$ is defined as the integral of a general function. Thus, we have

$$\mathcal{J}^{(p)}(\alpha,A,B,C) \approx \begin{cases} L_1 + L_2^{(p)}, A < \alpha < \infty \\ L_1, \alpha = A \quad \text{or} \quad \alpha = \infty \\ L_3^{(p)}, \alpha < A \end{cases}, \quad where \quad p \in \{0,\infty\} \ , \tag{9.26}$$

where

$$L_1 = \left[\tfrac{B^2A^3}{12} + \tfrac{BA^2}{2} + \tfrac{5A}{6} - \tfrac{ABC}{3} - \tfrac{2C}{3} + \tfrac{C^2}{12A}\right] \exp\left(-\left(AB + CA^{-1}\right)\right), \tag{9.27a}$$

$$\begin{aligned} L_2^{(p)} = -\Big[\alpha + \tfrac{5A}{6} + \tfrac{1}{2}\left(-B + \tfrac{C}{\alpha^2}\right)\alpha(-\alpha+A) + \tfrac{A}{3}(-\alpha+A)\left(-B+\tfrac{C}{\alpha^2}\right) \\ + \tfrac{\alpha}{6}(-\alpha+A)^2\left(-\tfrac{2C}{\alpha^3} + \left(-B+\tfrac{C}{\alpha^2}\right)^2\right)\Big]\Delta^{(p)}, \end{aligned} \tag{9.27b}$$

$$\begin{aligned} L_3^{(p)} = \Big[\tfrac{1}{12A}\left(-B^2\alpha^4 - C^2\right) + \tfrac{1}{6A}\left(B\alpha^3 + (3+BC)\alpha^2\right) + \tfrac{1}{6A^2}\left(B^2\alpha^5 + C^2\alpha\right) \\ + \tfrac{1}{3A^2}\left(B\alpha^4 + (1-BC)\alpha^3 - 2C\alpha^2\right)\Big]\Delta^{(p)}, \end{aligned} \tag{9.27c}$$

where if $B\alpha \to 0$, $\Delta^{(\infty)} = (1-B\alpha)\exp\left(-C\alpha^{-1}\right)$. Otherwise, $\Delta^{(0)} = \exp\left(-\left(B\alpha + C\alpha^{-1}\right)\right)$.

Proof: Let us define $\mathcal{G}(x) = \frac{x}{-x+A} = -1 + \frac{A}{-x+A}$ and $\mathcal{H}(x) = \exp\left(-\left(Bx+Cx^{-1}\right)\right)$. Because the derivation of $\mathcal{J}^{(p)}(\alpha,A,B,C)$ in close form is challenging, the second-order Taylor series expansion of $\mathcal{G}(x)\mathcal{H}(x)$ is applied in each region, including *i)* $\alpha > A$, *ii)* $\alpha = A$, or $\alpha = \infty$ and *iii)* $\alpha < A$.

Here, the second-order Taylor series expansion of $\mathcal{G}(x), \mathcal{H}(x)$ is defined as $\mathcal{G}^{(1)}(x) = \frac{A}{(-x+A)^2}$, $\mathcal{G}^{(2)}(x) = \frac{2A}{(-x+A)^3}$, $\mathcal{H}^{(1)}(x) = \left(-B + \frac{C}{x^2}\right)\mathcal{H}(x)$,
and $\mathcal{H}^{(2)}(x) = \left(-\frac{2C}{x^3} + \left(-B+\frac{C}{x^2}\right)^2\right)\mathcal{H}(x)$, respectively.

Here, each region *i)*, *ii)* and *iii)* is considered.

i). In case $\alpha > A$, we have the following expression as

$$\begin{aligned} \mathcal{J}^{(p)}(\alpha,A,B,C) &= \int_0^{\alpha} \frac{x}{-x+A} \exp\left(-\left(Bx+Cx^{-1}\right)\right) dx \\ &= \underbrace{\lim_{\varepsilon \to A^-} \int_0^{\varepsilon} \mathcal{G}(x)\mathcal{H}(x)\,dx}_{L_1} + \underbrace{\lim_{\varepsilon \to A^+} \int_{\varepsilon}^{\alpha} \mathcal{G}(x)\mathcal{H}(x)\,dx}_{L_2^{(p)}} . \end{aligned} \tag{9.28}$$

In terms of the first item, L_1 is as $\varepsilon \to A^-$, a one-dimensional Taylor series is an expansion of a real function $\mathcal{G}(x)$, $\mathcal{H}(x)$ at $x = 0$, $x = \varepsilon$, respectively. Thus, L_1 is presented similarly as in (9.27a).

Likewise, when $\varepsilon \to A^+$, Taylor series is an expansion of a real function, $\mathcal{G}(x)$, $\mathcal{H}(x)$ at $x = \alpha$. Therefore, $L_2^{(p)}$ follows from the result of (9.27b).

ii). When $\alpha = A$ or $\alpha \to \infty$, it can be known easily as $L_2^{(p)} = 0$. Thus, $\mathcal{J}^{(p)}(\alpha, A, B, C)$ can be computed by

$$\mathcal{J}^{(p)}(\alpha, A, B, C) = \lim_{\varepsilon \to A^-} \int_0^{\varepsilon} \mathcal{G}(x)\, \mathcal{H}(x)\, dx = L_1. \tag{9.29}$$

iii). When $0 < \alpha < A$, after some similar simple manipulations, where $\mathcal{J}^{(p)}(\alpha, A, B, C) = L_3^{(p)}$. L_3 is obtained as in (9.27c).

To this end, the desired result for *Lemma 9.2* is achieved to prove the proof.

Lemma 9.3. Let us define $\Upsilon_2^{(p)}(a, \alpha, \beta, \gamma) = \Pr\left([|X| \le \alpha], [|X|\,|Y| + a\,|Z| \le \beta], [|Z| \le \gamma]\right)$, where $\alpha, \beta, \gamma \in (0, \infty]$ and $a > 0$.

The exact expression is derived as

$$\Upsilon_2^{(p)}(a, \alpha, \beta, \gamma) = F_{|\mathrm{X}|}(\alpha)\, F_{|\mathrm{Z}|}(\delta) - \frac{1}{\Omega_X}\left[\exp\left(-\frac{\delta}{\Omega_Z}\right)\mathcal{J}_1 - \mathcal{J}_2\right], \tag{9.30}$$

where $\delta = \min\{\gamma, \beta a^{-1}\}$, $\mathcal{J}_1 = \int_{x=0}^{\alpha} \frac{x}{-x + a\Omega_Z\Omega_Y^{-1}} \exp\left(-\left(\frac{x}{\Omega_X} + \frac{\beta - a\delta}{x\Omega_Y}\right)\right) dx$,
$\mathcal{J}_2 = \int_{x=0}^{\alpha} \frac{x}{-x + a\Omega_Z\Omega_Y^{-1}} \exp\left(-\left(\frac{x}{\Omega_X} + \frac{\beta}{x\Omega_Y}\right)\right) dx$.

In principle, closed-form expressions for $\mathcal{J}_1$ and $\mathcal{J}_2$ are difficult to obtain, but based on *Lemma* 9.2, we can approximate them as

$$\mathcal{J}_1 \approx \mathcal{J}^{(p)}\left(\alpha, a\Omega_Z\Omega_Y^{-1}, \Omega_X^{-1}, (\beta - a\delta)\Omega_Y^{-1}\right), \tag{9.31a}$$

and

$$\mathcal{J}_2 \approx \mathcal{J}^{(p)}\left(\alpha, a\Omega_Z\Omega_Y^{-1}, \Omega_X^{-1}, \beta\Omega_Y^{-1}\right), \tag{9.31b}$$

where $p \in \{0, \infty\}$.

Proof: Using a similar argument used for the proof of *Lemma* 9.2 with the transformation, $\{U = |X|, S = |X|\,|Y| + a\,|Z|, T = |Z|\}$. We have

$$\begin{aligned}
&\Upsilon_2^{(p)}(a, \alpha, \beta, \delta) \\
&= \int_0^{\alpha}\left(\int_0^{\delta} f_{|\mathrm{X}|}(u)\, f_{|\mathrm{Z}|}(t)\, F_{|\mathrm{Y}|}\left(\frac{1}{u}(\beta - at)\right) dt\right) du \\
&= \int_0^{\alpha}\int_0^{\delta} f_{|\mathrm{X}|}(u)\, f_{|\mathrm{Z}|}(t)\, dt du - \Omega_Y \int_0^{\alpha}\left(\int_0^{\delta} f_{|\mathrm{X}|}(u)\, f_{|\mathrm{Z}|}(t)\, f_{|\mathrm{Y}|}\left(\frac{1}{u}(\beta - at)\right) dt\right) du \\
&= F_{|\mathrm{X}|}(\alpha)\, F_{|\mathrm{Z}|}(\delta) - \Omega_Y \int_0^{\alpha} \phi(u)\, du,
\end{aligned} \tag{9.32}$$

where

$$\begin{aligned}
\phi(u) &= (\Omega_Y\Omega_Z)^{-1} f_{|\mathrm{X}|}(u) \exp\left(-\tfrac{\beta}{u\Omega_Y}\right) \int_0^{\delta} \exp\left(-\left(\frac{1}{\Omega_Z} - \frac{a}{u\Omega_Y}\right) t\right) dt \\
&= \begin{cases} \delta(\Omega_Y\Omega_Z)^{-1} f_{|\mathrm{X}|}(u) \exp(-\varphi_2(u)), & \text{for} \quad \mathrm{u} = \frac{\mathrm{a}\Omega_{\mathrm{Z}}}{\Omega_{\mathrm{Y}}} \\ (\Omega_Y\Omega_Z)^{-1} f_{|\mathrm{X}|}(u) (-\varphi_1(u))^{-1} \exp(-\varphi_2(u)) \left[\exp(-\varphi_1(u)\,\delta) - 1\right], & \text{otherwise} \end{cases},
\end{aligned}$$

$\varphi_1(u) = \frac{1}{\Omega_Z} - \frac{a}{u\Omega_Y}$, $(\varphi_1(u))^{-1} = \frac{u\Omega_Y\Omega_Z}{u\Omega_Y - a\Omega_Z}$, and $\varphi_2(u) = \frac{\beta}{u\Omega_Y}$.

Eventually, we derive the desired result in (9.30) which ends the proof for *Lemma* 9.3.

A. Optimal power under individual power constrains (OPIPC)

For this RS scheme, the OP in (9.23) for OPIPC can be rewritten by

$$OP_{IPC}^{HTS} = \Pr\left(\left\{\min\left(\frac{P_S|X|}{P_{R_l}|W|}, \frac{P_{R_l}|Y|}{N_0} + \frac{P_S|Z|}{N_0}\right) \leq \Gamma_1\right\}, \left\{\min\left(P_S|X|, \frac{P_{R_k}|Y|}{N_0} + \frac{P_S|Z|}{N_0}\right) \leq \Gamma_2\right\}\right), \tag{9.33}$$

where P_{R_l}, P_{R_k} are the average transmit powers at R_l and R_k which were defined above. We are going to derive the analytical expression for OP_{IPC}^{HTS} in the next proposition.

Proposition 9.5. The exact closed-form expression for OP at high SNR in HTS RS scheme is calculated by

$$OP_{IPC}^{HTS} = \Theta_1\left(1 - \Theta_2 - \Theta_3\right) + \Theta_6\left(1 + \Theta_1 - \Theta_4 - \Theta_5\right) + \Theta_2\Theta_5 + \Theta_3\Theta_4, \tag{9.34}$$

where Θ_i, $i \in [1..6]$ is presented in detailed in the proof below.

Proof: Let us start with the simplification of notations used below for the following events as $\Phi_A = \left[\frac{|X|}{|W|} \leq \frac{P_{R_l}\Gamma_1}{P_S}\right]$, $\Phi_B = \left[\frac{P_{R_l}|Y|}{N_0} + \frac{P_S|Z|}{N_0} \leq \Gamma_1\right]$, $\Phi_C = \left[|X| \leq \frac{\Gamma_2}{P_S}\right]$ and $\Phi_D = \left[\frac{P_{R_k}|Y|}{N_0} + \frac{P_S|Z|}{N_0} \leq \Gamma_2\right]$.

It is worth noting that Φ_A is independent of Φ_B and Φ_D while Φ_C is independent of Φ_B and Φ_D. Following from [108], $\Pr\left(\min(U, V)\right) = \Pr\left(U \cup V\right)$ is the probability of all results of U or V, so $\Pr(U \cup V) = \Pr(U) + \Pr(V) - \Pr(UV)$. Thus, the probability in (9.33) can be expressed as

$$\begin{aligned} OP_{IPC}^{HTS} &= \Pr\left(\left(\Phi_A \cup \Phi_B\right), \left(\Phi_C \cup \Phi_D\right)\right) \\ &= \Pr\left(\Phi_A\Phi_C \cup \Phi_A\Phi_D\right) + \Pr\left(\Phi_B\Phi_C \cup \Phi_B\Phi_D\right) - \Pr\left(\Phi_A\Phi_B\left(\Phi_C \cup \Phi_D\right)\right) \\ &= \Pr\left(\Phi_A\Phi_C\right)\left[1 - \Pr\left(\Phi_B\right) - \Pr\left(\Phi_D\right)\right] \\ &+ \Pr\left(\Phi_B\Phi_D\right)\left[1 - \Pr\left(\Phi_A\right) - \Pr\left(\Phi_C\right) + \Pr\left(\Phi_A\Phi_C\right)\right] \\ &+ \Pr\left(\Phi_B\right)\Pr\left(\Phi_C\right) + \Pr\left(\Phi_A\right)\Pr\left(\Phi_D\right). \end{aligned} \tag{9.35}$$

Here, each probability in the above expression is going to studied. Let us start with $\Theta_1 = \Pr\left(\Phi_A\Phi_C\right)$ which can be given as

$$\Theta_1 = \Pr\left(\left[\frac{|X|}{|W|} \leq \frac{P_{R_l}\Gamma_1}{P_S}\right], E_1\right) + \Pr\left(\left[|X| \leq \frac{\Gamma_2}{P_S}\right], \overline{E}_1\right), \tag{9.36}$$

where E_1 is defined as $\left[|W| \leq \frac{\Gamma_2}{P_{R_l}\Gamma_1}\right]$ because $\left[\frac{|X|}{|W|} \leq \frac{P_{R_l}\Gamma_1}{P_S}\right]\left[|X| \leq \frac{\Gamma_2}{P_S}\right] = \left[|X| \leq \min\left\{\frac{P_{R_l}\Gamma_1}{P_S}|W|, \frac{\Gamma_2}{P_S}\right\}\right]$, and $\overline{E}_1$ is the complement of E_1.

Now, let us regard the first probability item in (9.36) as

$$\begin{aligned} \Theta_{1,a} &= \Pr\left(\left[\frac{|X|}{|W|} \leq \frac{P_{R_l}\Gamma_1}{P_S}\right], \left[|W| \leq \frac{\Gamma_2}{P_{R_l}\Gamma_1}\right]\right) \\ &= F_{|W|}\left(\frac{\Gamma_2}{P_{R_l}\Gamma_1}\right) - \frac{1}{\Omega_W}\int_0^{\frac{\Gamma_2}{P_{R_l}\Gamma_1}} e^{-\left(\frac{1}{\Omega_W} + \frac{P_{R_l}\Gamma_1}{P_S\Omega_X}\right)x} dx \\ &= 1 - e^{-\left(\frac{\Gamma_2}{P_{R_l}\Gamma_1\Omega_W}\right)} - \frac{1}{\Omega_W}\left(\frac{1}{\Omega_W} + \frac{P_{R_l}\Gamma_1}{P_S\Omega_X}\right)^{-1}\left(1 - e^{-\left(\frac{1}{\Omega_W} + \frac{P_{R_l}\Gamma_1}{P_S\Omega_X}\right)\frac{\Gamma_2}{P_{R_l}\Gamma_1}}\right). \end{aligned} \tag{9.37}$$

Next, due to the independence of RVs of $|X|$ and $|W|$, the second probability item is computed as

$$\begin{aligned}\Theta_{1,b} &= \Pr\left(\left[|X| \leq \tfrac{\Gamma_2}{P_S}\right], \left[|W| > \tfrac{\Gamma_2}{P_{R_l}\Gamma_1}\right]\right) \\ &= F_{|X|}\left(\tfrac{\Gamma_2}{P_S}\right)\left(1 - F_{|W|}\left(\tfrac{\Gamma_2}{P_{R_l}\Gamma_1}\right)\right) \\ &= \left(1 - e^{-\frac{\Gamma_2}{P_S\Omega_X}}\right) e^{-\frac{\Gamma_2}{P_{R_l}\Gamma_1\Omega_W}}.\end{aligned} \tag{9.38}$$

Replacing (9.37), (9.38) into (9.36), the result for Θ_1 is obtained as

$$\begin{aligned}\Theta_1 = 1 &- e^{-\left(\frac{1}{P_S\Omega_X} + \frac{1}{P_{R_l}\Gamma_1\Omega_W}\right)\Gamma_2} \\ &- \tfrac{1}{\Omega_W}\left(\tfrac{1}{\Omega_W} + \tfrac{P_{R_l}\Gamma_1}{P_S\Omega_X}\right)^{-1}\left(1 - e^{-\left(\frac{1}{P_S\Omega_X} + \frac{1}{P_{R_l}\Gamma_1\Omega_W}\right)\Gamma_2}\right).\end{aligned} \tag{9.39}$$

Firstly, using the result of (D.1.2) in Appendix D.1, the probability is as follows

$$\Theta_2 = \Pr\left(\Phi_B\right) = 1 + \frac{P_S\Omega_Z e^{-\frac{N_0\Gamma_1}{P_S\Omega_Z}} - P_{R_l}\Omega_Y e^{-\frac{N_0\Gamma_1}{P_{R_l}\Omega_Y}}}{P_{R_l}\Omega_Y - P_S\Omega_Z}, \tag{9.40a}$$

and

$$\Theta_3 = \Pr\left(\Phi_D\right) = 1 + \frac{P_S\Omega_Z e^{-\frac{N_0\Gamma_2}{P_S\Omega_Z}} - P_{R_k}\Omega_Y e^{-\frac{N_0\Gamma_2}{P_{R_k}\Omega_Y}}}{P_{R_k}\Omega_Y - P_S\Omega_Z}, \tag{9.40b}$$

Secondly, thanks to (D.1.1) in Appendix D.1, we compute the probability, Θ_4 as

$$\Theta_4 = \Pr\left(\Phi_A\right) = 1 - \frac{P_S\Omega_X}{P_{R_l}\Omega_W\Gamma_1 + P_S\Omega_X}. \tag{9.40c}$$

Thirdly, the following expression can be easily derived as

$$\Theta_5 = \Pr\left(\Phi_C\right) = 1 - e^{-\frac{\Gamma_2}{P_S\Omega_X}}. \tag{9.41}$$

Finally, considering $\Theta_6 = \Pr\left(\Phi_B\Phi_D\right)$, we see that $\Gamma_2 > \Gamma_1$ and $P_{R_k} > P_{R_l}$. Thus, we derive

$$\begin{aligned}&\left[a\left|Y\right| + c\left|Z\right| \leq \Gamma_1\right]\left[b\left|Y\right| + c\left|Z\right| \leq \Gamma_2\right] \\ &= \left[|Z| \leq c^{-1}\left(\Gamma_1 - a\left|Y\right|\right)\right]\left[|Z| \leq c^{-1}\left(\Gamma_2 - b\left|Y\right|\right)\right] \\ &= \left[|Z| \leq \min\left\{c^{-1}\left(\Gamma_1 - a\left|Y\right|\right), c^{-1}\left(\Gamma_2 - b\left|Y\right|\right)\right\}\right],\end{aligned}$$

where $a = \frac{P_{R_l}}{N_0}$, $b = \frac{P_{R_k}}{N_0}$, and $c = \frac{P_S}{N_0}$.

Therefore, Θ_6 is written as

$$\begin{aligned}\Theta_6 &= \Pr\left(\Phi_B, E_2\right) + \Pr\left(\Phi_D, \overline{E}_2\right) \\ &= \Pr\left(\Phi_B, E_2\right) + \Pr\left(\Phi_D\right) - \Pr\left(\Phi_D, E_2\right),\end{aligned} \tag{9.42}$$

where $E_2 = \left[\Gamma_1 - a\left|Y\right| \leq \Gamma_2 - b\left|Y\right|\right] = \left[|Y| \leq \Gamma_0\right]$, $\Gamma_0 = \left(b - a\right)^{-1}\left(\Gamma_2 - \Gamma_1\right)$, and we can derive the last equality following the fact that $\Pr(U, \overline{V}) = \Pr(U) - \Pr(U, V)$ in [108].

By reconsidering *Lemma* 9.1, Θ_6 can be easily obtained as

$$\Theta_6 = \Upsilon_1\left(\frac{P_{R_l}}{N_0}, \frac{P_S}{N_0}, \Gamma_1, \frac{N_0\left(\Gamma_2 - \Gamma_1\right)}{P_{R_k} - P_{R_l}}\right) + \Theta_3 - \Upsilon_1\left(\frac{P_{R_k}}{N_0}, \frac{P_S}{N_0}, \Gamma_2, \frac{N_0\left(\Gamma_2 - \Gamma_1\right)}{P_{R_k} - P_{R_l}}\right), \tag{9.43}$$

where Θ_3 is presented in (9.40b).

To this end, substituting the derived results from (9.39), (9.40a), (9.40b),(9.40c), (9.41) and (9.43) into (9.35), the desirable closed-form OP for HTS in case of OPIPC is obtained. This ends the proof for **Proposition** 9.5.

B. Optimal power with energy harvesting ability (OPEHA)

Regarding OPEHA policy, the OP in (9.23) can be expressed as

$$\begin{aligned} OP_{EHA}^{HTS} = \Pr\big(\{\min\left(\mathrm{a}_1\left|X\right|, \mathrm{a}_2\left|X\right|\left|Y\right| + \mathrm{a}_3\left|Z\right|\right) \le \Gamma_2\}, \\ \left\{\min\left(\tfrac{1}{\rho_l|W|}, \mathrm{a}_4\left|X\right|\left|Y\right| + \mathrm{a}_3\left|Z\right|\right) \le \Gamma_1\right\}\big), \end{aligned} \tag{9.44}$$

where based on the obtained expressions for OP in HDMRC and FDJD in OPEHA, $\rho_k = \frac{\eta\alpha_k}{1-\alpha_k}$ at R_k and $\rho_l = \frac{\eta\alpha_l}{1-\alpha_l}$ at R_l, respectively. In each definition, we denote $\mathrm{a}_1 = P_S, \mathrm{a}_2 = \rho_k P_S/N_0, \mathrm{a}_3 = P_S/N_0$ and $\mathrm{a}_4 = \rho_l P_S/N_0$. It is noted that $\Gamma_2 > \Gamma_1$ and $a_2 > a_4$.

It is challenging to obtain the exact analysis as in (9.44). Thus, thanks to the results of *Lemma 9.2* and *9.3*, the following proposition is going to be presented regarding the derivation of OP in this policy.

Proposition 9.6. The closed-form approximation of the OP in (9.44) for OPEHA policy is given by

(i) When $a_2\Gamma_1 - a_4\Gamma_2 \ge 0$,

$$OP_{EHA}^{HTS} \approx \Theta_1 + (1-\Theta_2)\,\Theta_3 + \Theta_2\,(\Theta_4 + \Theta_6 - \Theta_7) - (1-\Theta_2)\,\Theta_5 - \Theta_2\,(\Theta_8 - \Theta_9), \tag{9.45a}$$

(ii) Otherwise, when $a_2\Gamma_1 - a_4\Gamma_2 < 0$,

$$OP_{EHA}^{HTS} \approx \Theta_1 + (1-\Theta_2)\,\Theta_3 + \Theta_2\Theta_4 - (1-\Theta_2)\,\Theta_5, \tag{9.45b}$$

where Θ_i, $i \in [1..9]$ in the above expression is going to evaluated in the following proof.

Proof: Likewise, we denote $\Phi_A = \left[\left|X\right| \le \frac{\Gamma_2}{a_1}\right]$, $\Phi_B = \left[\left|X\right|\left|Y\right| \le \frac{\Gamma_2}{a_2} - \frac{a_3}{a_2}\left|Z\right|\right]$,
$\Phi_C = \left[\left|W\right| \ge \frac{1}{\rho_l\Gamma_1}\right]$, $\Phi_D = \left[\left|X\right|\left|Y\right| \le \frac{\Gamma_1}{a_4} - \frac{a_3}{a_4}\left|Z\right|\right]$, and
$\Phi_E = \left[\frac{\Gamma_2}{a_2} - \frac{a_3}{a_2}\left|Z\right| \le \frac{\Gamma_1}{a_4} - \frac{a_3}{a_4}\left|Z\right|\right] = [|Z| \le a_3^{-1}\,(a_2 - a_4)^{-1}\,(a_2\Gamma_1 - a_4\Gamma_2)]$.

The event, Φ_C is independent of Φ_A, Φ_B and Φ_D. Similar to the proof for (9.35) in **Proposition** 9.5, we can simplify the probability in (9.44) as

$$\begin{aligned} OP_{EHA}^{HTS} &= \Pr(\Phi_A)\Pr(\Phi_C) + \Pr(\Phi_B)\Pr(\Phi_C) \\ &\quad + \Pr\left(\overline{\Phi}_C\right)[\Pr(\Phi_B\Phi_E) + \Pr(\Phi_D) - \Pr(\Phi_D\Phi_E)] \\ &\quad - \Pr(\Phi_C)\Pr(\Phi_A\Phi_B) - \Pr\left(\overline{\Phi}_C\right)[\Pr(\Phi_A\Phi_B\Phi_E) - \Pr(\Phi_A\Phi_D\Phi_E)]. \end{aligned} \tag{9.46}$$

i) If $a_2\Gamma_1 - a_4\Gamma_2 \ge 0$, $\Phi_E \ne 0$. Firstly, we have

$$\Theta_1 = \Pr(\Phi_A)\Pr(\Phi_C) = \left(1 - \exp\left(-\frac{\Gamma_2}{a_1\Omega_X}\right)\right)\exp\left(-\tfrac{1}{\rho_l\Omega_W\Gamma_1}\right). \tag{9.47}$$

$$\Theta_2 = \Pr\left(\overline{\Phi}_C\right) = 1 - \exp\left(-\tfrac{1}{\rho_l\Omega_W\Gamma_1}\right). \tag{9.48}$$

Secondly, the following expressions are written based on Appendix D.2 and (D.2.8) as

$$\begin{aligned}\Theta_3 &= \Pr\left(\Phi_B\right) \\ &= 1 - e^{-\left(\frac{\Gamma_2}{a_3\Omega_Z}\right)} \left[1 + \tfrac{2}{a_3\Omega_Z} \int_{x=0}^{\sqrt{\Gamma_2}} \left(2x\sqrt{\frac{x^2}{a_2 N_0 \Omega_X \Omega_Y}} e^{\left(\frac{x^2}{a_3\Omega_Z}\right)} K_1\left(2\sqrt{\frac{x^2}{a_2 N_0 \Omega_X \Omega_Y}}\right)\right) dx\right],\end{aligned} \tag{9.49a}$$

and

$$\begin{aligned}\Theta_4 &= \Pr\left(\Phi_D\right) \\ &= 1 - e^{-\left(\frac{\Gamma_1}{a_3\Omega_Z}\right)} \left[1 + \tfrac{2}{a_3\Omega_Z} \int_{x=0}^{\sqrt{\Gamma_1}} \left(2x\sqrt{\frac{x^2}{a_4 N_0 \Omega_X \Omega_Y}} e^{\left(\frac{x^2}{a_3\Omega_Z}\right)} K_1\left(2\sqrt{\frac{x^2}{a_4 N_0 \Omega_X \Omega_Y}}\right)\right) dx\right].\end{aligned} \tag{9.49b}$$

Thanks to *Lemma* 9.2 and *Lemma* 9.3, the joint probability distributions is expressed as

$$\Theta_5 = \Pr\left(\Phi_A\Phi_B\right) \approx \Upsilon_2^{(p)}\left(\frac{a_3}{a_2}, \frac{\Gamma_2}{a_1}, \frac{\Gamma_2}{a_2}, \delta_1\right), \tag{9.50a}$$

$$\Theta_6 = \Pr\left(\Phi_B\Phi_E\right) \approx \Upsilon_2^{(p)}\left(\frac{a_3}{a_2}, \infty, \frac{\Gamma_2}{a_2}, \delta_2\right), \tag{9.50b}$$

$$\Theta_7 = \Pr\left(\Phi_D\Phi_E\right) \approx \Upsilon_2^{(p)}\left(\frac{a_3}{a_4}, \infty, \frac{\Gamma_1}{a_4}, \delta_3\right), \tag{9.50c}$$

$$\Theta_8 = \Pr\left(\Phi_A\Phi_B\Phi_E\right) \approx \Upsilon_2^{(p)}\left(\frac{a_3}{a_2}, \frac{\Gamma_2}{a_1}, \frac{\Gamma_2}{a_2}, \delta_4\right), \tag{9.50d}$$

$$\Theta_9 = \Pr\left(\Phi_A\Phi_D\Phi_E\right) \approx \Upsilon_2^{(p)}\left(\frac{a_3}{a_4}, \frac{\Gamma_2}{a_1}, \frac{\Gamma_1}{a_4}, \delta_5\right), \tag{9.50e}$$

where $\delta_1 = \min\left\{\infty, \frac{\Gamma_2}{a_2}\left(\frac{a_3}{a_2}\right)^{-1}\right\} = \frac{\Gamma_2}{a_3}$, $\delta_2 = \delta_4 = \min\left\{a_3^{-1}\left(a_2 - a_4\right)^{-1}\left(a_2\Gamma_1 - a_4\Gamma_2\right), \frac{\Gamma_2}{a_3}\right\}$, $\delta_3 = \min\left\{a_3^{-1}\left(a_2 - a_4\right)^{-1}\left(a_2\Gamma_1 - a_4\Gamma_2\right), \frac{\Gamma_1}{a_4}\right\}$, $\delta_5 = \min\left\{a_3^{-1}\left(a_2 - a_4\right)^{-1}\left(a_2\Gamma_1 - a_4\Gamma_2\right), \frac{\Gamma_1}{a_3}\right\}$, respectively.

ii) If $a_2\Gamma_1 - a_4\Gamma_2 < 0$, $\Phi_E = \emptyset$ which leads to the fact that $\Pr\left(\Phi_A\Phi_B\Phi_E\right) = \Pr\left(\Phi_A\Phi_D\Phi_E\right) = \Pr\left(\Phi_B\Phi_E\right) = \Pr\left(\Phi_D\Phi_E\right) = 0$, we rearrange the hybrid OP in (9.46) for simplicity as

$$OP_{EHA}^{HTS} = \Pr\left(\Phi_A\right)\Pr\left(\Phi_C\right) + \Pr\left(\Phi_B\right)\Pr\left(\Phi_C\right) + \Pr\left(\overline{\Phi}_C\right)\Pr\left(\Phi_D\right) - \Pr\left(\Phi_C\right)\Pr\left(\Phi_A\Phi_B\right). \tag{9.51}$$

This ends the proof for **Proposition** 9.6.

9.3.5 Power consumption model

There is no doubt that the demand for EE communication is high in future 5G wireless networks, the total power consumption must be deeply studied. In this chapter, the amount

of power consumed in the proposed RS schemes, the best relay is selected to minimize the total power consumption, where the quantity of bits received successfully per unit of energy into is examined while the QoS requirements are satisfied. In fact, the static power consumption falls, and the system EE increases [100, 101].

Thus, if HDMRC RS scheme is assumed to be selected to operate, the total power consumption is expressed as

$$P_{t,m}^{HDMRC} = P_C + \frac{1}{2}\left(a_S P_S + a_R \sum_{n=1}^{N} P_{R,m}^{HDMRC}\right), \qquad m \in [IPC, EHA] \tag{9.52}$$

where a_S and a_R are coefficients of power consumption considering the average radiated power, while the static power consumption is defined as $P_C = b_S + Nb_R$ with b_S and b_R being modelled as the stable power consumed in case of signal processing and cooling, with N being the number of relays [100]. For this formula, $P_{R,IPC}$ and $P_{R,EHA}$ are the maximum transmit powers at R in OPIPC and OPEHA, respectively.

Otherwise, when the system operates in FDJD RS scheme, although the static power, P_C is similar to that in HDMRC scheme, the average radiated power in in FDJD scheme is double compared to that in HDMRC. Therefore, the total power consumption in FDJD RS scheme can be expressed by

$$P_{t,m}^{FDJD} = P_C + a_S P_S + a_R \sum_{n=1}^{N} P_{R,m}^{FDJD}. \tag{9.53}$$

Likewise, in case of HTS RS scheme, the total of power consumption is obtained as

$$P_{t,m}^{HTS} = OP_m^{HDMRC}(\Gamma_2)\, P_{t,m}^{HDMRC} + \left[1 - OP_m^{HDMRC}(\Gamma_2)\right] P_{t,m}^{FDJD}. \tag{9.54}$$

Remark 9.3.

- The derived exact and approximate closed-form expressions for OP for the three proposed RS schemes are summarized in Table. 9.1. It is worth noting that the expressions for OP with constants, Φ_i, $i \in [1..9]$ are different in OPIPC and OPEHA.
- Thanks to the asymptotic characteristic of $K_1(x)$ which shows that $K_1(x) \to 1/x$, and $e^{-x} = 1 - x$ when $x \to 0$, the asymptotic expressions for OP at high SNR when $P_S \to \infty$ can be derived. Thanks to the derived results in Table. 9.1, Table. 9.2 provides approximate values for the derived analytical expressions in the above sections, with Φ_i^{∞}, $i \in [1..9]$.

9.4 Numerical Results

In this section, we provide numerical simulations to prove the OP, the total power consumption of the proposed RS schemes with regard to optimal power supply policies with

Tab. 9.1: The summary of derived OP expressions

I. In HDMRC, the OP is given by $OP_m(\Gamma_2) = 1 - [\Theta_1 \times \Theta_2]$, $m \in [IPC, EHA]$	
OPIPC	$\Theta_1 = e^{-\frac{\Gamma_2}{P_S\Omega_X}}$, $\Theta_2 = \frac{P_S\Omega_Z \mathrm{e}^{-\frac{N_0\Gamma_2}{P_S\Omega_Z}} - P_{R_k}\Omega_Y \mathrm{e}^{-\frac{N_0\Gamma_2}{P_{R_k}\Omega_Y}}}{P_S\Omega_Z - P_{R_k}\Omega_Y}$
OPEHA	$\Theta_1 = e^{-\left(\frac{N_0\Omega_X+\Omega_Z}{P_S\Omega_X\Omega_Z}\right)\Gamma_2}$, $\Theta_2 = 1 + \frac{2N_0}{P_S\Omega_Z}\int_{x=0}^{\sqrt{\Gamma_2}} x e^{\left(\frac{N_0x^2}{P_S\Omega_Z}\right)} 2\sqrt{\frac{x^2}{\rho_k P_S\Omega_X\Omega_Y}} K_1\left(2\sqrt{\frac{x^2}{\rho_k P_S\Omega_X\Omega_Y}}\right) dx$
II. In FDJD, the OP is given by $OP_m(\Gamma_1) = 1 - [\Theta_1 \times \Theta_2]$, $m \in [IPC, EHA]$	
OPIPC	$\Theta_1 = \frac{P_S\Omega_X}{P_{R_l}\Omega_W\Gamma_1 + P_S\Omega_X}$, $\Theta_2 = \frac{P_S\Omega_Z \mathrm{e}^{-\frac{N_0\Gamma_1}{P_S\Omega_Z}} - P_{R_l}\Omega_Y \mathrm{e}^{-\frac{N_0\Gamma_1}{P_{R_l}\Omega_Y}}}{P_S\Omega_Z - P_{R_l}\Omega_Y}$
OPEHA	$\Theta_1 = e^{-\left(\frac{N_0\Gamma_1}{P_S\Omega_Z}\right)}\left(1 - e^{\left(-\frac{1}{\rho_l\Gamma_1\Omega_W}\right)}\right)$, $\Theta_2 = 1 + \frac{2N_0}{P_S\Omega_Z}\int_{x=0}^{\sqrt{\Gamma_1}} x e^{\left(\frac{N_0x^2}{P_S\Omega_Z}\right)} 2\sqrt{\frac{x^2}{\rho_l P_S\Omega_X\Omega_Y}} K_1\left(2\sqrt{\frac{x^2}{\rho_l P_S\Omega_X\Omega_Y}}\right) dx$
III. In HTS The OP in OPIPC policy is given by $OP_{IPC}^{HTS} = \Theta_1(1 - \Theta_2 - \Theta_3) + \Theta_6(1 - \Theta_5 - \Theta_4 + \Theta_1) + \Theta_2\Theta_5 + \Theta_3\Theta_4$ The OP in OPEHA policy is given by (i) when $a_2\Gamma_1 - a_4\Gamma_2 \geq 0$, $OP_{EHA} \approx \Theta_1 + (1 - \Theta_2)\Theta_3 + \Theta_2(\Theta_4 + \Theta_6 - \Theta_7) - (1 - \Theta_2)\Theta_5 - \Theta_2(\Theta_8 - \Theta_9)$, (ii) Otherwise, when $a_2\Gamma_1 - a_4\Gamma_2 < 0$, $OP_{EHA} \approx \Theta_1 + (1 - \Theta_2)\Theta_3 + \Theta_2\Theta_4 - (1 - \Theta_2)\Theta_5$	
OPIPC	$\Theta_1 = 1 - e^{-\left(\frac{1}{P_S\Omega_X} + \frac{1}{P_{R_l}\Gamma_1\Omega_W}\right)\Gamma_2} - \frac{1}{\Omega_W}\left(\frac{1}{\Omega_W} + \frac{P_{R_l}\Gamma_1}{P_S\Omega_X}\right)^{-1}\left(1 - e^{-\left(\frac{1}{P_S\Omega_X} + \frac{1}{P_{R_l}\Gamma_1\Omega_W}\right)\Gamma_2}\right)$, $\Theta_2 = 1 - \frac{P_S\Omega_Z e^{-\frac{N_0\Gamma_1}{P_S\Omega_Z}} - P_{R_l}\Omega_Y e^{-\frac{N_0\Gamma_1}{P_{R_l}\Omega_Y}}}{P_S\Omega_Z - P_{R_l}\Omega_Y}$, $\Theta_3 = 1 - \frac{P_S\Omega_Z e^{-\frac{N_0\Gamma_2}{P_S\Omega_Z}} - P_{R_k}\Omega_Y e^{-\frac{N_0\Gamma_2}{P_{R_k}\Omega_Y}}}{P_S\Omega_Z - P_{R_k}\Omega_Y}$, $\Theta_4 = 1 - \frac{P_S\Omega_X}{P_{R_l}\Omega_W\Gamma_1 + P_S\Omega_X}$, $\Theta_5 = 1 - e^{-\frac{\Gamma_2}{P_S\Omega_X}}$, $\Theta_6 = \Upsilon_1\left(\frac{P_{R_l}}{N_0}, \frac{P_S}{N_0}, \Gamma_1, \frac{N_0(\Gamma_2 - \Gamma_1)}{P_{R_k} - P_{R_l}}\right) - \Upsilon_1\left(\frac{P_{R_k}}{N_0}, \frac{P_S}{N_0}, \Gamma_2, \frac{N_0(\Gamma_2 - \Gamma_1)}{P_{R_k} - P_{R_l}}\right) + \Theta_3$
OPEHA	$\Theta_1 = \left(1 - e^{\left(-\frac{\Gamma_2}{a_1\Omega_X}\right)}\right) e^{\left(-\frac{1}{\rho_l\Omega_W\Gamma_1}\right)}$, $\Theta_2 = 1 - e^{\left(-\frac{1}{\rho_l\Omega_W\Gamma_1}\right)}$, $\Theta_3 = 1 - e^{-\left(\frac{\Gamma_2}{a_3\Omega_Z}\right)}\left[1 + \frac{2}{a_3\Omega_Z}\int_{x=0}^{\sqrt{\Gamma_2}}\left(2x\sqrt{\frac{x^2}{a_2N_0\Omega_X\Omega_Y}} e^{\left(\frac{x^2}{a_3\Omega_Z}\right)} K_1\left(2\sqrt{\frac{x^2}{a_2N_0\Omega_X\Omega_Y}}\right)\right) dx\right]$, $\Theta_4 = 1 - e^{-\left(\frac{\Gamma_1}{a_3\Omega_Z}\right)}\left[1 + \frac{2}{a_3\Omega_Z}\int_{x=0}^{\sqrt{\Gamma_1}}\left(2x\sqrt{\frac{x^2}{a_4N_0\Omega_X\Omega_Y}} e^{\left(\frac{x^2}{a_3\Omega_Z}\right)} K_1\left(2\sqrt{\frac{x^2}{a_4N_0\Omega_X\Omega_Y}}\right)\right) dx\right]$, $\Theta_5 \approx \Upsilon_2^{(0)}\left(\frac{a_3}{a_2}, \frac{\Gamma_2}{a_1}, \frac{\Gamma_2}{a_2}, \delta_1\right)$, $\Theta_6 \approx \Upsilon_2^{(0)}\left(\frac{a_3}{a_2}, \infty, \frac{\Gamma_2}{a_2}, \delta_2\right)$, $\Theta_7 \approx \Upsilon_2^{(0)}\left(\frac{a_3}{a_3}, \infty, \frac{\Gamma_1}{a_4}, \delta_3\right)$, $\Theta_8 \approx \Upsilon_2^{(0)}\left(\frac{a_3}{a_2}, \frac{\Gamma_2}{a_1}, \frac{\Gamma_2}{a_2}, \delta_4\right)$, $\Theta_9 \approx \Upsilon_2^{(0)}\left(\frac{a_3}{a_4}, \frac{\Gamma_2}{a_1}, \frac{\Gamma_1}{a_4}, \delta_5\right)$, where used parameters are presented in **Proposition** 9.6.

Tab. 9.2: The summary of derived asymptotic OP expressions at high SNR when $P_S \to \infty$.

I. In HDMRC	
OPIPC	$\Theta_1^\infty \approx \frac{P_S\Omega_X-\Gamma_2}{P_S\Omega_X}$, $\Theta_2^\infty \approx \frac{P_S\Omega_Z-N_0\Gamma_2-P_{R_l}\Omega_Y \mathrm{e}^{-\frac{N_0\Gamma_2}{P_{R_l}\Omega_Y}}}{P_S\Omega_Z-P_{R_l}\Omega_Y}$
OPEHA	$\Theta_1^\infty \approx 1-\left(\frac{N_0\Omega_X+\Omega_Z}{P_S\Omega_X\Omega_Z}\right)\Gamma_2$, $\Theta_2^\infty \approx 1+\frac{N_0\Gamma_2}{P_S\Omega_Z}\left(1+\frac{N_0\Gamma_2}{2P_S\Omega_Z}\right)$
II. In FDJD	
OPIPC	$\Theta_1^\infty = \frac{P_S\Omega_X}{P_{R_l}\Omega_W\Gamma_1+P_S\Omega_X}$, $\Theta_2^\infty \approx \frac{P_S\Omega_Z-N_0\Gamma_1-P_{R_l}\Omega_Y \mathrm{e}^{-\frac{N_0\Gamma_1}{P_{R_l}\Omega_Y}}}{P_S\Omega_Z-P_{R_l}\Omega_Y}$
OPEHA	$\Theta_1^\infty \approx \left(\frac{P_S\Omega_Z-N_0\Gamma_1}{P_S\Omega_Z}\right)\left(1-e^{\left(-\frac{1}{\rho_l\Gamma_1\Omega_W}\right)}\right)$, $\Theta_2^\infty \approx 1+\frac{N_0\Gamma_1}{P_S\Omega_Z}\left(1+\frac{N_0\Gamma_1}{2P_S\Omega_Z}\right)$
III. In HTS	
OPIPC	$\Theta_1^\infty \approx \left(1-\left(1-\frac{\Gamma_2}{P_S\Omega_X}\right)e^{\left(-\frac{\Gamma_2}{P_{R_l}\Gamma_1\Omega_W}\right)}\right)\left(1-\frac{1}{\Omega_W}\left(\frac{1}{\Omega_W}+\frac{P_{R_l}\Gamma_1}{P_S\Omega_X}\right)^{-1}\right)$, $\Theta_2^\infty \approx 1-\frac{P_S\Omega_Z-N_0\Gamma_1-P_{R_l}\Omega_Y e^{-\frac{N_0\Gamma_1}{P_{R_l}\Omega_Y}}}{P_S\Omega_Z-P_{R_l}\Omega_Y}$, $\Theta_3^\infty \approx 1-\frac{P_S\Omega_Z-N_0\Gamma_2-P_{R_k}\Omega_Y e^{-\frac{N_0\Gamma_2}{P_{R_k}\Omega_Y}}}{P_S\Omega_Z-P_{R_k}\Omega_Y}$, $\Theta_4^\infty = \Theta_4$, $\Theta_5^\infty \approx \frac{\Gamma_2}{P_S\Omega_X}$, $\Theta_6^\infty = \Xi_1^\infty - \Xi_2^\infty + \Theta_3^\infty$, where $\Xi_1^\infty \approx 1-e^{-\frac{\epsilon_1}{\Omega_Y}}-\frac{1}{\Omega_Y}\left(1-e^{-\frac{\epsilon_1}{\Omega_Y}}\left(1+\frac{\epsilon_1 P_{R_l}}{P_S\Omega_Z}\right)\right)\left(\frac{1}{\Omega_Y}-\frac{P_{R_l}}{P_S\Omega_Z}\right)^{-1}\left(1-\frac{N_0\Gamma_1}{P_S\Omega_Z}\right)$, $\Xi_2^\infty \approx 1-e^{-\frac{\epsilon_2}{\Omega_Y}}-\frac{1}{\Omega_Y}\left(1-e^{-\frac{\epsilon_2}{\Omega_Y}}\left(1+\frac{\epsilon_2 P_{R_k}}{P_S\Omega_Z}\right)\right)\left(\frac{1}{\Omega_Y}-\frac{P_{R_k}}{P_S\Omega_Z}\right)^{-1}\left(1-\frac{N_0\Gamma_2}{P_S\Omega_Z}\right)$, $\epsilon_1 = \min\left\{\frac{N_0(\Gamma_2-\Gamma_1)}{P_{R_k}-P_{R_l}}, \frac{N_0\Gamma_1}{P_{R_l}}\right\}$, and $\epsilon_2 = \min\left\{\frac{N_0(\Gamma_2-\Gamma_1)}{P_{R_k}-P_{R_l}}, \frac{N_0\Gamma_2}{P_{R_k}}\right\}$.
OPEHA	$\Theta_1^\infty \approx \frac{\Gamma_2}{P_S\Omega_X}e^{\left(-\frac{1}{\rho_l\Omega_W\Gamma_1}\right)}$, $\Theta_2^\infty = \Theta_2$, $\Theta_3^\infty \approx 1-\left(1-\frac{N_0\Gamma_2}{P_S\Omega_Z}\right)\left[1+\frac{N_0\Gamma_2}{P_S\Omega_Z}\left(1+\frac{\Gamma_2 N_0}{2P_S\Omega_Z}\right)\right]$, $\Theta_4^\infty \approx 1-\left(1-\frac{N_0\Gamma_1}{P_S\Omega_Z}\right)\left[1+\frac{N_0\Gamma_1}{P_S\Omega_Z}\left(1+\frac{\Gamma_1 N_0}{2P_S\Omega_Z}\right)\right]$, $\Theta_5^\infty \approx \Upsilon_2^{(\infty)}\left(\frac{a_3}{a_2}, \frac{\Gamma_2}{a_1}, \frac{\Gamma_2}{a_2}, \delta_1\right)$, $\Theta_6^\infty \approx \Upsilon_2^{(\infty)}\left(\frac{a_3}{a_2}, \infty, \frac{\Gamma_2}{a_2}, \delta_2\right)$, $\Theta_7^\infty \approx \Upsilon_2^{(\infty)}\left(\frac{a_3}{a_3}, \infty, \frac{\Gamma_1}{a_4}, \delta_3\right)$, $\Theta_8^\infty \approx \Upsilon_2^{(\infty)}\left(\frac{a_3}{a_2}, \frac{\Gamma_2}{a_1}, \frac{\Gamma_2}{a_2}, \delta_4\right)$, $\Theta_9^\infty \approx \Upsilon_2^{(\infty)}\left(\frac{a_3}{a_4}, \frac{\Gamma_2}{a_1}, \frac{\Gamma_1}{a_4}, \delta_5\right)$, where used parameters are presented in Proposition 6.

Parameters	**Values**
Number relays, N	3
Power transmission, P_S	10 (dB)
Energy conversion efficiency, η	0.8
The SNR threshold, R_0	2 (bps/Hz)
The exponential distribution, $\Omega_X = \Omega_Y$	10 (dB)
The exponential distribution, Ω_W	10 (dB)
The exponential distribution, Ω_Z	$10\% \times \Omega_X$
The average radiated power at S, a_S	1/0.33
The average radiated power at R, a_R	1/0.38
The stable power consumed at S, b_S	120 (W)
The stable power consumed at R, b_R	22 (W)

Tab. 9.3: Main Simulation Parameters (Hybrid FD/HD RS).

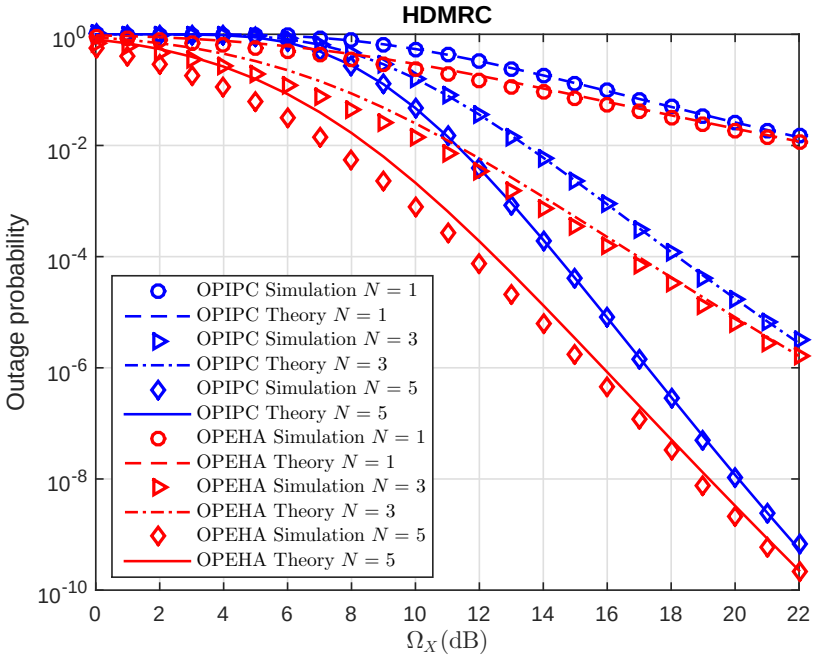

Fig. 9.2: OP vs. the average SNR links in HDMRC scheme

$\Omega_X = \Omega_Y$ being assumed, and the distance of each link is regarded as the average power. The simulation results follow some parameters specified in Table 9.3.

In Fig. 9.2 and Fig. 9.3, we illustrate the OP of HDMRC and FDJD schemes (a.k.a max-min RS) for the comparisons between OPIPC and OPEHA with $N = 1, 3, 5$ as function of the average SNRs of the S–R and R–D links. It is clear that in both figures, OPEHA is superior to OPIPC, since we obtained the optimal EH ratio to avoid the limited lifetime in most low-powered wireless networks, i.e., WSNs. Besides, the best

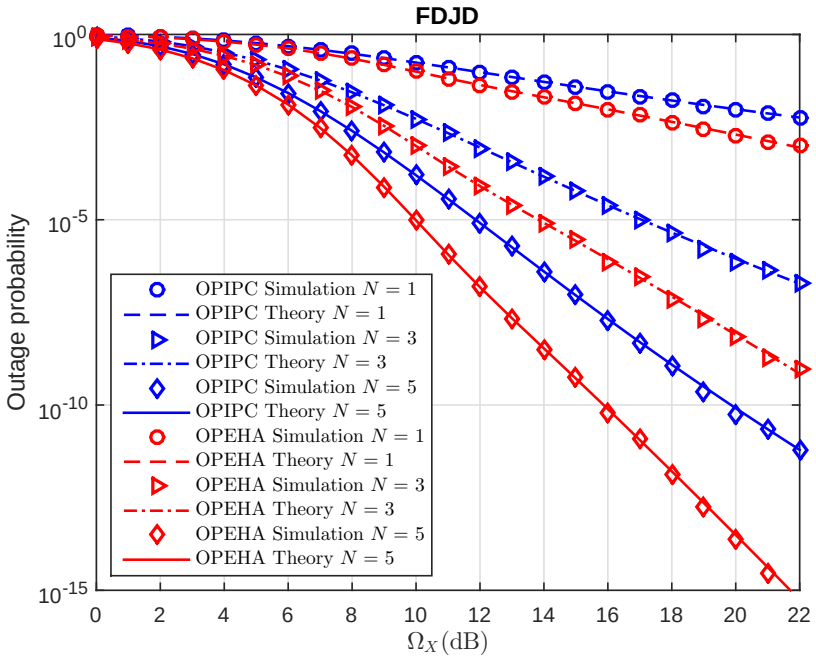

Fig. 9.3: OP vs. the average SNR links in FDJD scheme

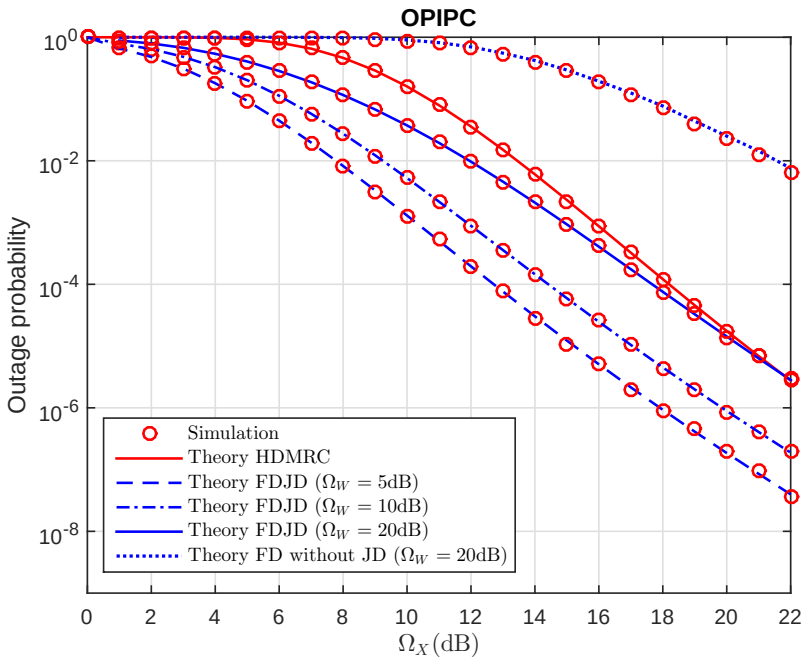

Fig. 9.4: OP vs. the average SNR links with different Ω_W in OPIPC policy.

outage performance is achieved in FDJD.

In Fig. 9.4 and Fig. 9.5, comparisons between HDMRC, FDJD and FD relaying without JD in the presence of SI in terms of OP are given with $N = 3$. Because the optimal power

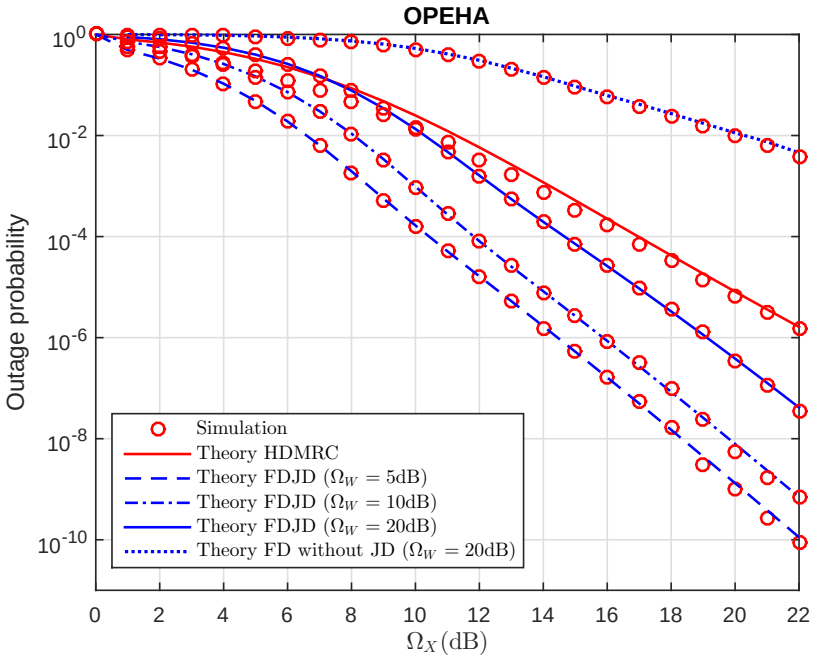

Fig. 9.5: OP vs. the average SNR links with different Ω_W in OPEHA policy.

supply policies are deployed to deal with SI which dominates grealy the power allocation of FD-based relays, interference will not affect FDJD at the receiving antenna if the residual self-interference (RSI) link is trivial ($\Omega_W \sim 0$). The SI can be cancelled if source signals are transmitted with the optimal power. OPEHA marks higher power efficiency than OPIPC, so OP in case of OPEHA is better than that in OPIPC. In particular, when Ω_W climbs to approximately 20dB, FDJD RS scheme is still positive compared to HDMRC in the first half of the average SNR link, but then as the values of average SNR links increase, outage performance of FDJD is worse than HDMRC. HDMRC scheme is superior to FDJD when Ω_W exceeds 20dB as in Fig. 9.4, FDJD is better than that of FD without JD [96] in the same scenario of Ω_W. Besides, with EH capacity in OPEHA in Fig. 9.5, FDJD RS scheme achieves better outage performance with $\Omega_W = 20$dB than HDMRC, it is proven to be prior to HDMRC by approximately 5dB.

Fig. 9.6 and Fig. 9.7 provide the comparisons between OPIPC and OPEHA. We can clearly see that HTS scheme outperform two conventional max-min RS schemes in terms of OP at high SNR. Note that if the system enjoys favourable SI cancellation, HTS selects FDJD to operate, since the OP in case of HTS deploying HD will deteriorate. Otherwise, if SI increases, the system performance in FDJD gets worse, and the OP in HTS approaches HDMRC. Furthermore, the performance of HTS scheme in OPIPC and OPEHA, where we examine OP versus P_S/N_0 with $N = 3$ and $\Omega_X = \Omega_Y = \Omega_W = 10$(dB) being fixed in Fig. 9.8 and Fig. 9.9. We illustrate the performance of the conventional max-min RS schemes for the comparison with HTS. We can easily observe that HTS is better than HDMRC and FDJD, and HTS is more efficient since it witnesses lower SI. Besides, the

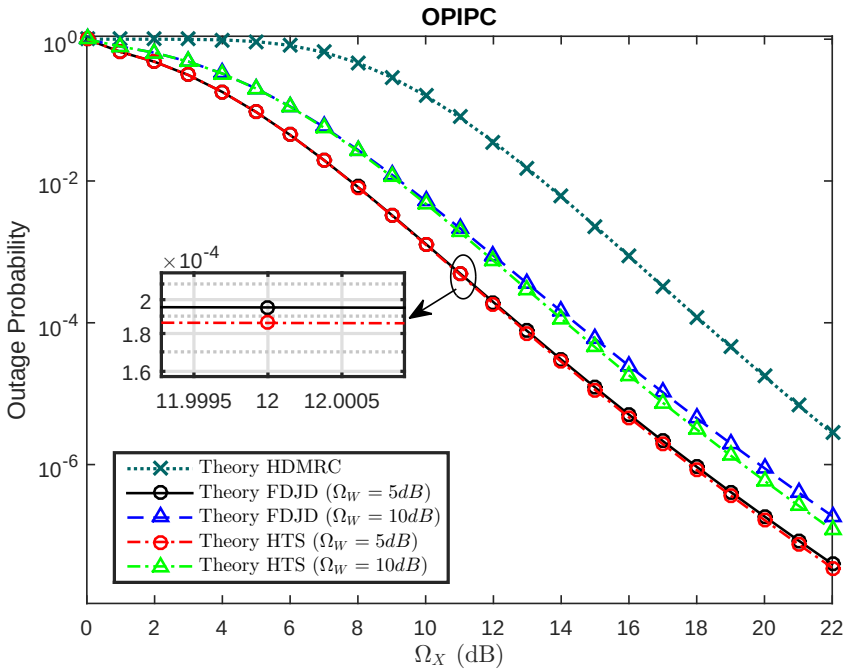

Fig. 9.6: OP for proposed RS schemes vs. the average SNR links with different Ω_W in OPIPC policy.

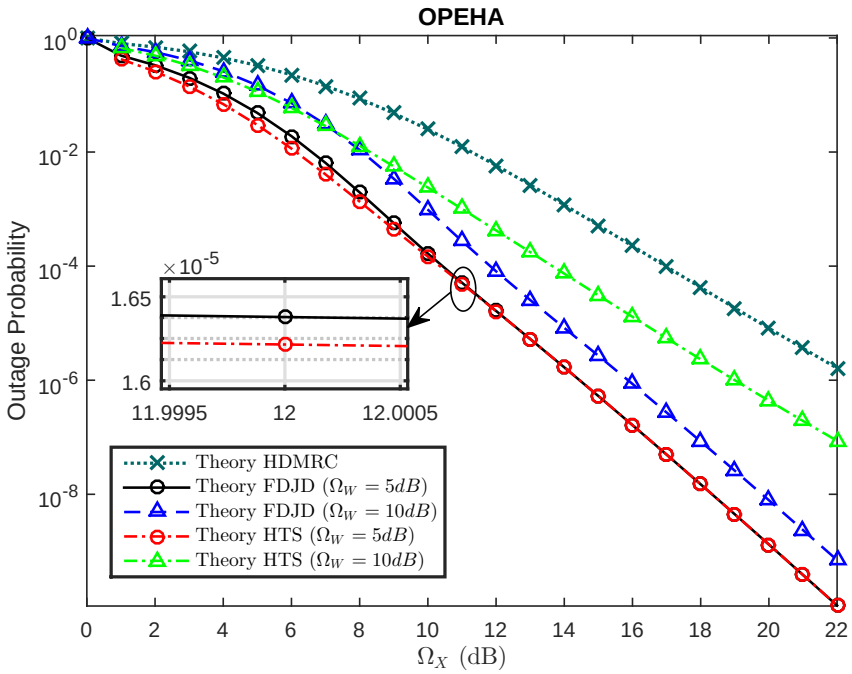

Fig. 9.7: OP for proposed RS schemes vs. the average SNR links with different Ω_W in OPEHA policy.

analytical results converge to the asymptotic line in high SNR.

The total power consumption is presented versus P_S with $\Omega_X = \Omega_Y = 20(dB)$, $\Omega_W =$

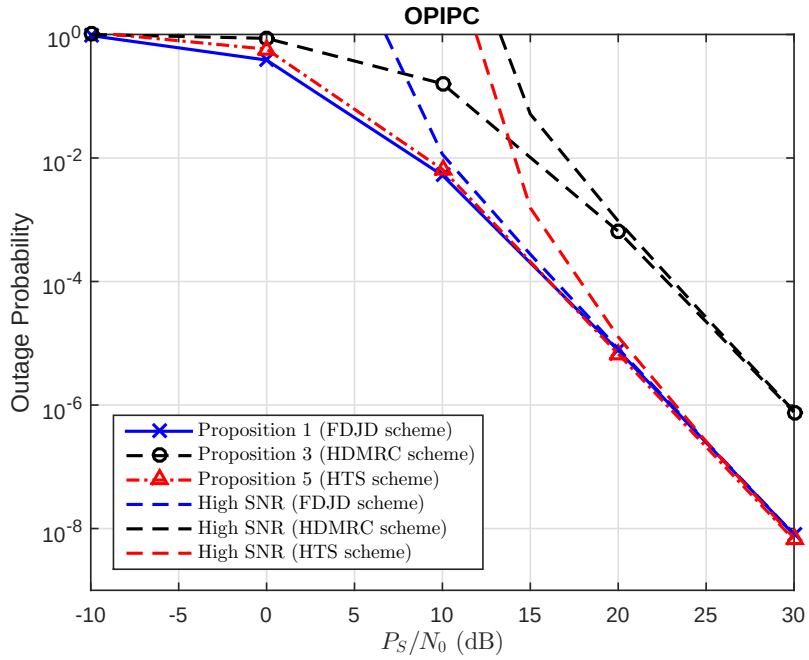

Fig. 9.8: OP for proposed RS schemes vs. P_S/N_0 in OPIPC policy.

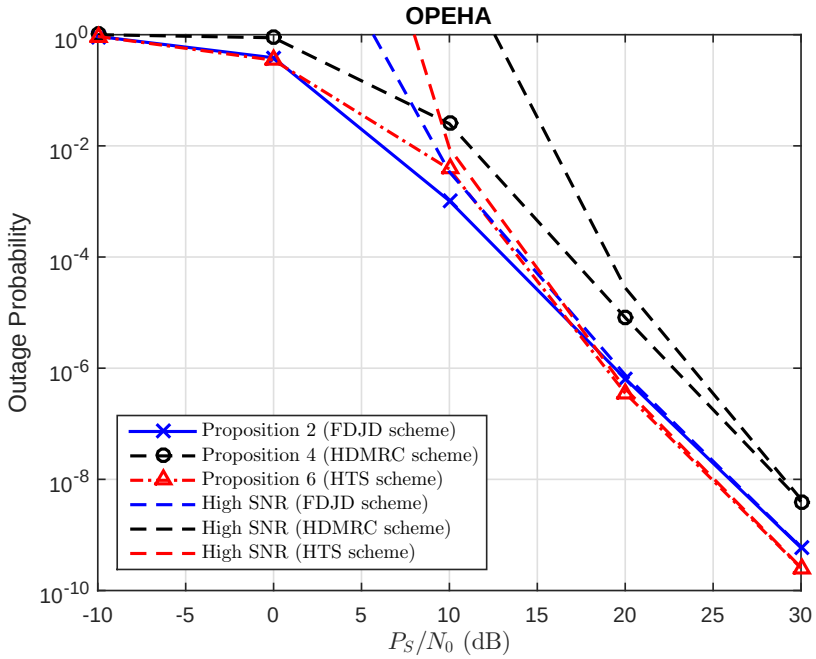

Fig. 9.9: OP for proposed RS schemes vs. P_S/N_0 in OPEHA policy.

$10(dB)$, and $N = 3$ in Fig. 9.10 and Fig. 9.11. The proposed RS schemes in terms of the total power consumption in OPIPC and OPEHA. The total power consumption climbs as P_S increases in each scheme, the weaker channel will dominate the performance of the

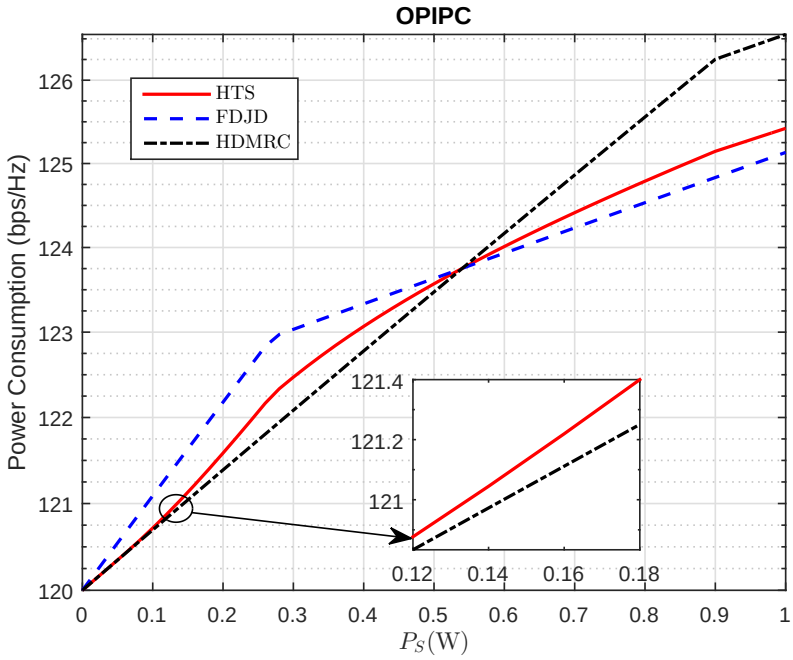

Fig. 9.10: Total power consumption vs. the transmit power, P_S in OPIPC policy.

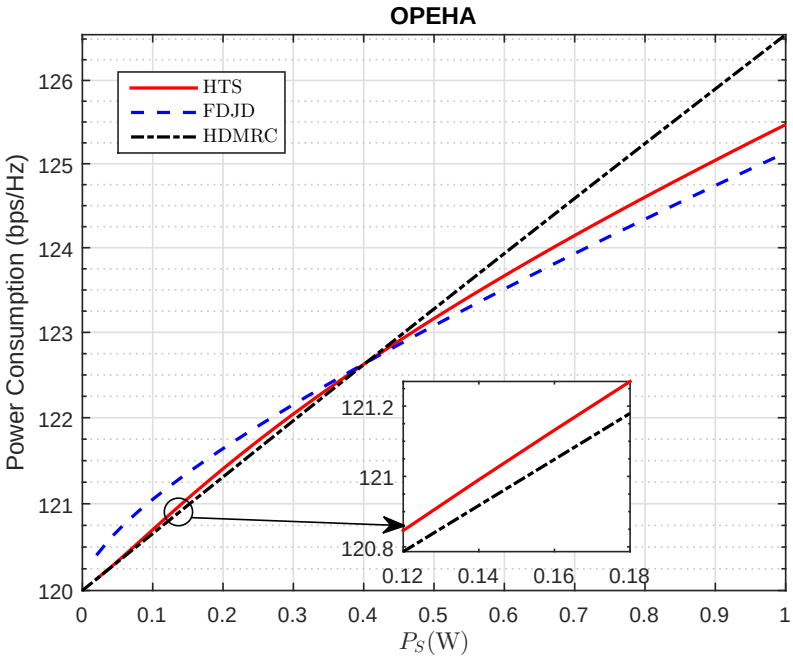

Fig. 9.11: Total power consumption vs. the transmit power, P_S in OPEHA policy.

relaying systems and more power will be consumed to ensure the QoS. These figures show that FDJD uses less power than HTS and HDMRC. In particular, OP does not exist at first until P_S approaches approximately 0.15W, HTS scheme adopts HDMRC. In contrast,

if OP starts increasing in HDMRC, FDJD will be automatically selected.

9.5 Summary

In this chapter, we proposed the optimal RS schemes in multi-relay cooperative RNs. In particular, OP is investigated at high SNR in our proposed otpimal RS schemes, including HDMRC and FDJD and HTS. Besides, two optimal optimal power supply policies called OPIPC and OPEHA were put forward which are used to evaluate each RS scheme. The asymptotic results are derived together with closed-form expressions for OP. Based on the designed power consumption model, EE was improved. The simulation results proved that HTS outperforms HDMRC and FDJD in terms of OP.

10 OPTIMAL TIME SWITCHING-BASED POLICIES FOR EFFICIENT TRANSMIT POWER IN WIRELESS EH SMALL CELL CRNS

In this final chapter, we take two TS policies, i.e., OTPS and OTPR to improve the maximum transmit power at S and R for a HD DF small-cell CRN. For system performance analysis, closed-form expressions for OP are derived for the proposed policies. Besides, throughput is evaluated delay-constraint transmission mode, and the average EE and the R-E trade-off are also studied [NHS10].

10.1 Motivation

In practice, the cross-tier interference has a negative impact on cognitive heterogeneous small cell networks, so the deployment of cognitive small cell networks is associated with several issues, i.e., cross-tier interference cancellation and resource management. In particular, a sensing-based power allocation policy in a cognitive small cell network was studied in [109] to maximize the sum rate in each cell. Additionally, the authors in [110] tried to optimize the radio resource allocation and sensing parameters to optimize the throughput in the precence of interference caused by PU. Meanwhile, the impact of HWIs in [111] was studied in underlay CRNs.

According to our best knowledge, the study of EH in small cell CRNs is still open so we are going to study and propose two novel EH policies, and the system performance is comprehensively investigated [NHS11].

10.2 System model

In Fig. 10.1, we present a HD small cell CRN. In particular, there is a macro cell network in tier 1 consisting of a BS a.k.a MPT and a mobile user representing a macro cell primary receiver (MPR) , while there are a secondary S and a secondary HD R in the small cell network in tier 2, and the secondary D is located in tier 3. It is worth noting that S and R can harvest energy from RF signals transmitted from MPT thanks to the communication between MPT and MPR. We assume the CSI of the link between the MPT and S is available at MPT.

We respectively denote the Rayleigh fading channels for links from MPT to S and R as t_1 and t_2 while h_1 and h_2 are the channel gain coefficients from S to R and from R to D. Similarly, r_1 and r_2 are for the links S and R to MPR, respectively. The energy used by S and R is constrained by the energy harvested which can be defined as E_S^h at S and E_R^h at R. The distances between MPT and S, and MPT and R are denoted as l_1, l_2, respectively, while we denote the distances from S, R to MP as l_3, l_4. Likewise, distances between S to R and R to D are l_5, l_6, respectively. We assume that the channel power

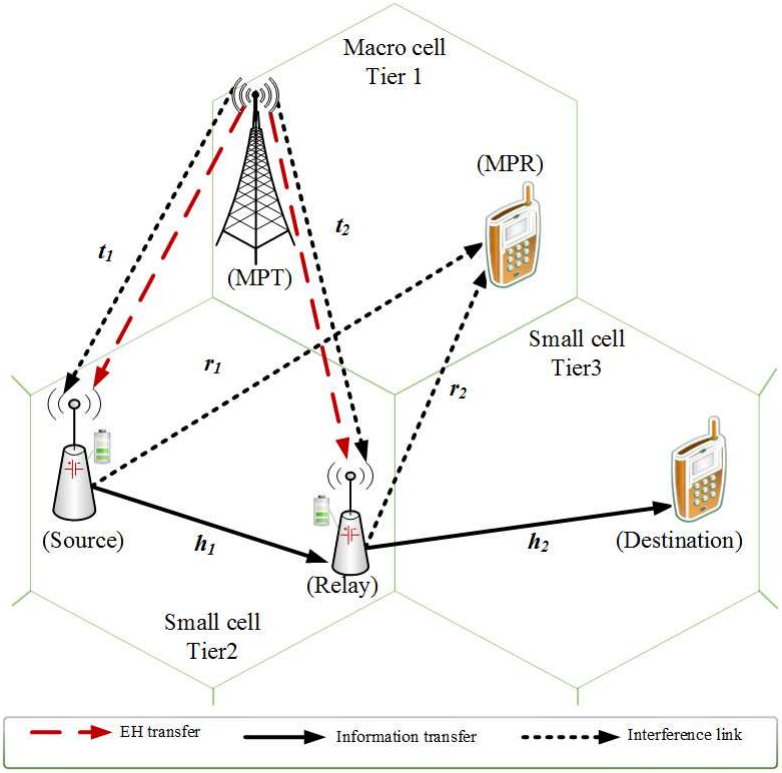

Fig. 10.1: System model.

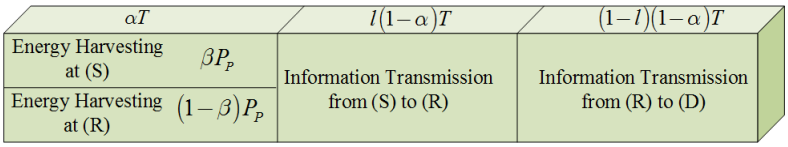

Fig. 10.2: TS protocol and power allocation for small cell CRNs.

gains are defined as $|t_1|^2$, $|t_2|^2$, $|r_1|^2$, $|r_2|^2$, $|h_1|^2$, and $|h_2|^2$, respectively. In addition, the channel coefficients are complex Gaussian distributed with zero mean and variances Ω_{t_1}, Ω_{t_2}, Ω_{r_1}, Ω_{r_2}, Ω_{h_1}, and Ω_{h_2}, respectively. We denote PLi as the path loss model with m being the path-loss exponent, where $i \in \{t_1, t_2, r_1, r_2, h_1, h_2\}$, (i.e, $PLt_1 = l_1^{-m}$), and the received signal at each node is perturbed by AWGN with mean N_0, and we can ignore the impact of noise.

We assume that the amount of energy harvested by S and R can be stored in capacitors or batteries to serve for the IT process, where they can help the switching between EH and IT. It is noted that S and R use the spectrum shared by MPT, in which they can transmit information simultaneously only when the interference at MPT is not higher than a peak interference threshold represented by P_M.

In Fig. 10.2, we use TS protocol to study EH, where S and R harvest energy within a duration of αT with T being the block time for each EH-IT time slot. Besides, the

interference signal transmitted from MPT to nodes in the small cell network in tier 1 makes up βP_P and $(1-\beta)P_P$, respectively. It is noted that P_P is the transmit power of MPT, and β is the power ratio, and $0 < \beta < 1$. Following that, R receives information from S for a duration of $l\,(1-\alpha)\,T$ before R forwards data to D in $(1-l)\,(1-\alpha)\,T$, where we assume $l = 1/2$ for simplicity.

To protect macro cell nodes, S and R must have the transmit powers satisfying the QoS in tier 1. Thus, the constant transmit powers of S and R are going to be studied during IT period to optimize the transmit power based on the knowledge of the harvested energy and the peak interference power. Thus, we have the following expressions

$$\begin{aligned} P_S &= \min\left(\tfrac{2E_S^h}{(1-\alpha)T}, \tfrac{P_M}{|r_1|^2 PLr_1}\right) \\ &= \min\left(\rho\beta P_P |t_1|^2 PLt_1, \tfrac{P_M}{|r_1|^2 PLr_1}\right) \end{aligned}, \tag{10.1a}$$

and

$$\begin{aligned} P_R &= \min\left(\tfrac{2E_R^h}{(1-\alpha)T}, \tfrac{P_M}{|r_2|^2 PLr_2}\right) \\ &= \min\left(\rho\,(1-\beta)\,P_P |t_2|^2 PLt_2, \tfrac{P_M}{|r_2|^2 PLr_2}\right) \end{aligned}, \tag{10.1b}$$

where the energy conversion efficiency is η with $0 < \eta < 1$, $E_S^h = \eta\alpha\beta P_P |t_1|^2 PLt_1 T$, $E_R^h = \eta\alpha\,(1-\beta)\,P_P |t_2|^2 PLt_2 T$, $\rho = 2\eta\frac{\alpha}{(1-\alpha)}$.

Remark 10.1. In practice, the communication of S and R suffers from MPR, because the same spectrum is allocated to S and R by MPT. The transmit power constraints of S and R affecting P_S, P_R make the interference power not exceed P_M. Besides, the choice of power allocation factor, β is important to balance the optimization the throughput performance and the harvested energy used for WPT which we are going to evaluate it by simulations. In particular, E_S^h falls, β decreases, but this accordingly leads to the rise in E_R^h.

Next, the gain is dependent solely on the instantaneous CSI. Therefore, the signal-to-interference ratio (SIR) (SIR = $|\text{signal}|^2/|\text{interference}|^2$) at R and D can be written as

$$\gamma_R = \frac{P_S |h_1|^2 PLh_1}{(1-\beta)\,P_P |t_2|^2 PLt_2}, \tag{10.2a}$$

$$\gamma_D = P_R |h_2|^2 PLh_2. \tag{10.2b}$$

To this point, we can obtain the achievable transmission rate at D as

$$R = \frac{(1-\alpha)}{2}\log_2\left(1+\gamma_{eq}\right), \tag{10.3}$$

where $\gamma_{eq} = \min\left(\gamma_R, \gamma_D\right)$ for DF small cell relay-assisted cognitive networks.

10.3 Performance analysis

In this section, the OP of HD small cell nodes using DF R and optimal TS policies are going to be addressed. It is worth noting that the optimal TS should be computed by an entity which gets access to the global instantaneous CSI while the optimal TS is updated only if the channel statistics changes. In principle, the interference power limits the maximum transmit powers at S and R which degrades the operation of the primary network. Due to this constraint, OTPS, OTPS are proposed by assuming that maximal transmit powers at S and R are permitted.

10.3.1 Outage probability

Here, we represent the OP in the DF CRN as OP, where OP is considered as the probability that the RVs of SIR for each time slot are set under a threshold value, γ_0. Therefore, we define it as

$$OP = \Pr\left\{\gamma_{eq} < \gamma_0\right\}. \tag{10.4}$$

Similarly, in case of the end-to-end SIR, we can express the probability at D (10.4) as

$$\begin{aligned} OP &= 1 - \Pr\left\{\gamma_{eq} \geq \gamma_0\right\} \\ &= 1 - \Pr\left\{\gamma_R \geq \gamma_0\right\} \times \Pr\left\{\gamma_D \geq \gamma_0\right\} \end{aligned}. \tag{10.5}$$

In this chapter, we are going to obtain the expressions (10.5) for OP in **Proposition** 10.1, and 10.2 in the following sections.

A. Optimal time for transmit power at source (OTPS):

In this work, the power transmitted to S is superior to the activation threshold, and EH circuits at S are always active. Due to the maximum transmit power at S, the optimal α_S is computed based on the following expression

$$\frac{\alpha_S}{(1-\alpha_S)} 2\eta\beta P_P |t_1|^2 PLt_1 = \frac{P_M}{|r_1|^2 PLr_1}. \tag{10.6}$$

Thus, the TS ratio, α_S is given by

$$\alpha_S = \frac{P_M}{2\eta\beta P_P |t_1|^2 |r_1|^2 PLt_1 PLr_1 + P_M}. \tag{10.7}$$

Proposition 10.1. The overall closed-form expression for OP at D for DF mode is expressed by

$$OP^{OTPS} = 1 - Q_1^{OTPS} \times \left(Q_2^{OTPS} + Q_3^{OTPS}\right), \tag{10.8}$$

where $Q_1^{OTPS} = \Phi_1^{OTPS} e^{\Phi_1^{OTPS}} E_1\left(\Phi_1^{OTPS}\right)$, $Q_3^{OTPS} = 2\Phi_3^{OTPS}\Phi_4^{OTPS} K_1\left(2\Phi_3^{OTPS}\right)$, $Q_2^{OTPS} = 2\Phi_2^{OTPS} K_1\left(2\Phi_2^{OTPS}\right) \times \left[1 - 2\Phi_3^{OTPS} K_1\left(2\Phi_3^{OTPS}\right)\right]$,

$\Phi_1^{OTPS} = \frac{P_M \Omega_{h_1} PLh_1}{(1-\beta)\gamma_0 P_P \Omega_{r_1} \Omega_{t_2} PLr_1 PLt_2}$, $\Phi_2^{OTPS} = \sqrt{\frac{\gamma_0}{\rho(1-\beta)P_P \Omega_{t_2} \Omega_{h_2} PLh_2 PLt_2}}$,
$\Phi_3^{OTPS} = \sqrt{\frac{P_M}{\rho(1-\beta)P_P \Omega_{r_2} \Omega_{t_2} PLr_2 PLt_2}}$, and $\Phi_4^{OTPS} = \frac{P_M \Omega_{h_2} PLh_2}{\gamma_0 \Omega_{r_2} PLr_2 + P_M \Omega_{h_2} PLh_2}$.

Proof: With the optimal α_S for maximum transmit power at S. Thus, the probability related to SIR at R can be written as

$$Q_1^{OTPS} = \Pr\left\{ |h_1|^2 \geq \frac{(1-\beta)\,\gamma_0 P_P |t_2|^2 |r_1|^2 PLt_2 PLr_1}{P_M PLh_1} \right\}. \tag{10.9}$$

Then, conditioning on $|t_2|^2$, the OP at R can be given by

$$\begin{aligned} Q_1^{OTPS} ||t_2|^2 &= \int_{x=0}^{\infty} \frac{1}{\Omega_{r_1}} e^{\left(-\frac{(1-\beta)\gamma_0 P_P |t_2|^2 PLt_2 PLr_1}{P_M \Omega_{h_1} PLh_1} - \frac{1}{\Omega_{r_1}} \right) x} dx \\ &= \omega_1 \left(\frac{1}{|t_2|^2 + \omega_1} \right) \end{aligned}, \tag{10.10}$$

where using formula $\int\limits_0^{\infty} e^{-px} dx = \frac{1}{p}$ in [[66], 3.310], and $\omega_1 = \frac{P_M \Omega_{h_1} PLh_1}{(1-\beta)\gamma_0 P_P \Omega_{r_1} PLr_1 PLt_2}$.

Consequently, the distribution of $|t_2|^2$ can be given as

$$\begin{aligned} Q_1^{OTPS} &= \tfrac{1}{\Omega_{t_2}} \omega_1 \int_{t=0}^{\infty} e^{-\frac{t}{\Omega_{t_2}}} \left(\frac{1}{t + \omega_1} \right) dt \\ &= \tfrac{\omega_1}{\Omega_{t_2}} e^{\frac{\omega_1}{\Omega_{t_2}}} E_1 \left(\tfrac{\omega_1}{\Omega_{t_2}} \right) \end{aligned}, \tag{10.11}$$

where the function $E_1(x)$ is from the exponential integral $E_i(x)$ thanks to the use of formula [[66], 3.352.4].

Thus, we obtain the probability for SIR at D by two probability terms as

$$\begin{aligned} \Pr\{\gamma_D \geq \gamma_0\} = &\Pr\left\{ |h_2|^2 \geq \tfrac{\gamma_0}{\rho(1-\beta)P_P |t_2|^2 PLh_2 PLt_2}, |r_2|^2 \leq \tfrac{P_M}{\rho(1-\beta)P_P |t_2|^2 PLr_2 PLt_2} \right\} \\ &+ \Pr\left\{ |h_2|^2 \geq \tfrac{\gamma_0 |r_2|^2 PLr_2}{P_M PLh_2}, |r_2|^2 \geq \tfrac{P_M}{\rho(1-\beta)P_P |t_2|^2 PLr_2 PLt_2} \right\} \end{aligned}. \tag{10.12}$$

Following that, the left joint probability of right-hand slide above is written by the product of two independent probabilities as

$$\begin{aligned} Q_2^{OTPS} = &\Pr\left\{ |h_2|^2 \geq \tfrac{\gamma_0}{\rho(1-\beta)P_P |t_2|^2 PLh_2 PLt_2} \right\} \\ &\times \Pr\left\{ |r_2|^2 \leq \tfrac{P_M}{\rho(1-\beta)P_P |t_2|^2 PLr_2 PLt_2} \right\} \end{aligned}. \tag{10.13}$$

Next, the term $\Pr\left\{ |h_2|^2 \geq \frac{\gamma_0}{\rho(1-\beta)P_P |t_2|^2 PLh_2 PLt_2} \right\}$ in Q_2^{OTPS} can be calculated by

$$\begin{aligned} Q_{2,a}^{OTPS} &= \tfrac{1}{\Omega_{t_2}} \int_{t=0}^{\infty} e^{-\frac{1}{t}\left(\frac{\gamma_0}{\rho(1-\beta)P_P \Omega_{h_2} PLh_2 PLt_2} \right) - \frac{t}{\Omega_{t_2}}} dt \\ &= 2\sqrt{\tfrac{\gamma_0}{\rho(1-\beta)P_P \Omega_{h_2} \Omega_{t_2} PLh_2 PLt_2}} K_1 \left(2\sqrt{\tfrac{\gamma_0}{\rho(1-\beta)P_P \Omega_{h_2} \Omega_{t_2} PLh_2 PLt_2}} \right) \end{aligned}, \tag{10.14}$$

where we take advantage of [[66], 3.324.1].

The term $\Pr\left\{ |r_2|^2 \leq \frac{P_M}{\rho(1-\beta)P_P |t_2|^2 PLr_2 PLt_2} \right\}$ in Q_2^{OTPS} can be given as

$$\begin{aligned} Q_{2,b}^{OTPS} &= 1 - \tfrac{1}{\Omega_{t_2}} \int_{t=0}^{\infty} e^{-\frac{1}{t}\left(\frac{P_M}{\rho(1-\beta)P_P \Omega_{r_2} PLr_2 PLt_2} \right) - \frac{t}{\Omega_{t_2}}} dt \\ &= 1 - 2\sqrt{\tfrac{P_M}{\rho(1-\beta)P_P \Omega_{r_2} \Omega_{t_2} PLr_2 PLt_2}} K_1 \left(2\sqrt{\tfrac{P_M}{\rho(1-\beta)P_P \Omega_{r_2} \Omega_{t_2} PLr_2 PLt_2}} \right) \end{aligned}. \tag{10.15}$$

Likewise, we derive the right joint probability of RHS of the above expression (10.12) by using the product of two independent probabilities

$$\begin{aligned} Q_3^{OTPS} = \Pr\left\{|h_2|^2 \geq \frac{\gamma_0 |r_2|^2 PLr_2}{P_M PLh_2}\right\} \\ \times \Pr\left\{|r_2|^2 \geq \frac{P_M}{\rho(1-\beta)P_P|t_2|^2 PLr_2 PLt_2}\right\} \end{aligned}. \tag{10.16}$$

Following from (10.16), we compute the left probability term of RHS as

$$\begin{aligned} Q_{3,a}^{OTPS} &= \frac{1}{\Omega_{r_2}} \int_0^\infty e^{\left(-\frac{\gamma_0 PLr_2}{P_M \Omega_{h_2} PLh_2} - \frac{1}{\Omega_{r_2}}\right)x} dx \\ &= \frac{P_M \Omega_{h_2} PLh_2}{\gamma_0 \Omega_{r_2} PLr_2 + P_M \Omega_{h_2} PLh_2} \end{aligned}. \tag{10.17}$$

To this end, we obtain the right term of RHS from (10.15) as

$$\begin{aligned} Q_{3,b}^{OTPS} &= 1 - Q_{2,b}^{OTPS} \\ &= 2\sqrt{\frac{P_M}{\rho(1-\beta)P_P \Omega_{r_2} \Omega_{t_2} PLr_2 PLt_2}} K_1\left(2\sqrt{\frac{P_M}{\rho(1-\beta)P_P \Omega_{r_2} \Omega_{t_2} PLr_2 PLt_2}}\right) \end{aligned}. \tag{10.18}$$

To this point, the **Proposition** 10.1 can be explained by (10.11), (10.14), (10.15), (10.17), and (10.18).

B. Optimal time for transmit power at relay (OTPR):

We depend on the characteristic of the SIR for R–D link and maximum transmit power at R. Here, we achieve the optimal α_R as

$$\rho\left(1-\beta\right) P_P |t_2|^2 PLt_2 = \frac{P_M}{|r_2|^2 PLr_2}. \tag{10.19}$$

Thus, the value of TS ratio, α_R is given as

$$\alpha_R = \frac{P_M}{2\eta\left(1-\beta\right) P_P |t_2|^2 |r_2|^2 PLr_2 PLt_2 + P_M}. \tag{10.20}$$

Proposition 10.2. Next, the closed-form expression for OP at D is written by

$$OP^{OTPR} = 1 - \left(Q_1^{OTPR} + Q_2^{OTPR}\right) \times Q_3^{OTPR}, \tag{10.21}$$

where $Q_1^{OTPR} = e^{\frac{1}{2}\Phi_1^{OTPR}} W_{-1,\frac{1}{2}}\left(\Phi_1^{OTPR}\right) \times \left[1 - 2\Phi_2^{OTPR} K_1\left(2\Phi_2^{OTPR}\right)\right]$,
$Q_2^{OTPR} = 2\Phi_2^{OTPR}\Phi_3^{OTPR} e^{\Phi_3^{OTPR}} E_1\left(\Phi_3^{OTPR}\right) K_1\left(2\Phi_2^{OTPR}\right)$, $Q_3^{OTPR} = 2\Phi_4^{OTPR} K_1\left(2\Phi_4^{OTPR}\right)$,
$\Phi_1^{OTPR} = \frac{(1-\beta)\gamma_0 \Omega_{t_2} PLt_2}{\rho\beta \Omega_{h_1} \Omega_{t_1} PLh_1 PLt_1}$, $\Phi_2^{OTPR} = \sqrt{\frac{P_M}{\rho\beta P_P \Omega_{r_1} \Omega_{t_1} PLr_1 PLt_1}}$,
$\Phi_3^{OTPR} = \frac{P_M \Omega_{h_1} PLh_1}{(1-\beta)P_P \gamma_0 \Omega_{r_1} \Omega_{t_2} PLr_1 PLt_2}$, and $\Phi_4^{OTPR} = \sqrt{\frac{\gamma_0}{\rho(1-\beta)P_P \Omega_{h_2} \Omega_{t_2} PLh_2 PLt_2}}$.
Proof: Similarly, the probability at R based on two probabilities and three independent power constraints can be given as

$$\begin{aligned} \Pr\left\{\gamma_R \geq \gamma_0\right\} = \Pr\left\{|h_1|^2 \geq \frac{(1-\beta)\gamma_0 |t_2|^2 PLt_2}{\rho\beta |t_1|^2 PLh_1 PLt_1}, |r_1|^2 \leq \frac{P_M}{\rho\beta P_P |t_1|^2 PLr_1 PLt_1}\right\} \\ + \Pr\left\{|h_1|^2 \geq \frac{(1-\beta)P_P \gamma_0 |t_2|^2 |r_1|^2 PLt_2 PLr_1}{P_M PLh_1}, \frac{P_M}{\rho\beta P_P |r_1|^2 PLr_1 PLt_1} \leq |t_1|^2\right\} \end{aligned}. \tag{10.22}$$

It is noted that each probability in the above formula is computed by the product of two terms as

$$\begin{aligned} Q_1^{OTPR} &= \Pr\left\{|h_1|^2 \geq \tfrac{(1-\beta)\gamma_0|t_2|^2 PLt_2}{\rho\beta|t_1|^2 PLh_1 PLt_1}\right\} \\ &\quad \times \Pr\left\{|r_1|^2 \leq \tfrac{P_M}{\rho\beta P_P|t_1|^2 PLr_1 PLt_1}\right\} \end{aligned}. \tag{10.23}$$

The left term of RHS of Q_1^{OTPR} when we condition on $|t_2|^2$ can be written as

$$\begin{aligned} Q_{1,a}^{OTPR}||t_2|^2 &= \tfrac{1}{\Omega_{t_1}} \int_{x=0}^{\infty} e^{-\frac{(1-\beta)\gamma_0|t_2|^2 PLt_2}{\rho\beta\Omega_{h_1} PLh_1 PLt_1 x} - \frac{x}{\Omega_{t_1}}} dx \\ &= 2\sqrt{\tfrac{(1-\beta)\gamma_0|t_2|^2 PLt_2}{\rho\beta\Omega_{h_1}\Omega_{t_1} PLh_1 PLt_1}} K_1\left(2\sqrt{\tfrac{(1-\beta)\gamma_0|t_2|^2 PLt_2}{\rho\beta\Omega_{h_1}\Omega_{t_1} PLh_1 PLt_1}}\right) \end{aligned}. \tag{10.24}$$

We average the results of $Q_{1,a}^{OTPR}$ over the PDF of $|t_2|^2$. Therefore, it can be obtained as

$$\begin{aligned} Q_{1,a}^{OTPR} &= \tfrac{2}{\Omega_{t_2}}\sqrt{\tfrac{(1-\beta)\gamma_0 PLt_2}{\rho\beta\Omega_{h_1}\Omega_{t_1} PLh_1 PLt_1}} \int_{t=0}^{\infty} e^{-\frac{t}{\Omega_{t_2}}} \sqrt{t} K_1\left(2\sqrt{\tfrac{(1-\beta)\gamma_0 PLt_2}{\rho\beta\Omega_{h_1}\Omega_{t_1} PLh_1 PLt_1} t}\right) dt \\ &= e^{\frac{(1-\beta)\gamma_0\Omega_{t_2} PLt_2}{2\rho\beta\Omega_{h_1}\Omega_{t_1} PLh_1 PLt_1}} W_{-1,\frac{1}{2}}\left(\tfrac{(1-\beta)\gamma_0\Omega_{t_2} PLt_2}{\rho\beta\Omega_{h_1}\Omega_{t_1} PLh_1 PLt_1}\right) \end{aligned}, \tag{10.25}$$

where we use the integral identity in [[66], 6.643.3].

The right term of RHS of Q_1^{OTPR} can be given by

$$\begin{aligned} Q_{1,b}^{OTPR} &= \tfrac{1}{\Omega_{t_1}} \int_{x=0}^{\infty} \left(1 - e^{-\frac{P_M}{\rho\beta P_P\Omega_{r_1} PLr_1 PLt_1 x}}\right) e^{-\frac{x}{\Omega_{t_1}}} dx \\ &= 1 - 2\sqrt{\tfrac{P_M}{\rho\beta P_P\Omega_{r_1}\Omega_{t_1} PLr_1 PLt_1}} K_1\left(2\sqrt{\tfrac{P_M}{\rho\beta P_P\Omega_{r_1}\Omega_{t_1} PLr_1 PLt_1}}\right) \end{aligned}. \tag{10.26}$$

By using (10.25), (10.26), (10.23) is achieved.

Likewise, the right term of RHS in (10.22) is derived as

$$\begin{aligned} Q_2^{OTPR} &= \Pr\left\{|h_1|^2 \geq \tfrac{(1-\beta)P_P\gamma_0|t_2|^2|r_1|^2 PLt_2 PLr_1}{P_M PLh_1}\right\} \\ &\quad \times \Pr\left\{|r_1|^2 \geq \tfrac{P_M}{\rho\beta P_P|t_1|^2 PLr_1 PLt_1}\right\} \end{aligned}. \tag{10.27}$$

Following that, we consider the first term of RHS based on (10.27) which can be given by conditioning on $|t_2|^2$ as

$$\begin{aligned} Q_{2,a}^{OTPR}||t_2|^2 &= \tfrac{1}{\Omega_{r_1}} \int_{x=0}^{\infty} e^{-\frac{x(1-\beta)P_P\gamma_0|t_2|^2 PLr_1 PLt_2}{P_M\Omega_{h_1} PLh_1} - \frac{x}{\Omega_{r_1}}} dx \\ &= \tfrac{P_M\Omega_{h_1} PLh_1}{(1-\beta)P_P\gamma_0\Omega_{r_1} PLr_1 PLt_2}\left(|t_2|^2 + \tfrac{P_M\Omega_{h_1} PLh_1}{(1-\beta)P_P\gamma_0\Omega_{r_1} PLr_1 PLt_2}\right)^{-1}. \end{aligned} \tag{10.28}$$

Then, using the certain values of the results over the distribution of $|t_2|^2$. Thus, we have

$$\begin{aligned} Q_{2,a}^{OTPR} &= \tfrac{1}{\Omega_{t_2}} \int_{t=0}^{\infty} \omega_2 \left(\tfrac{1}{t+\omega_2}\right) e^{-\frac{t}{\Omega_{t_2}}} dt \\ &= \tfrac{\omega_2}{\Omega_{t_2}} e^{\frac{\omega_2}{\Omega_{t_2}}} E_1\left(\tfrac{\omega_2}{\Omega_{t_2}}\right) \end{aligned}, \tag{10.29}$$

where $\omega_2 = \frac{P_M\Omega_{h_1} PLh_1}{(1-\beta)P_P\gamma_0\Omega_{r_1} PLr_1 PLt_2}$.

Eventually, with the help of (10.26), the expression for $Q_{2,b}^{OTPR}$ can be given as

$$\begin{aligned} Q_{2,b}^{OTPR} &= \Pr\left\{|r_1|^2 \geq \frac{P_M}{\rho\beta P_P |t_1|^2 PLr_1 PLt_1}\right\} = 1 - Q_{1,b}^{OTPR} \\ &= 2\sqrt{\frac{P_M}{\rho\beta P_P \Omega_{r_1}\Omega_{t_1} PLr_1 PLt_1}} K_1\left(2\sqrt{\frac{P_M}{\rho\beta P_P \Omega_{r_1}\Omega_{t_1} PLr_1 PLt_1}}\right) \end{aligned}. \tag{10.30}$$

We continue with the evaluation of OP at D as

$$\begin{aligned} Q_3^{OTPR} &= \frac{1}{\Omega_{t_2}} \int_{t=0}^{\infty} e^{-\frac{1}{t}\left(\frac{\gamma_0}{\rho(1-\beta)P_P \Omega_{h_2} PLh_2 PLt_2}\right) - \frac{t}{\Omega_{t_2}}} dt \\ &= 2\sqrt{\frac{\gamma_0}{\rho(1-\beta)P_P \Omega_{h_2}\Omega_{t_2} PLh_2 PLt_2}} K_1\left(2\sqrt{\frac{\gamma_0}{\rho(1-\beta)P_P \Omega_{h_2}\Omega_{t_2} PLh_2 PLt_2}}\right) \end{aligned}. \tag{10.31}$$

We complete the proof for **Proposition** 10.2 by using (10.25), (10.26), (10.29), (10.30), and (10.31).

Remark 10.1. We provided closed-form expressions for the OP in (10.8) and (10.21) for the small cells. Thanks to these expressions, the throughput is optimized. In particular, MPT is located near S and R for EH, so the small cell tier 2 can be deployed. Most importantly, it is necessary that S and R should be placed far from MPR to avoid interference.

10.3.2 Rate-Energy trade-off for small cell CRN

Here, the expression for the ergodic capacity and the average harvested energy for the considered system can be given as

$$E_h^{avg} = \left(E_h^S + E_h^R\right) = \frac{1}{2}\eta\alpha P_P \left(\beta\Omega_{t_1} PLt_1 + (1-\beta)\,\Omega_{t_1} PLt_1\right), \tag{10.32}$$

and

$$C = \frac{(1-\alpha)}{2}\left\{\log_2\left(1+\gamma_{eq}\right)\right\}, \tag{10.33}$$

Thanks to the expression for ergodic capacity in (10.33), α and C decline, because less α leads to more information to mitigate the interference power. Therefore, the trade-off between maximizing the average harvested energy for power transfer and the ergodic capacity for IT is considered. Thus, similar to [112], we can use rate-energy (R-E) region to clarify the considered trade-off, including the ergodic capacity and average harvested energy pairs. The R-E region is defined as follows

$$\Gamma_{R-E} \triangleq \bigcup_{0\leq\alpha\leq 1} \left\{(R,E) : R \leq C, E \leq E_h^{avg}\right\}. \tag{10.34}$$

10.3.3 Average energy efficiency

It is noted that EE is the number of bits associated with the consumption of unit-joule. There are two concepts of energy consumption, i.e., the power transmission for reliable data transmission and the other is defined as the circuit energy consumption which can be denoted as P_C.

Therefore, the average EE, n_{ee} can be given considering the transmit power and the circuit power as

$$n_{ee} = \frac{\sum\limits_{i\in\{R,D\}} (1-\alpha)\left\{\log_2\left(1+\gamma_i\right)\right\}}{2P_{total}}, \tag{10.35}$$

where $P_{total} = P_S + P_R + 2P_C$, and P_C is constant, standing for the associated circuit energy consumption at all nodes.

10.3.4 Throughput

The delay-constraint throughput is evaluated in this section which is equal to the successful transmission rate during the transmission time, $(1-\alpha)T/2$, when the requirement for SIR, γ_0 is satisfied at R and D. Thanks to the OP expressions obtained in (10.8) and (10.21), we are able to examine the delay-constraint throughput at fixed rate, $R_0 = \log_2(1+\gamma_0)$ as

$$\tau^k \underset{k\in\{OTPS,OTPR\}}{=} \frac{(1-\alpha)}{2} R_0 \left(1 - OP^k\left(\gamma_0\right)\right). \tag{10.36}$$

10.4 Numerical Results

In this section, the impacts of EH period, α, energy conversion efficiency, η, transmit power of primary source MPT, P_P, and the distances between nodes in the small cells and macro cell are going to be presented. It is noted that the network topology is designed on the X-Y plane. The simulation results follow some parameters specified in Table 10.4.

Parameters	**Values**
Located at MPT	$(0.5, 1)$
Located at S	$(0, 0)$
Located at R	$(0.5, 0)$
Located at D	$(1, 0)$
Power transmission, P_P	10(dB)
Energy conversion efficiency, η	0.8
The path loss exponent, m	4
The SNR threshold, γ_0	-5dB
The average channel gains, Ω_{h_1}=Ω_{h_2}=Ω_{r_1}=Ω_{r_2}=Ω_{t_1}=Ω_{t_2}=Ω	5

Tab. 10.1: Main Simulation Parameters (Optimal TS Polocies)

In Fig. 10.3, we present the OP at S and R as a function of the peak interference power at $\gamma_0 = -5dB$. We see that the outage performance depends on the placement of MPT, i.e. at $(0, 0.5)$, $(0, 1)$ and $(0.5, 1)$, respectively. Besides, as P_M increases, the outage performance improves, because as P_M rises, the power constraint is extended, more

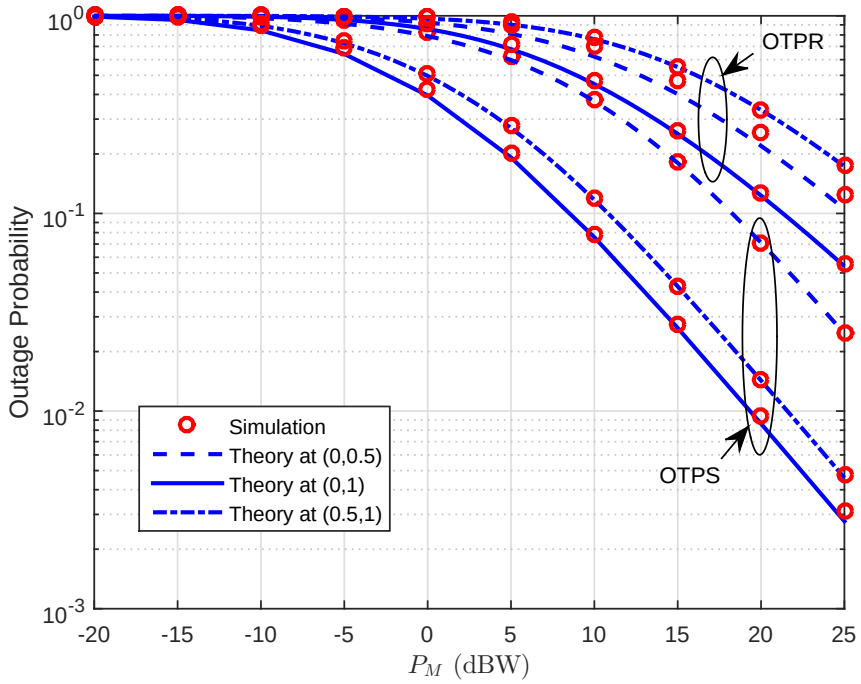

Fig. 10.3: OP vs. P_M(dB) with P_P=20dB, η=0.8, β=0.5, γ_0 =-5dB.

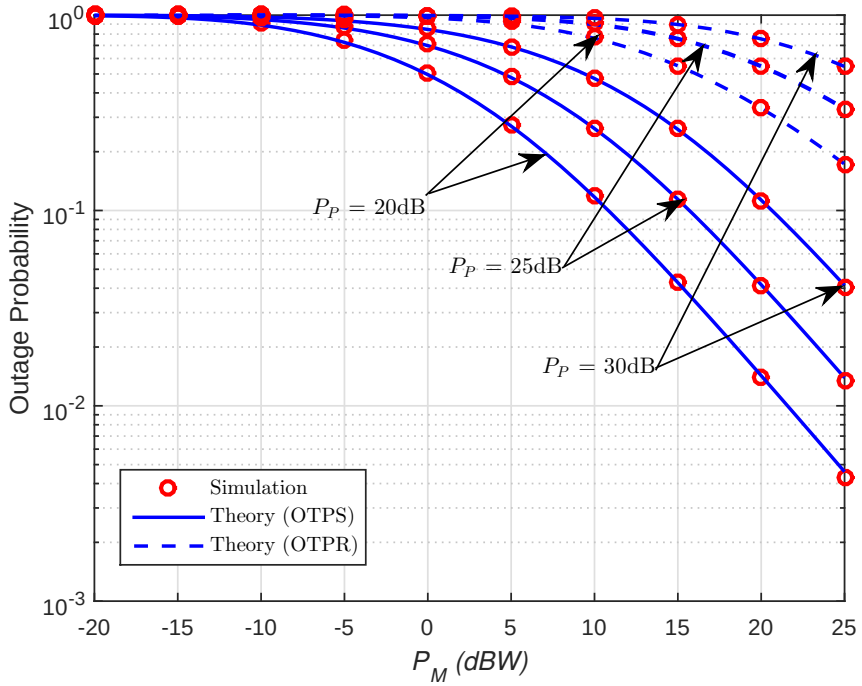

Fig. 10.4: OP vs. $P_M(dB)$ with difference power constraints, P_P, when MPT is at (0.5,1), η= 0.8, γ_0=-5dB.

energy is harvested at S and R from MPT, which accordingly enhances the small cell's outage performance. It is worth nothing that OTPS is superior to OTPR at $P_P = 20dB$. Particularly, in case of OTPS, when S is located near MPT, the OP is high, at $(0, 1)$, since more harvested power can be used for information decoding.

We illustrate the OP versus P_M for different values of transmit power at MPT, P_P in Fig. 10.4 with MPT being at $(0.5, 1)$. When P_M increases, the OP significantly enhances. Thanks to the achievement of α_S and α_R which are dependent on P_P, P_M, different levels of the transmit power at MPT lead to the changes of outage performance, because as P_P increases, S and R can use higher transmit power to replenish the interference affecting R and D from MPT. In contrast, as P_M rises, interference does not affect the transmit power at S and R.

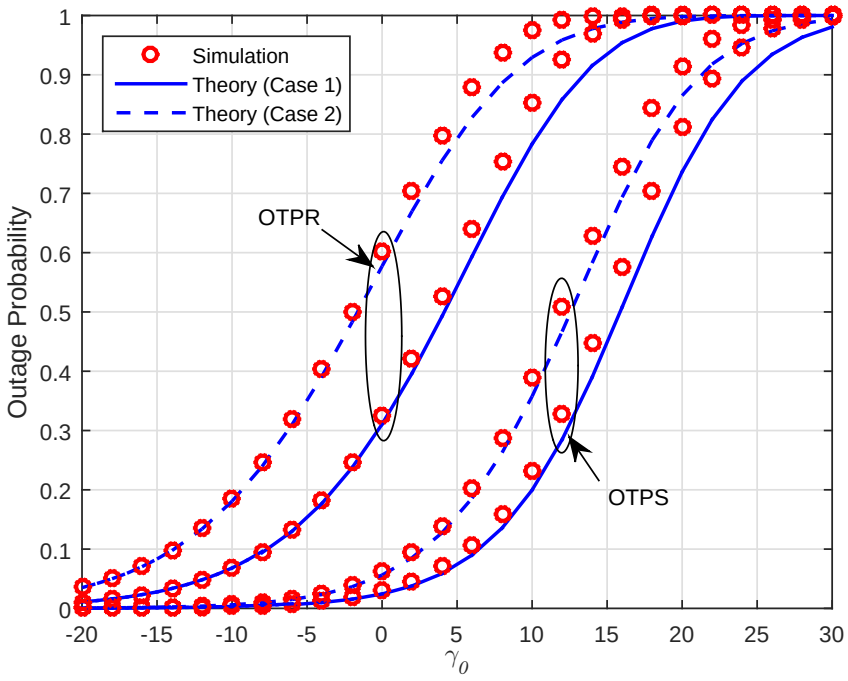

Fig. 10.5: OP vs. γ_0, with P_P=P_M=10(dBW), MPT at (0.5,1), and β=0.5 in two cases.

Fig. 10.5 presents the OP as a function of the SIR threshold, γ_0, where some parameters are used to simulate our results (i.e, P_P= 10dBW at $(0.5, 1)$), P_M = 10dBW, $\beta = 0.5$. We consider Case 1 and Case 2 with $\Omega = 1$ and $\Omega = 5$ for each case, respectively. In particular, as γ_0 increases, γ_0 is not satisfied at one of the communication links in the small cell, so the OP climbs. As γ_0 rises, the channel gain coefficients increase which result in a drop in the OP.

In Fig. 10.6, the delay-constraint throughput, α is depicted as a function of P_M, and we assume that MPT is located at $(0.5, 1)$. It is clear that the throughput increases and then falls as α rises. For each small α value, S and R do not have enough energy for

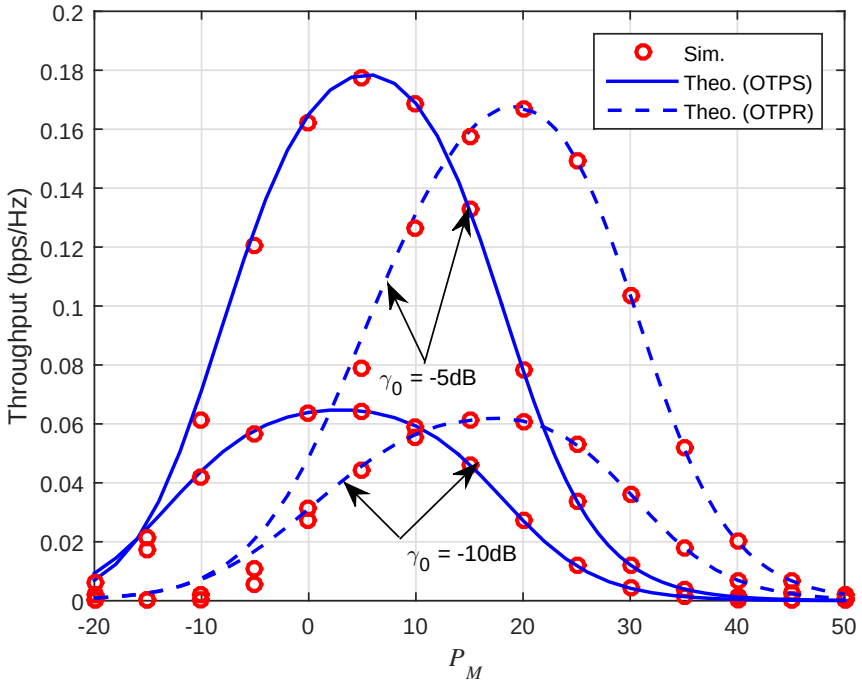

Fig. 10.6: Throughput vs. P_M(dBW) with different γ_0, and P_P=10(dBW) location (0.5,1), η=0.8, β=0.5.

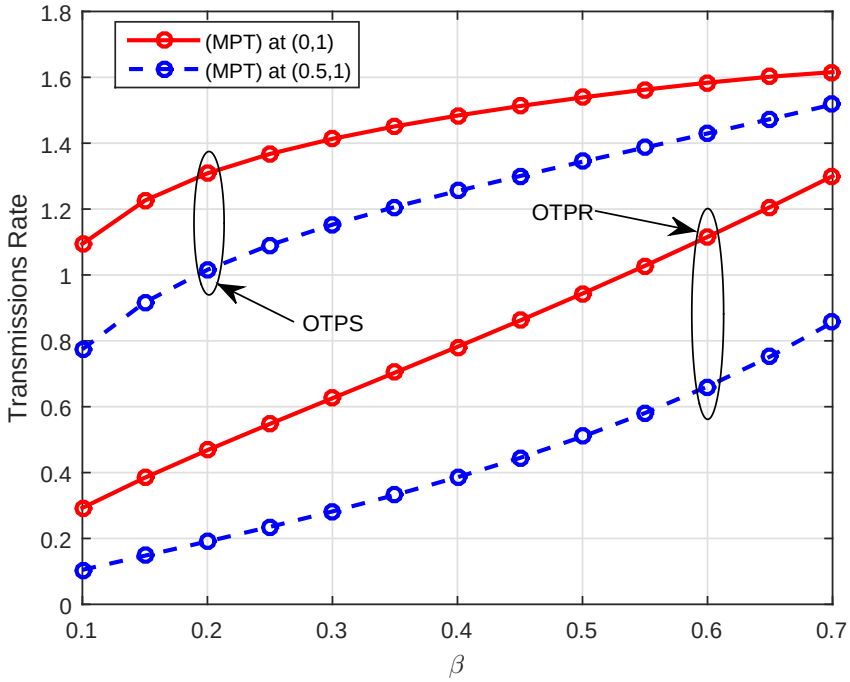

Fig. 10.7: Transmission Rate vs. β with different MPT at location, and $P_P = P_M$=10(dBW) , η=0.8, $\alpha_{optimal}$.

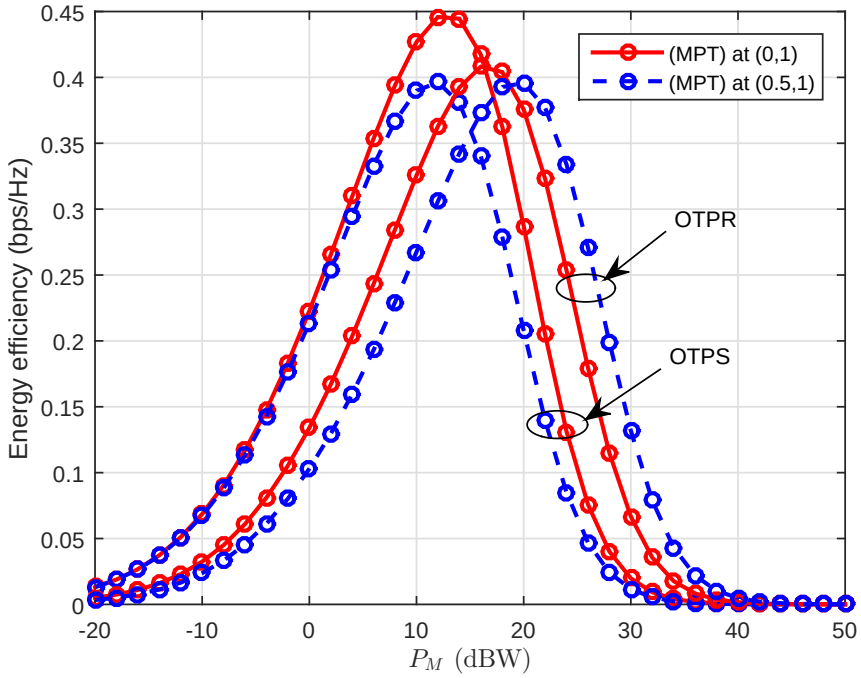

Fig. 10.8: Average energy efficiency with P_M (dBW) versus different locations of MPT, and P_P=P_C=10dBW , η=0.8, β=0.5.

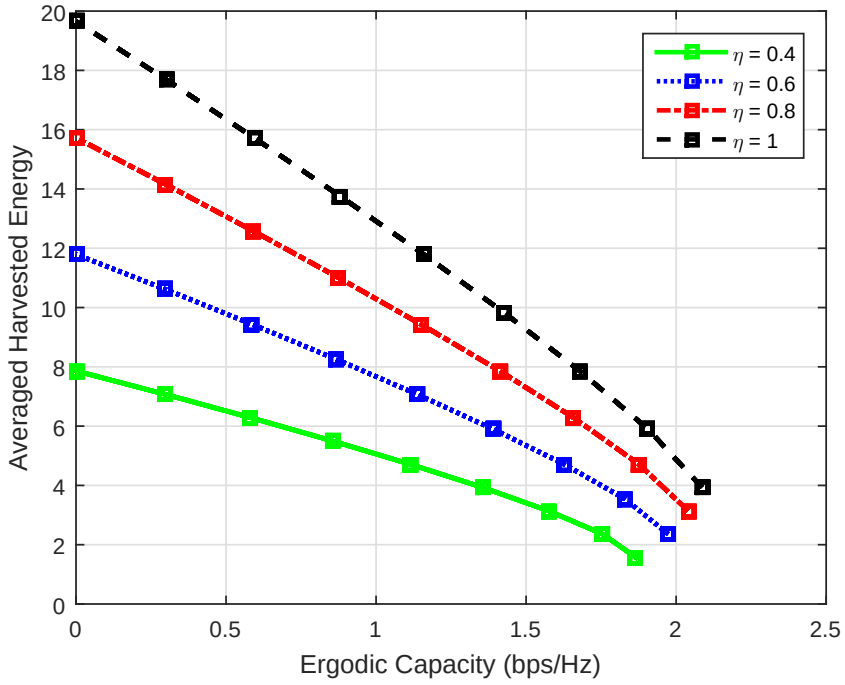

Fig. 10.9: Rate-energy trade-off versus different values of η, and MPT at (0.5,1), P_P=P_M= 10dBW.

successful IT because of the long time used for EH; as a result, the throughput is low. In contrast, regarding large values of α, S and R cannot transfer signals in a reliable way, since the IT periods are short.

The transmission rate versus different values of β is shown in Fig. 10.7. We can see that as β increases, the transmission rate of the small cell rises. Since β is low, less power is available for IT carried out by MPT. We can see that all curves go up as β increases, because the higher β means larger SIR, which improves the transmission rate in case of OTPS, because small β at S leads to less transmission rate, while large β at R associates with more transmission rate in case of OTPR. Note that the choice of β allows the proposed policies to achieve better transmission rate for the small cell.

We use different energy conversion efficiency, i.e, $\eta = 0.8$, $\eta = 0.4$, and $\eta = 0.1$ to study the average EE in Fig. 10.8. It is clear that the average EE increases as well as P_M. Subsequently, P_M falls to approximately 18(dB). Furthermore, the harvested energy is less dependent on P_P than η. Due to the impact of η on the transmitted signal in the small cell, the average EE is linear with η.

In Fig. 10.9, we present the energy conversion efficiency η which has the impact on the R-E trade-off. It is obvious that as ergodic capacity rises, the amount of harvested energy drops. The harvested energy is less sensitive to ergodic capacity than η, because E_h^{avg} is linear with η, but η affects both the transmitted signal to ensure the QoS of the macro cell.

10.5 Summary

In this chapter, we proposed two TS-based policies so-called OTPS and OTPR to greatly improve the maximum transmit power at S and R for a HD DF small cell CRN. Most importantly, we derived the closed-form expressions for OP in both single antenna, which result in better OP. For system performance analysis, the expressions for delay-constraint throughput, the average energy efficiency, and the R-E trade-off were obtained. With the numerical and simulation results, we can confirm that OTPR is better than OTPS in terms of all performance metrics due to the achievement of optimal TS ratio and the location of small cell nodes, but the QoS for the macro cell is still guaranteed.

11 CONCLUSIONS AND FUTURE WORK

In this thesis, new cooperative protocols were proposed, the system performance of different networks was analyzed. Each work is summarized in this chapter. Besides, our future developments to the existing works can also be presented.

11.1 Summary of results and insights

In Chapter 4, wireless power supply policies in FD RNs were proposed to address Aim 1. The choice of optimal time in HP mode assists R in sharing energy without consuming much energy like SP. Besides, the numerical results proved that an acceptable outage performance can be achieved between HP and SP mode. *Valuable understandings into the impact of SI, TS ratio and the transmit power* on the system throughput were presented systematically [NHS01].

Following that, Aim 2 presents the impact of CSI and HWIs in Chapter 5 and Chapter 6, respectively. There were several noticeable contributions of these works [NHS02], [NHS05]. Firstly, closed-form expressions for the achievable throughput, the STP and the average EE and SE were derived. Secondly, comparisons between AF and DF transmission schemes were provided to analyze the system performance. Last but not least, due to the fact that the optimization of STP is non-convex, TS and PS ratios were optimized by using the Genetic Algorithm.

In Aim 3, the development of SWIPT in bidirectional networks was focused, where PTSTW and PTSTH protocols were examined in Chapter 7 [NHS06], [NHS07]. This analysis provided closed-form expressions for OP in two considered protocols. Numerical results showed that *the throughput performance of PTSTW outperforms that of PTSTH.* In addition, *the delay-tolerant throughput is higher than that of the delay-limited throughput.* In fact, *the energy accumulation process in RNs should be examined with the placement of R nodes.*

Regarding RS techniques in Aim 4, optimal RS schemes in multi-relay cooperative RNs were studied in both Chapter 8 and Chapter 9. In particular, the trade-off between ergodic capacity, average EH, and OP were clearly investigated at high SNR in our new proposed schemes, i.e., HDMRC, FDJD, and HTS to combat self-interference with OPIPC and OPEHA. *In order to prove the correctness of the system, the asymptotic results were obtained along side with the closed-form expressions.* It is proven that *HTS is superior to HDMRC and FDJD* schemes in terms of OP [NHS08], [NHS09].

Finally, in Aim 5, OTPS and OTPR were designed to enhance the maximum transmit power at source and relay for a HD DF small-cell CRN in Chapter 10 [NHS10], [NHS11]. Our numerical and simulation results proved that *OTPR outperforms OTPS* in terms of all performance metrics.

11.2 Future work

We propose the following extensions to all the works presented in this thesis.

In Aim 1, some restrictions are associated with the power level, or the amount of energy that R can transfer requiring us to design a proper power transfer policy. In our future work, we are planning to formulate the optimal policy for SP and HP. Besides that, instead of using Rayleigh fading channel, Rician fading channel model will be applied.

The work in Aim 2 can be extended with multiple-antenna mode. In principle, this concept in wireless systems can ensure high SEs and EEs by exploiting the randomness in multipath propagation. In our future work, we are going to investigate the impact of CSI and HWIs in both AF and DF relaying protocol considering HTPSR in case R is equipped with multiple antennas. In this future work, we are going to determine how much HWIs will affect the process of RS.

To extend the work in Aim 3, we realize the security problems in TWRN are critical to comprehensively evaluate. Therefore, SWIPT is deployed at R to provide relay cooperation as R may not drain the energy from the limited battery.

Motivated from non-orthogonal multiple access (NOMA) which has attracted a lot of research attention thanks to its higher SE than traditional orthogonal multiple access (OMA) . These days, it has increasingly been recognized as a prime candidate multiple access scheme for future wireless networks. Therefore, the work in Aim 4 can be expanded with the the proposing of new RS schemes with fixed and adaptive power allocations at R nodes.

Regarding the work of Aim 5, the use of NOMA in CRN can be deployed to expand the work, where SUs can share the spectrum with the licensed PUs as long as the interference at PUs remains below a threshold. In principle, SU has to restrict its transmit power to deal with the interference to the PU, so the use of NOMA can significantly enhance the SU performance.

REFERENCES

[1] H. J. Visser and R. J. M. Vullers, "RF energy harvesting and transport for wireless sensor network applications: principles and requirements," *Proceedings of the IEEE*, vol. 101, no. 6, pp. 1410–1423, 2013.

[2] H. Nishimoto, Y. Kawahara, and T. Asami, "Prototype implementation of ambient RF energy harvesting wireless sensor networks," in *Proceedings of IEEE Sensors, Kona*, pp. 1282–1287, 2010.

[3] X. Zhang, H. Jiang, L. Zhang, C. Zhang, Z. Wang, and X. Chen, "An energy-efficient ASIC for wireless body sensor networks in medical applications," *IEEE Transactions on Biomedical Circuits and Systems*, vol. 4, no. 1, pp. 11–18, 2010.

[4] X. Lu, D. Niyato, P. Wang, D. I. Kim, and Z. Han, "Wireless charger networking for mobile devices: Fundamentals, standards, and applications," *IEEE Wireless Communications*, vol. 22, no. 2, pp. 126–135, 2015.

[5] D. Mishra, S. De, S. Jana, S. Basagni, K. Chowdhury, and W. Heinzelman, "Smart RF energy harvesting communications: challenges and opportunities," *IEEE Communications Magazine*, vol. 53, no. 4, pp. 70–78, Apr. 2015.

[6] S. Bi, C. K. Ho, and R. Zhang, "Wireless powered communication: Opportunities and challenges," *IEEE Communications Magazine*, vol. 53, no. 4, pp. 117–125, 2015.

[7] K. Ishibashi and H. Ochiai, "Analysis of instantaneous power distributions for non-regenerative and regenerative relaying signals," *IEEE Trans. Wireless Commun.*, vol. 11, no. 1, pp. 258–265, Jan. 2012.

[8] L. R. Varshney, "Transporting information and energy simultaneously," in *Proc. of International Symposium on Information Theory*, pp. 1612–1616, July 2008.

[9] P. Grover and A. Sahai, "Shannon meets tesla: wireless information and power transfer," in *Proc. of International Symposium on Information Theory*, pp. 2363–2367, June 2010.

[10] X. Zhou, R. Zhang, and C. K. Ho, "Wireless information and power transfer: Architecture design and rate-energy tradeoff," *IEEE Transactions on Communications*, vol. 61, no. 11, pp. 4754–4767, 2013.

[11] R. Zhang and C. K. Ho, "MIMO broadcasting for simultaneous wireless information and power transfer," *IEEE Transactions on Wireless Communications*, vol. 12, no. 5, pp. 1989–2001, 2013.

[12] L. Liu, R. Zhang, and K. C. Chua, "Wireless information transfer with opportunistic energy harvesting," *IEEE Trans. Wireless Commun.*, vol. 12, no. 1, pp. 288–300, Jan. 2013.

[13] A. A. Nasir, X. Zhou, S. Durrani, and R. A. Kennedy, "Relaying protocols for wireless energy harvesting and information processing," *IEEE Transactions on Wireless Communications*, vol. 12, no. 7, pp. 3622–3636, Jul. 2013.

[14] L. Liu, R. Zhang, and K. C. Chua, "Multi-antenna wireless powered communication with energy beamforming," *IEEE Trans. Wireless Commun.*, vol. 62, no. 12, pp. 4349–4361, Nov. 2014.

[15] G. Yang, C. K. Ho, and Y. L. Guan, "Dynamic resource allocation for multiple-antenna wireless power transfer," *IEEE Trans. on Signal Processing*, vol. 62, no. 14, pp. 3565–3577, July 2014.

[16] X. Chen, X. Wang, and X. Chen, "Energy-efficient optimization for wireless information and power transfer in large-scale mimo systems employing energy beamforming," *IEEE Wireless Comm. Letters*, vol. 2, no. 6, pp. 667–670, Dec. 2013.

[17] X. Lu, P. Wang, D. Niyato, and Z. Han, "Resource allocation in wireless networks with RF energy harvesting and transfer," *IEEE Network*, vol. 29, no. 6, pp. 68–75, 2015.

[18] C. A. Balanis, *Antenna theory: analysis and design*. John Wiley & Sons, 2012.

[19] R. Jabbar, Y. S. Song, and T. T. Jeong, "RF energy harvesting system and circuits for charging of mobile devices," *IEEE Trans. on Consumer Electronics*, vol. 56, no. 1, pp. 247–253, Feb. 2010.

[20] D. P. Bertsekas, *Dynamic Programming and Optimal Control*, vol. 1. MA: Athena Scientific„ 1995.

[21] A. Fu, E. Modiano, and J. Tsitsiklis, "Optimal energy allocation and admission control for communications satellites," *IEEE/ACM Transactions on Networking*, vol. 11, pp. 488–500, 2003.

[22] V. Sharma, U. Mukherji, V. Joseph, and S. Gupta, "Optimal energy management policies for energy harvesting sensor nodes," *IEEE Transactions on Wireless Communications*, vol. 9, p. 1326–1336, 2010.

[23] A. Kansal, J. Hsu, S. Zahedi, and M. B. Srivastava, "Power management in energy harvesting sensor networks," *ACM Transactions on Embedded Computing Systems (TECS)*, vol. 6, 2007.

[24] O. Ozel and S. Ulukus, "Information-theoretic analysis of an energy harvesting communication system," in *International Workshop on Green Wireless (W-GREEN) at IEEE Personal, Indoor and Mobile Radio Commun.*, 2010.

[25] O. Ozel, K. Tutuncuoglu, J. Yang, S. Ulukus, and A. Yener, "Transmission with energy harvesting nodes in fading wireless channels: Optimal policies," *IEEE J. Sel. Areas Commun.*, vol. 29, p. 1732–1743, 2011.

[26] T. Schenk, *RF Imperfections in High-Rate Wireless Systems: Impact and Digital Compensation*. Springer, 2008.

[27] E. Bjornson, M. Matthaiou, and M. Debbah, "A new look at dual-hop relaying: Performance limits with hardware impairments," *IEEE Trans. on Communications*, vol. 61, no. 11, pp. 4512–4525, Oct. 2013.

[28] O. Taghizadeh, V. Radhakrishnan, A. C. Cirik, R. Mathar, and L. Lampe, "Hardware impairments aware transceiver design for bidirectional full-duplex MIMO OFDM systems," *IEEE Transactions on Vehicular Technology*, vol. 67, no. 8, pp. 7450–7464, 2018.

[29] D. Li, C. Shen, and Z. Qiu, "Sum rate maximization and energy harvesting for two way AF relay systems with imperfect CSI," in *Proc. of International Conference on Acoustics, Speech and Signal Processing*, pp. 4958–4962, May 2013.

[30] Z. Xiang and M. Tao, "Robust beamforming for wireless information and power transmission," *IEEE Commun. Lett.*, vol. 1, no. 4, pp. 372–375, 2012.

[31] Z. Chen, B. Wang, B. Xia, and H. Liu, "Wireless information and power transfer in two-way amplify-and-forward relaying channels," in *IEEE Global Conference on Signal and Information Processing (GlobalSIP)*, pp. 168–172, 2014.

[32] Y. Liu, L. Wang, M. Elkashlan, T. Q. Duong, and A. Nallanathan, "Two-way relaying networks with wireless power transfer: Policies design and throughput analysis," in *Proc. of IEEE Global Conference on Signal and Information Processing (GlobalSIP)*, pp. 566–573, Dec. 2011.

[33] Y. Lu, W. Wang, L. Chen, Z. Zhang, and A. Huang, "Opportunistic forwarding in energy harvesting mobile delay tolerant networks," in *Proc. of IEEE International Conference on Communications (ICC)*, pp. 526–531, June 2014.

[34] Z. Ding, S. M. Perlaza, I. Esnaola, and H. V. Poor, "Power allocation strategies in energy harvesting wireless cooperative networks," *IEEE Trans. Wireless Commun.*, vol. 13, no. 2, pp. 846–860, Jan. 2014.

[35] Y. Wang, Y. Xu, N. Li, W. Xie, K. Xu, and X. Xia, "Relay selection of fullduplex decode-and-forward relaying over nakagami-m fading channels," *IET Communications*, vol. 10, no. pp, pp. 170–179, 2016.

[36] J. M. Moualeu, W. Hamouda, X. Hongjun, and F. Takawira, "Power assignment in multi-relay adaptive df cooperative networks," in *Proc. of: IEEE Global Communications Conference (GLOBECOM)*, pp. 2444–2449, 2012.

[37] A. Alsharoa, H. Ghazzai, and M. S. Alouini, "Near-optimal power allocation with PSO algorithm for MIMO cognitive networks using multiple AF two-way relays," in *Proc. of IEEE International Conference on Communications (ICC)*, p. 1580–1584, 2014.

[38] K. Pathak and A. Banerjee, "On energy cooperation in energy harvesting underlay cognitive radio network," in *Proc. of Twenty Second National Conference on Communication (NCC)*, pp. 1–6, 2016.

[39] T. Kalluri and V. A. Bohara, "Regenerative relaying in energy harvesting cognitive radio networks," in *Proc. of European Conference on Networks and Communications (EuCNC)*, pp. 84–88, 2016.

[40] T. Jing, S. Zhu, H. Li, X. Xing, X. Cheng, Y. Huo, R. Bie, and T. Znati, "Cooperative relay selection in cognitive radio networks," *IEEE Transactions on Vehicular Technology*, vol. 63, p. 1872–1881, 2015.

[41] K. Yamamoto, K. Haneda, H. Murata, and S. Yoshida, "Optimal transmission scheduling for hybrid of full-duplex and half-duplex relaying," *IEEE Commun. Lett.*, vol. 15, no. 3, pp. 305–307, 2011.

[42] T. Riihonen, S. Werner, and R. Wichman, "Mitigation of loopback self-interference in full-duplex mimo relays," *IEEE Trans. Signal Process.*, vol. 59, no. 12, pp. 5983–5993, 2011.

[43] B. Day, A. Margetts, D. Bliss, and P. Schniter, "Full-duplex mimo relaying: Achievable rates under limited dynamic range," *IEEE Journal on Selected Areas in Commun.*, vol. 30, no. 8, pp. 1541–1553, 2012.

[44] V. Aggarwal, M. Duarte, A. Sabharwal, and N. K. Shankaranarayanan, "Full-duplex or half-duplex? a capacity analysis with bounded radio resources," in *IEEE Information Theory Workshop*, pp. 207–211, 2012.

[45] S. Barghi, A. Khojastepour, and K. Sundaresan, "Charactarizing the throughput gain of single cell MIMO wireless systems with full-duplex radios," in *Proc. 10th International Symposium on Modeling and Optimization in Mobile, Ad Hoc and Wireless Networks*, pp. 68–74, 2012.

[46] E. Aryafar, M. A. Khojastepour, K. Sundaresan, S. Rangarajan, and M. Chiang, "Midu: enabling MIMO full-duplex," in *Proc. 18th Annual International Conference on Mobile Computing and Networking*, pp. 257–268, 2012.

[47] M. G. Khafagy, A. E. Shafie, and A.Sultan, "Throughput maximization for buffer-aided hybrid half-/full-duplex relaying with self-interference," in *Proc. 2015 IEEE International Conference on Communications (ICC)*, pp. 1926–1931, 2015.

[48] K. Tutuncuoglu and A. Yener, "Sum-rate optimal power policies for energy harvesting transmitters in an interference channel," *Journal of Commun. And Net. Special Issue on Energy Harvesting in Wireless Net.*, vol. 14, no. 2, pp. 151–161, 2012.

[49] Z. Zhang, K. Long, A. V. Vasilakos, and L. Hanzo, "Full-duplex wireless communications: Challenges, solutions, and future research directions," *Proc. of the IEEE*, vol. 104, no. 7, pp. 1369–1409, 2016.

[50] O. Orhan and E. Erkip, "Optimal transmission policies for energy harvesting two-hop networks," in *Proc. Annual Conf. Inform. Sciences Systems (CISS)*, pp. 1–6, 2012.

[51] C. Huang, R. Zhang, and S. Cui, "Throughput maximization for the gaussian relay channel with energy harvesting constraints," *IEEE J. Sel. Areas Com-mun.*, vol. 31, no. 8, pp. 1469–1479, 2013.

[52] H. Ju and R. Zhang, "User cooperation in wireless powered communication networks," in *Proc. IEEE GLOBECOM.*, pp. 1430–1435, 2014.

[53] C. Zhong, H. A. Suraweera, G. Zheng, I. Krikidis, and Z. Zhang, "Wireless information and power transfer with full duplex relaying," *IEEE Transactions on Communications*, vol. 62, no. 10, pp. 3447–3461, 2014.

[54] L. Chen-Feng, M. Marco, L. Subhash, L. Chia-Han, and Q. S. Q. Tony, "Simultaneous wireless information and power transfer under different CSI acquisition schemes," *IEEE Transactions on Wireless Communications*, vol. 14, no. 4, pp. 1911–1926, 2015.

[55] A. Imtiaz, I. Aissa, W. K. N. Derrick, and S. Robert, "Power allocation for a hybrid energy harvesting relay system with imperfect channel and energy state information," in *Proc. of IEEE Wireless Communications and Networking Conference (WCNC)*, pp. 990–995, 2014.

[56] C. Dongwook and H. L. Jae, "Outage probability of two-way full-duplex relaying with imperfect channel state information," *IEEE Communications Letters*, vol. 18, no. 6, pp. 933–936, 2014.

[57] P. Binod, D. R. Sanjay, and K. Sumit, "Secondary throughput in underlay cognitive radio network with imperfect CSI and energy harvesting relay," in *Proc. of IEEE International Conference on Advanced Networks and telecommunications Systems (ANTS)*, pp. 1–6, 2015.

[58] T. Kamel, A. Q. Khalid, and A. Mohamed-Slim, "Outage analysis for underlay cognitive networks using incremental regenerative relaying," *IEEE Transactions on Vehicular Technology*, vol. 62, no. 2, pp. 721–734, 2012.

[59] W. Fei and Z. Xi, "Resource allocation for multiuser cooperative overlay cognitive radio networks with RF energy harvesting capability," in *Proc. of IEEE Global Communications Conference (GLOBECOM)*, pp. 1–6, 2016.

[60] J. Hyungsik and Z. Rui, "Throughput maximization in wireless powered communication networks," *IEEE Transactions on Wireless Communications*, vol. 13, no. 2, pp. 418–428, 2014.

[61] P. Jaehyun and C. Bruno, "Transmission strategies for joint wireless information and energy transfer in a two-user MIMO interference channel," in *Proc. of IEEE International Conference on Communications Workshops (ICC)*, pp. 591–595, 2013.

[62] B. Fatma and A. Mohamed-Slim, "Simultaneous wireless information and power transfer for MIMO amplify-and-forward relay systems," in *Proc. of IEEE Global Communications Conference (GLOBECOM)*, pp. 1–6, 2015.

[63] L. Hongxin, Z. Rui, H. Yucheng, and H. Yongming, "Secrecy performance of transmit antenna selection with outdated CSI for MIMO relay systems," in *Proc. of IEEE International Conference on Communications Workshops (ICC)*, pp. 272–277, 2016.

[64] D. N. Van, D. V. Son, and S. Oh-Soon, "Opportunistic relaying with wireless energy harvesting in a cognitive radio system," in *Proc. of IEEE on Wireless Communications and Networking Conference (WCNC)*, pp. 87–92, 2015.

[65] R. Tanelili, W. Stefan, and W. Risto, "Hybrid full-duplex/half-duplex relaying with transmit power adaptation," *IEEE Transactions on Wireless Communications*, vol. 10, no. 9, pp. 3074–3085, 2011.

[66] I. S. Gradshteyn and I. M. Ryzhik, *Table of Integrals, Series, and Products, 4th ed,*. New York: Academic Press Inc.,, 1980.

[67] A. J. Goldsmith, *Wireless Communications*. Cambridge, U.K: Cambridge Univ. Press, 2005.

[68] Z. Yangyang, G. Jianhua, M. Jinjin, O. Fengchen, and Z. Chensi, "Joint relay selection and power allocation in energy harvesting AF relay systems with ICSI," *IET Microwaves, Antennas & Propagation*, vol. 10, no. 15, pp. 1656–1661, 2016.

[69] K. Doppler, M. Rinne, C. Wijting, C. Ribeiro, and K. Hugl, "Device-to-device communications as an underlay to lte-advanced networks," *IEEE Communications Magazine*, vol. 47, no. 12, pp. 42–49, 2010.

[70] S. T. Su, B. Y. Huang, C. Y. Wang, C. W. Yeh, and H. Y. Wei, "Protocol design and game theoretic solutions for device-to-device radio resource allocation," *IEEE Transactions on Vehicular Technology*, vol. 66, no. 5, pp. 4271–4286, 2017.

[71] Z. Xia, J. Yan, and Y. Liu, "Cooperative content delivery in multicast multihop device-to-device networks," *IEEE Access*, vol. 5, pp. 6314–6324, 2017.

[72] X. Chai, T. Liu, C. Xing, H. Xiao, and Z. Zhang, "Throughput improvement in cellular networks via full-duplex based device-to-device communications," *IEEE Access*, vol. 45, pp. 7645–7657, 2017.

[73] X. Xia, D. Zhang, K. Xu, W. Ma, and Y. Xu, "Hardware impairments aware transceiver for full-duplex massive mimo relaying," *IEEE Transactions on Signal Processing*, vol. 63, no. 24, pp. 6565–6580, 2015.

[74] N. T. Do, D. B. d. Costa, and B. An, "Performance analysis of multirelay RF energy harvesting cooperative networks with hardware impairments," *IET Communications*, vol. 10, no. 18, pp. 2551–2558, 2016.

[75] T. P. Huynh, H. S. Nguyen, D. T. Do, and M. Voznak, "Impact of hardware impairments in af relaying network for wipt: Tsr and performance analysis," in *Proc. of International Conference on Electronics, Information, and Communications, (ICEIC)*, pp. 1–4, 2016.

[76] H. S. Nguyen, H. Nguyen, S. D. Sau, M. Voznak, and T. Huynh, "Impact of hardware impairments for power splitting relay with wireless information and eh," in *Proc. of International Conference on Electronics, Information, and Communications, (ICEIC)*, pp. 1–4, 2016.

[77] T. N. Nguyen, P. T. Tran, H. G. Hoang, H. S. Nguyen, and M. Voznak, "On the performance of decode-and-forward half-duplex relaying with time switching based energy harvesting in the condition of hardware impairmen," in *Proc. of International Conference on Advances in Information and Communication Technology, (ICACT)*, pp. 421–430, 2017.

[78] M. Matthaiou, A. Papadogiannis, E. Bjornson, and M. Debbah, "Two-way relaying under the presence of relay transceiver hardware impairments," *IEEE Communications Letters*, vol. 17, no. 6, pp. 1136–1139, 2013.

[79] L. R. Varshney, "Proceedings of IEEE international symposium on information theory," *IEEE Wireless Communications Letters*, pp. 1612–1616, 2008.

[80] Z. Wang, Z. Chen, B. Xia, L. Luo, and J. Zhou, "Cognitive relay networks with energy harvesting and information transfer: Design, analysis and optimization," *IEEE Transactions on Wireless Communications*, vol. 15, no. 4, pp. 2562–2576, 2016.

[81] G. DE, *Genetic algorithms in search, optimization and machine learning.* Addison-Wesley Longman Publishing Co., Inc., Boston, MA, USA„ 1989.

[82] K. Man, K. Tang, and S. Kwong, "Genetic algorithms: concepts and applications," *IEEE Transactions on Industrial Electronics*, vol. 43, no. 5, pp. 519–534, 1996.

[83] G.Du, K. Xiong, Y. Zhang, and Z. Qiu, "Outage analysis and optimization for time switching-based two-way relaying with energy harvesting relay node," *KSII Transactions on Internet and Information Systems*, vol. 9, no. 2, pp. 1–19, 2014.

[84] Z. Chen, B. Xia, and H. Liu, "Wireless information and power transfer in two-way amplify-and-forward relaying channels," in *Proc. of IEEE Global Conference on Signal and Information Processing (GlobalSIP)*, pp. 168–172, Dec. 2014.

[85] Z. Fang, X. Yuan, and X. Wang, "Distributed energy beamforming for simultaneous wireless information and power transfer in the two-way relay channel," *IEEE Signal Processing Letters*, vol. 22, no. 6, pp. 656–660, 2015.

[86] Y. Zou, X. Wang, and W. Shen, "Optimal relay selection for physical-layer security in cooperative wireless networks," *IEEE Journal on Selected Areas in Communications*, vol. 31, no. 10, pp. 2099–2111, 2013.

[87] X. Xu, J. Bao, H. Cao, Y.-D. Yao, and S. Hu, "Energy-efficiency-based optimal relay selection scheme with a BER constraint in cooperative cognitive radio networks," *IEEE Transactions on Vehicular Technology*, vol. 65, no. 1, pp. 191–203, 2016.

[88] D. S. Michalopoulos, J. Ng, and R. Schober, "Optimal relay selection for outdated CSI," *IEEE Communications Letters*, vol. 17, no. 3, pp. 503–506, 2013.

[89] H. S. Nguyen, D. T. Do, and M. Voznak, "Two-way relaying networks in green communications for 5G: Optimal throughput and tradeoff between relay distance on power splitting-based and time switching-based relaying SWIPT," *AEU - International Journal of Electronics and Communications*, vol. 70, pp. 1637–1644, 2016.

[90] J. D. Leeuw and G. Michailidis, "Block-relaxation algorithms in statistics," *Journal of Computational and Graphical Statistics*, vol. 9, pp. 26–31, 2000.

[91] J. Gorski, F. Pfeuffer, and K. Klamroth, "Biconvex sets and optimization with biconvex functions: a survey and extensions," *Mathematical Methods of Operations Research*, vol. 66, no. 3, pp. 373–407, 2007.

[92] R. M. Starr, *General Equilibrium Theory: An Introduction.* Cambridge University Press, 1997.

[93] H. Cui, M. Ma, L. Song, and B. Jiao, "Relay selection for two-way full duplex relay networks with amplify-and-forward protocol," *IEEE Transactions on Wireless Communications*, vol. 13, pp. 3768–3777, 2014.

[94] D.-T. Do and H.-S. Nguyen, "A tractable approach to analyze the energy-aware two-way relaying networks in presence of co-channel interference," *EURASIP Journal on Wireless Communications and Networking*, vol. P.P, pp. 1–4, 2016.

[95] L. Liu, R. Zhang, and K. C. Chua, "Wireless information and power transfer: A dynamic power splitting approach," *IEEE Trans. Commun.*, vol. 61, pp. 3990–4001, 2013.

[96] K. Xiong, P. Fan, C. Zhang, and K. B. Letaief, "Wireless information and energy transfer for two-hop non-regenerative MIMO-OFDM relay network," *IEEE Journal on Selected Area in Communications*, vol. 33, pp. 1595–1611, 2015.

[97] P. C. Sofotasios, M. K. Fikadu, S. Muhaidat, S. Freear, G. K. Karagiannidis, and M. Valkama, "Relay selection based full-duplex cooperative systems under adaptive transmission," *IEEE Wireless Communications Letters*, vol. PP, pp. 1–1, 2017.

[98] T. Riihonen, S. Werner, and R. Wichman, "Hybrid full-duplex/half-duplex relaying with transmit power adaptation," *IEEE Transactions on Wireless Communications*, vol. 10, pp. 3074–3085, 2011.

[99] N. Zlatanov, V. Jamali, and R. Schober, "Achievable rates for the fading half-duplex single relay selection network using buffer-aided relaying," *IEEE Transactions on Wireless Communications*, vol. 14, pp. 4494–4507, 2015.

[100] O. Arnold, F. Richter, G. Fettweis, and O. Blume, "Power consumption modeling of different base station types in heterogeneous cellular networks," in *Proc. of Future Network & Mobile Summit*, pp. 1–8, 2010.

[101] S. Wang, M. Ge, and W. Zhao, "Energy-efficient resource allocation for OFDM-based cognitive radio networks," *IEEE Transactions on Communications*, vol. 61, pp. 3181–3191, 2013.

[102] M. Yu, A. Xiong, P. Yu, and W. Li, "Power consumption modeling of base stations based on dynamic factors," in *Proc. of 17th Asia-Pacific Network Operations and Management Symposium (APNOMS)*, pp. 8710–8715, 2015.

[103] Z. H. Abbas and F. Y. Li, "Power consumption analysis for mobile stations in hybrid relay-assisted wireless networks," in *Proc. of IEEE International Symposium on Wireless Pervasive Computing (ISWPC)*, pp. 16–21, 2010.

[104] I. Krikidis, H. Suraweera, P. Smith, and C. Yuen, "Full-duplex relay selection for amplify-and-forward cooperative networks," *IEEE Transactions on Wireless Communications*, vol. 11, pp. 4381–4393, 2012.

[105] E. E. B. Olivo, D. P. M. Osorio, H. Alves, J. C. S. S. Filho, and M. Latva-aho, "An Adaptive Transmission Scheme for Cognitive Decode-and-Forward Relaying

Networks Half Duplex, Full Duplex, or No Cooperation," *IEEE Transactions on Wireless Communications*, vol. 15, pp. 5586–5602, 2016.

[106] Y. Li, T. Wang, Z. Zhao, M. Peng, and W. Wang, "Relay Mode Selection and Power Allocation for Hybrid One-Way/Two-Way Half-Duplex/Full-Duplex Relaying," *IEEE Communications Letters*, vol. 19, pp. 1217–1220, 2015.

[107] S. Sudevalayam and P. Kulkarni, "Energy harvesting sensor nodes: Survey and implications," *Proc. IEEE Commun. Surveys & Tutorials*, vol. 13, no. 3, pp. 443–461, 2011.

[108] S. Ross, *Introduction to Probability Models.* MA: Athena Scientific,eleventh ed., Elsevier Science, 2014.

[109] X. Huang, S. Liu, Y. Li, F. Zhu, and Q. Chen, "Dynamic cell selection and resource allocation in cognitive small cell networks," in *IEEE 27th Annual International Symposium on Personal, Indoor, and Mobile Radio Communications (PIMRC)*, pp. 1–8, 2016.

[110] S. Sardellitti and S. Barbarossa, "Joint optimization of collaborative sensing and radio resource allocation in small-cell networks," *IEEE Trans. Signal Process.*, vol. 61, pp. 4506–4520, 2013.

[111] H. Huang, Z.Li, B. Ai, G.Wang, and M. S. Obaidat, "Impact of hardware impairment on spectrum underlay cognitive multiple relays network," in *Proc. of IEEE International Conference on Communications (ICC)*, pp. 1–6, 2016.

[112] L. Liu, R. Zhang, and K. C. Chua, "Wireless information and power transfer: A dynamic power splitting approach," *IEEE Transactions on Communications*, vol. 61, no. 9, pp. 3990–4001, 2013.

CANDIDATE'S RESEARCH CITED IN THIS WORK INDEXED IN SCIE/WEB OF SCIENCE JOURNALS

[NHS01] Hoang-Sy Nguyen, M. Voznak, M.-T. Nguyen, L. Sevcik, Performance analysis with wireless power transfer constraint policies in full-duplex relaying networks (2017), In: *Elektronika ir Elektrotechnika*, Vol. 23, Issue 4, pp. 70-76. DOI: 10.5755/j01.eie.23.4.18725

[NHS02] Hoang-Sy Nguyen, Bui, A.-H., Do, D.-T., Voznak, M. Imperfect channel state information of AF and DF energy harvesting cooperative networks (2016), In: *China Communications*, 13 (10), art. no. 7732008, pp. 11-19. DOI: 10.1109/CC.2016.7732008

[NHS03] Hoang-Sy Nguyen, D. T. Do, M. Voznak, Exploiting hybrid time switching-based and power splitting-based relaying protocol in wireless powered communication networks with outdated channel state information (2017), In: *Automatika*, Vol. 58, No. 1, pp. 111-118, DOI: 10.1080/00051144.2017.1372124

[NHS04] D. T. Do, Hoang-Sy Nguyen, M. Voznak, T. S. Nguyen, Wireless Powered Relaying Networks Under Imperfect Channel State Information: System Performance and Optimal Policy for Instantaneous Rate (2017), In: *Radioengineering*, Vol. 26, No. 3, pp. 869-877, DOI: 10.13164/re.2017.0869

[NHS05] Hoang-Sy Nguyen, TS. Nguyen, M. Voznak, Successful transmission probability of cognitive device-to-device communications underlaying cellular networks in the presence of hardware impairments (2017), In: *EURASIP Journal on Wireless Communications*, 2017 (1), art. no. 208, DOI: 10.1186/s13638-017-0994-0

[NHS06] Hoang-Sy Nguyen, D.T. Do, A. H. Bui, M. Voznak, Self-Powered Wireless Two-Way Relaying Networks: Model and Throughput Performance with Three Practical Schemes (2017), In: *Wireless Personal Communications*, vol. 97, no. 1, pp. 613-631, DOI: 10.1007/s11277-017-4526-3

[NHS07] Hoang-Sy Nguyen , D.T. Do, M. Voznak, Two-Way Relaying Networks in Green Communications for 5G: Optimal Throughput and Tradeoff between Relay Distance on Power Splitting-based and Time Switching-based Relaying SWIPT, In: *AEU - International Journal of Electronics and Communications*, vol. 70, no. 12, pp. 1637-1644. DOI: 10.1016/j.aeue.2016.10.002

[NHS08] Hoang-Sy Nguyen, TS. Nguyen, M. Voznak, Relay Selection for SWIPT: Performance Analysis of Optimization problems and the Trade-off between Ergodic Capacity and Energy Harvesting (2018), In: *AEU - International Journal of Electronics and Communications*,vol. 85, pp. 59-67. DOI: 10.1016/j.aeue.2017.12.012

[NHS09] Hoang-Sy Nguyen, TS. Nguyen, VT. Vo, M. Voznak, Hybrid full-duplex/half-duplex relay selection scheme with optimal power under individual power constraints and energy harvesting (2018), In: *Computer Communications*, vol. 124, pp. 31-44, DOI: 10.1016/j.comcom.2018.04.014

[NHS10] Hoang-Sy Nguyen, TS. Nguyen, MT. Nguyen, M. Voznak, Optimal Time Switching-Based Policies for Efficient Transmit Power in Wireless Energy Harvesting Small Cell Cognitive Relaying Networks (2018), In: *Wireless Personal Communications*, vol. 99, no. 4, pp. 1605-1624, DOI: 10.1007/s11277-018-5296-2

[NHS11] Hoang-Sy Nguyen, T. S. Nguyen, M. Voznak, Wireless powered D2D communications underlying cellular networks: design and performance of the extended coverage (2018), In: *Automatika*, vol. 58, no. 4, pp. 391-399. DOI: 10.1080/00051144.2018.1455016

LIST OF CANDIDATE'S RESEARCH RESULTS AND ACTIVITIES

Publication activities

I provide the following list indexed results in relevant scientific databases, in order to document my research activities within the entire period of my doctoral study:

- ORCID: orcid.org/0000-0002-1547-8416
- Research ID: K-5701-2016
- records in Journal of ISI/SCIE/Web of Science: 13 articles in journals
- records in Processing of ISI/IEEE-Xplore/Web of Science: 13 conference papers
- h-index according to ISI/Web of Science: 3 (32 citations)
- h-index according to Scopus: 3 (56 citations)

Project memberships and participations

- In 2015-2018, a member of WiCOM group in TDTU, **Wireless Communications Research Group**, head of group: prof. Vozňák.
- In 2017, Specific research, SGS FEI VSB-TU Ostrava, project SP2017/82 **Networks and Security, Modelling, Simulation, Knowledge Retrieval and Communication Technologies for Smart Cities**, project coordinator: prof. Vozňák.
- In 2018, Specific research, SGS FEI VSB-TU Ostrava, project SP2018/170 **Networks and Communication Technologies for Smart Cities**, project coordinator: Dr. Řezáč.
- In 2018, The Czech Ministry of Education, Youth and Sports, project **Large Infrastructures for Research, Experimental Development and Innovations**, project No. LM2015070, project coordinator: doc. Vondrák.

Results with wider relation to the topic of dissertation indexed in SCI/SCIE/Web of Science journals

1. Do, D.-T., Hoang-Sy Nguyen, A tractable approach to analyzing the energy-aware two-way relaying networks in the presence of co-channel interference (2017), In: *EURASIP Journal on Wireless Communications and Networking*, 2016:271. DOI: 10.1186/s13638-016-0777-z
2. T. N. Nguyen, P. T. Tran, Hoang-Sy Nguyen , D. T. Do, M. Voznak, On the Performance of a Wireless Powered Communication System Using a Helping Relay (2017), In: *Radioengineering*, Vol. 26, No. 3, pp. 860-868, DOI: 10.13164/re.2017.0860

Other results indexed in conference proceedings of WoS, Scopus, IEEE-Xplore

I achieved next results not directly related to the dissertation within my study period and which are indexed in conference proceedings of WoS, Scopus, IEEE-Xplore.

1. Hoang-Sy Nguyen, T.-S.Nguyen, Tin Phu, and Miroslav Voznak, Outage performance of time switching energy harvesting wireless sensor network deploying NOMA, *In Proc. of 20th International Conference on e-Health Networking, Application & Services - Healthcom2018*, Czech Republic, 2018.DOI: 10.1109/HealthCom.2018.8531184
2. Hoang-Sy Nguyen, T-S. Nguyen, Tan N. Nguyen and Miroslav Voznak, Average bit error probability analysis for cooperative DF relaying in wireless energy harvesting networks, the 5th International Conference on Advanced Engineering - Theory and Applications 2018, Ostrava, Czech Republic
3. T.-S.Nguyen, N.M. Duc, Hoang-Sy Nguyen, and M. Voznak, Outage Probability Analysis in Multiple-RelayNetworks for Wireless Energy Harvesting, *in Proc. of 41th International Conference on Telecommunications and Signal Processing (TSP)*, Greece, July 2018. DOI: 10.1109/TSP.2018.8441296
4. T.-S.Nguyen, H.H.K. Duy, Hoang-Sy Nguyen, and M. Voznak, Throughput Analysis in Relaying Cooperative Systems Considering Time-switching with NOMA, *in Proc. of 41th International Conference on Telecommunications and Signal Processing (TSP)*, Greece, July 2018. DOI:10.1109/TSP.2018.8441516
5. Hoang-Sy Nguyen, AT. Bui, NT. Nguyen and M. Voznak, Opportunistic Multiple Relay Selection Schemes in both Full-Duplex and Half-Duplex Operation for Decode-and-Forward Cooperative Networks, *in SPRINGER Advances in Intelligent Systems and Computing*, Volume 538, 2017, pp. 431-441. DOI 10.1007/978-3-319-49073-1_47
6. TN. Nguyen, PT. Tran, HG. Hoang, Hoang-Sy Nguyen, and M. Voznak, On the Performance of Decode-and-Forward Half-Duplex Relaying with Time Switching Based Energy Harvesting in the Condition of Hardware Impairment, *in SPRINGER Advances in Intelligent Systems and Computing*, Volume 538, 2017, pp. 421-430. DOI 10.1007/978-3-319-49073-1_46
7. TN. Nguyen, PT. Tran, Hoang-Sy Nguyen, TT. Nguyen, M. Voznak, On the Performance of Energy Harvesting for Decode-and-Forward Full-Duplex Relay Networks in Imperfect CSI Condition, *in SPRINGER (AETA 2016): Recent Advances in Electrical Engineering and Related Sciences*, Volume 415, Busan, Korea December 8–10, 2016, pp. 838-849. DOI: 10.1007/978-3-319-50904-4_85
8. Hoang-Sy Nguyen , D. T. Do, M. Voznak, L. Sevcik, A Straightforward Method to Evaluate the Energy Aware Two-way Relaying Networks Under Effect of Co-channel Interference, *in Proc. XI International Symposium on Telecommunications-BIHTEL 2016*, Sarajevo, October 24-26, 2016. DOI: 10.1109/BIHTEL.2016.7775737
9. Hoang-Sy Nguyen , D. T. Do, M. Voznak, L. Sevcik, Two-Way Relay Networks

with Energy Harvesting and Information Transfer: Throughput Performance with Distance Allocation, *in Proc. XI International Symposium on Telecommunications-BIHTEL 2016*, Sarajevo, October 24-26, 2016. DOI: 10.1109/BIHTEL.2016.7775727

10. Hoang-Sy Nguyen, H. Bui, D.-T. Do, M.-T Nguyen, M. Voznak, and M. Mikulec, Wireless Information and Energy Harvesting for Bidirectional Relay Channels: Trade off between Relay Distance and Optimal Throughput, *in Proc. of 39th International Conference on Telecommunications and Signal Processing (TSP)*, Vienna, June 27-29, 2016, pp. 83-86. DOI: 10.1109/TSP.2016.7760834
11. Hoang-Sy Nguyen, D.-T. Do, H. B., and M. Voznak, Optimal Throughput of Time Power Switching Relaying Protocol with Imperfect Channel State Information, *in book Communication, Management and Information Technology Proceedings of the International Conference on Communication, Management and Information Technology (ICCMIT)*, Cosenza, April 26-29, 2016, pp. 261-268, ISBN : 978-1-138-02972-9
12. T.-P. Huynh, Hoang-Sy Nguyen , D.-T. Do, M. Voznak, Impact of hardware impairments in AF relaying network for WIPT: TSR and performance analysis, (2016) *in International Conference on Electronics, Information, and Communications, ICEIC 2016*, art. no. 7562967, 4p. DOI: 10.1109/ELINFOCOM.2016.7562967
13. Hoang-Sy Nguyen , H. Nguyen, S. Dang-Sau, M. Voznak, T.-P. Huynh, Impact of hardware impairments for power splitting relay with wireless information and EH, *in International Conference on Electronics, Information, and Communications, ICEIC 2016*, art. no. 7562941, 4p. DOI: 10.1109/ELINFOCOM.2016.7562941

APPENDIX A.1

Proof of Proposition 4.1

We provide this appendix to explain how OP at D using TSR protocol is obtained. In the first hop, the PDF and CDF of SNR are derived. In particular, the PDF is written as

$$f_{|h|^2}(x) = \frac{1}{\Omega_h} \exp\left(-\frac{x}{\Omega_h}\right), x \geq 0. \tag{A.1.1}$$

Next, we obtain the CDF as

$$F_{|h|^2}(x) = 1 - \exp\left(-\frac{x}{\Omega_h}\right). \tag{A.1.2}$$

The distribution function of SI can be defined as

$$f_{|f|^2}(x) = \frac{1}{\Omega_f} \exp\left(-\frac{x}{\Omega_f}\right). \tag{A.1.3}$$

Next, the the overall OP of the system is as

$$\begin{aligned} F_{\gamma_R}(x) &= \Pr\{\gamma_R < x\} = \Pr\left\{\frac{P_S|h|^2}{P_R|f|^2} < x\right\} \\ &= 1 - \frac{P_S\Omega_h}{P_R\Omega_f x + P_S\Omega_h} \end{aligned}. \tag{A.1.4}$$

Note that the end-to-end SNR in DF scheme is defined as $Y = \min\{\gamma_R, \gamma_D\}$. We have the general outage probability

$$\begin{aligned} F_Y(x) &= 1 - (1 - F_{\gamma_D}(x)) \times (1 - F_{\gamma_R}(x)) \\ &= 1 - P_S\Omega_h(P_S\Omega_h + P_R\Omega_f x)^{-1} \exp\left(-\frac{\sigma^2}{P_R\Omega_g}x\right) \end{aligned}, \tag{A.1.5}$$

where $F_{\gamma_D}(x) = 1 - \exp\left\{-\frac{\sigma^2}{P_R\Omega_g}x\right\}$.

This ends the proof for Proposition 4.1.

APPENDIX A.2

Proof of Proposition 4.2

Likewise, the PDF of the SNR for SI must be first given as

$$f_{|f|^2}(x) = \frac{1}{\Omega_f} \exp\left(-\frac{x}{\Omega_f}\right). \tag{A.2.1}$$

Following this, we have the CDF of the SNR at R as

$$F_{\gamma_R}(x) = 1 - \left(1 - \exp\left(-\frac{1}{\rho x\Omega_f}\right)\right). \tag{A.2.2}$$

Using the integral identity [47], the OP is computed by

$$F_{\gamma_D}(x) = 1 - 2\sigma^2\sqrt{\frac{x}{\rho P_S\Omega_h\Omega_g}}K_1\left(2\sigma^2\sqrt{\frac{x}{\rho P_S\Omega_h\Omega_g}}\right). \tag{A.2.3}$$

To this end, the overall OP is as follows

$$P_{out}^{HP}(x) = 1 - 2\sigma^2\left(1 - \exp\left(-\tfrac{1}{\rho x\Omega_f}\right)\right) \times \sqrt{\tfrac{x}{\rho P_S\Omega_h\Omega_g}}K_1\left(2\sigma^2\sqrt{\tfrac{x}{\rho P_S\Omega_h\Omega_g}}\right) \tag{A.2.4}$$

This ends the proof for Proposition 4.2.

APPENDIX B

Proof of Proposition 7.1:
It is established to depict the outage probability and the output SNRs at source A and B for both transmission schemes which is rewritten by

$$Z = \frac{U_1 XY}{U_2 X + U_3}, \tag{B.1}$$

where variables X and Y are $|f_A|^2$ and $|f_B|^2$ and constant $U_1 \geq 0$, $U_2 \geq 0$ and $U_3 \geq 0$ are distinguished factors from X and Y.

The outage probability at high SNRs is given by

$$P_{out} = \Pr\left\{Z = \frac{U_1 XY}{U_2 X + U_3} < \gamma_0\right\}. \tag{B.2}$$

Following (B.2), the OP can be rewritten as

$$\begin{aligned} P_{out} &= F_{|f_B|^2}(z) + \int\limits_{z=\gamma_0 U_2/U_1}^{\infty} f_{|f_B|^2}(z) \Pr\left(X < \frac{\gamma_0 U_3}{U_1 z - \gamma_0 U_2}\right) dz \\ &= 1 - \tfrac{1}{\Omega_B} \int\limits_{z=\gamma_0 U_2/U_1}^{\infty} \exp\left(-\frac{z}{\Omega_B} - \frac{\gamma_0 U_3}{(U_1 z - \gamma_0 U_2)\,\Omega_A}\right) dz, \end{aligned} \tag{B.3}$$

where $1_{Y<\frac{\gamma_0 U_2}{U_1}}: Pr\left(X > \frac{\gamma_0 U_3}{U_1 Y - \gamma_0 U_2}\right) = 1$ because $U_1 Y - \gamma_0 U_2$ is a negative number and the probability of X is always 1.

The cumulative distribution function (CDF) of Ω_A that is the exponential random variable by $|f_A|^2$ and $F_X(z) \triangleq Pr(X < z) = 1 - \exp(-z/\Omega_X)$. Moreover, the probability density function (PDF) of Ω_B that is the average of the exponential random variable $|f_B|^2$ and $f_{|f_B|^2}(z) \triangleq \frac{1}{\Omega_B} \exp(-z/\Omega_B)$.

We have

$$P_{out} = 1 - \frac{1}{\exp\left(\frac{U_2 \gamma_0}{U_1 \Omega_B}\right) \Omega_B} \int\limits_{x=0}^{\infty} \exp\left(-\frac{x}{U_1 \Omega_B} - \frac{\gamma_0 U_3}{x \Omega_A}\right) dx, \tag{B.4}$$

where new integration is set $x \triangleq U_1 z - \gamma_0 U_2$ and the modified Bessel function of the second kind with order n in [66] is depicted by $K_n\{.\}$ and $\int\limits_0^{\infty} e^{-\frac{\beta}{4x} - \gamma x} dx = \sqrt{\frac{\beta}{\gamma}} K_1\left(\sqrt{\beta\gamma}\right)$.

Thus, the CDF of Z is calculated by

$$F_Z(\gamma_0) = 1 - \exp\left(-\frac{U_2 \gamma_0}{U_1 \Omega_B}\right) \mu K_1(\mu), \tag{B.5}$$

where $\mu = \sqrt{\frac{(4U_3)\gamma_0}{U_1(\Omega_A \Omega_B)}}$.
This ends the proof for Proposition 7.1.

APPENDIX C

Proof for Proposition 8.1.

Based on (8.8), the PDF of γ_D for a Rayleigh fading channel can be computed by

$$\begin{aligned} F_{\gamma_D} &= Pr\left(\frac{\frac{\eta\alpha\beta(1-\beta)}{(1-\alpha)}P_S^2X^2Y}{\frac{\eta\alpha\beta}{(1-\alpha)}l_1^m P_S N_0 XY + l_1^m l_2^m(1-\beta)P_S N_0 X + l_1^{2m} l_2^m N_0 N_0} < \gamma_0\right) \\ &= Pr\left(\left(Q_3X^2 - Q_4X\right)Y < \left(Q_1X + Q_2\right)\right), \end{aligned} \tag{C.1}$$

where $Q_1 = l_1^m l_2^m \left(1-\beta\right) P_S N_0 \gamma_0$, $Q_2 = l_1^{2m} l_2^m N_0 N_0 \gamma_0$, $Q_3 = \frac{\eta\alpha\beta(1-\beta)}{(1-\alpha)}P_S^2$, and $Q_4 = \frac{\eta\alpha\beta}{(1-\alpha)}l_1^m P_S N_0 \gamma_0$.

It is clear that $(Q_3X^2 - Q_4X)$ has both negative or positive values. If $(X > Q_4/Q_3)$, it will be a negative value, and the greater figure than the negative value is 1. Therefore, we derive the following equations as follows

$$\begin{aligned} F_{\gamma_D} &= Pr\left(Y < \tfrac{Q_1X+Q_2}{Q_3X^2-Q_4X}\right) \\ &= Pr\left(Y < \tfrac{Q_1X+Q_2}{Q_3X^2-Q_4X}\right)1_{(X<Q_4/Q_3)} + Pr\left(Y > \tfrac{Q_1X+Q_2}{Q_3X^2-Q_4X}\right)1_{(X>Q_4/Q_3)}. \end{aligned} \tag{C.2}$$

From (C.2), the CDF of γ_D can be expressed as

$$\begin{aligned} F_{\gamma_D} &= \int_{x=0}^{Q_4/Q_3} f_X(x) Pr\left(Y > \frac{Q_1X+Q_2}{Q_3X^2-Q_4X}\right)\mathrm{dx} + \int_{x=Q_4/Q_3}^{\infty} f_X(x) Pr\left(Y < \frac{Q_1X+Q_2}{Q_3X^2-Q_4X}\right)\mathrm{d}x \\ &= \int_{x=0}^{Q_4/Q_3} f_X(x)dx + \int_{x=Q_4/Q_3}^{\infty} f_X(x) Pr\left(1 - e^{-\frac{\omega X+\zeta}{(\varphi x^2-\upsilon x)\Omega_D}}\right)dx \\ &= 1 - \tfrac{1}{\Omega_S}\int_{x=Q_4/Q_3}^{\infty} \exp\left[-\left(\frac{x}{\Omega_S} + \frac{Q_1x+Q_2}{\left(Q_3x^2-Q_4x\right)\Omega_D}\right)\right]\mathrm{d}x, \end{aligned} \tag{C.3}$$

where the integration variable is x, the PDF of random variable, X is $f_X(x) \triangleq \frac{1}{\Omega_S}e^{-\frac{x}{\Omega_S}}$. The CDF of the random variable Y is $F_Y(x) \triangleq Pr(Y < x) = 1 - e^{-\frac{x}{\Omega_D}}$. Although it is obvious that the integration of the formula in (C.3) cannot be simplified, thanks to the product of the two noise variance terms in (8.8), the approximated SNR is derived since the constant, $l_1^{2m} l_2^m N_0 N_0$ is approximately 0. Consequently, the CDF of γ_D can be rewritten by

$$F_{\gamma_D} \approx 1 - \frac{1}{\Omega_S}\int_{x=Q_4/Q_3}^{\infty} \exp\left[-\left(\frac{x}{\Omega_S} + \frac{Q_1}{(Q_3x - Q_4)\Omega_D}\right)\right]dx. \tag{C.4}$$

Thanks to the final equation in [[66], 3.324.1], the approximated CDF at high SNR is written as

$$\begin{aligned} F_{\gamma_D} &\approx 1 - \frac{e^{-\frac{Q_4}{Q_3\Omega_{h_S}}}}{Q_3\Omega_{h_S}}\int_{y=0}^{\infty} \exp\left[-\left(\frac{y}{Q_3\Omega_{h_S}} + \frac{Q_1}{y\Omega_{h_D}}\right)\right]dy \\ &= 1 - 2\exp\left(-\tfrac{Q_4}{Q_3\Omega_{h_S}}\right)\sqrt{\tfrac{Q_1}{Q_3\Omega_{h_S}\Omega_{h_D}}}K_1\left(2\sqrt{\tfrac{Q_1}{Q_3\Omega_{h_S}\Omega_{h_D}}}\right). \end{aligned} \tag{C.5}$$

This ends the proof for Proposition 8.1.

APPENDIX D.1

Proof of Proposition 9.1

This appendix derives the outage probability at D node for FDJD relay selection in OPIPC policy.

Let us first calculate the CDF at R_l as

$$\begin{aligned} F_{\Gamma_{SR_l}}(x) &= \Pr\left\{\Gamma_{SR_l} < x\right\} = \Pr\left\{\frac{P_S|X|}{P_{R_l}|W|} < x\right\} \\ &= 1 - \frac{P_S\Omega_X}{P_{R_l}\Omega_W x + P_S\Omega_X}. \end{aligned} \tag{D.1.1}$$

Next, the CDF for FDJD mode at D node can be expressed by

$$\begin{aligned} F_{\Gamma_{R_lD}} &= \Pr\left(Z = Z_1 + Z_2 < x\right) \\ &= \frac{1}{\Omega_{Z_1}}\frac{1}{\Omega_{Z_2}}\int_{z=0}^{x}\int_{z_1=0}^{z} \mathrm{e}^{-\frac{z_1}{\Omega_{Z_1}}}\mathrm{e}^{-\frac{(z-z_1)}{\Omega_{Z_2}}}dz_1dz \\ &= 1 + \frac{P_S\Omega_Z\mathrm{e}^{-\frac{N_0x}{P_S\Omega_Z}} - P_{R_l}\Omega_Y\mathrm{e}^{-\frac{N_0x}{P_{R_l}\Omega_Y}}}{P_{R_l}\Omega_Y - P_S\Omega_Z}, \end{aligned} \tag{D.1.2}$$

where $Z_1 = \frac{P_{R_l}|Y|}{N_0}$, and $Z_2 = \frac{P_S|Z|}{N_0}$ with mean variables $\Omega_{Z_1} = \frac{P_{R_l}\Omega_Y}{N_0}$ and $\Omega_{Z_2} = \frac{P_S\Omega_Z}{N_0}$, respectively.

It is noted that the e2e SNR in DF scheme can be calculated as $\Gamma_{eq,l} = \min\left\{\Gamma_{SR_l}, \Gamma_{R_lD}\right\}$. Therefore, the outage probability can be obtained as

$$F_{\Gamma_{eq,l}}(x) = 1 - \left(\frac{P_S\Omega_X}{R_l\Omega_W x + P_S\Omega_X}\right)\left(\frac{P_S\Omega_Z\mathrm{e}^{-\frac{N_0x}{P_S\Omega_Z}} - P_{R_l}\Omega_Y\mathrm{e}^{-\frac{N_0x}{P_{R_l}\Omega_Y}}}{P_S\Omega_Z - P_{R_l}\Omega_Y}\right). \tag{D.1.3}$$

This ends the proof for *Proposition 9.1*.

APPENDIX D.2

Proof of Proposition 9.2

We have the CDF of the high SNR at R_l in OPEHA policy as

$$F_{\Gamma_{SR_l}}(x) = 1 - \left(1 - e^{\left(-\frac{1}{\rho_l x\Omega_W}\right)}\right), \tag{D.2.1}$$

where applying the PDF is $f_{|W|}(x) = \frac{1}{\Omega_W}e^{\left(-\frac{x}{\Omega_W}\right)}$.

Thanks to the use of [[66],324.1], $\int_0^\infty e\left(-\frac{\beta}{4x} - \gamma x\right)dx = \sqrt{\frac{\beta}{\gamma}}K_1\left(\sqrt{\beta\gamma}\right)$, we denote $\Gamma_{XY} = \frac{\rho_l P_S|X||Y|}{N_0}$. Hence, the CDF of Γ_{XY} can be calculated as

$$F_{\Gamma_{XY}}(x) = 1 - 2\sqrt{\frac{N_0x}{\rho_l P_S\Omega_X\Omega_Y}}K_1\left(2\sqrt{\frac{N_0x}{\rho_l P_S\Omega_X\Omega_Y}}\right). \tag{D.2.2}$$

Following that, the SNR at D as $\Gamma_{R_lD} = \frac{\rho_l P_S |X||Y|}{N_0} + P_S \frac{|Z|}{N_0}$, the CDF at D node can be expressed by

$$F_{\Gamma_{R_lD}}(x) = \Pr\left[\Gamma_{XY} < x - P_S \frac{|Z|}{N_0}\right]. \tag{D.2.3}$$

Based on (D.2.3), the CDF is expressed as

$$F_{\Gamma_{R_lD}}(x) = \frac{1}{\Omega_Z}\int_{z=0}^{\infty}\left[1 - 2\sqrt{\frac{(N_0 x - P_S z)}{\rho_l P_S \Omega_X \Omega_Y}} K_1\left(2\sqrt{\frac{(N_0 x - P_S z)}{\rho_l P_S \Omega_X \Omega_Y}}\right)\right] e^{-\frac{z}{\Omega_Z}} dz. \tag{D.2.4}$$

Now we define a new integration variable, $t^2 \triangleq (N_0 x - P_S z)$. Therefore, the outage probability at D node can be written by

$$\begin{aligned} F_{\Gamma_{R_lD}}(x) = {} & \tfrac{2N_0}{P_S\Omega_Z} e^{-\left(\frac{N_0 x}{P_S\Omega_Z}\right)} \int_{t=0}^{\sqrt{x}} t e^{\left(\frac{N_0 t^2}{P_S\Omega_Z}\right)} dt \\ & + \tfrac{2N_0}{P_S\Omega_Z} e^{-\left(\frac{N_0 x}{P_S\Omega_Z}\right)} \int_{t=\sqrt{x}}^{0} \left(2t\sqrt{\frac{t^2}{\rho_l P_S \Omega_X \Omega_Y}} e^{\left(\frac{N_0 t^2}{P_S\Omega_Z}\right)} K_1\left(2\sqrt{\frac{t^2}{\rho_l P_S \Omega_X \Omega_Y}}\right)\right) dt \end{aligned}. \tag{D.2.5}$$

We obtain the first term of (D.2.5) as follow

$$\mathcal{I}_1 = 1 - e^{-\left(\frac{N_0 x}{P_S\Omega_Z}\right)}, \tag{D.2.6}$$

where we use the formula, $\int_0^u x e^{-q^2x^2} dx = \frac{1}{2q^2}\left(1 - e^{-q^2u^2}\right)$ in [[66],3.321.4].

The second term of (D.2.5) can be expressed as

$$\mathcal{I}_2 = -\frac{2N_0}{P_S\Omega_Z} e^{-\left(\frac{N_0 x}{P_S\Omega_Z}\right)} \int_0^{\sqrt{x}} \left(2t\sqrt{\frac{t^2}{\rho_l P_S \Omega_X \Omega_Y}} e^{\left(\frac{N_0 t^2}{P_S\Omega_Z}\right)} K_1\left(2\sqrt{\frac{t^2}{\rho_l P_S \Omega_X \Omega_Y}}\right)\right) dt. \tag{D.2.7}$$

Thus, base on (D.2.6), (D.2.7), the CDF at D node can be calculated as

$$F_{\Gamma_{R_lD}}(x) = 1 - e^{-\left(\frac{N_0 x}{P_S\Omega_Z}\right)}\left[1 + \frac{2N_0}{P_S\Omega_Z}\int_{t=0}^{\sqrt{x}} \left(2te^{\left(\frac{N_0 t^2}{P_S\Omega_Z}\right)}\sqrt{\frac{t^2}{\rho_l P_S \Omega_X \Omega_Y}} K_1\left(2\sqrt{\frac{t^2}{\rho_l P_S \Omega_X \Omega_Y}}\right)\right) dt\right]. \tag{D.2.8}$$

Finally, based on (D.2.1), (D.2.8), we compute the overall outage probability as

$$F_{\Gamma_{eq,l}}(x) = 1 - \left(1 - F_{\Gamma_{SR_l}}(x)\right).\left(1 - F_{\Gamma_{R_lD}}(x)\right). \tag{D.2.9}$$

This ends the proof for *Proposition 9.2*.